INAUGURAL - DISSERTATION

for the degree of Doctor of Natural Sciences
of the Ruperto-Carola-University of Heidelberg, Germany

presented by
Dipl.-Phys. Anne Katrin Wackerbarth
born in: Rotenburg a.d. Fulda, Germany
Oral examination: 19.1.2012

Towards a better understanding of climate proxies in stalagmites
-
Modelling processes from surface to cave

Referees: Prof. Dr. Augusto Mangini
Prof. Dr. Werner Aeschbach-Hertig

Dedicated to my parents.

Abstract

In recent years stalagmites revealed their high potential as archives for palaeo climate variability. However, the quantitative interpretation of the climate-related features - proxies - is still a challenging task.
In this work two numerical models assessing the influence of climate parameters on two stalagmite proxies - the Mg/Ca ratio and the δ^{18}O value - were developed. The models describe quantitatively how the proxies evolve from the atmospheric signals to the incorporation into stalagmite calcite. Both models were successfully applied to stalagmites from caves in western Germany.
The models were used to establish two novel approaches of inverse modelling yielding simultaneously palaeo-temperatures and palaeo-precipitation from δ^{18}O and Mg/Ca values. Although both models are based on substantially different setups, their climate reconstructions show remarkable similarities applied on a Holocene stalagmite from western Germany.
In addition, for the first time a stalagmite model (the δ^{18}O model developed in this thesis) was forced with the output data of a General Circulation Model, as a new concept to understand the climate impact on δ^{18}O values of speleothems. The advantage is that this method can be applied to caves worldwide and for any given point in time without requiring observational climate data. An experiment including twelve European caves at 6ka before present shows the potential of this method to analyse synoptic-scale patterns of the climate of the past.

Zusammenfassung

Seit einigen Jahren beweisen Stalagmiten ihr hohes Potenzial als Archive der Variabilität des Paläoklimas. Die quantitative Interpretation ihrer vom Klima beeinflussten Merkmale - Proxys - ist jedoch eine herausfordernde Aufgabe.
In dieser Arbeit wurden zwei numerische Modelle entwickelt, die den Einfluss klimatischer Parameter auf zwei verschiedene Stalagmitenproxys bestimmen - das Mg/Ca Verhältnis sowie den δ^{18}O Wert. Sie wurden entwickelt um quantitativ zu beschreiben, wie sich diese Proxys vom atmosphärischen Signal bis hin zum Einbau in den Stalagmiten entwickeln. Beide Modelle konnten erfolgreich an Stalagmiten in Westdeutschland angewendet werden. Die Modelle wurden desweiteren benutzt, um zwei neuartige Ansätze der Inversmodellierung zu implementieren. Beide bestimmen gleichzeitig Paläotemperaturen sowie Paläoniederschläge anhand der gegebenen δ^{18}O und Mg/Ca Werte. Obwohl beide Modelle auf unterschiedlichen Voraussetzungen beruhen, weisen doch ihre Klimarekonstruktionen an einem holozänen Stalagmiten aus dem Westen Deutschlands bemerkenwerte Übereinstimmungen auf.
Zusätzlich wurde in dieser Arbeit zum ersten Mal ein Stalagmitenmodel (das entwickelte δ^{18}O Modell) mit den simulierten Klimadaten eines 'General Circulation'-Modells angetrieben, als ein neuer Ansatz um die Auswirkungen des Klimas auf den δ^{18}O Wert von Stalagmiten zu verstehen. Der Vorteil dieses Verfahrens ist die Anwendbarkeit zu jedem Zeitpunkt weltweit, ohne die Notwendigkeit Beobachtungsdaten einzubeziehen. Ein Experiment anhand von zwölf europäischen Höhlen für den Zeitpunkt 6000 Jahre vor heute zeigt das Potenzial der Methode, großskalige, meteorologische Muster zu analysieren.

Contents

1. Introduction

People throughout history have been influenced by the climate conditions of their environment and strong climatic changes. During the last decades we have experienced a strong temperature increase which needs to be evaluated and classified. It is especially important to understand how much of this trend is associated with an anthropogenic influence and how much can be ascribed to the internal and natural variations of the climate system. On the other hand it is relevant to estimate where this trend is leading to and which impact on our daily life we have to anticipate.
To estimate the influence of natural climate variation in modern times, the climate variability of the past must be assessed with the help of climate archives.
Climate archives are characterised by two attributes: i) the possibility to derive a temporal assignment of the measured samples and ii) a feature which is sensitive to climate parameters (proxy). Pollen records, deep sea corals, ice cores or tree rings are some of them which can supply insights to the whole range of climate forming parameters like temperature of land and ocean, precipitation or circulation changes of ocean and atmosphere. Since few decades stalagmites have established as valuable components of climate archives.
They qualify as valuable climate archive for two reasons: i) they grow sheltered and continuous over long periods and can be absolutely dated by the Th/U method [Richards and Dorale, 2003] and ii) they provide several proxies (δ^{18}O , δ^{13}C, Mg/Ca and other trace elements, growth rate, noble gases in their fluid inclusions) which react in different ways to climate conditions. These criteria lead to a continuous recording of the climate conditions over periods from decades to hundred thousands of years.
However, the decoding of climate information from stalagmites is a challenging task, since the proxies are influenced by several climate parameters. Various case studies show that it depends on the particular location of the cave how climate affects the stalagmite proxies[1].
Assessing the influence of climate parameters at a specific location can be approached either by comparing stalagmite proxy time series with observational data or other established climate archives or models can be designed which describe the processes influencing the respective climate proxy mathematically.
In this work the latter attempt is aimed for by developing two models for the proxies δ^{18}O and the Mg/Ca ratio. The first model (chapter 4) describes the evolution of the δ^{18}O value from precipitation to stalagmite calcite depending on climate parameters. The second model (chapter 5) was designed to understand the many parameters influencing the Mg/Ca ratio of stalagmites and determine the relation to climate proxies.
The advantage of modelling is that the influence of different parameters included in the model can be determined very fast by sensitivity experiments - provided that the model

[1] Section 2.4, 2.5 and 2.6 give insights to the influence of climate on δ^{18}O and Mg/Ca incorporated in stalagmites and an overview of important case studies.

represents the actual conditions and processes correctly. Therefore the presented models are thoroughly calibrated with observed climate and cave parameters and tested by comparison with measured values (for Mg/Ca or δ^{18}O respectively) for a cave in western Germany.
In addition, modelling offers the possibility of reversing the models under certain conditions to derive climate information from stalagmite proxy time series. This work presents two approaches for climate reconstruction from stalagmite records (chapter 6).
The third major part (chapter 7) of this work describes a novel approach how models can be used to analyse climate changes of the past. In this part a forcing of the developed model for δ^{18}O in stalagmites by a General Circulation Model is presented. This leads to artificial δ^{18}O values (present days or past times) that can be compared to stalagmite samples. Applied to several European Caves it is a valuable tool to enlighten the European climate pattern in past times.
This thesis is embedded in the DAPHNE research group by the DFG (Deutsche Forschungsgemeinschaft Forschergruppe 668).

2. Basics

This section supplies an overview of state-of-the-art research on different topics, which are touched by this work and required to understand the model design presented here. Since the studied climate archives in this work are stalagmites, the conditions of their growth are described first (section 2.1). The next section (section 2.2) introduces the evapotranspiration, which is in many ways an important factor in this work, as it determines the fraction of meteoric water that can form cave drip water.
The third, fourth and fifth section are dedicated to isotopes and the oxygen isotopes in particular, which is the main climate proxy investigated for this thesis. The third section (section 2.3) describes the principles of isotope fractionation in general, while the fourth section (section 2.4) focusses on the oxygen isotopes and pictures the processes influencing the oxygen isotope ratio from source (ocean) to target (stalagmite). The fifth section (section 2.5) finally gives an overview of case studies using oxygen isotopes to draw conclusions of climate variability.
The sixth section (section 2.6) turns towards the Mg/Ca ratio in speleothems and outlines the link of this proxy to climate. In addition, several case studies are presented, which are able to prove the validity of Mg/Ca as a climate proxy.
The last section is concerned with a meteorological phenomenon - the North Atlantic Oscillation. Although this synoptic pattern is not directly connected to stalagmites, it plays an important role in this work. The developed models are applied to stalagmites from European regions, whose winter climate conditions are ruled by the North Atlantic Oscillation. Therefore, it can be enlightening to interpret stalagmite proxies in this context. The basics of the North Atlantic Oscillation and the impact on European winter climate are approached in section 2.7.

2.1. Stalagmite growth

A stalagmite is a calcite formation in a cave which can develop over thousands of years in caves due to constant dripping of a calcite supersaturated solution from the cave ceiling to the floor. Stalagmite growth occurs in karstic areas due to the following processes.
Meteoric precipitation has a specific partial pressure of CO_2 depending of the atmospheric signal (presently about 380ppm). After the loss due to evapotranspiration (see section 2.2) a fraction of the water infiltrates the soil layer where it is faced with a significantly higher pCO_2. McDermott [2004] gives an average value between ≈5000-35000 ppm. The exact value depends on the type and state of the vegetation and the activity of micro organism in the soil. The partial pressure is subject to a characteristic annual cycle caused by the growing season of the vegetation and long term trends like the formation of a soil layer between the last glacial period and the early Holocene.
The water from meteoric precipitation equilibrates with this pCO_2 by the uptake of CO_2. In the upper soil the pCO_2 clearly shows a seasonal pattern which is smoothed towards greater depth to a rather constant annual signal [Scheffer and Schachtschabel, 1984]. Depending on the properties of the soil layer the water either infiltrates deeper layer rather fast or resides in the upper layer experiencing an extensive mixing with water from several months. [1] The soil pCO_2 value is important because it determines the formation of bicarbonate in the solution. The chemical reaction can be expressed as

$$\begin{aligned} H_2O + CO_2 &\rightleftharpoons H_2CO_3 \\ H_2O + H_2CO_3 &\rightleftharpoons H_3O^+ + HCO_3^- \\ H_2O + HCO_3^- &\rightleftharpoons H_3O^+ + CO_3^{2-} \end{aligned} \tag{2.1}$$

When the karst matrix is approached, the solution starts to dissolve calcite until saturation is reached.
In principle two flow characteristics of water in the karst matrix can be distinguished - seepage and fissured flow. In the first case the water percolates slowly through the matrix and is therefore well mixed, when it enters the cave. In the latter case the infiltration water uses cracks and fissures in the host rock leading to a rather short residence time in this layer. In most cases the cave drip water is well mixed indicating that seepage flow often prevails. In both cases the solution is saturated with respect to calcite, when it enters a cave, since the time constant for dissolution is short compared to typical residence times (month to years [Lachniet, 2009]).
Calcite dissolution is described by

$$CaCO_3 + HCO_3^- + H_3O^+ \rightleftharpoons Ca^{2+} + 2HCO_3^- + H_2O \tag{2.2}$$

In most cases a cave has a lower pCO_2 than soil air. This value can reveal also high seasonal variations [Spötl *et al.*, 2005] due to cave ventilation. The gradient between the pCO_2 of the drip water solution and the cave environment forces degassing of CO_2

[1] If the residence time of the water is short, it is possible that the drip water in a cave shows strong variation in pCO_2. If the residence time is long, the pCO_2 will show a more constant and stable value.

from the drip water solution starting immediately, when the drip water is exposed to cave air. Due to the loss of CO_2 calcite is forced to precipitate from the solution for electroneutrality.
Where the drip water solution hits the ground constantly, a stalagmite forms.

$$Ca^{2+} + 2HCO_3^- \rightleftharpoons CaCO_3 + H_2O + CO_2 \tag{2.3}$$

If this occurs in small gaps or voids in the karst layer, before the stalagmite is reached, the process is called Prior Calcite Precipitation. This can happen also on the cave ceiling. The principles of stalagmite growth are illustrated in figure 2.1.

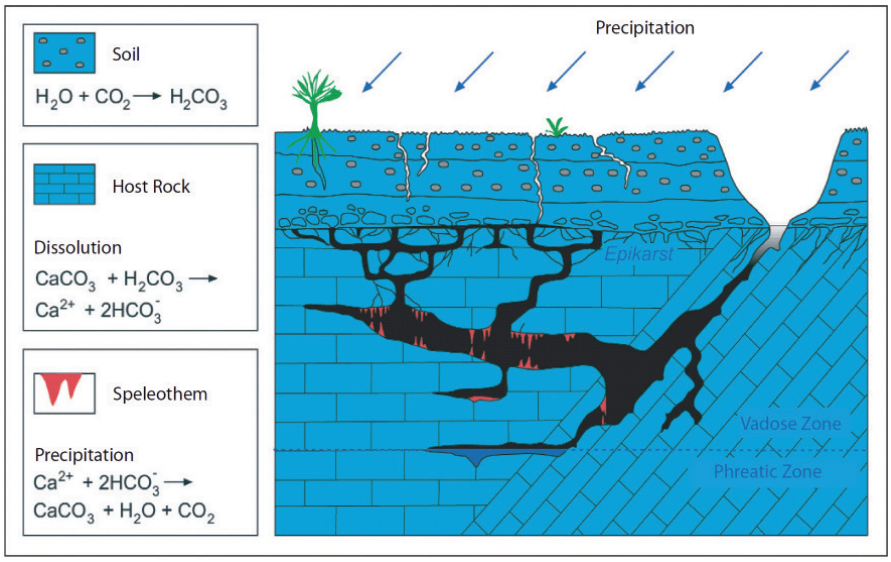

Figure 2.1.: Principle of stalagmite growth (extracted from Spötl *et al.* [2007])

2.2. Evapotranspiration

The evapotranspiration plays a major role in this thesis, as it determines how much water from meteoric precipitation contributes to the drip water in caves. Evapotranspiration combines the processes of evaporation and transpiration. The former depends on physical parameters like temperature, humidity or wind velocity. Transpiration describes the evaporation of water through leaf stomata, which was taken up by the roots for nutrient transport and water supply. Therefore transpiration depends on the type and state of vegetation. Plants from arid regions show small transpiration rates by adaption to the low water supply [Häckel, 1999].
The quantitative calculation of these combined processes are complex due to many parameters influencing the system. Several empirical equations have been developed, which differ in the number of input parameters. The choice of the equation depends on the respective application.
The most comprehensive equation which yields the best results worldwide was published by Penman [1948]. It includes temperature, global insolation, actual hours of sunshine, humidity, wind velocity, saturation vapour pressure and the albedo.
However, the number of input parameters complicates an application, since these parameters might not be easy to retrieve for each location in the world in particular in the context of palaeo climate research. For this application more simple, yet adequate equations must be used.
Two equations will be applied in the following studies. One was developed by Haude [1954] and Haude [1955] (see equation 2.4). As input parameters it requires only temperature and humidity at 2 p.m. (or daily maximum) and a vegetation coefficient describing the type of vegetation.

$$ET_{pot} = D \cdot m \cdot P_{2p.m.} \cdot (1 - \frac{F_{2p.m.}}{100}) \left[\frac{mm}{month}\right] \tag{2.4}$$

where

$$P_{2p.m.} = 4.58 \cdot 10^{\frac{7.45 \cdot T_{2p.m.}}{235 + T_{2p.m.}}} \; [hPa] \tag{2.5}$$

In the equation represents:
D the number of days per month
m the vegetation coefficient
$\mathbf{P}_{2p.m.}$ the saturation vapour pressure
$\mathbf{T}_{2p.m.}$ the mean monthly temperature at 2p.m. in °C[2]
$\mathbf{F}_{2p.m.}$ the relative humidity at 2p.m.

Schiff [1975] showed that this equation describing the potential evapotranspiration is close to the actual evapotranspiration measured with lysimeters in Germany.
For some applications the number of input parameters is still too high. In these cases the established equation published by Thornthwaite and Mather [1957], which depends only on temperature, is recommended (equation 2.6).

$$ET_{pot} = 16 \cdot (10 \cdot T/I)^{0.9262188/(2.4232459 - log_{10}(I))} \cdot C \tag{2.6}$$

[2]Note, that temperature is generally given in °C in this thesis.

where I is

$$I = \sum_{i=1}^{12} \frac{T_{i_{std}}}{5}^{1.514} \tag{2.7}$$

and C is a coefficient which depends on the geographical location and can be derived from tables in Thornthwaite and Mather [1957].

2.3. Isotopes and fractionation

Mook [2006] describes the phenomenon of isotope fractionation as follows.
Isotope cores (atoms of the same element with different numbers of neutrons) have the same electrical charge, but can be distinguished by their physiochemical properties due to their different masses. The mass difference results in two features in which isotopes differ from each other:

- The thermal energy is equal for each particle. The mass of the particle (E=$\frac{1}{2}mv^2$) determines therefore their velocity. Lighter and therefore faster particles have a higher diffusion velocity and in addition a higher collision frequency, which is the driver of chemical reactions.
- The binding energy of particles depends on mass. Lighter molecules have lower binding energies. Heavier isotopes remain statistically more often in a solid state than lighter isotopes. Example: Evaporation removes preferentially lighter isotopes which more often exceed the energy to pass from liquid phase to gaseous phase.

These differences cause a shift in the ratio of different isotopes during chemical or physical reaction, which is defined as the **isotope fractionation**.
The **fractionation factor,** α describes the fractionation from state A to state B mathematically:

$$\alpha_{B/A} = \frac{R_B}{R_A} \tag{2.8}$$

where R is the isotope ratio

$$R = \frac{\text{abundance of rare isotopes}}{\text{abundance of abundant isotopes}} \tag{2.9}$$

Since isotope effects are small resulting in $\alpha \approx 1$, the fractionation is referred to as deviation of α from 1. The deviation is called fractionation (ϵ) and describes enrichment ($\epsilon > 0$) or depletion ($\epsilon < 0$).

$$\epsilon = \alpha_{B/A} - 1 = \frac{R_B}{R_A} - 1 \tag{2.10}$$

Fractionation can occur in principle under three different conditions:

- **equilibrium fractionation.** A and B are in a state of thermodynamical equilibrium. The reaction between A and B is fully reversible and the mass transport is identical in both directions. This happens in a closed system where no fraction is removed, while the reaction occurs. Example: water and water vapour in a closed volume.
- **kinetic fractionation.** The reaction from A to B is irreversible. The mass transport is permanent from A to B and immediately removed from the system. In a pure kinetic process no mass transport can occur from B to A.

- **disequilibrium fractionation.** The mass transfer between A and B occurs in both directions, however, with a dominant transport in one direction. A net mass transfer results from this process which can therefore, not be describes as a purely kinetic process. Example: evaporation of water in an open volume. Although evaporation prevails, a small fraction water vapour will condense before it is removed from the volume.

δ-notation Isotope ratios are commonly given not in absolute values, but relative to a reference ratio as a deviation, δ.

$$\delta = \frac{R_A}{R_{std}} - 1(10^3‰) \tag{2.11}$$

It should be noted that δ values are nearly additive when the isotopic fractionation is small (‰ range).

Standards in the calcite system The standard ratios R_{std} which are used in this work are the $^{18}O/^{16}O$ standard samples. For calcite this thesis refers to the Vienna PeeDee Belemnite and for the ratio measured in water the Vienna Standard Mean Ocean Water Mook and de Vriess [2000]. Absolute values are:

$$R_{VPDB} = 0.0020672 \tag{2.12}$$

$$R_{VSMOW} = 0.0020052 \tag{2.13}$$

2.4. Oxygen isotopes in the hydrological cycle

The main focus of this study lies upon the $\delta^{18}O_{calcite}$ value of speleothems. This section gives an introduction to the processes which influence the $\delta^{18}O$ value from ocean water to speleothem calcite. Many of these processes will be approached in the model section. Lachniet [2009] gave a profound and comprehensive analysis of this topic. This summary relies on his study.
Meteoric precipitation originates mainly from the ocean. Water evaporates from the surface experiencing an isotopic fractionation since the lighter ^{16}O is preferentially removed during this process. Hence, the formed air mass containing water vapour is isotopically lighter and the remaining ocean water is enriched. Therefore the $\delta^{18}O$ value of ocean water reveals a characteristical pattern with heavier values where evaporation rate is high (figure 2.2 a) adapted from Lachniet [2009]). The pattern is interfered by the input to the ocean by fresh water sources like ice or huge rivers (for example: Amazon river). The vapour parcel is transported in the atmosphere where clouds can form causing precipitation. The formation of liquid water in the cloud depends on temperature as well as the resulting isotopic fractionation. In contrast to evaporation, the formation of liquid water is an equilibrium process, as long as no rain-out occurs. If the cloud is cooled by a confronting air mass or by orographic lifting, the air mass is supersaturated with water leading to precipitation. Since the $\delta^{18}O$ value of the liquid phase in the air mass is higher than the vapour, the remaining air mass reveals a lighter isotopic composition with progressive rain-out. The isotopic composition of precipitation on the continent is therefore influenced by three parameters: i) temperature, ii) state of remaining fraction of water in the air parcel compared to the initial amount and iii) the isotopic composition of the moisture source. A geographical pattern of $\delta^{18}O_{prec}$ is given in figure 2.2 b). A trend towards lighter $\delta^{18}O_{prec}$ values can be observed with increasing latitude, increasing altitude and increasing distance from the ocean. These effects described Mook [2006] as the isotopic latitude-, altitude- and continental effect.
Three effects are not shown in figure 2.2 b), yet they have an important impact on $\delta^{18}O_{prec}$ - the source-effect, the amount-effect and the ice volume effect.
The source-effect accounts for changes in the source of moisture forming precipitation. A change in the synoptic pattern can change the geographical origin of precipitation (for detailed examples see section 2.5). Due to the different $\delta^{18}O$ values of the ocean, the precipitation at a cave location will show a significantly different $\delta^{18}O_{prec}$ value if the origin of moisture shifts [Denniston *et al.*, 1999].
The amount effect is closely connected to the rain-out process of a cloud. In strong downdrafts of precipitation initiated during thunderstorms an enormous amount of water precipitates in a short time. Due to the fractional removal of heavy isotopes by rain the remaining air mass depletes strongly (Dansgaard [1964], Lee and Fung [2007]). Until the cave location is not subject to the initial rain falling from the air mass, the precipitation at the cave is strongly depleted during thunderstorms.
The ice volume effect can be observed on times scales in which a glaciation or deglaciation occurs. During glacials the volume of ice on the continent increases due to precipitation accompanied with less melting. When meteoric precipitation is stored in continental ice, the ocean $\delta^{18}O$ value increases [Lachniet, 2009].
However, during the Holocene, the geographical $\delta^{18}O$ pattern is dominated by the three

effects named above (i.-iii.).
The temperature is the parameter whose correlation to $\delta^{18}O_{prec}$ can be measured best. Dansgaard [1964] was the first who published a spatial temperature gradient which was calculated from mean annual temperatures and the corresponding $\delta^{18}O_{prec}$ values. The derived value was 0.69‰/°C. In later studies values between 0.17 and 0.9‰/°C were found (Mook [2006], Rozanski *et al.* [1993], Schmidt *et al.* [2007]) However, this gradient is a spatial gradient. The rain-out effect occurring with increasing latitude amplifies the pure temperature gradient. The temporal temperature gradient measured at one location is about 0.3‰/°C for Central and Northern Europe [Fricke and O'Neil, 1999].
The next process in the hydrological cycle which is faced by meteoric precipitation is the fractional recycling of water due to direct evaporation from soil to the atmosphere or transpiration by plants - the evapotranspiration (section 2.2). During evaporation an isotopic enrichment occurs due to the preferential removal of lighter isotopes (Clark and Fritz [1997], Majoube [1971]). This is described in section 4.1.1.
The remaining water percolates through the soil to the epikarst layer and the host rock matrix. Due to chemical reactions which can be summarised as the carbonate system describes by Hendy [1971] the water dissolves calcite until saturation and enters finally the cave.
Simultaneous to the degassing of the drip water (stalagmite formation - section 2.1) calcite precipitates from the drip water solution. Both processes are accompanied by an isotopic fractionation. For calcite precipitation under equilibrium conditions many equations have been developed describing the fractionation between H_2O and $CaCO_3$ (Friedmann and O'Neil [1977], Kim and O'Neil [1997], O'Neil *et al.* [1969]). The derived temperature gradients are negatively correlated to temperature and the value is ≈-0.23‰/°C. If the fractionation occurs under disequilibrium conditions, more sophisticated models must be applied (Dreybrodt [2008], Mühlinghaus *et al.* [2009], Romanov *et al.* [2008], Scholz *et al.* [2009]). This topic is further discussed in section 4.1.1.

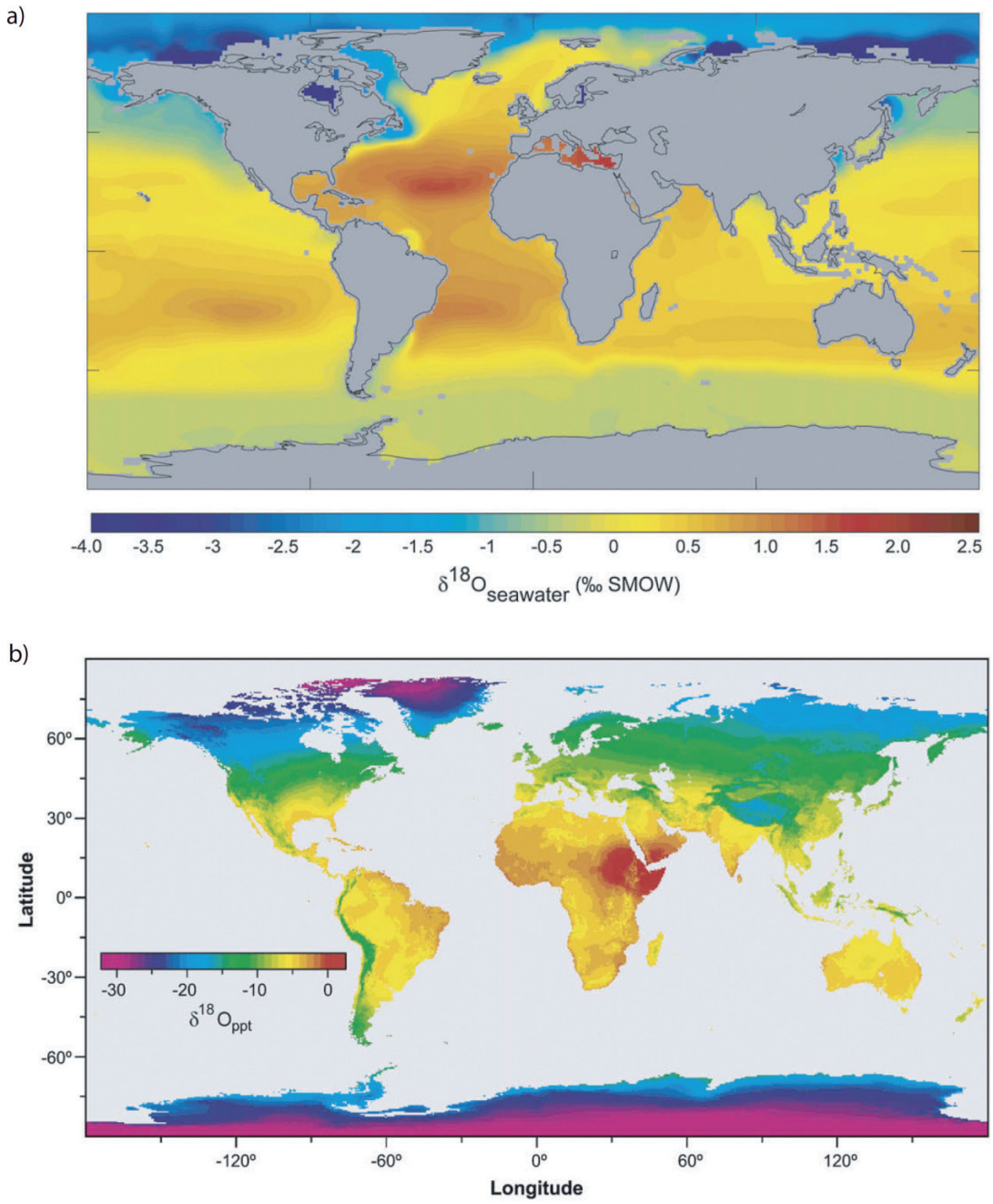

Figure 2.2.: Spatial δ^{18}O distribution in the surface ocean (a) and spatial distribution of $\delta^{18}O_{prec}$ (b). Figures extracted from Lachniet [2009]

2.5. $\delta^{18}O_{calcite}$ as climate proxy

The use of $\delta^{18}O_{calcite}$ is established as a valuable proxy for the climate of past times since several decades [Hendy and Wilson, 1968]. Regarding the hydrological cycle during which the $\delta^{18}O$ value faces many processes, it is obvious that $\delta^{18}O$ is sensitive to parameters characterising the climate of a region. Temperature, precipitation, moisture source and pathway, shift in storm tracks or synoptic pattern as well as effects due to the ice volume variation during deglaciation reflect in the isotope signal of speleothem records on different time scales.
The references given here are restricted to few representative examples. A more comprehensive overview was given by McDermott [2004] or Fairchild *et al.* [2006].

On long timescales (ten- to hundred thousand years) stalagmite records were used to identify changes between glacial periods and warmer phases where significant changes in the $\delta^{18}O$ value of the ocean occurred. Winograd *et al.* [1992] compared ice core data to the $\delta^{18}O_{calcite}$ record of stalagmites from Devil's Hole, USA, and derived a correlation between the stalagmite record and ice volume through the varying $\delta^{18}O$ value of ocean water with growing glaciers (see 2.4)[3]. In this context Cheng *et al.* [2009], Henderson and Slowey [2000] and Linge *et al.* [2001] can be referred to who also showed evidence that the $\delta^{18}O$ records of stalagmites are sensitive to deglaciation and ice age termination. Spötl and Mangini [2002] revealed a correlation with Daansgaard-Oeschger Events similar to the work by Wang *et al.* [2001] and Genty *et al.* [2003]. In addition Cruz *et al.* [2005] pointed out that large scale variation of $\delta^{18}O_{calcite}$ records can be connected to insolation changes which influence the atmospheric circulation.
These massive changes of climate reflect very clearly upon the $\delta^{18}O$ signal of stalagmites. The changes in the $\delta^{18}O$ signal of the ocean and the heavy drop or rise of annual temperature prevail all the other effects which cause smaller impact on the $\delta^{18}O_{calcite}$ signal. These variations dominate on shorter timescales where the climate modes does not change, e.g. the Holocene.

On shorter timescales different parameters rule the $\delta^{18}O_{calcite}$ value of speleothems depending on the specific location of a cave. While Lauritzen and Lundberg [1999] (Norway) or Mangini *et al.* [2005] (Austria) correlated the $\delta^{18}O_{calcite}$ value to surface temperature, at other locations a shift of the moisture source turned out to dominate the $\delta^{18}O$ variations (Denniston *et al.* [1999] (USA), Partin *et al.* [2007] (Borneo)). Also the pathway of precipitation in combination with atmospheric circulation modes was proven to be an important factor for $\delta^{18}O_{calcite}$ variability (Fensterer [2011] (Cuba), Vollweiler *et al.* [2006] (Austria)) Stalagmites from other caves, where the regional climate is highly sensitive to amount and seasonality of precipitation (monsoon area), revealed a prevailing influence of this parameter and proved that the $\delta^{18}O_{calcite}$ value is also a valuable proxy for amount of precipitation (Burns *et al.* [2001] (Oman), Neff *et al.* [2001] (Oman)). The influence of the vapour source was emphasised by Bar-Matthews *et al.* [1999]) for an Israelean cave.

[3] Due to the existence of a correlation stalagmites can also help to refine the chronology of other climate archive - in this case ice core data.

The named studies used different approaches to assess the correlation between $\delta^{18}O_{calcite}$ and the dominant parameter. One option is to compare $\delta^{18}O_{calcite}$ values with other climate archive which are better understood to identify relationships between climate and $\delta^{18}O_{calcite}$ (see above).
A more recent approach was enabled with increasing resolution of the $\delta^{18}O$ records due to an improved measuring technique. Small samples size can supply $\delta^{18}O$ time series in annual to subannual resolution. Such a time series offers the possibility of a tight calibration between observational climate data and $\delta^{18}O_{calcite}$ of speleothems, which can be used analyse the parameter influences [Jex *et al.*, 2010]. With these insights models for the $\delta^{18}O_{calcite}$ value can be designed (Baker and Bradley [2010], Bradley *et al.* [2010], Wackerbarth *et al.* [2010]).

2.6. Mg/Ca as climate proxy

The Mg/Ca ratio of speleothem calcite has over the last decade been established as a valuable proxy for palaeo precipitation or water supply. In contrast to the $\delta^{18}O_{calcite}$ value the Mg/Ca ratio is not directly linked to atmospheric processes and therefore to climate. The Mg/Ca value in speleothems does not originate from sea salt but is inherited from the host rock signature [Fairchild and Treble, 2009]. Nevertheless the Mg/Ca ratio has been proven to respond to wetter or drier conditions and can be regarded as a proxy for effective rainfall [Fairchild and Treble, 2009] due to processes which control the Mg/Ca ratio and are linked to the infiltration.
McDonald and Drysdale [2004] showed an anti-correlation of a 2.5 year record between the high resolution Mg/Ca record of a speleothem and the water supply in Wombeyan Cave, Australia. In another Australian Cave (Moondyne Cave) Treble *et al.* [2003] identified the same anticorrelation for a record covering the 20th century. McMillan *et al.* [2005] stated that these correlations on a shorter timescale are also valid for longer time scales. Cruz *et al.* [2007] published a important example which proves this relationship for a Brazilian stalagmite which has grown from 120ka to present day. In this study the Mg/Ca clearly correlates with $\delta^{18}O_{calcite}$ which is a proxy for the strength of the summer monsoon in this region.
The major reasons for the correlation to rainfall are i) the correlation between Prior Calcite Precipitation, PCP, and ii) the characteristics of calcite precipitation at the stalagmite [Fairchild and Treble, 2009].

PCP and the correlation to infiltration Many studies show that the Mg/Ca ratio of drip water or stalagmites is driven by the extent of PCP (Baldini *et al.* [2006], Fairchild *et al.* [2006], Karmann *et al.* [2007], McDonald and Drysdale [2004], Tooth and Fairchild [2003]). Johnson *et al.* [2006] presented a correlation between the strength of the monsoon and the extent of PCP.
PCP describes calcite precipitation which occurs in the host rock matrix or at the cave ceiling. When calcite precipitates from a solution, Mg^{2+} is incorporated as a trace element. The Mg/Ca ratio of the resulting calcite is much lower than the ratio of the solution due to the very low partition coefficient (0.019) [Morse and Bender, 1990]. This results in a preferential removal of Ca^{2+} ions during calcite precipitation. The Mg^{2+} enriches in the remaining solution. The partition coefficient is also temperature dependent, but the gradient is too small ($0.0006°C^{-1}$ [Huang and Fairchild, 2001]) to explain the variations in stalagmite records.
PCP in the karst matric can occur, when air filled gaps exist, which is the case, if infiltration is low. Therefore the Mg/Ca of the drip water solution increases during dry conditions due to a higher extent of PCP. This is in detail described in chapter 5.
The cave ceiling also offers the conditions for calcite to precipitate from the solution, which can bias the Mg/Ca of the stalagmite strongly, if the stalagmite of interest is fed from a large calcite drapery. The effect can be reduced by using stalagmites which are fed by a soda straw stalactite in which the solution enters the cave through a channel inside and is exposed to the cave atmosphere not until the drop forms at the tip of the stalactite.

Calcite precipitation at the stalagmite The second reason why infiltration is related to the Mg/Ca ratio of stalagmites is due to the general relationship of a higher drip rate during wetter conditions. The mechanism of calcite precipitation at the stalagmite surface is identical to PCP. The calcite of the speleothem shows a lower Mg/Ca ratio than the solution. However, due to proceeding calcite precipitation the solution enriches successively, which leads to an increase of the Mg/Ca ratio in the instantaneously precipitating calcite (since the partition coefficient is constant but the initial Mg/Ca increases). This process is stopped by the fresh impinging drop. If the drip interval is short (high infiltration), the solution at the top of the stalagmite is less enriched regarding Mg/Ca than in dry conditions, when the solution lies for a longer time interval undisturbed at the top of the stalagmite. This process is explained thoroughly in section 5.

Both effects lead to the correlation between Mg/Ca and hydrological changes [Fairchild and Treble, 2009]. The basic idea of this correlation is illustrated in figure 2.3. An extensive discussion of the topic is given in section 5.

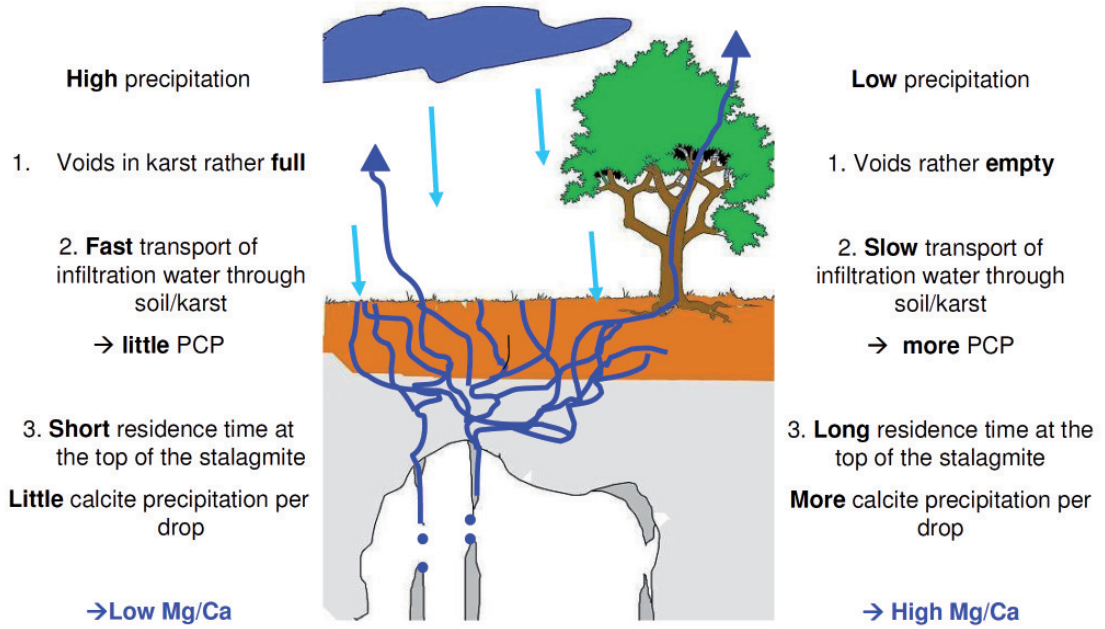

Figure 2.3.: Principle of the anti-correlation between Mg/Ca ratio of a stalagmite and the amount of infiltration/precipitation

2.7. European winter climate - the regime of the North Atlantic Oscillation

The North Atlantic Oscillation, NAO, is a meteorological phenomenon, that rules the European winter climate.
The NAO originates from the pressure gradient in the atmosphere above the North Atlantic caused by the Azores High and Icelandic Low. The gradient shows pronounced values during winter month, while during summer the gradient is lower due to a weakening and splitted Icelandic Low [Hurrell, 1995].
The absolute value of the gradient is not constant in time, but oscillates with varying frequencies between 6-10 years [Hurrell and van Loon, 1997] due to interference of the internal variability of the atmosphere and the oscillation of sea surface temperatures Rodwell *et al.* [1999].
The NAO index describes the pressure gradient of the normalised sea level pressure values at two different location. First, the index was defined by Hurrell [1995] between Lisbon (Portugal) and Stykkismholmur (Iceland). More often used is the index established by Jones *et al.* [1997] which is defined by the difference of normalised pressure values of Gibraltar and south-west Iceland for the month from November to March (see figure 2.4).

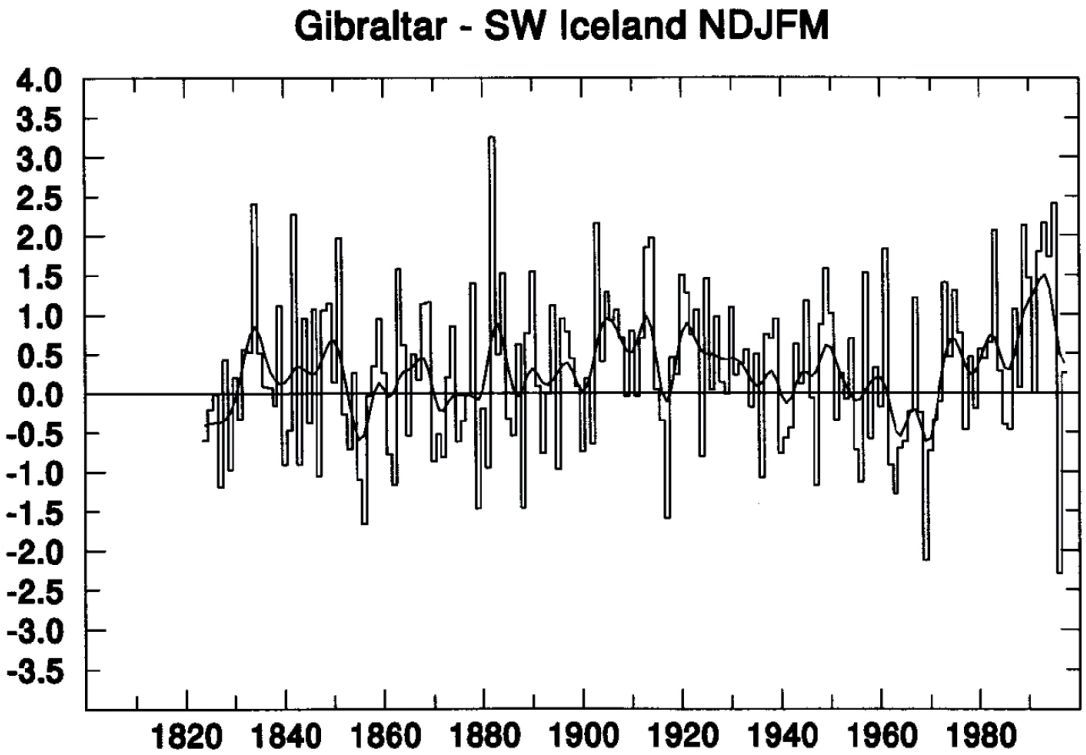

Figure 2.4.: Index of the North Atlantic Oscillation as determined by Jones *et al.* [1997] for winter month (NDJFM) from observational data

The NAO index can be reconstructed back to 1820, which is the start of observational

data for the relevant locations. However, by the use of different, appropriate proxies [Luterbacher *et al.*, 2002] published a reconstruction back to 1500 A.D.. Even further reaches the reconstruction of Trouet *et al.* [2009] who derived the index from two significant studies from Northern Scotland and Morocco for the last thousand years. The proxies which were used cannot be regarded as archives for atmospheric pressure, but record the climate variation which result from the oscillating pressure gradient.
The impact on winter climate generated by the NAO index is explained by different authors (Hurrell [1995], Wanner [2001] see also figure 2.5) as follows.
The NAO mode is divided into a positive (NAO+) and a negative anomaly situation (NAO-). When the pressure gradient is strong (NAO+), the westerlies from the Atlantic to European continent strengthen and follow a north-east trajectory covering Mid and Northern Europe. In the Mediterranean area winter precipitation is reduced accompanied with higher temperatures resulting from air masses from the south, which can spread in this situation. For the northern and mid part of Europe the Atlantic air masses lead to rather wet but warm winter conditions.
In the opposite situation (NAO-) the pressure gradient is less pronounced and the westerlies shift to an eastern trajectory moving across Mediterranean Europe. Winter climate in this area experience humid conditions and slightly decreased temperatures. The air masses from the north (high Norwegian See) are not repelled by the southern storm tracks and spread cold and dry air across Mid- and Northern Europe.
Trigo *et al.* [2002] and Baldini *et al.* [2008] approached these general relationships by calculating correlation coefficients between NAO index, precipitation, temperature and δ^{18}O of precipitation. The results show strong correlations to temperature and $\delta^{18}O_{prec}$, but significantly lower correlations to precipitation. The reason for this is that the correlation coefficients are calculated from GNIP [IAEA/WMO, 2006] station values which can only supply spatially discrete climate information. Temperature is spatially more stable parameter than precipitation which is influenced by all kind of geographical conditions. A detailed discussion of the work of Baldini *et al.* [2008] is given in section 7.3.4.

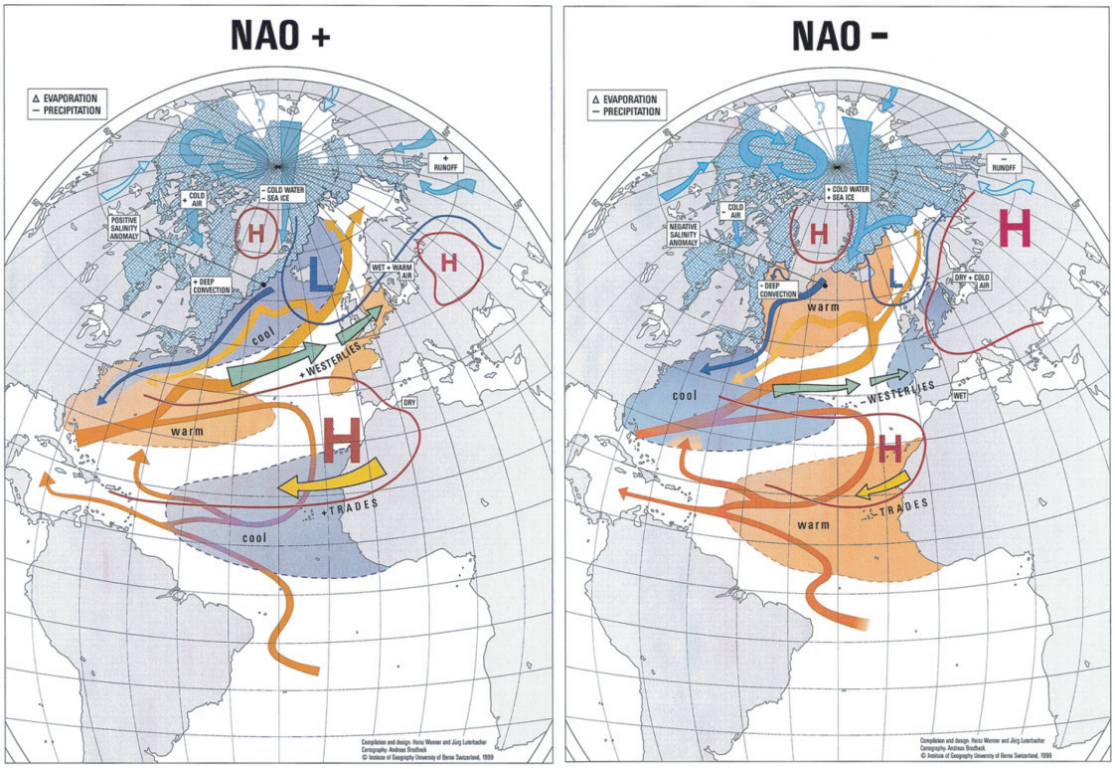

Figure 2.5.: Positive (NAO+) and negative (NAO-) mode of the North Atlantic Oscillation and the impact on European climate extracted from Wanner [2001]

3. Model preface

The following three chapters present the models which were developed during this work. The first two chapters discuss the forward models, while the third chapter introduces two approaches to inverse the models.

Forward modelling in this context means, that a model is designed that uses climate signals as input parameters and simulates the processes occurring from surface via soil and karst matrix to calcite precipitation at the stalagmite to derive the resulting $\delta^{18}O_{calcite}$ value (chapter 4) and the Mg/Ca ratio (chapter 5) of speleothem calcite.

Inverse modelling aims for reconstructing palaeo climate conditions from proxy data. This work presents two approaches to interpret the $\delta^{18}O_{calcite}$ signal in this context. One approach is based only on the $\delta^{18}O_{calcite}$ value, while the other relies on both, $\delta^{18}O_{calcite}$ and Mg/Ca ratio. Since the reconstruction is performed for stalagmite BU4 from Bunker Cave the respective values are illustrated in figure 3.1.

The models have been implemented and compiled using the program MATLAB 6.5 (The MathWorks, Inc., Natick, MA, USA).

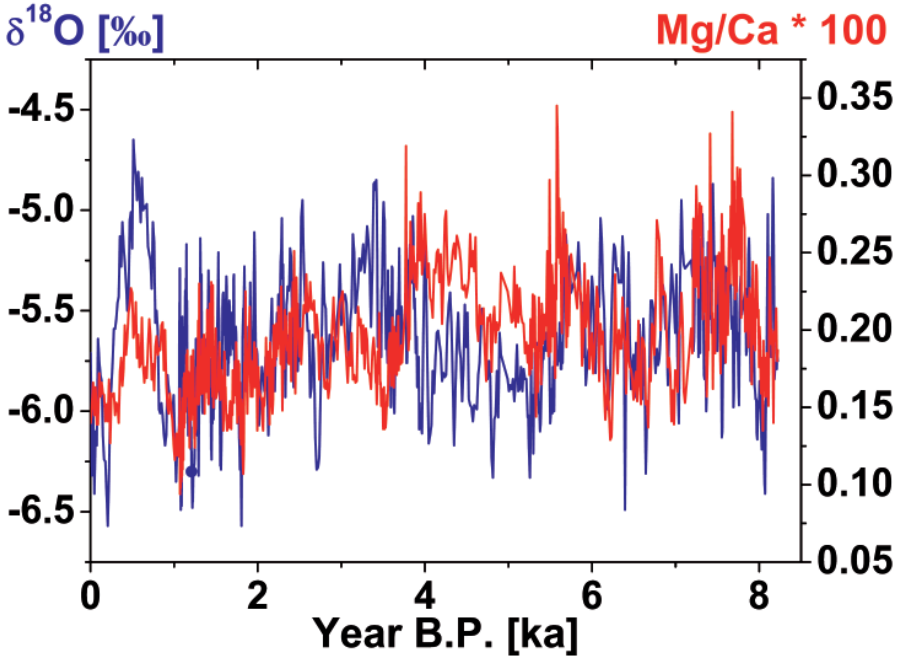

Figure 3.1.: The Mg/Ca and $\delta^{18}O_{calcite}$ record from stalagmite BU4 from Bunker Cave in western Germany [Riechelmann, 2010]

4. δ^{18}O model

In the following chapter the key issue of this work is presented - the model describing the modification and evolution of δ^{18}O from rain water to speleothem calcite.
First, the forward model is introduced and described, which is applied to Bunker Cave in western Germany. This is followed by a discussion about the model's sensitivity with respect to several input parameters. In section 6.2 an application of the model - the model reversion in the context of climate reconstruction - is shown.

4.1. The forward model

This chapter describes the structure, setup and included equations of the developed **O**xygen isotope **D**rip water and **S**talagmite **M**odel - ODSM. As an overview the concept of the model is given in figure 4.1 illustrating the segments which are modelled by the ODSM. In the following they are described in detail.

Overview Cave drip water inherits the δ^{18}O signature from meteoric precipitation above the cave modified in the soil-karst system before it enters the cave and feeds the stalagmite. As shown in figure 4.1, the parameters influencing the δ^{18}O signal can in principle be separated into four groups: atmosphere, bio- and pedosphere, karst system and cave environment.
Atmospheric parameters (e.g. surface temperature and amount of precipitation) and related processes (e.g. moisture source, pathway from source to cave, seasonality of meteoric precipitation) influence the δ^{18}O value of meteoric precipitation (e.g., Lachniet [2009], McDermott [2004], Mook [2006]).
In biosphere, pedosphere and karst system the signal is influenced by processes like evapotranspiration, mixing of water of different ages and calcite dissolution, which depends on different parameters like temperature, properties of the soil and karst layer, the pCO_2 of soil air as well as type and seasonal state of vegetation.
The conditions at the cave described by parameters such as cave temperature, drip interval and supersaturation of the drip water solution with respect to calcite determine the amplitude of the isotopic fractionation between the $\delta^{18}O_{drip}$ and $\delta^{18}O_{calcite}$ (e.g., Dreybrodt [2008], Mühlinghaus *et al.* [2009], O'Neil *et al.* [1969], Scholz *et al.* [2009]).

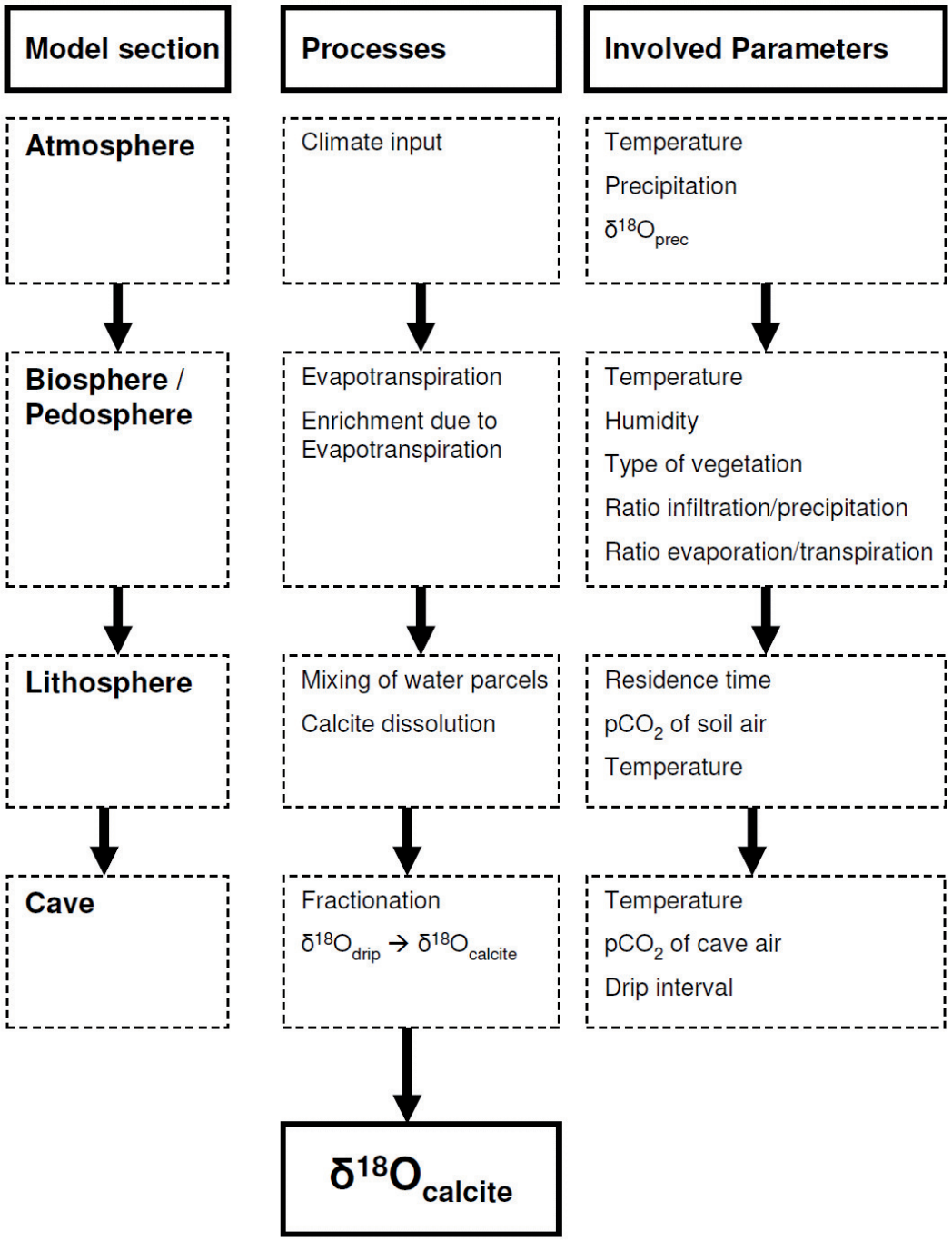

Figure 4.1.: The scheme of the ODSM shows the different model sections, the processes occurring in these sections and the involved parameters in the processes.

4.1.1. Model description

The OSDM describes the modification of δ^{18}O during the processes named above and was developed to understand how and to which extent the input parameters affect the $\delta^{18}O_{calcite}$.
To model the annual mean δ^{18}O value of cave drip water and the resulting $\delta^{18}O_{calcite}$ value two factors must be determined: i) the δ^{18}O value of monthly water parcels calculated according to the processes named above and described in detail below and ii) the weight of these water parcels which is defined as the contribution of a water parcel to the annual amount of drip water.

4.1.1.1. Weighting function for drip water

The ODSM establishes a weighting function and calculates the resulting isotopic composition of the drip water (equation 4.1). The resulting mean $\delta^{18}O_{drip}$ value is the mean value of n month (if the annual mean is modelled n=12).

$$\delta^{18}O_{drip} = \sum_{i=1}^{n} G_i(P, ET_{pot}) \cdot \delta^{18}O_{soil_i}(T) \tag{4.1}$$

Determination of Infiltration. The weighting function depends on the amount of precipitation, **P**, and the amount of evapotranspiration, $\mathbf{ET_{pot}}$. The difference of these parameters determines the amount of infiltration, **Inf**.

$$G_i(P, ET_{pot}) = \frac{Inf_i}{\sum_{i=1}^{n} Inf_i} \tag{4.2}$$

For the evapotranspiration several equations have been developed (Haude [1954], Haude [1955], Penman [1948], Thornthwaite and Mather [1957]). As discussed in section 2.2, if not stated differently, the equation used from Haude [1954] is applied. Therefore, the weighting coefficient depends also on temperature, humidity and the type and state of vegetation.

Determination of $\delta^{18}\mathbf{O_{soil}}$. The $\delta^{18}\mathbf{O_{soil}}$ is defined as the isotopic composition of a monthly precipitation parcel after the process of evapotranspiration which enriches the remaining water in heavy isotopes [Mook, 2006]. This enrichment is described as a Rayleigh process with one reservoir (monthly precipitation parcel) and two sinks (evaporation and transpiration) (equation 4.3).

$$\delta^{18}O_{soil} = \left(\left(1 + \frac{\delta^{18}O_{prec}(T)}{1000} \right) \cdot \left(\frac{N_{remain}}{N_{prec}} \right)^{\epsilon_e \cdot f_e + \epsilon_t \cdot f_t} - 1 \right) \cdot 1000 \tag{4.3}$$

in which $\delta^{18}O_{prec}$ is the initial δ^{18}O value of meteoric precipitation, before evapotranspiration occurs. Evapotranspiration can be separated into physical evaporation and the uptake of water by plants - transpiration. $\mathbf{f}_e$ is the fraction of water which is lost through evaporation and $\mathbf{f}_t$ the fraction of water lost due to transpiration. $f_e + f_t$ is defined as 1. While the process of transpiration is not accompanied by isotopic fractionation [Mook,

2006], the evaporation from a water body leads to isotopic enrichment. The enrichment was described by Majoube [1971]:

$$\epsilon_e = (-7356/T + 15.38)‰ \tag{4.4}$$

The Rayleigh fractionation depends on temperature and on the ratio of infiltration to precipitation. As the influence of the temperature on the enrichment is rather small (+2.7‰ over the temperature range from 0°C and 30°C - see figure 4.2), the ratio of infiltration to precipitation is the driving factor of the enrichment as illustrated in figure 4.2.

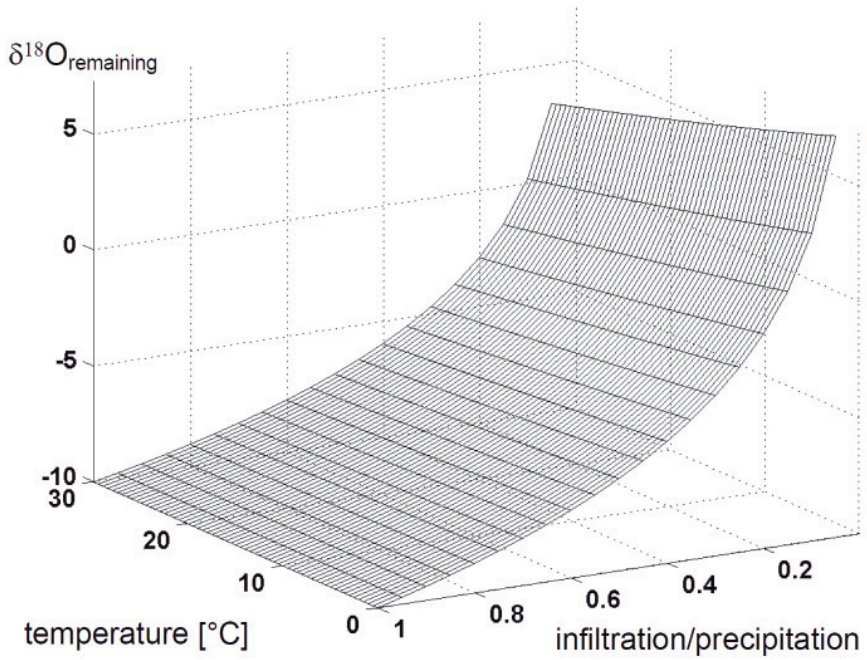

Figure 4.2.: Enrichment of $\delta^{18}O$ in an evaporating water parcel depending on temperature (influencing the fractionation factor) and on the ratio of infiltration to precipitation. The figure is based on equation 4.3. f_e is in this figure defined as 0.5.

The model calculates the $\delta^{18}O_{soil}$ for the individual months and calculates the weighted mean $\delta^{18}O$ value according to equation 4.1. The value represents the $\delta^{18}O$ value of the drip water feeding the stalagmite, which is used in the next step.

4.1.1.2. Fractionation from $\delta^{18}O_{drip}$ to $\delta^{18}O_{calcite}$

The isotopic fractionation between $\delta^{18}O_{drip}$ and $\delta^{18}O_{calcite}$ results from the degassing of CO_2 and simultaneous precipitation of calcite from the drip water solution. The process is driven by the gradient between the pCO_2 of cave air and the drip water solution, that have been in equilibrium with the higher soil air pCO_2, when it enters the cave. Degassing enriches the solution due to the preferential removal of lighter oxygen isotopes, while calcite precipitation removes statistically more heavy isotopes. If calcite

precipitation occurs under equilibrium conditions, the resulting fractionation depends only on temperature. In the ODSM the equation by Friedmann and O'Neil [1977] is used (equation 4.5).

$$1000 \cdot ln\alpha = \frac{2.78 \cdot 10^6}{T^2} - 2.89 \tag{4.5}$$

in which α can be expressed in the δ-notation with equation 2.11

$$\alpha = \frac{R_{CaCO_3}}{R_{H_2O}} = \frac{\delta^{18}O_{CaCO_3} + 1000}{\delta^{18}O_{H_2O} + 1000} \cdot \frac{R_{VPDB}}{R_{SMOW}} \tag{4.6}$$

This results in equation 4.7 for the fractionation between drip water and calcite in the δ-notation:

$$\delta^{18}O_{calcite}(\delta^{18}O_{drip}, T) = \frac{\delta^{18}O_{drip} + 1000}{1.03086} \cdot exp(2780/T^2 - 2.89/1000) - 1000 \tag{4.7}$$

In most applications (in the ODSM as well as for the Mg/Ca model (section 5) and for the model inversions (chapter 6)) equilibrium fractionation does not describe natural conditions realistically. Therefore kinetic fractionation must be included in the ODSM. The module describing disequilibrium fractionation is adopted from Mühlinghaus *et al.* [2009]. For this type of fractionation more parameters are required.

- The pCO_2 of the cave and soil air must be known, since their difference controls the degassing of CO_2 and precipitation of calcite. Calcite precipitation takes place until the solution is in equilibrium with the pCO_2 of cave air (stalagmite growth - see section 2.1).

- The drip interval is the third, important parameter. The $\delta^{18}O$ value of the drip water solution on top of the stalagmite degasses continuously accompanied by calcite precipitation. The $\delta^{18}O$ value of the solution as well as of the instantaneously precipitating calcite enriches successively. However, due to hydration and hydroxylation oxygen isotopes exchange between calcite and the large H_2O reservoir. This so-called buffering finally inhibits the enrichment of $\delta^{18}O_{calcite}$ and leads to depletion. If the buffering is fully developed, the $\delta^{18}O$ value of the calcite is the same as it would be under equilibrium conditions. The drip interval determines the time in which the solution on top of the stalagmite can evolve freely and subsequently the extent of the buffering effect.

- The parameter ϕ must be determined. These parameters describes the mixing between the solution layer on the stalagmite surface and the new drop. It can range between 0 and 1. If only 10% of the impinging drop remain at the place where the drop hits the stalagmite (center of growth) while the rest is lost by splashing to outer areas of the stalagmite, ϕ has the value 0.1. If the new drop replaces the solution layer at the growth axis completely pushing the existing solution to outer areas of the stalagmite surface, ϕ is defined as 1.

4.1.1.3. Weighting function for calcite

. For the $\delta^{18}O_{calcite}$ it is not only important how much water infiltrates to deeper soil layers but also how much Ca^{2+} precipitates at the stalagmite top from the drip water parcel. If water without the possibility to precipitate $CaCO_3$ feeds the stalagmite, the $\delta^{18}O_{drip}$ value cannot contribute to the isotopic composition of the stalagmite. For the $\delta^{18}O_{calcite}$ the weighting function must be extended involving Ca^{2+} ions.

Determination of Ca^{2+} content of the drip water solution. The Ca^{2+} content of the drip water solution arriving at the cave ceiling depends on three driving factors:

- The CO_2 of soil air dissolves in precipitation and forms acid which dissolves calcite from the host rock (see section 2.1). The pCO_2 of soil air determines how much calcite can be dissolved.
- The temperature of soil and karst influences the chemical reactions involved in calcite dissolution.
- The residence time of water parcels in the soil and karst layer determines how much influence the additional weighting coefficient, Ca^{2+}, has (see below).
- The pCO_2 of cave air drives the degassing and precipitation from the drip water solution at the stalagmite because it is generally lower than the pCO_2 in equilibrium with the CO_2 dissolved in drip water. The bigger the gradient between the two CO_2 contents is, the more calcite precipitates from the solution.

These parameters are included in the calcite dissolution model by Hendy [1971] (routine written by Jens Fohlmeister [Fohlmeister *et al.*, 2011]) which calculates the concentrations of the different species involved in the carbonate system (i.e., H^+, CO_2 (aq), OH^-, ${CO_3}^{2-}$, HCO_3^- and Ca^{2+}) in dependence of soil air pCO_2 (g) and temperature. This module determines how much calcite is dissolved under the given temperature and pCO_2 conditions for open system dissolution. This determines the Ca^{2+} concentration of the drip water entering the cave.
Calcite precipitation is forced by the gradient between the dissolved inorganic CO_2 of the drip water in equilibrium with soil air pCO_2 and cave air pCO_2. Due to low pCO_2 values of the cave air environment compared to the drip water solution, the solution is highly supersaturated as it enters the cave. CO_2 degasses until the solution reaches a certain saturation index. Here, the saturation index (SI: from here on) is kept constant at 0.5 (Lebrón and Suárez [1998], Nielsen and Toft [1984]). The gradient finally determines how much calcite precipitate from a water parcel. The factor $\mathbf{Ca^{2+}}$ comprises this parameter as a coefficient in equation 4.8.
In the model Prior Calcite Precipitation is not included, i.e. calcite precipitates only at the stalagmite.

$$\delta^{18}O_{drip} = \sum_i G_i(P, ET_{pot}, Ca^{2+}) \cdot \delta^{18}O_{soil_i}(T) \tag{4.8}$$

However, the importance of this additional weighting depends strongly on the residence time of the water parcels in the soil and karst. In most cave systems the residence

time is long (one or more years) leading to extensive mixing in the upper soil layers [Riechelmann *et al.* [b], in review]. If the water parcels stay for months or longer in the layers in which the uptake of CO_2 in the solution occurs, the pCO_2 of the solution can be assumed as the mean pCO_2 value of the soil air over this time. The particular month of precipitation is therefore less important. The same holds for the temperature. Hence, for long residence times the drip water bears more or less a similar Ca^{2+} content throughout the year.
Under these conditions (constant Ca^{2+} content AND constant $\delta^{18}O_{drip}$ value due to extensive mixing) it is not important to know in which month calcite precipitation occurs preferentially. The $pCO_{2\ cave}$ can be defined as constant.
In case of a short residence time the annual pattern of $pCO_{2\ soil}$ and $pCO_{2\ cave}$ cannot be regarded as constant. If no (or less) mixing of the water occurs in soil and karst, which can occur in a fissured flow situation, the drip water in the cave reveals neither a constant Ca^{2+} content nor a constant $\delta^{18}O_{drip}$ value.
Under these conditions it is important to know from which water parcel the amount of Ca^{2+} ions precipitates. Hence, both the $pCO_{2\ soil}$ and $pCO_{2\ cave}$ must be included in the weighting function.

4.2. Application and evaluation of ODSM

In general a model can only be validated by comparison to measured data. In the case of the ODSM the input data for the model are

- surface parameters
  - temperature
  - precipitation
  - evapotranspiration (or humidity and temperature at 2 p.m. Haude [1955])
- measured data
  - pCO_2 of soil and cave air
  - cave temperature
  - drip interval
  - residence time in soil and karst

These data should be supplied in a monthly resolution. It is not enough to know annual mean temperature or the annual amount of precipitation, since seasonality is one of the most important features of regional climate (season of precipitation results in pronounced weighting of this season for the $\delta^{18}O_{drip}$ value). The parameters which must be simulated correctly for a validation by the ODSM are

- mean annual $\delta^{18}O_{drip}$ value
- $\delta^{18}O_{calcite}$ value of modern precipitates

Although the input data must be provided in a monthly resolution, a comparison between simulated and measured monthly $\delta^{18}O_{drip}$ and $\delta^{18}O_{calcite}$ values is not aimed for. The ODSM can be regarded as successfully validated, if it is able to simulate the measured mean annual $\delta^{18}O_{drip}$ and $\delta^{18}O_{calcite}$ correctly. In the context of palaeo climate analyses mean values are the important feature of stalagmite records, since they represent the climate conditions of the past instead of short scale variations. In addition growth rates are commonly low yielding proxy information in a temporal resolution from years to decades. Only very rarely stalagmite can supply annual or subannual resolution [Jex *et al.*, 2010].
It should be noted, that the best assessment of the validity of the model can be achieved by comparing model results and the measured values from the same time period. However, the measurement values ($\delta^{18}O_{drip}$ and $\delta^{18}O_{calcite}$) are only available for a rather short period depending on the respective cave monitoring period. Five years are generally a long time for a monitoring program. However, it is not advisable to use the input data from atmosphere and cave for the model from the same period for two reasons: i) the cave system reacts slowly and delayed to surface climate variations and ii) although five years of cave monitoring provide a sound database, five years of surface climate observation can accidently not represent the long term climate means. For a comparison it is important to use good representatives of the long term climate mean as input values.

4.2.1. Application to Bunker Cave

This work is funded by the DAPHNE Forschergruppe which focus mainly on Bunker Cave in Sauerland, Germany. Five years of cave monitoring [Riechelmann *et al.* [a], in press] supply a reliable set of observed parameters which allow a sound testing of the ODSM at this location.

Parameters to determine the monthly infiltration
For Bunker Cave the input weather parameters are supplied by the German Weather Service (Deutscher Wetterdienst - DWD, www.dwd.de) from the nearby station Hagen Fley. The data set includes monthly temperature, monthly amount of precipitation, monthly values for the humidity and temperature at 2 p.m. from 1988 to 2007. These parameters are required to determine the monthly amount of infiltration, P-ET_{pot}. The calculation of evapotranspiration by Haude [1954] requires besides temperature and humidity the type of vegetation. According to the vegetation found today above the cave (observations from Riechelmann *et al.* [a] [in press] and Bundesamt für Naturschutz (the German Federal Agency for Nature Conservation, www.bfn.de), the type of vegetation is defined as a representative composition of beech and spruce. The values of the vegetation coefficient used in the calculations are taken from Häckel [1999] (see table 4.1).

Parameters to determine the $\delta^{18}O_{soil}$
For the same period as the climate data the GNIP station from Bad Salzuflen supplies $\delta^{18}O_{prec}$ in monthly resolution, which is the initial $\delta^{18}O$ value in the ODSM. During evapotranspiration the $\delta^{18}O$ value enriches. Therefore the ratio of evaporation to transpiration (see section 4.1) is required according to equation 4.3. Unfortunately this value is hard to evaluate due to a lack of studies on this topic. By default the ratio could be defined as 1. However, the study of Tang and Feng [2001] on twig water suggests that during summer, the fraction of transpiration, f_t, to the total amount of evapotranspiration is bigger than the fraction of evaporation, f_e. They show that trees use mainly water from soil layers near the surface from spring and summer. Although the temperature is high in summer intensifying physical evaporation in theory, a large part of the water is absorbed by plants during their growing season [Tang and Feng, 2001]. In addition, after strong precipitation events humidity tends to be high reducing the factor of direct evaporation from soil. The third reason that evaporation does not prevail during summer is that the canopy of the trees shields the soil from direct solar insolation reducing direct evaporation. Therefore f_e (fraction of evaporation to the total amount of evapotranspiration - equation 4.3) is defined as 0.5 for winter months (October–March) and 0.2 for summer months (April–September).

Determination of mixing characteristics
As the next step, the residence time of the precipitation water in the soil and karst must be determined to evaluate if the ODSM should be applied with the additional weighting coefficient for the calcite (see section 4.1.1).
The study by Kluge *et al.* [2010] with tritium tracers suggested a residence time of 2-3 years for the drip site above BU4. This stalagmite is selected, because it was recently growing and supplied therefore a sample of modern calcite.

The assumption from Kluge *et al.* [2010] is confirmed by the monitoring of the monthly Ca^{2+} content of the drip water which reveals no seasonal pattern but a rather constant level for the drip site suggesting an extensive mixing of the water in soil and karst. Accordingly, the ODSM is applied in the setup for long residence times.

Parameters to determine the fractionation between $\delta^{18}O_{drip}$ and $\delta^{18}O_{calcite}$
For the calculation of the kinetic fractionation the relevant data can be retrieved from the monitoring program. The mean pCO_2 values for soil and cave air are given in table 4.1. The drip interval of the drip site TS8 showed an average value of about 3600s. For the modelling the new drop is assumed to replace the solution at the center box on top of the stalagmite completely (which in the model is represented by the mixing coefficient ϕ=1).

4.2.2. Model results

With this set of input the ODSM yields the following results:

- $\delta^{18}O$ =-7.8‰ (precipitation weighted mean $\delta^{18}O_{prec}$)
- $\delta^{18}O$ =-8.5‰ (infiltration weighted mean $\delta^{18}O_{prec}$)
- $\delta^{18}O$ =-7.9‰ (mean $\delta^{18}O_{drip}$)
- $\delta^{18}O$ =-6.6‰ (mean $\delta^{18}O_{calcite}$ - equilibrium fractionation)
- $\delta^{18}O$ =-5.8‰ (mean $\delta^{18}O_{calcite}$ - kinetic fractionation)

The infiltration is higher in winter than in summer due to higher evapotranspiration rates under warm conditions. The $\delta^{18}O_{drip}$ signal is by this process biased towards isotopically lighter winter $\delta^{18}O_{prec}$ values. The enrichment during evaporation causes the $\delta^{18}O$ signal to increase compared to the $\delta^{18}O$ value of meteoric water. The $\delta^{18}O_{drip}$ is nearly on the same level as the precipitation weighted mean $\delta^{18}O$ value. The measured $\delta^{18}O_{drip}$ value and the modern $\delta^{18}O_{calcite}$ sample from BU4 are

- $\delta^{18}O$ =-7.9‰(mean $\delta^{18}O_{drip}$ - May 2006 to July 2009)
- $\delta^{18}O$ =-5.7‰(mean $\delta^{18}O_{calcite}$ - recent sample from BU4)

The simulated drip water $\delta^{18}O$ agrees well with the observed value. The $\delta^{18}O_{calcite}$ shows that the calcite sample has not grown under equilibrium conditions but reveals a kinetic offset of about 0.8‰.
The ODSM seems to be a good representative of the cave system at Bunker Cave.

Error estimation A classical error estimation of the simulated values cannot be applied to the model. The equations in the model do not cause a statistical error (which could occur due to errors of parameters included in the equations). The parameters which are afflicted with uncertainties are the input parameters (climate and isotope parameters), which in principle bear a measurement uncertainty. However, these are not given by the DWD (www.dwd.de).
The more interesting feature of the model is the sensitivity of the model to the input parameter. A sensitivity test is performed in the following section.

4.3. Sensitivity of the ODSM

4.3.1. Preparatory model adjustments

In the context of climate research it is important to know how the model results change, if temperature and the amount of precipitation change. The sensitivity of the model results to these parameters is the main focus of this section.
In addition the sensitivity to different calculation of the evapotranspiration, short and long residence times, the effect of varying parameters in the kinetic fractionation are evaluated.
For these experiments standard years for precipitation and temperature are defined (table 4.1) using the mean monthly values of the weather service data from Hagen Fley (Deutscher Wetterdienst- www.dwd.de) from 1988-2007. This allows to calculate the difference between the $\delta^{18}O_{calcite}$ results for the current valid mean parameters and parameter deviations.
In order to investigate the temperature- and precipitation sensitivity, the numbers of input parameters must be reduced. In this context some parameter are kept constant (see table 4.1). These are

- ratio evaporation/transpiration
- vegetation coefficient (used for the calculation of the evapotranspiration)
- pCO_2 of soil and cave air

Month	Temperature [°C]	Precipitation [mm/month]	CO_2 soil air [ppm]	CO_2 cave air [ppm]	veg. coeff.
1	3	77.5	3293	600	0.05
2	3.5	57.6	2547	650	0.02
3	6.1	72.8	3644	700	0.09
4	9.3	67.3	4725	750	0.23
5	13.7	72.3	5195	800	0.31
6	16.7	87.6	4944	850	0.31
7	18.4	90.6	5154	900	0.32
8	18.0	77.2	4867	900	0.26
9	15.1	66.7	4370	800	0.19
10	11.4	62.2	4430	700	0.12
11	6.8	78.4	4393	650	0.04
12	4.1	90.4	3212	600	0.03

Table 4.1.: Standard months used as input for the ODSM sensitivity experiment. Sensitivity is investigated as deviation from these standard values. Temperature and precipitation are mean monthly values from Hagen Fley (DWD), pCO_2 of cave air and soil air are derived as average monthly values from the monitoring program (Riechelmann [2010], Riechelmann *et al.* [a] [in press]) and the vegetation coefficient is taken from Häckel [1999].

Other parameter should not be set to fix values, since a close relationship to temperature exists, and must be included in the model for a realistic sensitivity experiment. These are:

- humidity of surface air at 2 p.m.
- surface temperature at 2 p.m.
- $\delta^{18}O_{prec}$ value

These parameters can be linked to surface mean monthly temperature using a linear fit of the respective data from meteorologic data sets (for humidity, $F_{2p.m.}$, and temperature, $T_{2p.m.}$, at 2 p.m. the weather data from Hagen Fley, for $\delta^{18}O_{prec}$ the data from the monitoring program).

$$F_{2p.m.}(T) = 76.72(\pm 1.07) - 1.21(\pm 0.07) \cdot T \text{ (where } R^2 = 0.56) \tag{4.9}$$

$$T_{2p.m.}(T) = 1.77(\pm 0.12) + 1.13(\pm 0.01) \cdot T \text{ (where } R^2 = 0.98) \tag{4.10}$$

$$\delta^{18}O_{prec}(T) = -9.53(\pm 0.47) + 0.18(\pm 0.04) \cdot T \text{ (where } R^2 = 0.47) \tag{4.11}$$

Since the monitoring period is rather short for a robust and reliable correlation, the values of the linear regression between $\delta^{18}O_{prec}$ and temperature must be compared to long term values from the surrounding GNIP stations before the regression from Bunker Cave monitoring is applied. The results are shown in table 4.2. Since the slope observed at Bunker cave agrees within the errors with the surrounding GNIP stations, the monitoring period seems to be sufficient to establish a robust relation. Therefore equation 4.11 is used in the following to link the $\delta^{18}O_{prec}$ value to temperature.
The values of the linear regression seem rather small in comparison to the often-cited 0.69‰/°C [Dansgaard, 1964] or the global values that range between +0.17 to +0.9‰/°C (Dansgaard [1964], Mook [2006], Rozanski *et al.* [1993], Schmidt *et al.* [2007]). However, these values are spatial temperature gradients from linear regressions between annual temperature and $\delta^{18}O_{prec}$ values. For the ODSM a temporal temperature gradient should be used as determined above. The temporal gradients are known to be smaller than spatial gradients for locations from all over the world [Fricke and O'Neil, 1999]. Schmidt *et al.* [2007] determined the temporal temperature gradient to be 0.3‰/°C for central and northern Europe.
Using equations 4.9, 4.10 and 4.11 the weighting function which determines the mean annual drip water $\delta^{18}O$ value (equation 4.1) depends only on precipitation and temperature and the influence of these parameters on the $\delta^{18}O$ signal can be assessed.

4.3.2. Results of the sensitivity experiment

In figure 4.3 the influence on $\delta^{18}O_{drip}$ and $\delta^{18}O_{calcite}$ can be observed. It should be noted that the respective temperature and precipitation variations correspond to annual mean

GNIP station	y-axis intercept [‰]	Slope [‰/°C]	R^2	p-value	mean $\delta^{18}O_{prec}$ [‰]
Bad Salzuflen (51.2°N, 8.73°E)	-9.61±0.27	0.19±0.02	0.25	<0.0001	-7.8
Emmerich (51.83°N, 6.6°E)	-8.80±0.24	0.16±0.02	0.22	<0.0001	-7.14
Braunschweig (52.3°N,10.45°E)	-8.83±0.25	0.17±0.02	0.23	<0.0001	-7.23
Koblenz (53.35°N, 7.58°E)	-10.09±0.29	0.27±0.02	0.42	<0.0001	-6.91
Mean (51.38°N,7.52°E)	-9.34±0.27	0.20±0.01	0.28	<0.0001	-7.35
Bunker Cave (51.2°N, 8.73°E)	-9.53±0.47	0.18±0.04	0.47	<0.0001	-7.84

Table 4.2.: Relationship between the $\delta^{18}O_{prec}$ and temperature at four GNIP stations and at the Bunker Cave.

values as well as monthly mean values. For example: 1°C warmer annual temperature results from 1°C warmer, individual months. 10% less annual precipitation also means 10% less precipitation in each month. The seasonal pattern is not changed. The sensitivity is given as $\Delta\delta^{18}O$ values. This refers for each figure to the respective present day value.

For the $\delta^{18}O_{drip}$ value in figure 4.3 a clear, positive temperature dependence can be observed which originates from the relationship between temperature and $\delta^{18}O_{prec}$ (equation 4.11).
The influence of the amount of precipitation is less dominant than temperature.
For low temperatures there is little variation in the $\delta^{18}O_{drip}$ signal with the precipitation change. Only for very dry conditions the $\delta^{18}O_{drip}$ depletes. This is caused by the dominance of winter precipitation, which has still a significant contribution under dry conditions while summer infiltration (and warmer spring and autumn months) are reduced to zero.
For warmer conditions (e.g. 5°C) a wavy pattern can be observed which see-saws between enrichment and depletion with a decrease of precipitation. A decrease of precipitation diminishes on the one hand the infiltration/precipitation ratio (leading to heavier $\delta^{18}O$ values) but adds more and more weight to colder (isotopically lighter) seasons on the other hand. Under warm conditions this behaviour is more pronounced than in colder conditions due to higher evaporation values.

The $\delta^{18}O_{calcite}$ value inherits this wavy pattern. However, the basic sensitivity features are different. Note, that the axes are differently displayed than for $\delta^{18}O_{drip}$.
In general the temperature sensitivity is lower (one third) than the $\delta^{18}O_{drip}$ sensitivity and with an inverted gradient. $\delta^{18}O_{calcite}$ enriches with decreasing temperature due to the isotopic fractionation (equation 4.7) between drip water and calcite which counter-

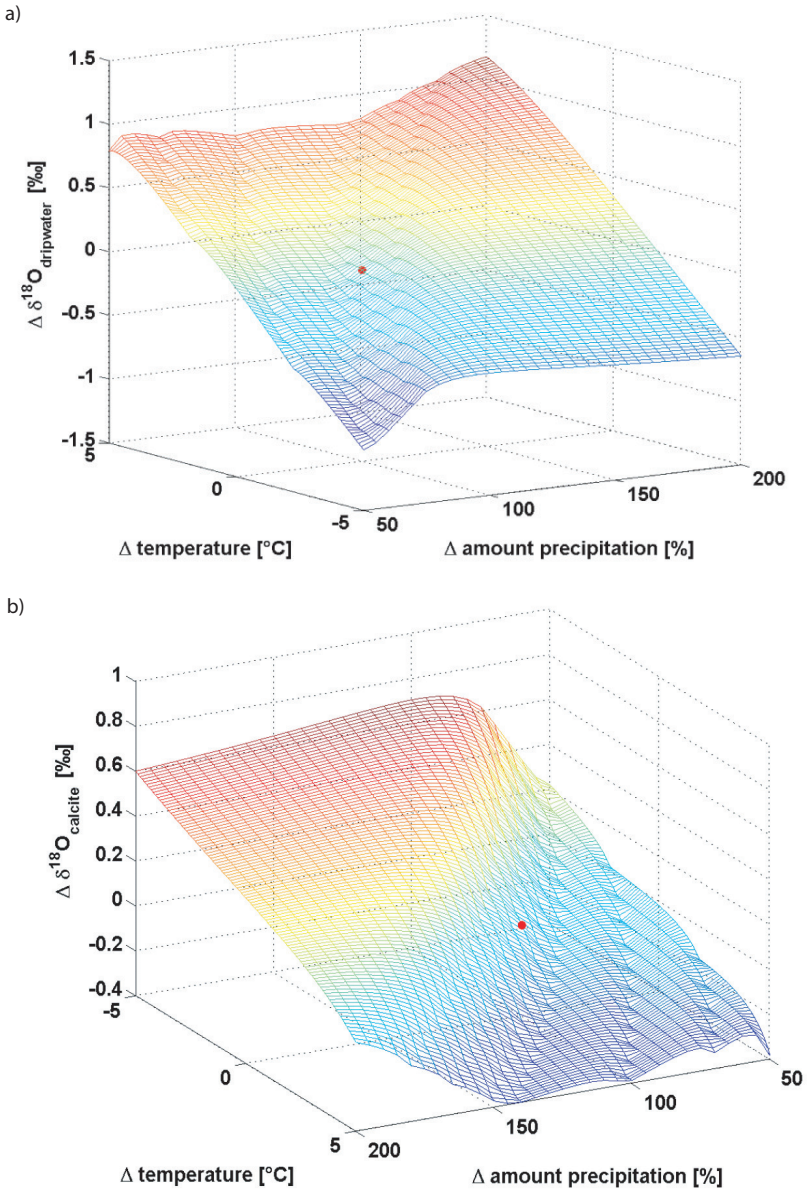

Figure 4.3.: Sensitivity of δ^{18}O on temperature and precipitation variations plotted as $\Delta\delta^{18}O_{drip}$ (a) and $\Delta\delta^{18}O_{calcite}$ (b) (deviation from the respective present day values). Temperature deviation is given in °C from the present day annual mean temperature T=10.5°C, precipitation in % from the present day amount (100%). The red dot represents the present day conditions.

acts the temperature dependence of $\delta^{18}O_{prec}$ and prevails.
For low temperatures there is a soft increase of $\delta^{18}O_{calcite}$ with an decrease of precipitation identically to the $\delta^{18}O_{drip}$ evolution. For warmer temperatures the $\delta^{18}O_{calcite}$ see-saws between depletion and enrichment like the $\delta^{18}O_{drip}$.

It is obvious that both the $\delta^{18}O_{drip}$ and $\delta^{18}O_{calcite}$ signal are highly sensitive to the ratio of infiltration to precipitation.

4.3.2.1. Influence of different ET_{pot} calculation

As discussed in section 2.2 the equation for the calculation of evapotranspiration by Haude [1954] (equation 2.4) is the preferred choice for the ODSM. However, in many cases the required input parameters (type of vegetation, humidity and temperature at 2 p.m.) are not available at the cave. For these cases the equation by Thornthwaite and Mather [1957] can be applied (equation 2.6).
In general the evapotranspiration by Thornthwaite and Mather [1957] results in higher evapotranspiration rates than calculated by Haude [1954] (figure 4.4). This leads to lower infiltration rates throughout the year enriching the soil water isotopically more than calculated by Haude's equation. For the present day, climatic conditions the equation by Thornthwaite and Mather [1957] yields 0.7‰ heavier $\delta^{18}O_{drip}$ and $\delta^{18}O_{calcite}$ values. This difference cannot be regarded as an offset as the sensitivity of the $\delta^{18}O$ values is also different between the setups. The differences of the sensitivities of $\delta^{18}O_{drip}$ and $\delta^{18}O_{calcite}$ to temperature and precipitation variations are shown in figure 4.5.

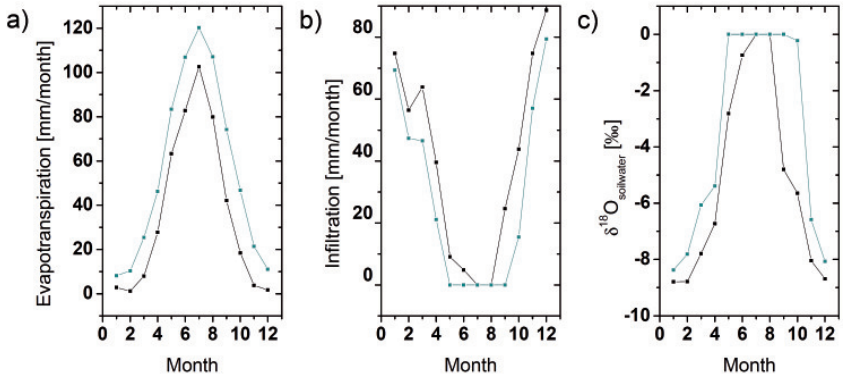

Figure 4.4.: Comparison of the amount of evapotranspiration (a), infiltration (b) and the $\delta^{18}O$ value of soil water enriched due to evapotranspiration calculated by Haude [1954] (black) and Thornthwaite and Mather [1957] (cyan)

For both setups the temperature sensitivity is higher than the precipitation sensitivity. The drip water $\delta^{18}O$ value is in the setup using Thornthwaite and Mather [1957] (red layer) even more sensitive to temperature than in the Haude setup. Both setups inherit the temperature gradient from the relationship between $\delta^{18}O_{prec}$ and temperature. In the Thornthwaite & Mather setup this gradient is amplified by the stronger, additional enrichment occurring during evapotranspiration with increasing temperatures. This effect is more pronounced, when precipitation is low.
For these low precipitation rates the pronounced positive temperature gradient is strong enough to dominate the negative temperature gradient of the fractionation between drip water and calcite [Friedmann and O'Neil, 1977]. In contrast to the Haude setup, the

resulting temperature gradient of $\delta^{18}O_{calcite}$ is positive ($\delta^{18}O_{calcite}$ in figure 4.5). For wetter conditions the temperature slope has nearly the same magnitude as the temperature gradient in the fractionation. Hence, the $\delta^{18}O_{calcite}$ is nearly constant over the whole temperature range.
To conclude, the temperature sensitivity is higher in the Thornthwaite and Mather [1957] setup and in general the equation by Thornthwaite and Mather [1957] leads to heavier $\delta^{18}O_{drip}$ and $\delta^{18}O_{calcite}$.

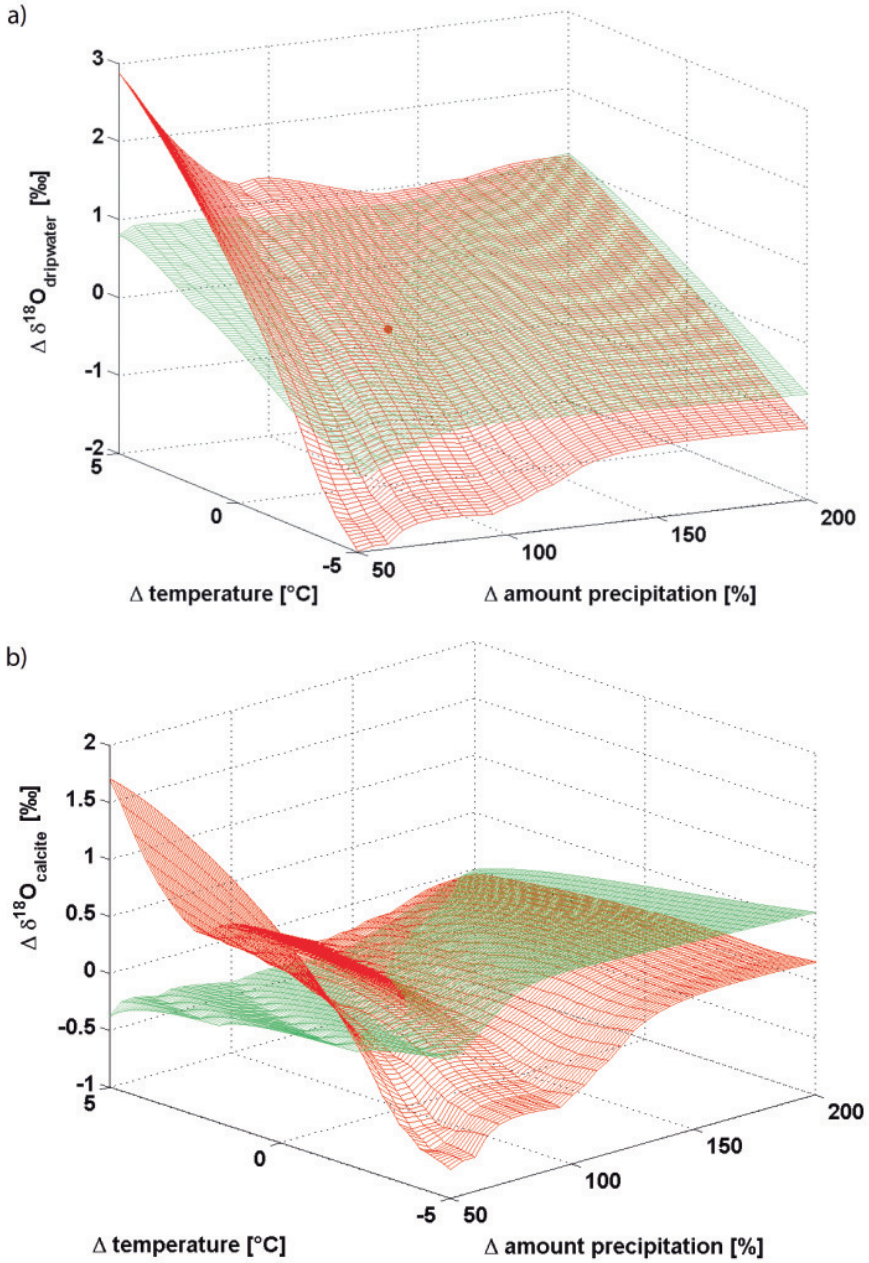

Figure 4.5.: Sensitivity of δ^{18}O on temperature and precipitation variations plotted as $\Delta\delta^{18}O_{drip}$ (a) and $\Delta\delta^{18}O_{calcite}$ (b) (deviation from the respective present day values). Temperature deviation is given in °C from the present day annual mean temperature T=10.5°C, precipitation in % from the present day amount (100%). The red dot represents the present day condition. Red Layer: Thornthwaite calculation. Green Layer: Haude calculation

4.3.2.2. Influence of short and long residence time

The residence time might differ from drip site to drip site in one cave depending on the flow situation[1]. It is useful to understand the influence of this parameter on the δ^{18}O values. As discussed before, the residence time changes the weighting function, when the amount of Ca^{2+} ions which precipitate from monthly water parcels is included. If a short residence time is assumed, monthly rainfall water dissolves calcite under the pCO_2 conditions of the respective month. For the same soil pCO_2 less calcite is dissolved at higher temperatures than at lower temperatures. Thus, calcite dissolution should be more effective during winter months [Riechelmann, 2010]. However, higher temperatures promote higher soil pCO_2 values, which counteract the above mentioned effect. For Bunker Cave the difference between winter and summer pCO_2 of soil air (about 1600ppmv) is too small to compensate for the temperature effect. In addition, the gradient between the pCO_2 of soil and cave air is higher during winter months, resulting in more calcite precipitation. This is reflected in the weighting coefficient which assigns even more weight to the winter season. However, the difference is small. For short residence times the ODSM yields a $\delta^{18}O_{calcite}$ value which is 0.1‰ lighter than under the assumption of a long residence time.
For caves revealing more pronounced seasonal variations in soil and cave air pCO_2, this difference might be higher.
The sensitivity is not illustrated graphically, because it is the same for both setups.

4.3.2.3. Influence of kinetic fractionation

The sensitivity experiment for kinetic fractionation has an additional problem - the drip interval (in the following $\mathbf{dT_i}$) of the stalactite is bound to change depending on the amount of infiltration (Cobb *et al.* [2007], Hu *et al.* [2008], Zhou *et al.* [2005]). For this purpose a correlation must be established between drip rate and the amount of infiltration. This correlation is extremely difficult to derive from data of the monitoring program, since short term variations of soil conditions and flow characteristics influence the drip rate. For long term climate variations the influence of precipitation on the drip rate should prevail. Such a correlation cannot be derived from five years of monitoring. In the lack of knowledge, the equation 4.12 is used. This equation assumes the simplest, possible relationship between precipitation and drip interval as illustrated in figure 4.6 and discussed in the following.

$$dT_i(INF_i) = (dT_{max} - dT_{min}) * exp(INF_i \cdot C) + dT_{min} \tag{4.12}$$

where C forces the function to include the pair of values for the present day situation

$$C = \left[log \frac{dT_{std} - dT_{min}}{dT_{max} - dT_{min}} \right] / INF_{std} \tag{4.13}$$

If climatic conditions become very dry, the drip interval increases. In figure 4.6 the maximum drip interval (dT_{max}=10000s) is approached when the annual infiltration is zero. When conditions become wetter the drip interval decreases and converges to the lower drip interval level (dT_{min}=500s). The minimum and maximum drip rates are chosen

[1] fissured or seepage flow

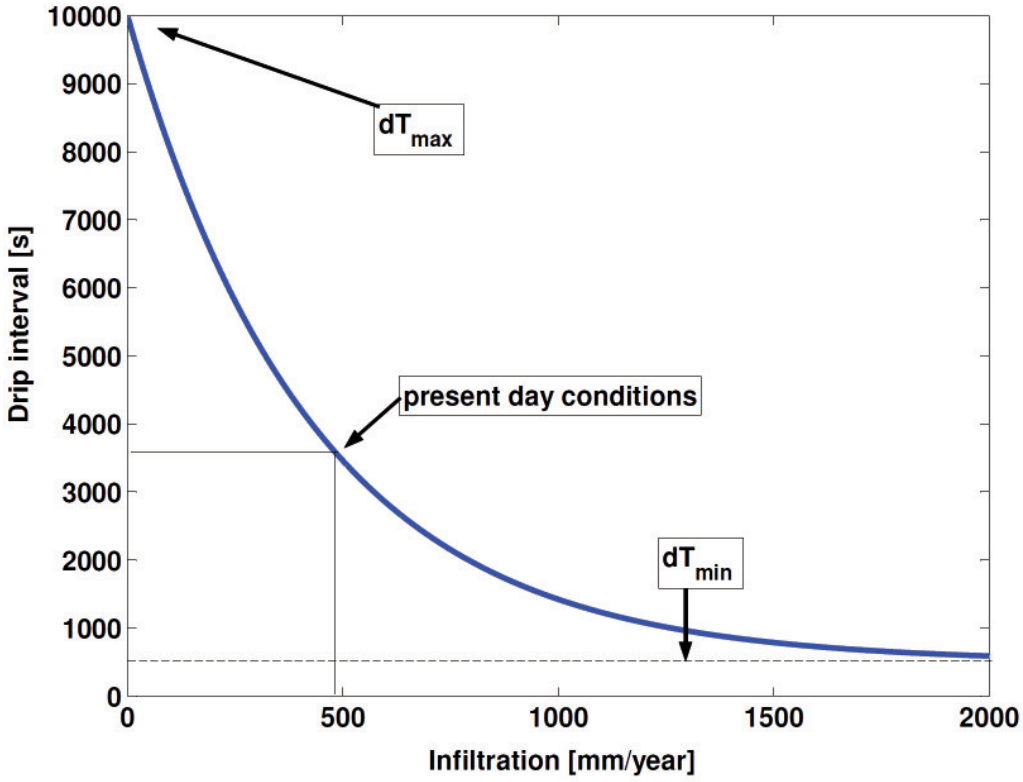

Figure 4.6.: Assumed relation between drip interval and the amount of infiltration

here to be suitable to drip site TS8 which is the drip site above stalagmite BU4 from Bunker cave. The drip site shows clear seepage flow characteristics with an extremely long average drip interval (dT_{std}=3600s) [Riechelmann *et al.* [a], in press]. If the climatic conditions provide much infiltration, this drip site tends to show a higher flow rate, but will unlikely turn into a fissured flow drip site. Hence, the drip interval will still be rather long. If the climate reaches a very dry level, the drip site will possible run dry totally resulting in a very long drip interval (dT_{max}). Stalagmite growth nearly ceases. The kinetic offset for present day conditions was shown in 4.2 (0.7‰ heavier than under equilibrium conditions). The sensitivity of $\delta^{18}O_{calcite}$ under kinetic fractionation compared to equilibrium conditions is presented in figure 4.7.

In general, the temperature gradient under disequilibrium conditions is inverse to the amplitude of isotopic fractionation [Mühlinghaus, 2008] resembling the gradient under equilibrium fractionation. The sensitivity of $\delta^{18}O_{calcite}$ to changes of precipitation is also inherited from the drip water variation. The drip interval is a factor which is influenced by temperature and precipitation and could in principle also influence the sensitivity of $\delta^{18}O_{calcite}$. However, for a wide range of deviations from the present day situation (red dot) both setups show a rather similar behaviour. Only for cold and wet conditions the sensitivity behaviour is different. The influence of the drip interval on $\delta^{18}O_{calcite}$ was proven to be not linear and smaller for lower drip rates. Therefore the influence of the

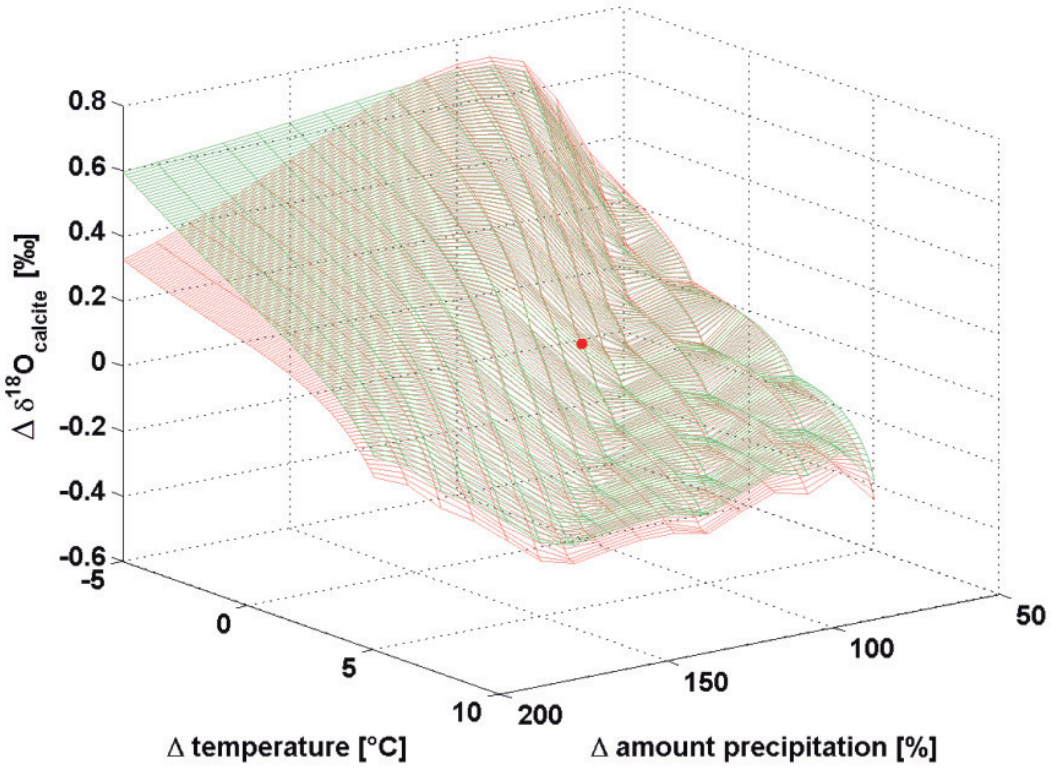

Figure 4.7.: Sensitivity of δ^{18}O on temperature and precipitation variations plotted as $\Delta\delta^{18}O_{calcite}$ (deviation from present day value). Temperature deviation is given in °C from the present day annual mean temperature T=10.5°C, precipitation in % from the present day amount (100%). The red dot represents the present day conditions. Red Layer: Kinetic fractionation calculation. Green Layer: Equilibrium calculation

drip interval becomes relevant in wet conditions (high precipitation, low temperatures). Note, that figure 4.7 shows only the different sensitivity behaviour. The offset of 0.7‰ between kinetic and equilibrium fractionation causes the $\delta^{18}O_{calcite}$ signal to be heavier under kinetic conditions in general.

Influence of relationship between drip interval and infiltration The correlation between drip interval and infiltration is a critical point in the ODSM as it is just based on an assumption. Figure 4.8 shows the sensitivity results for different minimum and maximum drip intervals in equations 4.13 and 4.12. The larger the difference is between these boundary conditions, the higher is the sensitivity of $\delta^{18}O_{calcite}$. However, the principle gradients of temperature and precipitation are not changed.

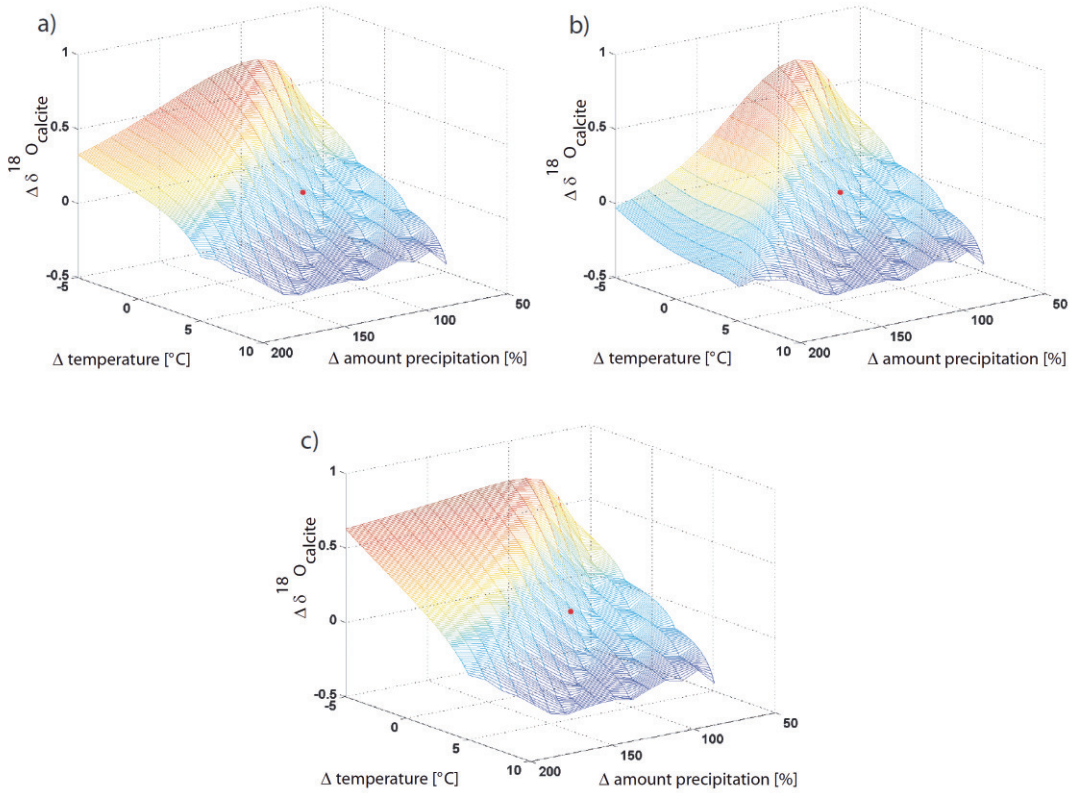

Figure 4.8.: Sensitivity of δ^{18}O on temperature and precipitation variations plotted as $\Delta\delta^{18}O_{calcite}$ (deviation from present day value). Temperature deviation is given in °C from the present day annual mean temperature T=10.5°C, precipitation in % from the present day amount (100%). The red dot represents the present day conditions. The figures represent the sensitivity for different boundary parameters in equation 4.13 and 4.12 a) dT_{min}=500s, dT_{max}=10000s, b) dT_{min}=100s, dT_{max}=20000s, c) constant drip interval dT=3600s

Influence of the mixing coefficient The mixing coefficient is a parameters describing the strength of kinetic fractionation. It ranges between 0 and 1 and describes which fraction of the impinging drop remains at the growth axis [Mühlinghaus, 2008]. If the parameter is 0.1, 10% of the drop contribute to the solution layer directly at the top of the stalagmite while 90% are splashed to outer parts of the stalagmite surface. This also indicates that 90% of the existing solution layer at the top of the stalagmite remain in this center box and 10% are pushed to outer boxes (compare [Mühlinghaus *et al.*, 2009]). The mixing parameter is poorly investigated in literature so far. However, the parameter is important, because the existing solution layer at the stalagmite has already changed its isotopic composition due to calcite precipitation and CO_2 degassing, when the fresh drop arrives. Since stalagmites grow extremely slowly and the mixing characteristics depend on the drop height, the mixing coefficient is assumed to be constant in time. In figure 4.9 the results for the $\delta^{18}O_{calcite}$ sensitivity for different mixing coefficients are shown.

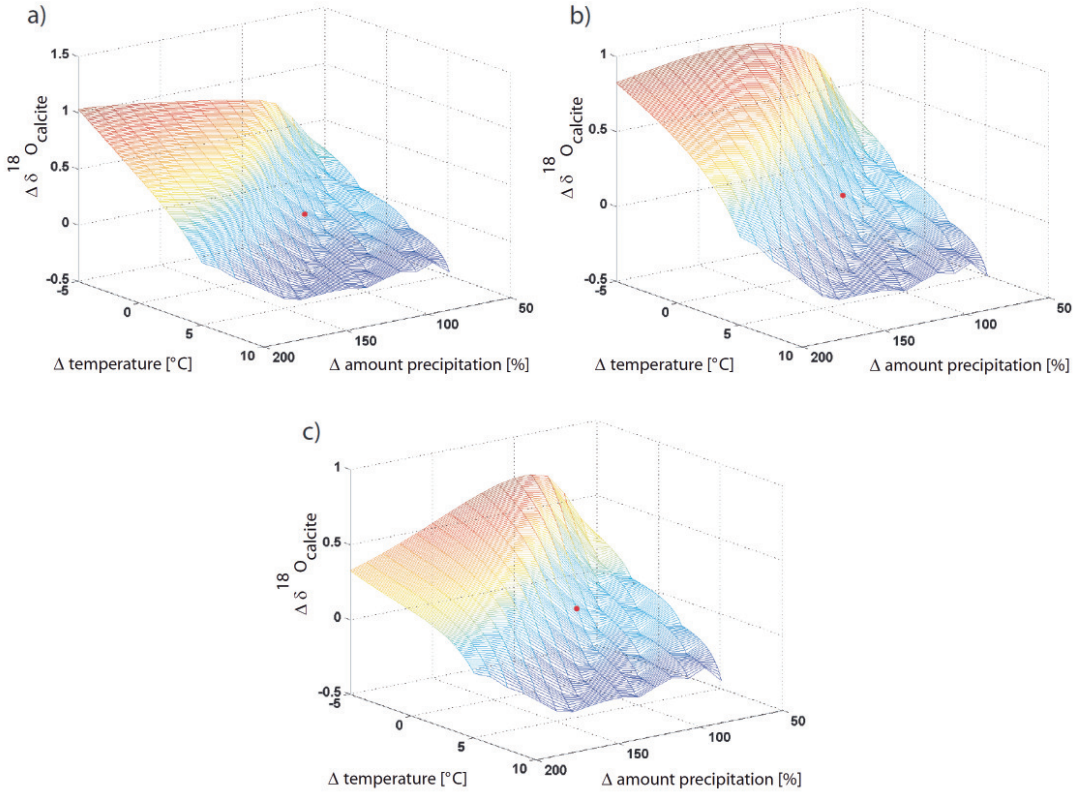

Figure 4.9.: Sensitivity of $\delta^{18}O$ on temperature and precipitation variations plotted as $\Delta\delta^{18}O_{calcite}$ (deviation from present day value) for different mixing coefficients. Temperature deviation is given in °C from the present day annual mean temperature T=10.5°C, precipitation in % from the present day amount (100%). The red dot represents the present day conditions. The figures represent the results for different mixing coefficients: a) ϕ=0.1, b) ϕ=0.5 and c) ϕ=1

To understand the pattern it is important to know how the $\delta^{18}O$ value of a solution from which calcite precipitates and CO_2 degasses evolves. On one hand the solution enriches, because CO_2 degasses leaving heavy isotopes in the solution. On the other hand precipitating calcite removes preferentially heavy isotopes. The latter fractionation factor is smaller than the fractionation during degassing. Therefore, the solution enriches successively as well as the calcite precipitating from the solution. Further effects (e.g. evaporation) can also alter the $\delta^{18}O$ signal of the solution layer. For detailed information see Deininger *et al.* [in review] or Mühlinghaus *et al.* [2009].
As time progresses, the time constant of the buffering (exchange of oxygen isotopes from the huge H_2O reservoir with the bicarbonate-ions due to hydration and hydroxylation) becomes relevant (Mühlinghaus *et al.* [2009], Scholz *et al.* [2009]). The buffering depletes the precipitating calcite. When the solution is fully buffered, the $\delta^{18}O_{calcite}$ value is identical to the oxygen isotopic composition from calcite precipitated under equilibrium conditions. For a low mixing coefficient, ϕ=0.1 (figure 4.9), the slope of the

$\delta^{18}O_{calcite}$ sensitivity is negative with increasing temperature and decreasing amount of precipitation. This indicates that the $\delta^{18}O_{calcite}$ is heavier when infiltration is high. When infiltration is low, the drip interval is long providing enough time for the solution layer to be buffered by hydration and hydroxylation (biasing the solution to lighter values) [Mühlinghaus, 2008]. In contrast, in shorter drip intervals the solution is not fully buffered and therefore enriched.
For a high mixing coefficient, ϕ=1, the pattern is the same as for low infiltration (low precipitation and high temperatures). Above a certain amount of infiltration the slope of the layer decreases again with lower temperatures and wetter conditions. The reason is that the solution does not have enough time to get enriched before the next drip arrives supplying fresh water.
The results for $\delta^{18}O_{calcite}$ differ also in their absolute values for present day conditions:

- ϕ=0.1 $\Rightarrow$ $\delta^{18}O_{calcite}$ =-6.4‰
- ϕ=0.5 $\Rightarrow$ $\delta^{18}O_{calcite}$ =-6.0‰
- ϕ=1 $\Rightarrow$ $\delta^{18}O_{calcite}$ =-5.8‰

The reason for the offset is again the buffering process. If the new drop replaces the existing solution layer, the temporal evolution starts with every drop from the beginning. If only 10% of the new drop mix with 90% of the old layer, the temporal evolution is slightly diminished but buffering is more important (leading to lighter isotopic conditions).
However, this is only the case for these long drip intervals observed at TS8. For short drip intervals the relation is the other way round.
Though the mixing coefficient influences the sensitivity strongly, it should be kept in mind that switching between the mixing characteristics on short term scales is not realistic.

4.3.2.4. Error estimation

As discussed in the previous section the sensitivity study itself replaces the classical error analysis. However, in order to perform the sensitivity experiment three linear regressions were used to relate the $\delta^{18}O_{prec}$ value, the humidity and the monthly 2 p.m. temperature to the mean monthly temperature. These regressions reveal correlation coefficients < 1. Therefore the error of the regressions should be used to evaluate the uncertainty of the ODSM.
For the error analysis the Monte-Carlo-Method is used performing the sensitivity experiment for $\delta^{18}O_{drip}$, $\delta^{18}O_{calcite}$ under equilibrium conditions and $\delta^{18}O_{calcite}$ under disequilibrium conditions 2000 times. The linear regression is arbitrary varied within the standard deviations of the respective fit characteristics (see section 4.3.1). In figure 4.10 the resulting mean $\delta^{18}O$ value is displayed (green layer), which is identical with the calculated $\delta^{18}O$ values above. The red and blue layers show the mean value matrix the calculated standard deviation in positive and negative direction for each value. The values of the standard deviation range from 0.48 to 0.7‰ for $\delta^{18}O_{drip}$ and the $\delta^{18}O_{calcite}$.

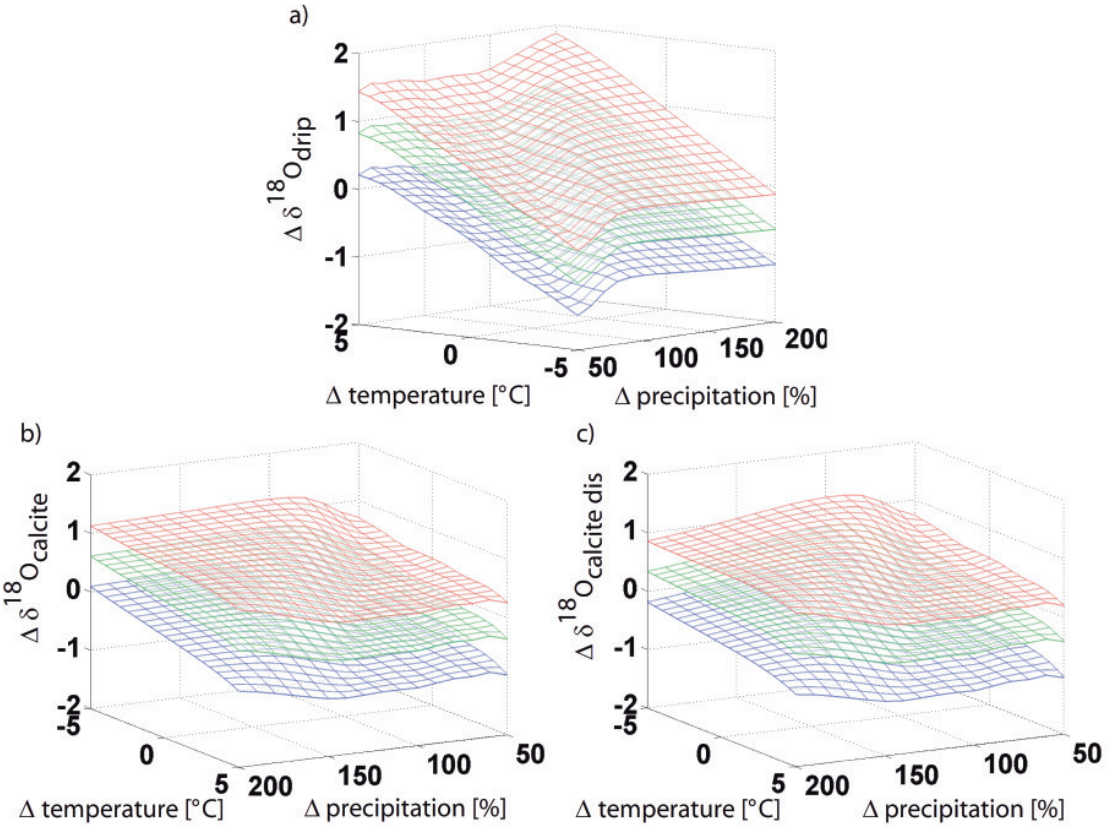

Figure 4.10.: Illustration of the standard deviation of the ODSM results ($\Delta\delta^{18}O_{drip}$, $\Delta\delta^{18}O_{calcite}$ and $\Delta\delta^{18}O_{calcite}$ under disequilibrium conditions). The green layer shows the mean value, the blue and red layers represent the corresponding standard deviation of each of the values from the green layer.

4.3.2.5. Sensitivity to different seasonality

The main assumption for the sensitivity experiment so far was that the parameters vary simultaneously and uniformly throughout the year. The seasonality was not touched. However, the European winter climate is known to be ruled by strong hydrologic patterns above the North Atlantic - called the North Atlantic Oscillation - and to show stronger variations than the other seasons (see section 2.7). Therefore, the observed variations in stalagmite records can also be caused by a changing seasonality.
To assess the influence of changing climatic winter conditions, the ODSM must be run in a different setup using the following assumptions:

- If climate (not short term weather conditions) lead to warmer winter conditions, it can be assumed that the other seasons will experience the same temperature trend though less pronounced. Analyses of data from the GHCN Network (Global Historical Climate Network [Vose *et al.*, 1998]) prove that temperature variations are larger in winter than in summer. However, precise values are hard to determine. The value is hence set to $\Delta T_{AMJJASO} = 0.5 \Delta T_{NDJFM}$. The temperature variation of April-October affects the $\delta^{18}O_{prec}$, the enrichment of soil water during evaporation, the amount of evapotranspiration and the cave temperature.

- A relationship between summer and winter precipitation can not be proven by GHCN. The amount of precipitation of the month from April to October is therefore set to the present day values. Thereby the influence of more or less contribution of winter precipitation can be assessed.

In figure 4.11 b) and d) the sensitivity of $\delta^{18}O_{calcite}$ of the new model setup is compared to the regular setup (a) and c)).
Both, the $\delta^{18}O_{drip}$ sensitivity and the $\delta^{18}O_{calcite}$ sensitivity in the new setup (figure 4.11 b) and d)) reveal a stronger precipitation dependence than the original setup. If the amount of winter precipitation increases, it contributes more water to the annual amount of drip water. Since winter precipitation is isotopically lighter than precipitation from warmer seasons, the mean $\delta^{18}O_{drip}$ depletes as well as the $\delta^{18}O_{calcite}$.
The temperature dependence is slightly smaller in the modified setup, because the monthly temperature are not varied equally. Nevertheless the temperature dependence is negative.
According to the modulated model setup lower $\delta^{18}O_{calcite}$ values in a stalagmite time series can be invoked by wetter winter conditions.

Error estimation For the model reduced to a variation of the winter season the error evaluation is performed in the same way as for the basic model (Monte-Carlo-Method with 2000 runs). The results are illustrated in figure 4.12. The standard deviation range for the $\delta^{18}O_{drip}$ value from 0.49 to 0.65‰ identically to the $\delta^{18}O_{calcite}$ standard deviation.

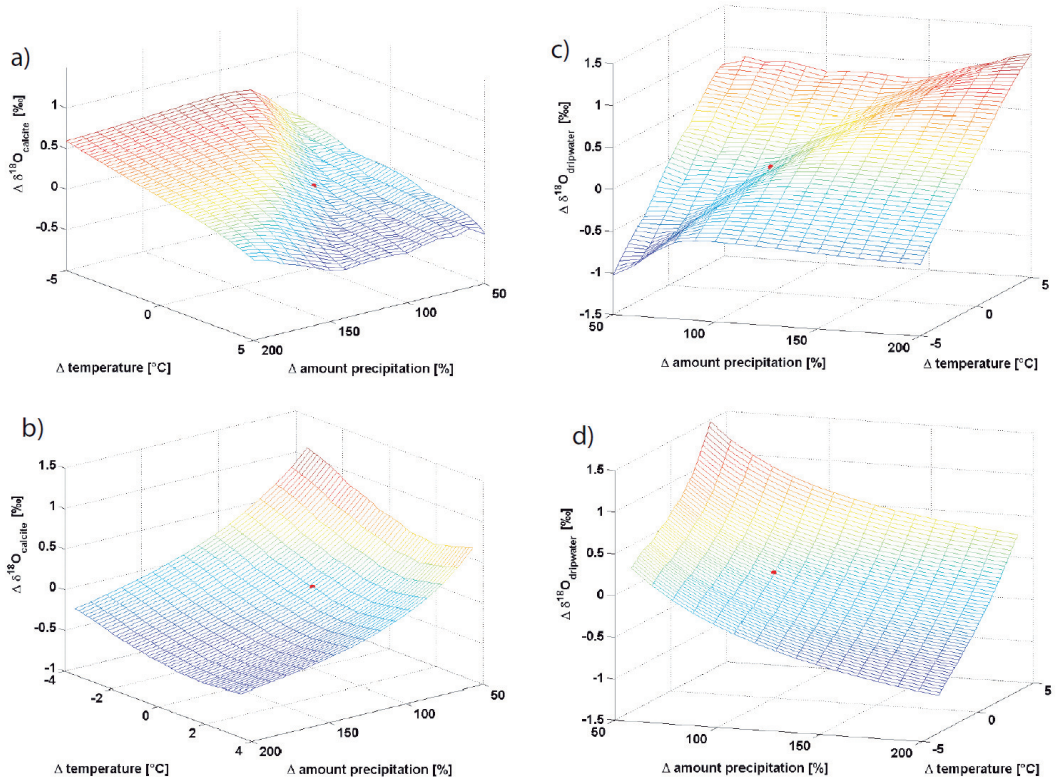

Figure 4.11.: Sensitivity of δ^{18}O on temperature and precipitation variations plotted as $\Delta\delta^{18}$O (deviation from the respective present day values). Temperature deviation is given in °C from the present day annual mean temperature T=10.5°C, precipitation in % from present day amount (100%) of winter precipitation. The red dot represents present day conditions. a) and c) $\delta^{18}O_{calcite}$ and $\delta^{18}O_{drip}$ from the regular model setup, b) and d) $\delta^{18}O_{drip}$ and $\delta^{18}O_{calcite}$ calculated with stronger variation during winter.

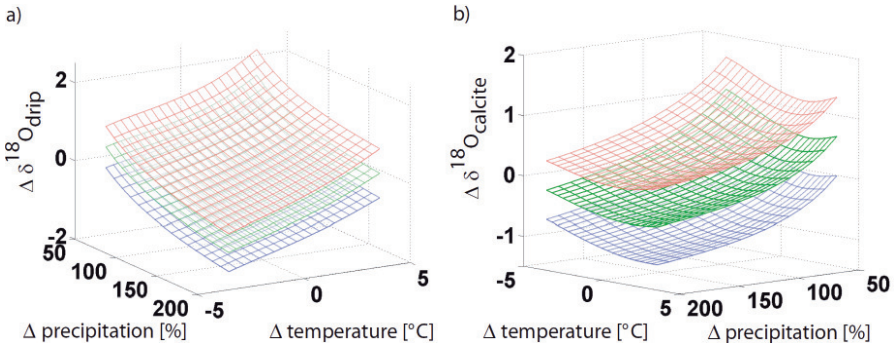

Figure 4.12.: Standard deviation of the ODSM ($\Delta\delta^{18}O_{drip}$, $\Delta\delta^{18}O_{calcite}$)in the mode in which only the winter season varies. The green layer shows the mean value, the blue and red layers represent the corresponding standard deviation of each of the values from the green layer.

4.3.3. Conclusions from the sensitivity experiments

In this section the sensitivity and influence of $\delta^{18}O_{drip}$ and $\delta^{18}O_{calcite}$ to variations of different parameters were analysed. It is important to compare these values to the observed variability of the stalagmite record. For the present day conditions the modelled $\delta^{18}O_{calcite}$ value under disequilibrium conditions agrees with the measured value:

- $\delta^{18}O$ =-5.7‰ (observed $\delta^{18}O_{calcite}$ value of stalagmite BU4)
- $\delta^{18}O$ =-5.8‰ (modelled $\delta^{18}O_{calcite}$ value under disequilibrium conditions)

The stalagmite record shows 1.9‰ variation from peak to peak between present day and 8.2 ka before present and a standard deviation of 0.3‰(see figure 3.1). The results of the sensitivity experiments must be regarded in context of these values.
In context of palaeo climate analyses, the important parameters are temperature and precipitation. However, in the model implementation there are several setups (mixing coefficient, determination of evapotranspiration, residence time) which are constant in one model run. The sensitivity of the $\delta^{18}O$ value on these features is compiled in table 4.3 and discussed first.

Model Modification	$\delta^{18}O_{calcite}$ offset from basic model [‰]
ET_{pot} by Thornthwaite (vs. Haude)	+0.7
Short residence time (vs. long residence time)	-0.1
Kinetic fractionation (ϕ=0.1) (vs. equilibrium)	+0.2
Kinetic fractionation (ϕ=0.5) (vs. equilibrium)	+0.4
Kinetic fractionation (ϕ= 1) (vs. equilibrium)	+0.8

Table 4.3.: The $\delta^{18}O_{calcite}$ offset between the basic model setup as presented in section 4.1 and the setup modification in this section

The smallest offset results from a modification of the residence time (between 'short' and 'long') of the water in soil and karst. This parameter can be neglected for Bunker Cave.
The determination of evapotranspiration (Thornthwaite [Thornthwaite and Mather, 1957] vs. Haude [Haude, 1955]) changes the mean $\delta^{18}O$ by a relevant number. For Bunker Cave it is known that Haude's equation [Haude, 1954] is the preferred choice due to i) a study by Schiff [1975] and ii) the fact that the model results for $\delta^{18}O_{drip}$ do not agree with the observed values, if the equation by Thornthwaite and Mather [1957] is applied. However, for other cave systems it is possible that Thornthwaite and Mather [1957] yield a realistic evaluation of the actual evapotranspiration. In addition, in the context of palaeo climate research the equation by Thornthwaite and Mather [1957] is a very useful tool, if it is kept in mind that the equation seems to overestimate evapotranspiration in the winter season.
The kinetic fractionation can affect the $\delta^{18}O$ to a large extent. If the calcite of the investigated stalagmite does not precipitate under equilibrium conditions, kinetic fractionation must be applied in the ODSM. The possible $\delta^{18}O_{calcite}$ range resulting from

varying mixing coefficients (table 4.3) would dominate any climatic signal leading to complicated analyses of the stalagmite δ^{18}O signal. However, during the growing period it is rather realistic that the mixing coefficient does not vary much, because the drip characteristics (drip point at the ceiling, drop height, stalagmite surface) can change only very slowly. Since the mixing coefficient depends on these parameters, the mixing characteristics are rather stable.
The parameters that can be changed in the model implementation (determination of evapotranspiration, equilibrium vs. kinetic fractionation, relationship between drip rate and infiltration, mixing coefficient between drip water and solution layer) influence the δ^{18}O sensitivity to temperature and precipitation variations in many ways. For each cave and stalagmite which is used for palaeo climate research, the relevant parameters must be assessed and carefully considered to evaluate the δ^{18}O sensitivity correctly. However, it is encouraging that for small variation of the climate conditions from the present day situation, the sensitivity is similar for all the varied features. They all show a decrease of the $\delta^{18}O_{calcite}$ signal with increasing temperature and a less significant gradient with precipitation.

The range of the calculated $\delta^{18}O_{calcite}$ values in the sensitivity experiment for the given temperature and precipitation variations is about 1.1‰ in the basic model setup, which is about 0.8‰ smaller than the observed range of the stalagmite record of BU4. The model modification with stronger variation during the winter months increases the modelled $\delta^{18}O_{calcite}$ range to about 1.6‰, indicating that a varying contribution of winter precipitation can be an explanation for the natural variability of the $\delta^{18}O_{calcite}$ signal.
This model modification of the ODSM setup is one of the most important adjustments that should be involved for stalagmites from Bunker Cave as well as other European caves. From different studies (Mangini *et al.* [2007], Trouet *et al.* [2009], Vollweiler *et al.* [2006]) we gain the knowledge that stalagmite $\delta^{18}O_{calcite}$ time series seem to covary with winter climate proxies. The impact of this factor in the context of model inversion is shown in section 6.2.
The comparison between the basic ODSM and the sensitivity of the ODSM with a stronger winter variability shows that the general sensitivity is very different. However, under the assumption that climate conditions tend to be warm and wet or cold and dry, the sensitivity results resemble each other following the respective trajectory. Both model realisation reveal decreasing $\delta^{18}O_{calcite}$ values from cold and dry to warm and wet conditions.

5. Mg/Ca model

In recent publications Mg/Ca got acknowledged as a valuable palaeo hydrology tracer. The relationship between the Mg/Ca ratio and precipitation can supply additional information about past hydrological characteristics or water supply and was investigated in many studies (Cruz *et al.* [2007], Fairchild *et al.* [2000], McDonald and Drysdale [2004], McDonald *et al.* [2007], Roberts *et al.* [1998], Treble *et al.* [2003]). A review of this subject was given by Fairchild and Treble [2009]. The underlying principle of the relationship was also given in section 2.6.
Compared to the $\delta^{18}O$ system, the Mg/Ca system from its origin in the host rock to the inclusion in speleothem calcite is even more complex. The $\delta^{18}O_{calcite}$ value inherits its signature from meteoric precipitation modified by different processes which are more or less directly linked to climate. The influence and origin of the $\delta^{18}O_{drip}$ value can be assessed in a monitoring program. In contrast the Mg/Ca system is sensitive to many processes which do not directly count as climate parameters or can only indirectly be linked to climate (e.g. Prior Calcite Precipitation (PCP)). The Mg/Ca signature of a drip site originates from the host rock type and processes in the karst, which alter the signal depend also on features of the karst environment in addition to climate parameters. An approach to simulate the Mg/Ca system is presented in this section.

5.1. The forward Mg/Ca model

Overview In the following section a forward model is developed which traces the Mg/Ca ratio from the initial solution to the growing stalagmite. The sequences of the model are illustrated in figure 5.1.
In contrast to $\delta^{18}O$ which bears the atmospheric signal, the Mg/Ca ratio of the drip water is mainly influenced by the Mg ratio of the host rock above the cave. Mg is carried with the sea salt or aerosols in precipitation and deposits during precipitation also above caves, but compared to the huge amount of Mg and Ca in the host rock, this contribution is only marginal.
The Mg/Ca model requires a monthly amount of precipitation and temperature to determine the amount of infiltrating water which forms acids dissolving the host rock. The dissolution process is identically to that of the ODSM. After dissolution the solution has the same Mg/Ca as the host rock.
The solution percolates downwards from the surface to the cave. If the water enters voids in the karst area, where the pCO_2 is smaller than the original soil air pCO_2 , CO_2 is forced to degas from the solution and calcite precipitates - so called Prior Calcite Precipitation hereafter referred to as PCP. The amount of calcite that can possibly precipitate is determined by the difference of the initial Ca^{2+} content of the drip water and the Ca^{2+} than can remain in the solution depending on the pCO_2 of the air in the gaps (precipitation down to SI=0.5 according to Lebrón and Suárez [1998] and Nielsen

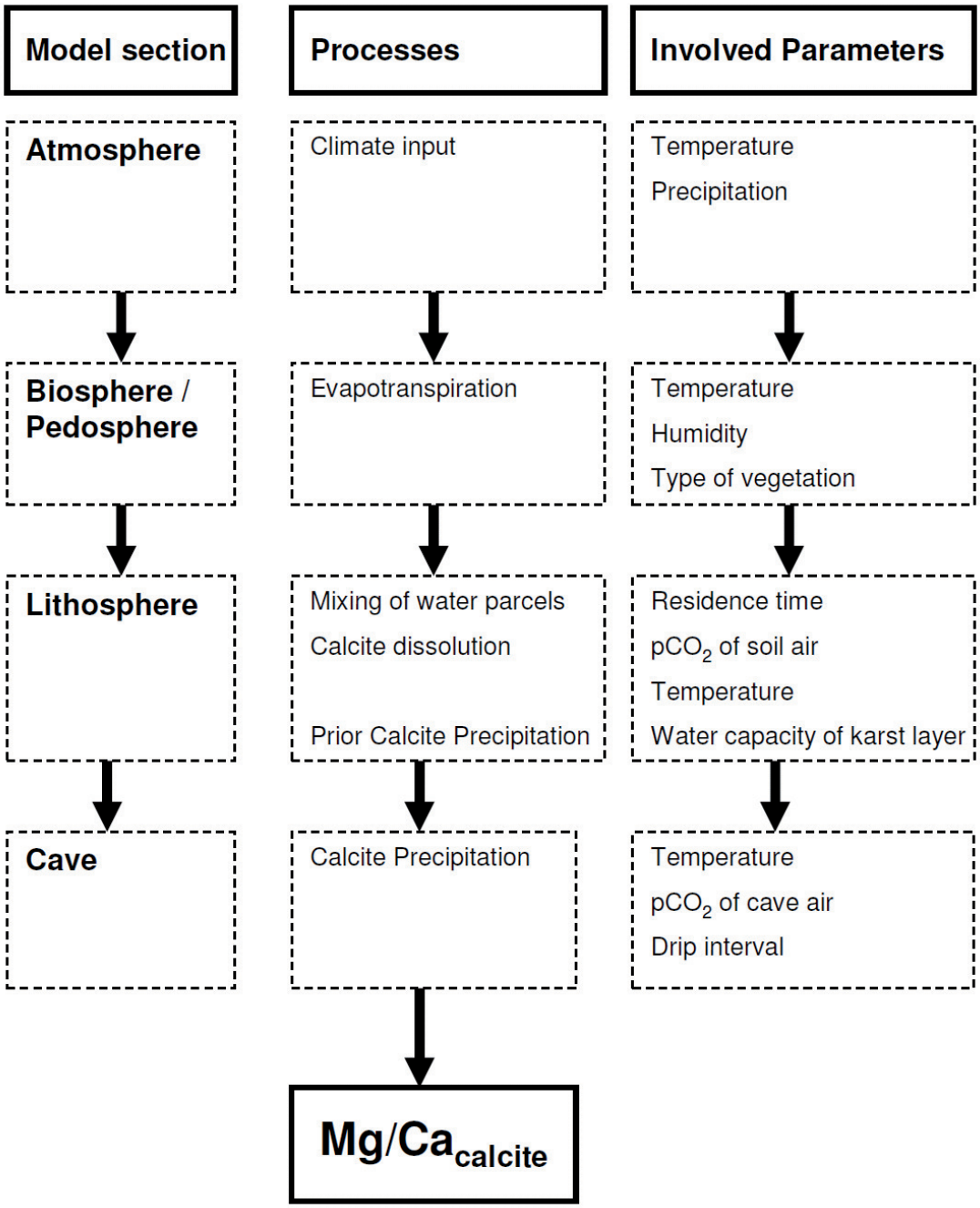

Figure 5.1.: Scheme of the forward Mg/Ca model

and Toft [1984]). During calcite precipitation a shift occurs between the Mg/Ca ratio of drip water and the stalagmite caused by the Mg/Ca partition coefficient. Ca^{2+} is preferentially removed while Mg^{2+} enriches in the remaining solution.
Depending of the drip interval, the gradient between the dissolved carbon of the solu-

tion in equilibrium with the soil air pCO_2[1] and cave air and the temperature, a certain amount of calcite precipitates from the drip water solution at the stalagmite. The Mg/Ca ratio of this stalagmite can be derived by a Rayleigh process where the fractionation is describes by the partition coefficient. In the following section the forward model is described in detail. Afterwards it is adjusted and applied to Bunker Cave.

5.1.1. Model description

Calcite dissolution The Mg/Ca model determines the infiltration in the same way as the ODSM (section 4.1). This monthly water parcel is exposed to the monthly varying pCO_2 of soil air. The formation of carbon acids and the amount of dissolved Ca^{2+} in the solution, Ca^{2+}_{inital} is determined by the model of Hendy [Hendy, 1971] modelled by Fohlmeister *et al.* [2011]. The water parcels are mixed over a certain number of months.

Prior Calcite Precipitation During the downward percolation the solution can approach air filled gaps in the karst matrix. If a gradient between the solution in equilibrium with soil air pCO_2 and the air in the void exists, CO_2 is forced to degas from the solution causing simultaneous calcite precipitation.
The critical point is to parameterise the extent of PCP and how to correlate this to the input parameters (temperature and precipitation). The presence of air filled gaps in the karst matrix is bound to depend on the amount of water in the matrix. In wet conditions the matrix fills with water diminishing the potential for PCP. If the climatic conditions are rather dry, the gaps are filled with air enhancing the possibility for CO_2 degassing. The degassing proceeds until pCO_2 equilibrium between solution and surrounding air is reached[2].
These two cases (extremely wet conditions - no PCP, extremely dry conditions - maximum PCP) can be regarded as boundary for the simulation of PCP. The behaviour between both cases is difficult to describe, since the knowledge of the state of dryness under which the maximum PCP occurs needs very detailed and comprehensive investigation of the karst layer. For the model realization the simplest correlation is used (figure 5.2 and equation 5.1) in which the full PCP takes place, if the soil wetness approaches zero[3].
Depending on the CO_2 gradient the remaining amount of Ca^{2+} ions in the solution can be determined.

$$Ca_{prec}(SW_{\text{capacity}}) = (Ca^{2+}_{\max}) - (Ca^{2+}_{\max}) \cdot \frac{SW_{\text{amount}}}{SW_{\text{capacity}}} \tag{5.1}$$

In equation 5.1 Ca_{prec} is the fraction of ions leaving the solution during PCP depending on the actual amount of water in the soil and karst layer between surface and cave,

[1] 'Soil air' refers to the initial pCO_2 value or the pCO_2 which was present in the gaps, where PCP occurred

[2] It is very important here to note, that the degassing does not proceed until the saturation index is 0 but it stops at about 0.5 in the model (Lebrón and Suárez [1998], Nielsen and Toft [1984])

[3] This inhibits calcite precipitation at the stalagmite, which is a good assumption, since without infiltration a stalagmite cannot grow.

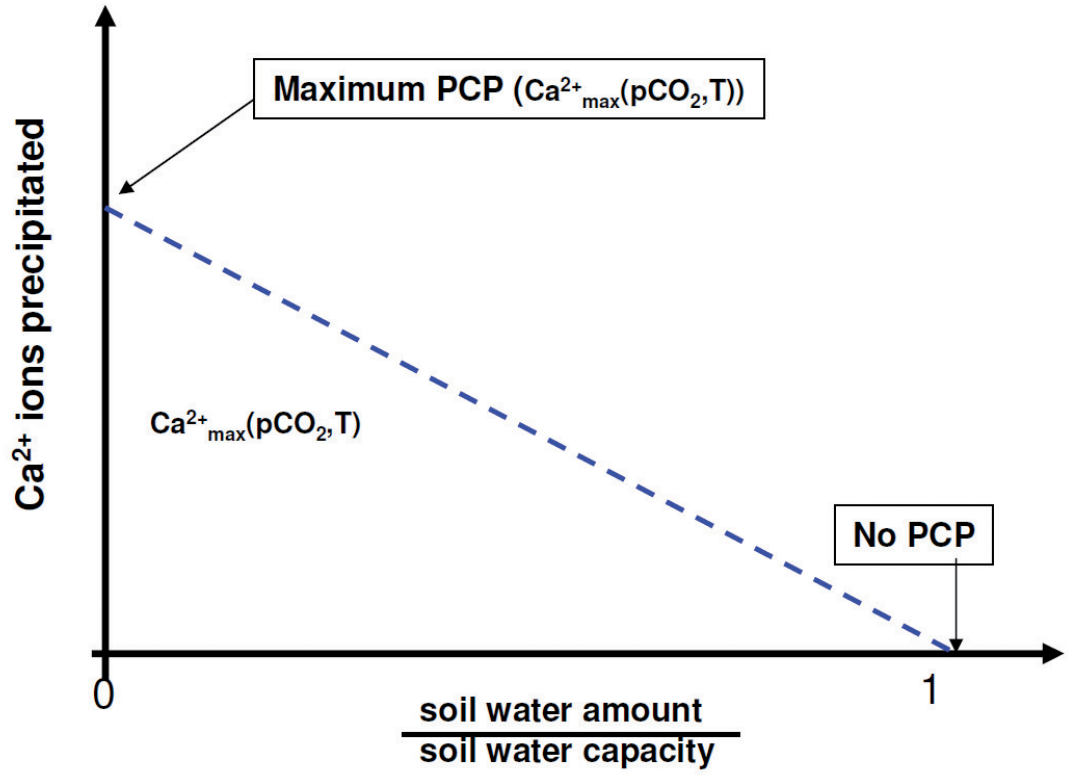

Figure 5.2.: Scheme for the PCP parameterization

SW_{amount}. $Ca^{2+}{}_{max}$ is the highest possible amount of calcite precipitation (in the model given in % from the initial solution). The soil water capacity, $SW_{capacity}$, is the maximum amount of water that the layer between surface and cave is able to absorb. How this parameter is determined for Bunker Cave is written section 5.2.2. This parameter depends on the amount of infiltration in the period of mixing or in other words the amount of infiltration that resides at the same time in the layer.
During calcite precipitation Mg/Ca increases in the solution described by a Rayleigh process (equation 5.2). $N_{remain}/N_{initial}$ is identic with 1-Ca_{prec} from equation 5.1 (the amount of Ca^{2+} which after PCP is still in the solution). The partition coefficient, D=0.019, of Mg compared to Ca is very small [Huang and Fairchild, 2001]. Due to this low partition coefficient, the remaining solution enriches in Mg^{2+} ions during PCP.

$$Mg/Ca_{\text{resulting}} = Mg/Ca_{\text{ini}} \cdot \left(\frac{N_{\text{remain}}}{N_{\text{initial}}}\right)^{D-1} \tag{5.2}$$

Precipitation on top of the stalagmite The soil water with modified Ca^{2+} content and Mg/Ca ratio forming the drip water enters the cave. The simulation of calcite precipitation at the stalagmite is performed identically to the ODSM.
One drop falls onto the stalagmite, the solution degasses and calcite precipitate undis-

turbed until the next drop arrives. Four parameter decide how much calcite precipitates during one drip interval:

- the gradient between the pCO_2 of soil air and the cave air
- the cave temperature
- the drip interval
- the mixing coefficient

The pCO_2 gradient forces the degassing from the drip water, which would proceed until the solution is in equilibrium with cave air identical to the PCP sequence. However, the drip interval is a limiting factor, because the solution on the top of the layer is replaced by the new drip bearing the Ca^{2+} imprint of the soil water. If the mixing coefficient between impinging drop and solution layer is 1 (complete replacement of the solution layer by the new drop), the calcite precipitation starts again with the initial Ca^{2+} content of the soil water. If the mixing coefficient is lower, the starting Ca^{2+} content of the solution layer after the mixing with the new drop is lower than the Ca^{2+} content of the new drop. This is illustrated in figure 5.3.
The initial Ca^{2+} content of each new drop is in figure 5.3 represented by the 'Ca^{2+} soil air' line and illustrates the Ca^{2+} content of the solution in equilibrium with the soil/gap air pCO_2. If the mixing coefficient is 1, the Ca^{2+} content of the solution at the stalagmite surface starts with this value for each new drop. If the mixing coefficient is $\neq 1$, the Ca^{2+} of the solution is lower than the drip water level.
The model calculates the mixing between drip water and solution until an equilibrium has established in which the solution has the same Ca^{2+} value each time a new drop arrives. In this model sequence only the first drop at the stalagmite has the Ca^{2+} content of the drip water. When the second drop replaces the solution partially, the Ca^{2+} content of the solution is mixed with a certain ratio with the Ca^{2+} concentration of the fresh drop. The resulting Ca^{2+} content is smaller.
The calculations of the temporal evolution of the Ca^{2+} in the solution is identical to the kinetic model sequence in the ODSM. The $\delta^{18}O$ ratio is replaced by the Mg/Ca ratio.
When the equilibrium is established, the Ca^{2+} content decreases during one drip interval from an upper to a lower Ca^{2+} content due to calcite precipitation (in figure 5.3 Ca_{upper} to Ca_{lower}). Precipitation is accompanied by a change of the Mg/Ca ratio in the solution film on the stalagmite (equivalent to equation 5.2 calculated with equation 5.3 and figure 5.4: black line). The Mg/Ca ratio of calcite which forms on top of the stalagmite depends on the Mg/Ca ratio of the parent drip water. These ratios are related by the partition coefficient, D. It is obvious that, if the Mg/Ca ratio of the solution evolves during calcite precipitation, the Mg/Ca ratio of instantaneously precipitating calcite changes simultaneously. To determine the resulting Mg/Ca ratio of the calcite after one drip interval (which is equal to the stalagmite Mg/Ca value under the respective conditions), the Mg/Ca ratios of the instantaneous calcite over the whole drip interval must be integrated (realized by adding up the instantaneous Mg/Ca ratios). The temporal evolution of Mg/Ca ratio of solution, instantaneous and total calcite is illustrated in figure 5.4. An identical picture can be found in Johnson *et al.* [2006]. The underlying

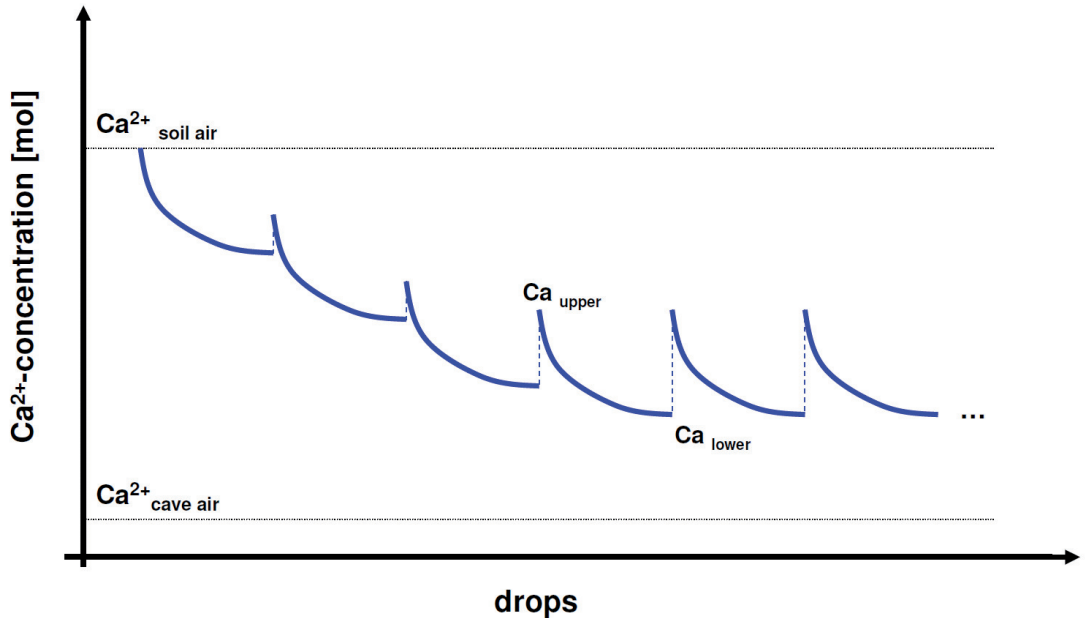

Figure 5.3.: Evolution of Ca^{2+} in the solution film on the stalagmite surface with time depends on the drops falling onto the stalagmite. The Ca^{2+} content decreases due to the gradient between soil air and cave air pCO_2. The upper dashed line 'Ca^{2+} soil air' represents the amount of dissolved Ca^{2+} in the solution in equilibrium with the soil air (Soil air: either original soil air pCO_2 or altered due to PCP). The lower dashed line illustrates the amount of dissolved Ca^{2+} which can remain in the solution in equilibrium with cave air pCO_2. The mixing coefficient $\phi \neq 1$. Therefore the initial Mg/Ca ratio is after one drip different from the Mg/Ca ratio of the first drop. If the input parameters of the model stay constant, an equilibrium establishes with an invariant, initial Ca^{2+} and Mg/Ca ratio decreasing to constant lower Ca^{2+} and Mg/Ca values.

equations are given in the following. Equation 5.3 describes the Mg/Ca ratio of the solution depending on the fraction of Ca^{2+} which precipitates at the stalagmite, Ca^{2+}_{prec}.

$$Mg/Ca_{\text{solution}} = Mg/Ca_{\text{ini}} \cdot (\frac{100 - Ca_{\text{prec}}[\%]}{100})^{D-1} \tag{5.3}$$

The Mg/Ca ratio of the instantaneous calcite depends on the solution and the partition coefficient.

$$Mg/Ca_{\text{inst.calcite}} = Mg/Ca_{\text{solution}} \cdot D \tag{5.4}$$

The resulting Mg/Ca of stalagmite calcite can be added up as in the following equation.

$$Mg/Ca_{\text{sum.calcite}} = \frac{\sum_0^{Ca_{\text{prec}}[\%]} Mg/Ca_{\text{inst.calcite}}}{Ca_{\text{prec}}[\%]} \tag{5.5}$$

This last equation yields the Mg/Ca ratio of a stalagmite for given conditions.

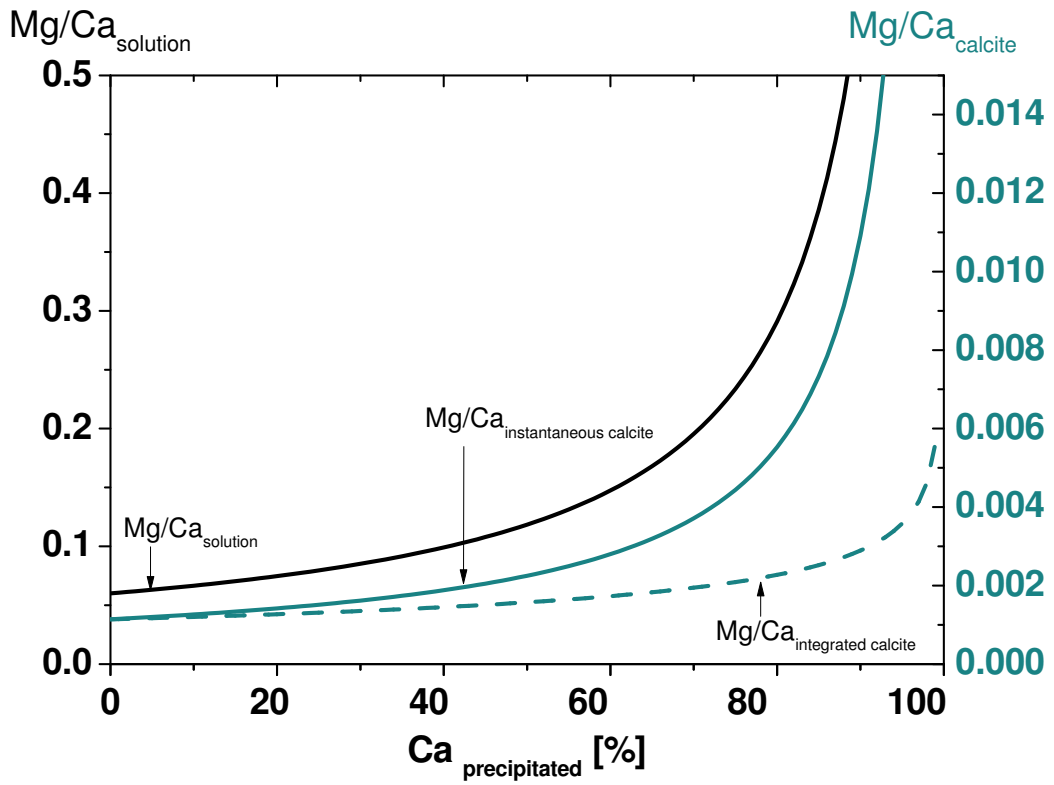

Figure 5.4.: Evolution of Mg/Ca ratio of the drip water solution (black line), the instantaneous calcite (cyan line) and the integrated calcite (cyan line dashed). The latter is the integral of the function describing the instantaneous calcite.

Growth rate The sequence of calcite precipitation at the stalagmite yields an additional feature that can help to evaluate the model results - the growth rate of the stalagmite. Since the amount of Ca^{2+} from the solution is calculated, the amount of calcite ($CaCO_3$) which is deposited during one drip interval can be assessed (one mol Ca^{2+} yields one mol $CaCO_3$). The volume per drip interval is calculated by equation 5.6.

$$CaCO_3(\text{Volume})[cm^3] = \frac{CaCO_{3\ \text{prec}}[mol/l].\cdot 0.0001[l]\cdot 100.9[g/mol]}{2.7[g/cm^3]} \tag{5.6}$$

$CaCO_{3prec}$ is the amount of precipitated calcite in mol/l as calculated by the model sequence, 0.0001l is the volume of one drop, 100.9g/mol is the molecular weight of calcite and 2.7g/cm^3 the density. This results in a height of the calcite volume in the center box of the stalagmite (size=10cm^2 as proposed by Mühlinghaus [2008]) given in equation 5.7

$$H_{\text{growth}}[cm] = CaCO_3(\text{Volume})[cm^3]/10[cm^2] \tag{5.7}$$

During one year N=31557600s/dT drops approach the stalagmite (dT: drip interval [s]) resulting in equation 5.8 which yields the growth per year, H_{growth} per year.

$$H_{\text{growth}}[cm/year] = CaCO_3(\text{Volume})[cm^3]/10[cm^2]\cdot N \tag{5.8}$$

5.2. Application and evaluation of Mg/Ca Model

5.2.1. General application comments

In contrast to the OSDM the Mg/Ca Model yields multiple output parameters. This is an advantage in the context of model validation. The model is applied here to Bunker Cave, which provides a comprehensive and long monitoring of the required parameters. The following input parameters of the Mg/Ca model are supplied by the monitoring program:

- Climate data (temperature, precipitation, humidity, vegetation)
- pCO_2 of soil air
- samples of the cave host rock
- residence time of water in the soil and karst
- pCO_2 of cave air
- drip interval

The output parameters simulated by the Mg/Ca model which can be compared to observed values are:

- the Mg/Ca ratio of drip water
- the Ca^{2+} content of the drip water
- the Mg^{2+} content of the drip water
- the Mg/Ca ratio of the speleothem calcite
- the growth rate of the stalagmite

However, some required information for the model setup have not been monitored so far or cannot be monitored at all (initial Ca^{2+} content of the solution, initial Mg/Ca ratio of the solution and the extent of PCP). These are the parameters that must be linked to one of the known input parameters, estimated or parameterized. The following paragraphs describe how these factors can be approached in general. Specific numbers of the parameters are given in the application in section 5.2.2.

Initial Ca^{2+} content of the solution Though in principle this parameter is determined by the pCO_2 of soil air, the resulting Ca^{2+} of the drip water can be not in agreement with the observed value at one particular drip site. A modelled Ca^{2+} content of the soil water solution after calcite dissolution (depending on the pCO_2 of the soil) that is lower than any measured value at any drip site at the cave might indicate that other acids (humins) are present in the soil dissolving additional calcite or even a higher pCO_2 than measured. Therefore cations measurements of the drip water (example for Bunker Cave: figure 5.5) can help to determine the initial Ca^{2+} content. The figure displays all the

Ca^{2+} content and Mg/Ca ratio pairs of values measured at all drip sites in Bunker Cave during the period from July 2006 to July 2009. The dashed line illustrates the Rayleigh equation for PCP. If we focus now on drip site TS8, it is obvious that monthly drip water values follow the predicted behaviour of PCP. For the drip sites whose values group along the PCP line, it is sound to assume that the initial Ca^{2+} concentration of the solution directly after host rock dissolution lies in the upper part of the Ca^{2+} range and on the curve (for example: 110mg/l for TS8). Of course the initial Ca^{2+} concentration can be above this value, but when simulated and measured end member values are compared, it becomes clear that only a certain range of initial Ca^{2+} concentration values yields good model results (see section 5.2.2).

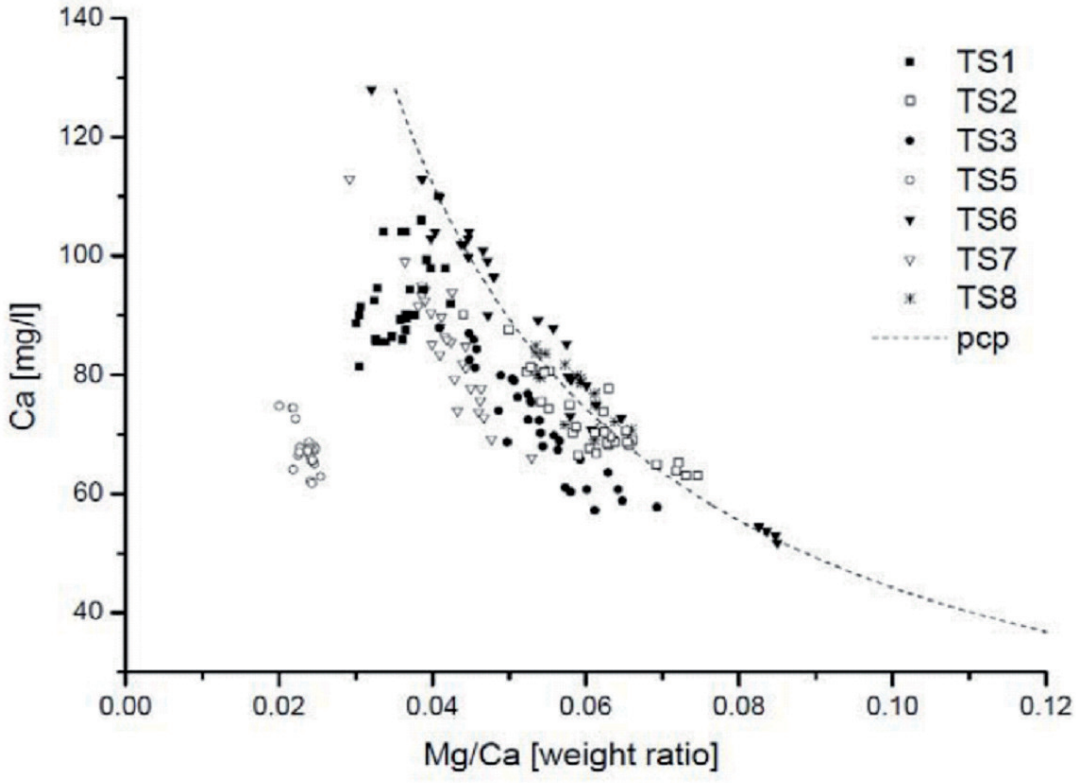

Figure 5.5.: Ca^{2+} content and Mg/Ca ratio monthly drip water samples of all monitored drip sites in Bunker Cave. Figure taken from Riechelmann *et al.* [a] [in press].

Initial Mg/Ca ratio This value can be estimated by analysing host rock samples. However, it is not possible to analyse a whole host rock cross section above the cave. It is possible that randomly collected host rock samples do not represent the average host rock type for example if dolomite veins exist in between calcite. These might not be grasped by the random samples, but will change the Mg/Ca essentially. Hence, the Mg/Ca ratio of the initial solution is chosen according to the initial Ca^{2+} content on the hypothetical line of PCP (dashed line in figure 5.5). Of course it is advisable to compare this to the grab samples of the host rock.

Extent of PCP For the model there is no difference where PCP takes place. Every precipitation before the calcite precipitation at the top of a growing stalagmite is defined as PCP including calcite precipitation in the karst layer as well as at the ceiling of the cave. The pCO_2 of the air filled gaps is by default set to the mean cave air pCO_2 =740ppm (the cave monitoring reveals a standard deviation of this value of 100ppm).
To determine the amount of PCP two parameters were introduced in section 5.1 - the soil water amount and the soil water capacity. The soil water amount is the actual amount of water in the matrix which is correlated to the residence time. Twelve month residence time mean that the infiltration of twelve months is present in the area between surface and cave.
The soil water capacity describes how much water the layer between surface and cave can contain. There is little knowledge of this parameter, but certain indicators help to assess a realistic value.
In humid regions (where the soil and karst is wet during all seasons) the residence time gives an impression how many months of infiltration the layer between surface and cave contains. The matrix from surface to cave is obviously able to contain at least this amount of water parcels. The minimum capacity can therefore be defined as the mean amount of infiltration over as many months as the residence time suggests.
The drip site characteristics show that PCP takes actually place at Bunker Cave indicating that voids and air filled gaps must exist in the host rock. Hence, the real soil water capacity should be bigger by a factor, F, than the minimum capacity derived from the residence time. This factor, F, can be estimated by comparing the initial Ca^{2+} value of percolating water after host rock dissolution and drip water Ca^{2+} values. The difference indicates how much calcite is lost due to PCP.
Only a small range of values for the factor of soil water capacity simulate the correctly measured drip water characteristics. The calibration of this factor for TS8 is shown in section 5.2.2.

5.2.2. Application to Bunker Cave

In contrast to the ODSM the Mg/Ca model needs calibration for several parameters, which can only be achieved during application of the model, since these parameters are characteristic for each individual cave and drip site. In the following the model is adjusted to the trace element values of TS8 and the recent growth rate and Mg/Ca value of BU4.
The calibration should lead to the following observed values which were measured at the drip site between May 2007 to August 2011:

- $Ca^{2+}_{drip} = 78 \pm 5$ mg/l (mean value between May 2007 and September 2009)
- $Mg^{2+}_{drip} = 4.5 \pm 0.2$ mg/l (mean value between May 2007 and September 2009)
- $Mg/Ca_{drip} = 0.058 \pm 0.004$ (mean value between May 2007 and September 2009)
- $Mg/Ca_{calcite} = 0.0013$ (BU4 recent sample)
- growth rate = 14μm/year

Only the first three parameters are relevant to calibrate the initial Ca^{2+} content, the initial Mg/Ca ratio and the soil water capacity. Without the monitored drip site it would be nearly impossible to calibrate these parameters.

Initial Ca^{2+} content of the solution for TS8 The mean soil air pCO_2 above Bunker Cave is ≈4200ppm [Riechelmann *et al.* [a], in press]. This amount dissolves ≈60mg/l Ca^{2+} (see table 5.1). From figure 5.5 can be derived that this value is lower than the smallest Ca^{2+} content at TS8. The highest Ca^{2+} value at the drip site is about 85mg/l. This amount can be dissolved by a solution, if the pCO_2 of soil air is about 10500ppm. The highest measured pCO_2 during the monitoring period has this value. However, it is possible that a problem with the CO_2-sensor occurred (personal communication: Andrea Schröder-Ritzrau) which diminished the measured pCO_2 values. Values about 10000ppm are therefore realistic. It is also possible that other acids with an anthropogenic origin (SO_4) dissolve additional calcite. In table 5.1 some pCO_2 value are listed together with the resulting Ca^{2+} content of the saturated solution.
85mg/l seem to be a realistic value for Ca^{2+}, that does not disagree with the drip site characteristics.

pCO_2 of solution [*ppm*]	Ca^{2+} dissolved [mg/l]	Comment
380	27	atmospheric pCO_2
740	34	mean cave air pCO_2
740	50	mean cave air pCO_2 (SI = 0.5)
4200	61	mean soil air pCO_2
10500	85	maximum soil air pCO_2
20000	107	
40000	138	

Table 5.1.: Resulting dissolved Ca^{2+} of calcite saturated conditions depending on the surrounding pCO_2.

Initial Mg/Ca ratio of TS8 According to the initial Ca^{2+} value the initial Mg/Ca ratio of 0.052 is chosen from the hypothetical curve of PCP.

Soil water capacity of TS8 Since monitoring suggests that PCP occurs at the drip site, the soil water capacity is obviously not reached. For the given initial Ca^{2+} content, the capacity can be determined by comparing the modelled and the measured drip water. If the solution starts at 85mg/l and the mean measured Ca^{2+} content is 78mg/l, the difference must be lost due to PCP. This can be achieved, if the soil water capacity is defined as a factor 1.5 of the mean annual present day infiltration.
In this setup the Mg/Ca model yields the following drip water values.

- $Ca^{2+}_{drip} = 74$ mg/l
- $Mg^{2+}_{drip} = 4.2$ mg/l

- $Mg/Ca_{drip} = 0.057$

5.2.2.1. Parameter discussion

The calibrated values are in a realistic range and the results of the model agree with observed values. Nevertheless, it is important to investigate how the model reacts, if one of the parameters is chosen differently.

- **Initial Ca^{2+} content.** If the initial Ca^{2+} content is increased (third line table 5.2), the gradient between the Ca^{2+} content in equilibrium with soil air pCO_2 and the air filled void pCO_2 is larger. This leads to a steeper slope in figure 5.2 and to a higher percentage of PCP calcite which enriches Mg^{2+} in the solution. Therefore the Mg/Ca ratio of the drip water increases.

- **Initial Mg/Ca ratio.** An increase of the initial Mg/Ca ratio (fourth line in table 5.2) is accompanied by an increase of the amount of Mg^{2+} in the solution and a slight decrease of Ca^{2+}. The drip water Mg/Ca ratio increases subsequently.

- **Soil water capacity.** If the soil water capacity is increased (fifth line in table 5.2), more calcite precipitates due to more space in the soil diminishing the Ca^{2+} content in the drip water. During PCP the Mg^{2+} enriches in the solution which leads to a higher Mg^{2+} and Mg/Ca ratios of the drip water.

It is obvious that each calibrated parameter can bias the output values toward different directions. Hence, it is reasonable to assume that a different setup of parameters than the stated can also lead to correct output values. However, a different set of initial values leads to some problems:
i) The soil water capacity could be chosen to be smaller (but bigger than one times the mean annual infiltration). In this case, the initial Ca^{2+} must also be chosen smaller, since less PCP occurs. However, the initial Ca^{2+} value was so far chosen to include also the highest Ca^{2+} content measured at the drip site. A lower initial Ca^{2+} content then contradicts the highest Ca^{2+} content of the drip water.
ii) The case of a larger soil capacity is represented by the last line in table 5.2). The soil water capacity is increased there to 2.5 times the mean annual infiltration. To model the correct measured drip water values, the initial Ca^{2+} content 110mg/l (which is the biggest value of all the drip sites in Bunker Cave). Under these conditions about 30% of Ca^{2+} must be lost from the solution on the way to the stalagmite. In principle it is possible that a stalactite forms above the stalagmite incorporating the calcite which is lost during PCP, but at BU4 only a soda straw grows at the ceiling. The calcite must be primarily precipitated in the karst matrix above the cave. The question then arises, if it is possible that a stalagmite grows for over about 10 thousands of years, if 30% of the dissolves Ca^{2+} precipitates in the karst without leading to closing of the water-bearing channels.
For the studies to come we use the first set of input parameters as default values (second line in table 5.2).

In the model sequence which calculates the calcite precipitation at the stalagmite the parameters known from the ODSM are required: mixing coefficient (ϕ=1) and drip interval (3600s). The Mg/Ca model yields for recent calcite grown under the named conditions:

- Mg/Ca = 0.0013
- growth rate = 19μm/year

These values are both within the order of the measured value.

		Input			**Output**		
	Comment	Ca^{2+}_{ini} [mg/l]	Mg/Ca_{ini}	$Factor_{Cap.}$	Ca^{2+} [mg/l]	Mg^{2+} [mg/l]	Mg/Ca
1	Observed Data				78±5	4.5±0.2	0.058 ± 0.004
2	Basic setup	85	0.05	1.5	74	4.2	0.057
3	increased Ca^{2+}	150	0.052	1.5	106	6.9	0.065
4	increased Mg/Ca	85	0.06	1.5	73	5	0.069
5	increased $Factor_{Cap.}$	85	0.052	2	67	4.4	0.064
6	Top point on PCP curve for all TS	110	0.04	2.5	74	4.4	0.058

Table 5.2.: Model input and output of the Mg/Ca model

5.3. Sensitivity of the Mg/Ca model

In this section the sensitivity of the Mg/Ca model is determined in analogy to the $\delta^{18}O$ model. The results are presented in dependence of mean annual temperature and annual amount of precipitation. The sensitivity relies therefore on the defined standard monthly values (table 4.1) from section 4.3. The model results for Ca^{2+}, Mg^{2+} and Mg/Ca of the drip water, the Mg/Ca and the growth rate of the stalagmite and the fraction of calcite that precipitates at the stalagmite are discussed in the following.
First, the sensitivity of drip water values of temperature and precipitation is focussed on. In figure 5.6 the Ca^{2+} content, the Mg^{2+} content and the Mg/Ca ratio of the drip water is displayed depending on variation of annual temperature and precipitation.

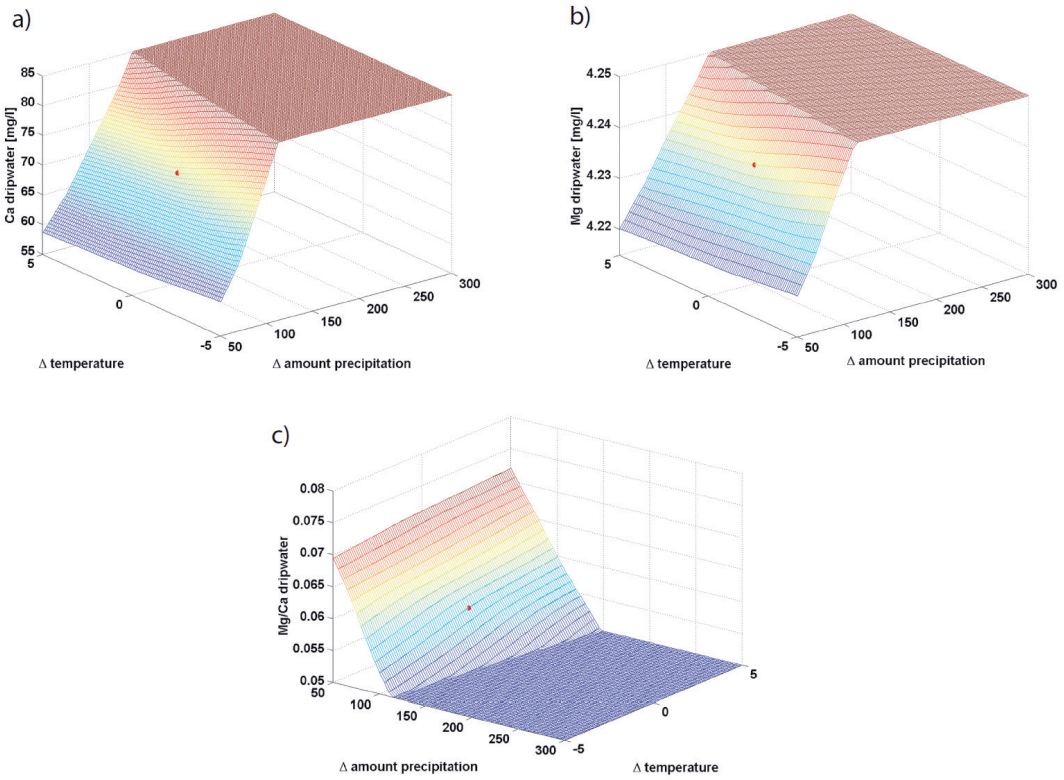

Figure 5.6.: Sensitivity on temperature and precipitation variations of a) Ca^{2+}, b) Mg^{2+} and c) Mg/Ca ratio of cave drip water. The temperature deviation is given in °C from the present day annual mean temperature T=10.5°C, precipitation in % from the present day amount (100%). The red dot represent present day conditions.

Drip water sensitivity The **Ca^{2+} content** shows a clear correlation to the amount of precipitation. Drier conditions than the present day situation (red dot) generate more air filled voids in the karst where PCP can occur reducing the Ca^{2+} in the drip water. If the conditions are wetter, less Ca^{2+} is lost during PCP leading to an increased Ca^{2+} content. The Ca^{2+} reaches finally a plateau at 85mg/l - the initial Ca^{2+} content. Here the infiltration is 1.5 times the present-day amount of annual infiltration which equals

the soil water capacity. No PCP takes place under these conditions.
The **Mg^{2+} content** reveals a similar pattern. As long as the conditions are wet enough to prevent PCP, the Mg^{2+} content of drip water shows the initial Mg^{2+} concentration which is determined by the initial ratio Mg/Ca. The precipitation gradient is less steep compared to Ca^{2+} , since calcite precipitation preferentially removes Ca^{2+} from the solution (Partition coefficient D=0.019)
Regarding the temperature, both parameters show an anticorrelation. This originates from the anticorrelation between temperature and infiltration. Lower temperatures lead to higher infiltration values, leading to less PCP and higher Ca^{2+} and Mg^{2+} values in the drip water.
The **Mg/Ca ratio** shows an opposite pattern. Without PCP the value remains constant at the initial Mg/Ca ratio. When the climate conditions yield potential for PCP the Mg/Ca ratio increases, due to the preferential removal of Ca^{2+} during calcite precipitation.

Speleothem calcite sensitivity The sensitivity results for the mixing coefficient ϕ=1 are shown in figure 5.7 in the right column. To understand the pattern the explanation must start with the **percentage of Ca^{2+} precipitating** from the solution (figure 5.7 i)). For dry conditions the percentage is very small. This pattern is inherited from the Ca^{2+} content of the parent drip water. The higher the gradient between the Ca^{2+} content of the drip water and the Ca^{2+} content of water according to the pCO_2 of cave air (≈50mg/l), the more the percentage of precipitating calcite increases. This increases up to a plateau value, which is delimited by the maximum value of Ca^{2+} in the drip water. Here, the drip interval is long enough for complete calcite precipitation down to the saturation index SI=0.5. It is important to note, that the maximum percentage is about 40% of the calcite in the solution.
For wetter conditions (high precipitation and cold temperatures) and higher drip rates the percentage of precipitating calcite decreases again, as for high drip rates calcite precipitation is disturbed by the new impinging drop.
The sensitivity of the **growth rate** matches the sensitivity pattern of the percentage of calcite that precipitates but also shows a general higher growth rate with increasing infiltration. Wetter conditions lead to less PCP increasing the Ca^{2+} content of the drip water which allows more calcite precipitation at the stalagmite and under wetter conditions the drip rate is higher and more drops per year transport more Ca^{2+} ions to the stalagmite.
The **Mg/Ca ratio** of the stalagmite depends on two principles. On the one hand it inherits the Mg/Ca ratio of the drip water, on the other hand the Mg/Ca ratio of calcite is influenced by the extent of calcite precipitation (more calcite precipitation leading to higher Mg/Ca values). Therefore the Mg/Ca ratio of calcite increases from wet to dry conditions (although at higher precipitation the drip water Mg/Ca ratio remains constant, see figure 5.6). However, when the Mg/Ca ratio of the drip water increases, this mechanism prevails resulting in increasing Mg/Ca ratio of the calcite. The increase would even be more pronounced, if the percentage of precipitating calcite did not decrease.

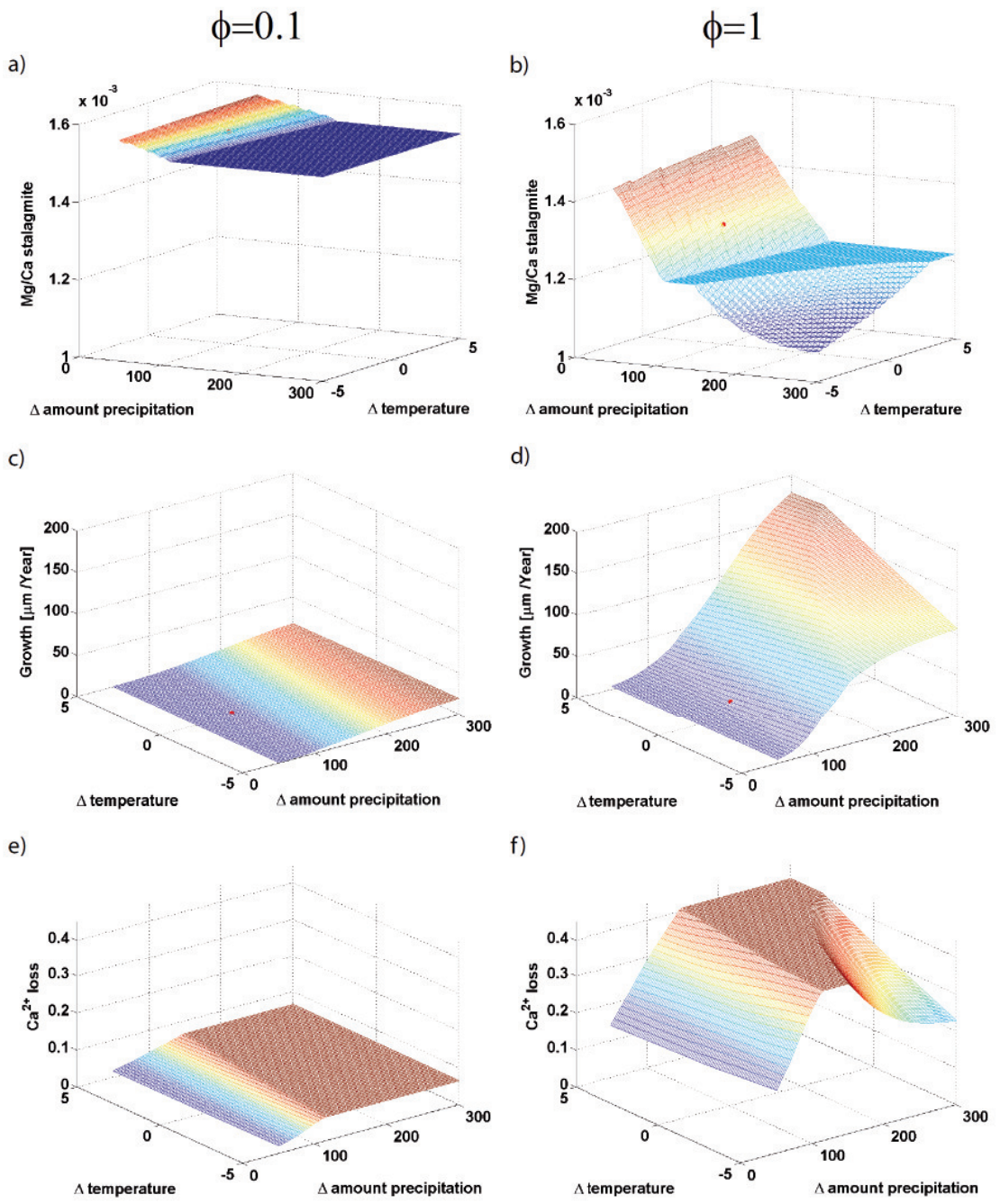

Figure 5.7.: Sensitivity for different mixing coefficients, ϕ, on temperature and precipitation variation of the Mg/Ca ratio of speleothem calcite (a and b), growth rate (c and d) and percentage of calcite precipitation during one drip interval from the water film on top of the stalagmite (e and f). Temperature deviation is given in °C from the present day annual mean temperature T=10.5°C, precipitation in % from the present day amount (100%). The red dot represents the present day condition.

Different mixing coefficient The results for Mg/Ca ratio of calcite, the growth rate and the percentage of calcite precipitating from the solution for different mixing coefficients can be observed in figure 5.7.
The growth rate decreases significantly with decreasing mixing coefficient, because less Ca^{2+} ions are added to the solution in the center box of the stalagmite by the impinging drip. This can also be observed in the percentage of precipitated calcite. The sensitivity of the Mg/Ca ratio of the stalagmite is presented in figure 5.7 a)-c). Two main characteristics are obvious: i) with increasing ϕ the Mg/Ca decrease and ii) with increasing ϕ the range of Mg/Ca increases. The reason for i) is that the solution (with already enriched Mg/Ca) at the top of the stalagmite is replaced only by 10% by the drip water solution (less enriched Mg/Ca) when the mixing coefficient is small. This leads to a higher Mg/Ca ratio in comparison to the situation when the solution layer is replaced completely (ϕ=1).
The explanation for the second feature is again the influence of the Mg/Ca ratio of the drip water in combination with the percentage of precipitating calcite similar to the previous paragraph.

Comment on seasonality For the Mg/Ca model it is not necessary to investigate the model to a changing seasonality as for the ODSM. The $\delta^{18}O$ of drip water inherits an atmospheric signal bearing relevant, seasonal variations. In contrast, for the Mg/Ca system the season of infiltration and calcite dissolution is not important due to extensive mixing. Therefore the Mg/Ca model is always used in the presented setup.

5.3.1. Error estimation

The sensitivity study itself gives comprehensive information about the variability of the modelled systems. The errors occurring due to the linear regressions (between humidity/monthly maximum temperature and mean monthly temperature - identical to the linear regressions in the ODSM) are very small and listed below:

- Range of standard deviation of $\mathbf{Mg/Ca_{drip}}$: $7{\cdot}10^{-10}$-$5{\cdot}10^{-4}$
- Range of standard deviation of $\mathbf{Ca_{drip}}$: 0-0.88 mg/l
- Range of standard deviation of $\mathbf{Mg_{drip}}$: 0-0.007 mg/l
- Range of standard deviation of $\mathbf{Mg/Ca_{calcite}}$: $2{\cdot}10^{-18}$-$7{\cdot}10^{-6}$
- Range of standard deviation of $\mathbf{Percent\ Ca_{prec}}$: 0%-0.6%
- Range of standard deviation of **Growth rate**: 0.03-3.65[μm/year]

5.4. Additional modules: dolomite and PCP dissolution

The Mg/Ca model as presented above was established to represent the Mg/Ca system with a minimal set of assumptions and parameters. The model yields good results compared to present day values. The sensitivity study has shown the range of possible variations in the Mg/Ca ratio of speleothem calcite for different climate parameters.
The Mg/Ca record of BU4 suggests that the natural range is much bigger (0.0025) than the simulated range (0.0005). Obviously some parameters in the natural cave system, which are not included in the Mg/Ca model so far change the Mg/Ca ratio significantly. A higher range of Mg/Ca values can be caused by more or less calcite precipitation at the stalagmite. In figure 5.4 the Mg/Ca ratio of calcite is illustrated in dependence on the percentage of the precipitated calcite. The ratio of calcite (integrated, not instantaneous) is nearly a flat line up to 70% precipitation. This value must be approached to increase the Mg/Ca ratio. As discussed in the previous section the maximum percentage of calcite precipitation from present day drip water at BU4 is about 40%. This leaves a major change of the long term mean Mg/Ca ratio of drip water to be the only possibility for a significant change of the Mg/Ca ratio of speleothem calcite.
In the following section two factors are introduced, that are able to generate a shift of the mean Mg/Ca ratio of the drip water.
These are

- **Dolomite dissolution.** So far the host rock was assumed to be pure calcite. However, it is possible that the host rock also contains dolomite veins. The chemical structure of dolomite is $CaMg(CO_3)_2$. Dolomite dissolution therefore leads to a higher Mg/Ca ratio of the drip water.

- **Dissolution of calcite$_{PCP}$.** The calcite which precipitated due to PCP in the karst matrix before entering the cave has a very low Mg/Ca content. If this calcite is dissolved by a water parcel which did not reach saturation with respect to calcite and is carried to the cave, the Mg/Ca ratio of the drip water diminishes.

5.4.1. Dolomite dissolution

Dolomite is a crystal fabric similar to calcite, but the magnesium content is 50% ($CaMg(CO_3)_2$) in contrast to calcite where it occurs only as a trace element by definition. The solubility of dolomite compared to calcite is low [Fairchild and Treble, 2009]. Due to the small size of the Mg^{2+} ions compared to Ca^{2+} the ion exchange with water ions is slower for dolomite in the process of dissolution than for calcite [Fairchild and Treble, 2009].
The dissolution characteristics reveal a very important feature: dolomite can be dissolved also after the solution is saturated with respect to calcite [Fairchild *et al.*, 2000]. Due to the relative long time constant, only if the solution has enough time to dissolve calcite and dolomite, a significant contribution of dissolved dolomite is added to the drip water solution. This was discussed and summarised in Fairchild *et al.* [2000].
In the model dolomite dissolution is included for dry conditions. When little water is in the karst matrix, the water is not pushed downwards to the cave like it is in wet conditions, but the solution has enough time to dissolve dolomite.
The scheme for the mixing is shown in figure 5.8.

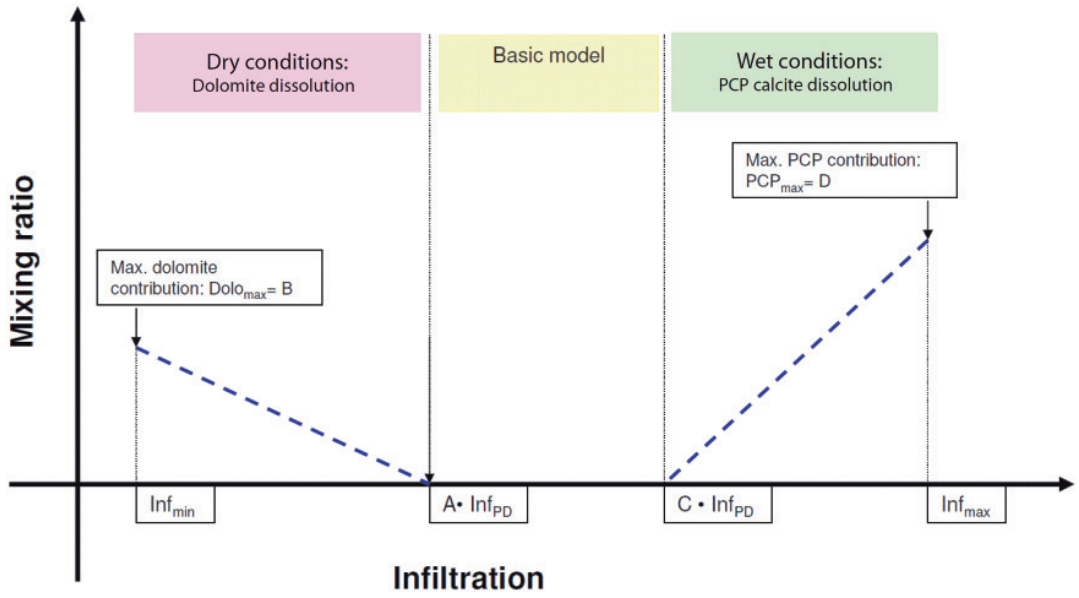

Figure 5.8.: Scheme of the extended Mg/Ca model. Under dry conditions dolomite is dissolved in the drip water solution while under wet conditions calcite which formed due to PCP is added to the solution. The x-axis represents the infiltration. The boundaries are defined in dependence on the present day amount of annual infiltration, Inf_{PD}. The parameters A, B, C, D must be determined in the model.

If the infiltration in the model is lower than a certain boundary (A·Infiltration$_{PD}$), infiltrating water dissolves dolomite. Below this boundary, the model assumes that a certain amount of the dissolved calcite is dolomite. The mixing reaches a maximum value (Dolo$_{max}$=B in figure 5.8) when infiltration is at the minimum value.
Unfortunately, determining parameters A and B is difficult. An experiment of Fairchild *et al.* [2000] showed that a solution is able to dissolve dolomite to calcite in a ratio of 0.2. However, the karst system is much more complex than the controlled conditions of a laboratory experiment. Since for the cave the ratio cannot be determined, 0.2 is set as a default value for B.
The boundary, A·Infiltration$_{PD}$, must be at a smaller infiltration value than the present day value, Inf_{PD}, as for the present day situation the basic model yields the correct measured Mg/Ca values (default value A=0.8 in figure 5.8).

5.4.2. PCP dissolution

In the basic Mg/Ca model PCP occurs, when the current amount of infiltration is smaller than the water capacity of soil and karst layer. If the capacity is reached or exceeded, PCP stops. The constant calcite precipitation in the karst matrix leads to a problem: the accumulation of calcite$_{PCP}$ would finally close the small fissures which the drip water uses on the way to the cave. For a constant stalagmite growth over thousands of years

it is necessary that this calcite is dissolved at some point and the fissures reopen.
For the dissolution of this calcite, the solution must arrive undersaturated at the layer where calcite_{PCP} exists. This can only happen, if the solution is not fully saturated with respect to calcite during dissolution of the host rock.
After saturation is reached more calcite can only be dissolved, when the pCO_2 of the surrounding air increases. However, the highest pCO_2 is found in the soil layer where plant activity produces pCO_2. The pCO_2 of the cave is lower and in the same order as the atmospheric CO_2 content. Air filled spaces in which PCP can occur must provide also low pCO_2. Otherwise no PCP could have taken place before in this area. This indicates that the solution is exposed to the highest pCO_2 in the soil layer and after this faces lower pCO_2 pressures on the path to the cave.
The only possibility for the dissolution of calcite_{PCP} are wet conditions when the soil water capacity is exceeded. The boundary for the mixture with a contribution of calcite_{PCP} to the drip water is therefore the soil water capacity (C=1.5 in figure 5.8).
Under wet conditions, undersaturated water can reach deeper karst layers due to a high downwards flux, where calcite_{PCP} has formed before. The solution can then dissolve calcite_{PCP}.
This calcite reveals a very low Mg/Ca ratio in contrast to the host rock due to the small partition coefficient. From the forward Mg/Ca model and section 5.3 the Mg/Ca ratio of calcite_{PCP} over the whole range of the sensitivity parameters can be calculated. The mean value is $Mg/Ca_{PCP}=8.3\cdot10^{4}$ ($Mg/Ca_{PCP\ min}=7\cdot10^{4}$ and $Mg/Ca_{PCP\ max}=11\cdot10^{4}$). Since the range is small compared to the host rock Mg/Ca the mean value is defined as the Mg/Ca ratio of calcite_{PCP} (for comparison: host rock Mg/Ca=0.052).
The upper mixing limit is the maximum infiltration where the contribution of calcite_{PCP} reaches at a maximum value (by default D=0.5 in figure 5.8).

5.4.3. Results of extended Mg/Ca model

The results for the Mg/Ca_{stal} sensitivity compared to the basic model are illustrated in figure 5.9. It is obvious that the Mg/Ca_{stal} range is strongly increased by the model extensions. In the range of infiltration, where the basic model (see figure 5.8) is applied, the old and the new model agree with each other. In drier conditions, the slope of Mg/Ca goes steeply upwards, since the contribution of dolomite leads to a higher Mg/Ca of the drip water. Under wetter conditions, the Mg/Ca ratio is reduced due to the small Mg/Ca ratio of calcite_{PCP} .
For different mixing coefficients, ϕ, the difference in the range of Mg/Ca_{stal} is less pronounced as in the basic model setup, because the effects of the dolomite-module and the PCP dissolution-module dominate the variations.
In a natural system the junction between the different situations which are represented in the model by the different model modules will be more smooth and less clearly defined. This should be kept in mind in the context of model inversion.

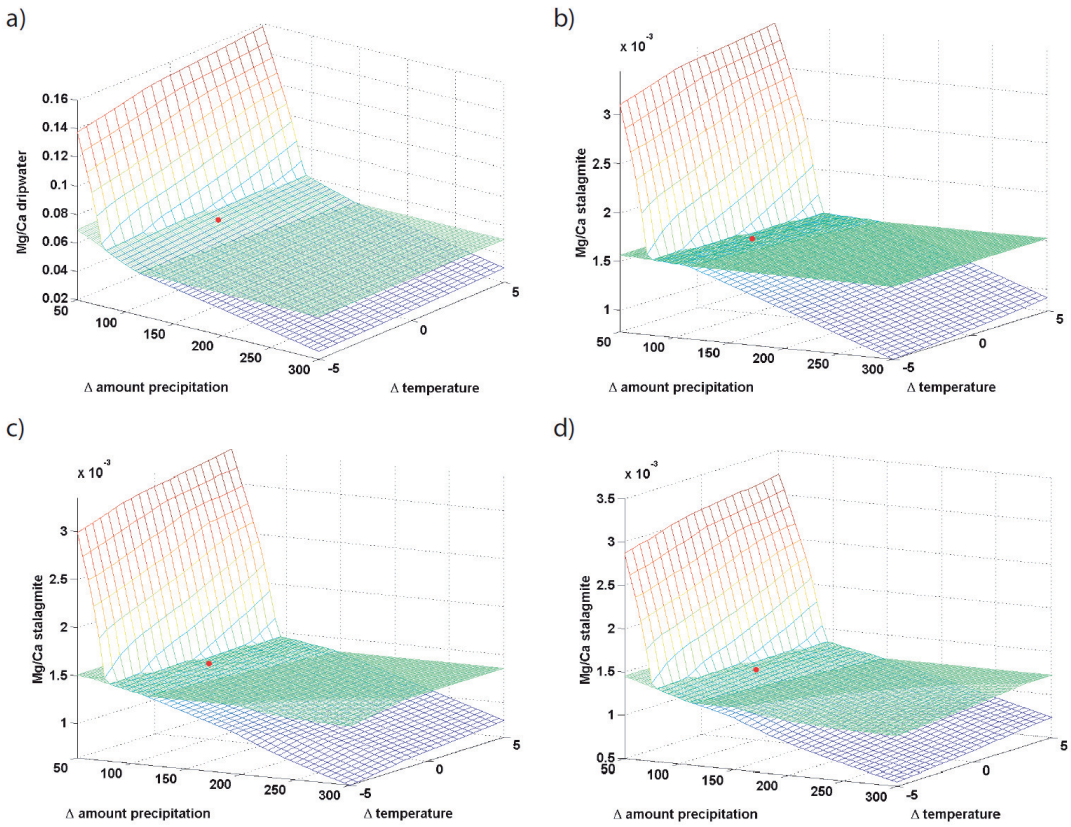

Figure 5.9.: Sensitivity on temperature and precipitation variations of the Mg/Ca ratio of drip water (a) and speleothem calcite (b)(ϕ=0.1), c) (ϕ=0.5), d) (ϕ=1)) of the basic model (green layer) and the extended model (multi-coloured layer). Temperature deviation is given in °C from the present day annual mean temperature T=10.5°C, precipitation in % from the present day amount (100%). The red dot represents present day condition.

6. Inverse Models

Forward models are an essential tool to understand palaeo archive proxies. The assessment of the parameters influencing the system leads to deeper insights and offers the potential to interpret the proxy in the context of palaeo climate research. For quantitative climate reconstructions it is necessary to reverse the forward model - a complicated task, as the models depend on a set of parameters but yield only one output parameter ($\delta^{18}O_{calcite}$ or $Mg/Ca_{calcite}$)). The modeller faces the classical problem of an underdetermined system of equations.
For the presented models the aim was to establish a model setup in which the output parameters ($\delta^{18}O_{calcite}$ and $Mg/Ca_{calcite}$) depend on two parameters: temperature and precipitation. All the other input parameters should be related to temperature or default values could be defined.
Deriving a temperature reconstruction from a stalagmite record by reversing the presented forward models can only be achieved, if the amount of meteoric precipitation is calculated simultaneously. This section presents two approaches how the inversion can be performed - a Dual-Proxy Approach which uses both models - the Mg/Ca model and the ODSM - and the Correlation Approach in which a relationship between temperature and precipitation permits the model inversion.

6.1. Model inversion: the Dual-Proxy Approach

The approach is based on the fact that the Mg/Ca ratio and the $\delta^{18}O_{calcite}$ value are measured along the growth axis. Therefore two stalagmite proxies which depend on temperature and precipitation are given for a specific depth which is equivalent with a point in time.
The sensitivity experiments showed how the proxies depend on temperature and precipitation. For a given calcite sample the $\delta^{18}O_{calcite}$ value as well as the Mg/Ca value can be achieved by a multitude of temperature-precipitation pairs. The advantage of the Dual-Proxy method is that the model finds the one temperature-precipitation pair which could have caused both, the measured Mg/Ca value and the measured $\delta^{18}O_{calcite}$ of the sample.

6.1.1. Procedure description

First, the values of Mg/Ca and $\delta^{18}O_{calcite}$ (matrices in figure 6.1) depending on mean annual temperature and annual precipitation are determined at the same, high resolution for both proxies.
Second, the stalagmite data is used. For one particular depth on the stalagmite's growth axis a pair of Mg/Ca and $\delta^{18}O_{calcite}$ exists. An algorithm searches for the respective Mg/Ca and $\delta^{18}O_{calcite}$ values in the matrices including small tolerance values (0.05‰ for the $\delta^{18}O_{calcite}$ and 0.00001 for the Mg/Ca ratio) and derives the associated temperature-precipitation values. Next, the model compares the temperature-precipitation pairs derived from both sets and if a pair of parameters matches to both models, the temperature and precipitation pair is saved. If more than one matching pair is found, the mean value is given. The error of the value is calculated by a Monte-Carlo experiment, in which the same procedure is applied 2000 times during which the Mg/Ca and $\delta^{18}O_{calcite}$ matrices vary within the standard deviation, as presented in section 5.3.1 (for Mg/Ca) and section 4.3.2.4 (for $\delta^{18}O_{calcite}$).
Example. In figure 6.1 an example for one model run is illustrated. The example shows the calcite sample from BU4 in 1.2mm distance from top (age about 85 years) whose Mg/Ca value is 0.0015 and $\delta^{18}O_{calcite}$ =-5.64‰.
The $\delta^{18}O$ model was run in the basic setup and with $\phi = 1$. The Mg/Ca model yields slightly too high values for the modern $Mg/Ca_{calcite}$ (0.0002) with this mixing coefficient. This discrepancy is added as a constant offset for the model inversion.
Figure 6.1a) is the matrix for $\delta^{18}O_{calcite}$ depending on mean annual temperature and annual amount of precipitation. The red crosses show grid points with the value $\delta^{18}O_{calcite}$ =-5.64±0.05‰. The same is shown in figure 6.1b) (red crosses for the Mg/Ca value Mg/Ca=0.0015±0.0002. Figure 6.1c) represents the projection of the marked Mg/Ca and $\delta^{18}O_{calcite}$ values on the x-y-plane which are the associated axes for temperature and precipitation. The blue circles represent the possible temperature-precipitation pairs according to the $\delta^{18}O_{calcite}$ model for the specific $\delta^{18}O_{calcite}$ value. The red circles represent the possible temperature-precipitation pairs according to the Mg/Ca model. Two pairs of temperature and precipitation values are detected in this model run which are identical for both models (points where the red and the blue curve match). For the mean value follows: $T_{annualmean}$=-0.8°C (deviation from present day temperature) and $P_{annualmean}$=90% (from present day annual value). In this way the whole stalagmite record is analysed.

6.1.2. Model results

The presented routine was applied to stalagmite BU4. As the Mg/Ca values were determined in a higher spatial resolution than the $\delta^{18}O_{calcite}$ values, the same resolution in both data sets was achieved by averaging the higher resolution data of Mg/Ca over the intervals of the $\delta^{18}O$ data (here: 2mm intervals along the growth axis). The climate reconstruction resulting from this new stalagmite record for BU4 can be observed in figure 6.2.
The range of temperature variations is unexpectedly high for the Holocene (11°C peak to peak maximum). In figure 6.1 one can observe what is causing the large temperature range. The temperature-precipitation pairs bearing the same Mg/Ca value form

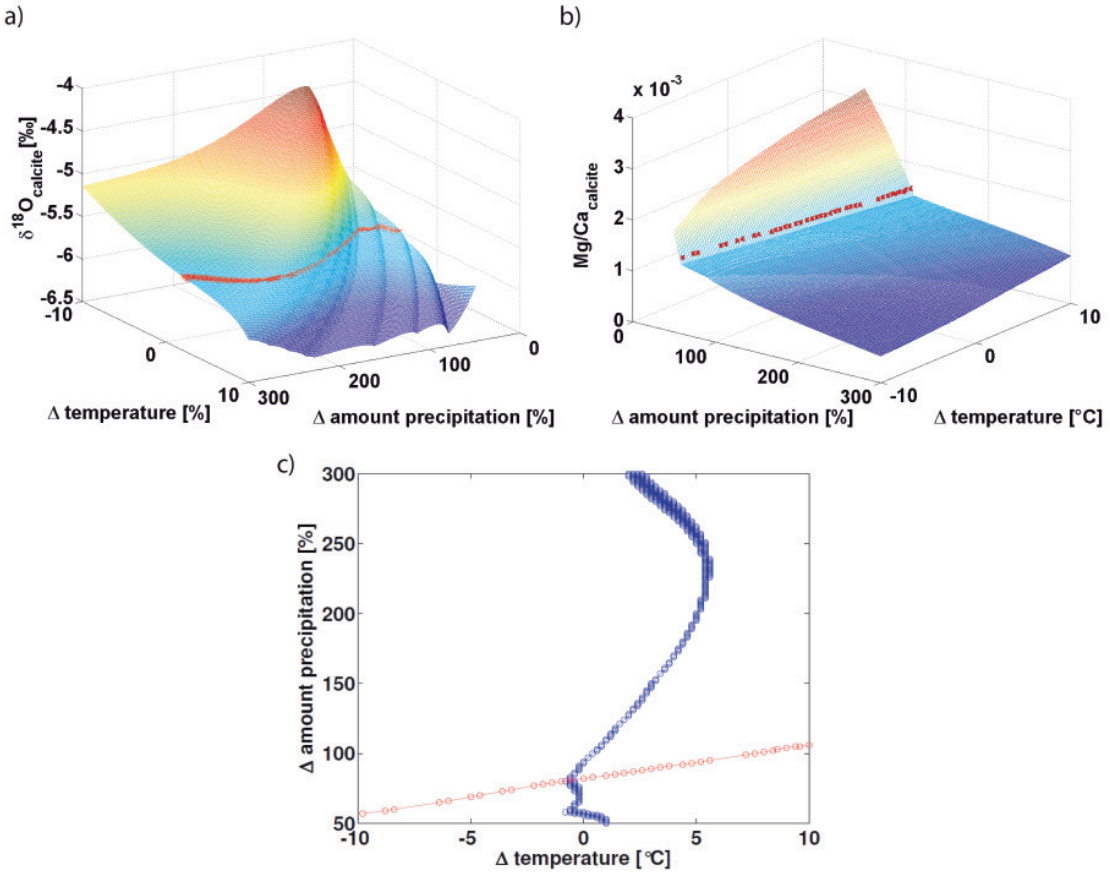

Figure 6.1.: Model realisation of the inverse model in the Dual-Proxy approach. For explanation see text in section 6.1.1

a line rather parallel to the temperature axis. Instead, the temperature dependence of Mg/Ca is rather low while its precipitation dependence is rather high (figure 6.1b). The $\delta^{18}O_{calcite}$ matrix is much more sensitive to temperature and the position of the respective $\delta^{18}O_{calcite}$ level determines the resulting temperature. Therefore, the slope of $\delta^{18}O_{calcite}$ with temperature can be assessed as the driver for the temperature reconstruction. If the $\delta^{18}O$ matrix had a steeper slope with temperature, the calculated temperature variations would diminish. Hence, the simulated temperatures reveal a clear correlation to the $\delta^{18}O_{calcite}$ record in contrast to the Mg/Ca record (figure 6.3). In contrast to the temperature reconstruction the reconstructed precipitation record shows rather small variations and the amount of precipitation are in most cases less than 100%. The reason is a soft general trend in the Mg/Ca record towards higher Mg/Ca ratios with increasing age (see figure 3.1). This trend is not assumed to be a real precipitation trend, because this would represent progressively drier conditions from present day to early Holocene. It is more likely, that this trend results from the progressive removal of loess bearing a high Mg^{2+} content, which was deposited during the last glacial (pers. communication Andrea Schröder Ritzrau, Jens Fohlmeister). Therefore, it is advisable to detrend the record. The values of the trend (linear regression) are,

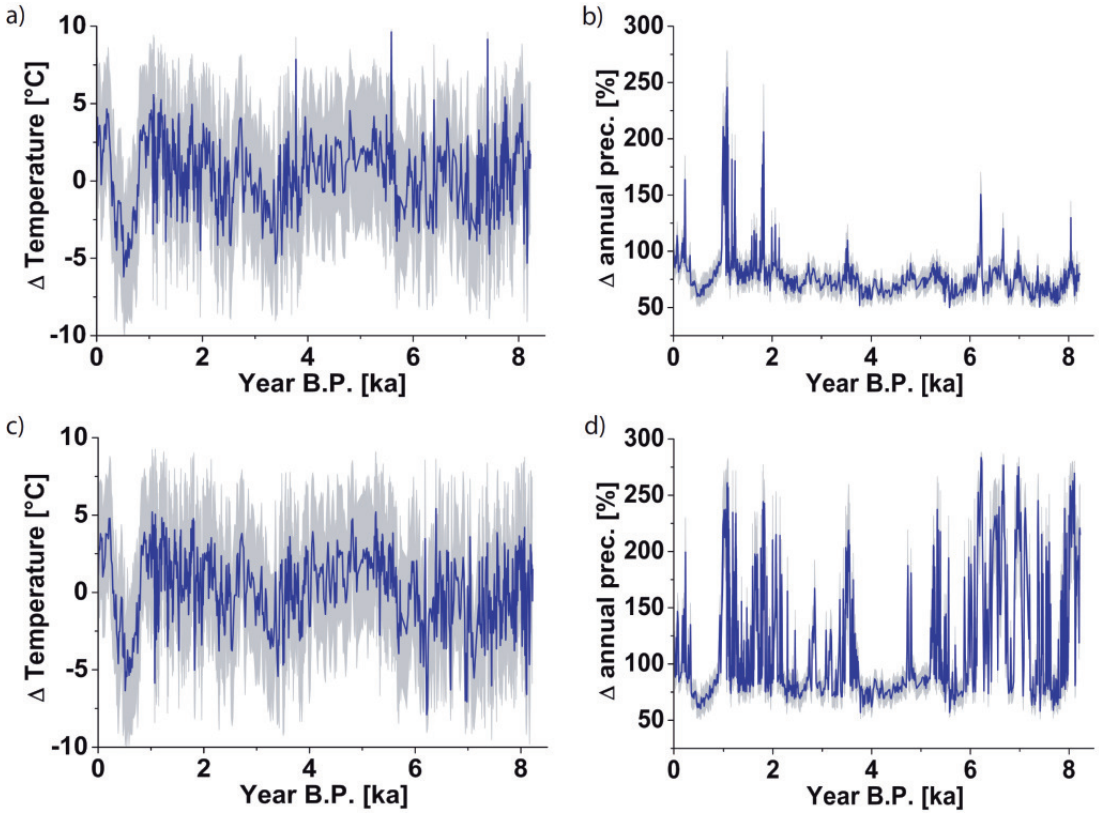

Figure 6.2.: Temperature (a) and c)) and precipitation (b) and d)) reconstruction according to the Dual-Proxy approach from stalagmite BU4. c) and d) show the results for the detrended Mg/Ca record. The 1σ-errors (grey shaded areas) are calculated using a Monte-Carlo simulation with 2000 runs.

therefore, subtracted from the measured values. Afterwards a constant offset is added to shift the mean value of the detrended record to the recent value. The results of this detrending can be observed in figure 6.2 c) and d). The precipitation record shows strong variations between 60% and 260%. In particular the early Holocene shows large short term variations[1]. This can be explained, since the Mg/Ca values are shifted to lower values towards the early Holocene by the detrending. In the lower part of the Mg/Ca matrix (figure 6.1), the slope becomes steeper with increasing precipitation. This explains the pronounced precipitation variance in the model results of the detrended Mg/Ca values. In the following the detrended record is used, since the trend may deliver false temperature and precipitation information otherwise.

6.1.3. Variance of the simulated temperature reconstruction

The presented temperature reconstruction is based on estimating sound values for the parameters describing the mixing with dolomite and $\text{calcite}_{\text{PCP}}$ (parameters A, B, C, D in

[1]For comparison: Annual precipitation values from Gütersloh (1837-1975) and Hannover (1856-2006) show variations about 50% for this short period compared to the Holocene scale.

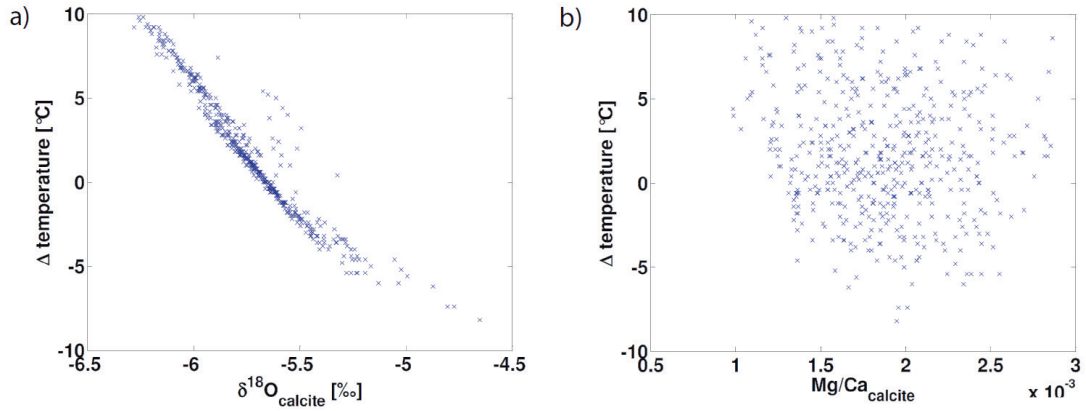

Figure 6.3.: The simulated temperature deviation in dependence with a) $\delta^{18}O_{calcite}$ and b) Mg/Ca ratio of the stalagmite.

figure 5.8). A and B represent the factor of present day infiltration, where dolomite and $calcite_{PCP}$ dissolution starts, respectively, while B and D define the fraction of dolomite and $calcite_{PCP}$ to the total amount of dissolved rock in the drip water, respectively . These parameters are afflicted with major uncertainties. Therefore the difference of the reconstructed temperatures must be analysed, if these parameters are changed. Table 6.1 shows the standard deviation of the simulated temperatures derived from BU4 depending on variations of the parameters. The standard deviation of the temperature time series changes to a very small extent, when the parameters A-D are varied.

Model configuration	**A** Infiltration boundary for dolomite contribution	**B** Maximum dolomite contribution	**C** Infiltration boundary for $\text{calcite}_{\text{PCP}}$ contribution	**D** Maximum $\text{calcite}_{\text{PCP}}$ contribution	Standard Deviation [°C]
Basic configuration	0.8	0.2	1.5	0.5	3.4
Small contribution	0.8	0.1	1.5	0.2	3.8
High contribution	0.8	0.4	1.5	0.7	3.5
Wide inf. boundaries	0.7	0.2	2.0	0.5	3.6
Narrow inf. boundaries	0.9	0.2	1.2	0.5	3.3

Table 6.1.: Variation of the standard deviation of the simulated temperature record from BU4 depending on the values for A, B, C, D in figure 5.8

6.2. Model inversion: the Correlation Approach

Another possibility to reduce the parameters of the $\delta^{18}O$ system in order to derive temperature information from the $\delta^{18}O_{calcite}$ record of a stalagmite is to find a relationship between the two parameters - temperature and precipitation. The method described in the following was published in Wackerbarth *et al.* [2010].
To define a relation between mean annual surface temperature and precipitation the dataset from the weather station close to Bunker Cave (Hagen Fley - DWD www.dwd.de) was analysed. Unfortunately such a general relationship could not be detected. However, the winter climate in the region of Bunker Cave reveals a relationship between winter temperature and the amount of winter precipitation. The correlation is positive and reveals a slope of 9%/°C (see equation 6.1, where R^2=0.21 and p=0.03)[2].

$$Precipitation_{winter} = 226.56(\pm 77.21) + 33.14(\pm 15.34) \cdot T_{winter} \tag{6.1}$$

This relationship might be linked to the North Atlantic Oscillation, NAO, (see section 2.7). The phenomenon was investigated by observations during the last two centuries and analysed with the help of proxy data for larger time scales (e.g. Trouet *et al.* [2009]). Though for present day the correlation is as described in equation 6.1, in former times the slope might have essentially changed.
The observed relationship can be used to reduce the degrees of freedom of the $\delta^{18}O_{calcite}$ system and to achieve a non-ambiguous correlation between $\delta^{18}O_{calcite}$ and temperature. Therefore the ODSM must be used in the setup described in section 4.3.2.5, which is the forward $\delta^{18}O$ model in which the precipitation is only varied in the winter season. In contrast, the Dual-Proxy Approach can be based on the basic model setup which varies temperature and precipitation identically for all months. This setup cannot be used in the Correlation-Approach, since the measured correlation between temperature and precipitation exists only for the winter season. If a relation between precipitation in winter (NDJFM) and the precipitation during the rest of the months existed, the correlation between winter temperature and winter precipitation could be applied also in the basic model setup. However, such a correlation was not detected in the weather service data. Therefore, the only option to run the ODSM is by varying only winter precipitation. The setup of this model mode was described in section 4.3.2.5.
Two factors encourage the use of this model setup for the reconstruction using the Correlation Approach: i) In contrast to the Mg/Ca system the $\delta^{18}O_{calcite}$ is highly sensitive to a change in the seasonality of meteoric precipitation, because it inherits the atmospheric signal through $\delta^{18}O_{prec}$. Therefore it is useful to reconstruct temperatures using a model setup which is able to grasp this seasonal variability. ii) The reduction to only the winter season leads only to small distortions, since this is anyway the season contributing most water to the annual amount of drip water.
The function which finally determines the resulting temperature from $\delta^{18}O_{calcite}$ values is established by calculating the $\delta^{18}O_{calcite}$ value for each temperature-precipitation value

[2]Note: In the following the slopes are given in %/°C. Mathematically this does not result in a linear function but an exponential. However, the descriptions of the slopes refer to the mean precipitation value. For example, in equation 6.1 9% corresponds to 33.14mm/T°C, which is actually the linear slope in the model implementation. The slope is in % to give a more descriptive value of the increase or decrease. % is easier to envision than mm/month.

pair (according to the slope of 10%/°C). This curve is shown in figure 6.4 e) and f) (black curve). In addition, the figure shows other slopes between $\delta^{18}O_{calcite}$ and temperature (the values range between 5%/°C and 30%/°C) in order to analyse the effect of a varying strength of the NAO system (see figure 6.4).
These curves yield a negative relationship between $\delta^{18}O_{calcite}$ (figure 6.4 e)) and surface temperature. This might not seem to be surprising, because the temperature gradient of the isotopic fractionation is negative. However, the gradient between surface temperature and $\delta^{18}O_{prec}$ which influences the drip water $\delta^{18}O$ value is positive. These gradients nearly compensate each other. In fact, the negative relationship between temperature and $\delta^{18}O_{calcite}$ originates here from the relationship between winter temperature and winter precipitation what changes the contribution of winter precipitation.

6.2.1. Discussion of the resulting $\delta^{18}O$ -temperature relations

First, I focus on the correlation between temperature and $\delta^{18}O_{drip}$ figure 6.4d). A temperature change causes two counteracting effects on the $\delta^{18}O_{drip}$. On the one hand lower temperatures result in decreasing amount of winter precipitation reducing the contribution of the isotopically lighter winter precipitation. Therefore, summer precipitation becomes more dominant and the $\delta^{18}O_{drip}$ value increases at lower temperatures. On the other hand the $\delta^{18}O_{prec}$ signal is decreased by lower temperatures resulting in lower isotopic composition of the drip water. For lower temperature the former effect prevails while for increasing temperature the latter effects dominates from a certain temperature value on. This pattern is then confronted with the negative temperature gradient in the fractionation between drip water and calcite, which ranges from 0.21‰ to 0.25‰ in the investigated temperature range. For the part, where the $\delta^{18}O_{drip}$ -temperature relationship shows a decreasing trend with temperature, both gradients intensify each other resulting in a steeper slope for $\delta^{18}O_{calcite}$ with temperature compared to the gradient occurring alone due to the fractionation. In the part in which the $\delta^{18}O_{drip}$ increases again with temperature, the slope between temperature and $\delta^{18}O_{calcite}$ becomes successively less steep until both gradients have the same absolute value. Under this condition the minimum value of the curve in $\delta^{18}O_{calcite}$ is reached. If the temperature increases further, the gradient between temperature and $\delta^{18}O_{calcite}$ (figure 6.4e) is positive. However, this is only the case for a rather high temperature deviation from today (+7.5°C for the curve yielded by 10%/°C).
The differences between the coloured curves are derived from the different correlation between temperature and precipitation. For 30%/°C, the $\delta^{18}O_{calcite}$ reacts more sensitive for the same temperature change as the curve which assumes 10%/°C to be the correlation between winter precipitation and winter temperature. For the same temperature variation the contribution of winter precipitation varies stronger resulting in a higher variation in the $\delta^{18}O_{cal}$. The higher the slope between winter temperature and winter precipitation, the steeper is the slope between temperature and $\delta^{18}O_{cal}$.
The feature that is shared by all the curves is the higher sensitivity for negative temperature changes. According to the model the response to decreasing temperatures in natural stalagmites should be more pronounced compared to increasing temperature conditions.

It should be noted, that the difference between kinetic and equilibrium fractionation is very small. The main difference is the offset between the types of fractionation discussed in section 5.2.2.

6.2.2. Model results

The coloured curves in figure 6.4 f) can be used to reconstruct temperature variations of the past. The used stalagmite $\delta^{18}O_{calcite}$ values are imported in a model routine and the temperature can be read out according to one of the curves in figure 6.4. However, it is possible that the slope between precipitation and temperature might have changed significantly in the past. In phases of a stronger NAO like pattern the slope between winter temperature and winter precipitation can for instance be 30%/°C.

In figure 6.5 simulated temperatures and precipitation values are shown using the $\delta^{18}O_{calcite}$ of BU4 under the assumption of 10%/°C and 30%/°C. Assuming 10%/°C seems advisable regarding the present day situation. In figure 6.5 a) the temperature reconstruction under this assumption is shown. The standard deviation of the time series is 1°C. The temperature reconstruction bears three different main uncertainties. i) The critical point concerning the modelling of kinetic fractionation in the ODSM is the relationship between drip interval and the amount of infiltration, which is poorly investigated and must be defined. If the relationship changes in time or if the system lacks any clear relationship between the parameters, the kinetic fractionation in the model can be over- or underestimated resulting in different temperature values. ii) The correlation between $\delta^{18}O_{prec}$ and surface temperature yielded by observational data might have changed in the past induced by a change in the synoptic pattern. In the model it is assumed to be constant. iii) The slope between winter temperature and winter precipitation is also defined to be constant over the whole period. This might not be a realistic assumption, but the only possibility to reconstruct temperatures for lack of knowledge of the circulation pattern in the past. If stronger westerlies featured periods in the past in which the slope between winter temperature and winter precipitation was higher, the variations of the reconstructed temperatures would diminish, because the variations in the $\delta^{18}O_{calcite}$ value can be ascribed to varying contribution of winter precipitation. Such a situation is illustrated in figure 6.5 d) and f). It is obvious that the temperature variation is smaller (standard deviation = 0.5°C), if the assumed slope is 30%/°C, due to the enhancement of the precipitation variability.

Error estimation The uncertainty of the reconstructed temperature and precipitation values is calculated by a Monte-Carlo simulation with 2000 runs. The errors occurring in the model are as in the forward model evoked by the linear regression between monthly mean temperature and humidity, $\delta^{18}O_{prec}$ and the monthly mean temperature at 2 p.m.. The curves (see figure 6.4) in this simulation are calculated 2000 times with different values for the regressions (arbitrary choice of the values within the bounds of the standard deviation according to the Monte-Carlo theory) and the resulting temperatures are determined according to the respective curve. The mean and standard values for each data point are calculated afterwards.

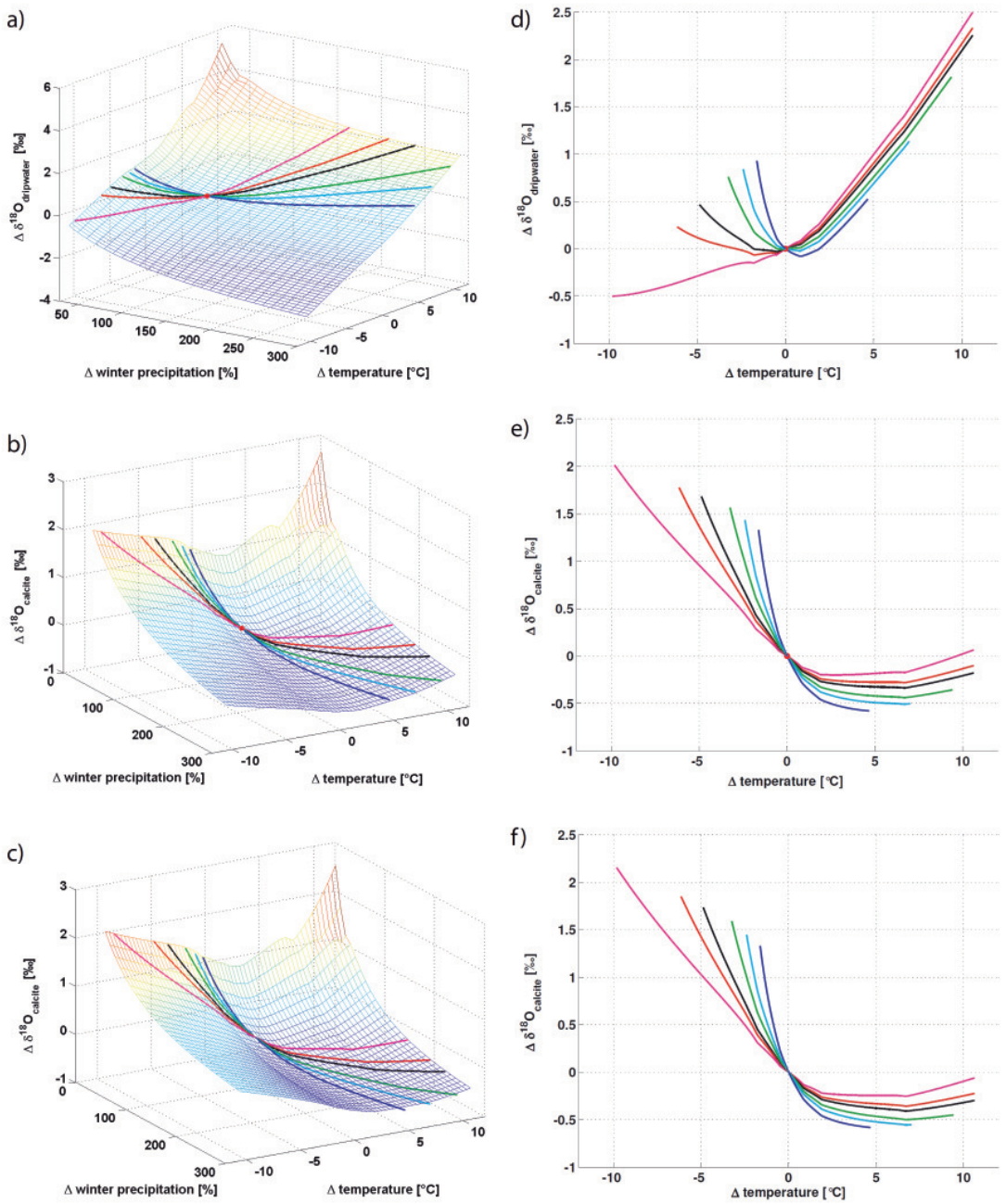

Figure 6.4.: Forward ODSM including the curves for different correlations between winter temperature and precipitation (30%/°C: dark blue, 20%/°C: light blue, 15%/°C: black, 10%/°C: black, 8%/°C: red, 5%/°C: magenta). a) shows the $\delta^{18}O_{drip}$ dependence on temperature and precipitation and d) the curves again and the resulting temperature dependence. The same is plotted for $\delta^{18}O_{calcite}$ assuming equilibrium fractionation in b) and e) and for $\delta^{18}O_{calcite}$ assuming kinetic fractionation in c) and f).

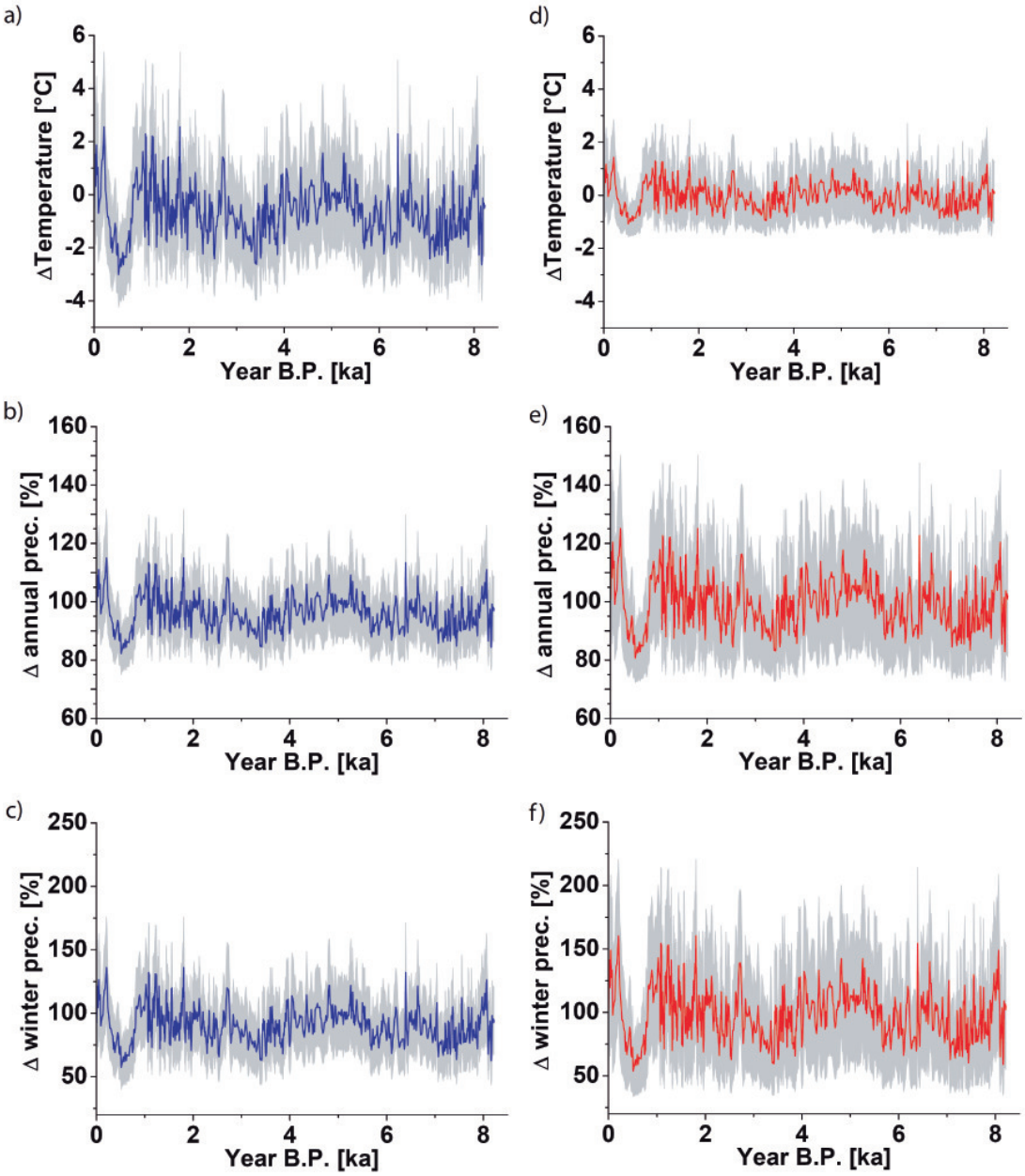

Figure 6.5.: Simulated temperature and precipitation reconstructions using the $\delta^{18}O_{calcite}$ data from BU4 for two slopes between winter temperature and winter precipitation (a)-c): 10%°C and d)-f): 30%/°C). a) und d) show reconstructed temperatures, b) and e) the annual amount of precipitation and c) and f) show the resulting winter precipitation in % of the respective present day amount. The grey shadowed areas correspond to 1σ uncertainties.

6.2.3. Results for other stalagmites

The model inversion showed that temperature reconstructions have several uncertainties and the temperature information of one single stalagmite must be handled with care. The evaluation of the simulated temperature can be improved, by applying the inverse model to two or more stalagmites from the same cave or the same geographical region. By comparison of the resulting temperature histories real temperature signals can be distinguished from $\delta^{18}O$ variations which originate from parameters which are not directly linked to climate (mixing characteristics, flow conditions, pCO_2 values). Similarities in the simulated temperature values indicate a real climate signal.
The temperature reconstruction using BU4 can be tested applying two other stalagmites - BU1, also from Bunker Cave [Riechelmann, 2010], and AH1 [Niggemann *et al.*, 2003] from Atta Cave.
The curve describing the relation between $\delta^{18}O_{calcite}$ and temperature must be adjusted to the respective stalagmite by selecting the climate input parameters from the closest DWD station and the parameters describing the calcite precipitation (pCO_2 of cave air and soil air, drip interval) from cave monitoring. Table 6.2 comprises the applied data.

Parameters	**BU1**	**AH1**
Climate Data		
DWD station	Hagen Fley	Attendorn
$\delta^{18}O_{prec}$ (T) relation	Bunker Cave Monitoring	Bunker Cave Monitoring
Cave Data		
drip interval	410s	300s
residence time	long	long
pCO_2 of soil air	as BU4	as BU4
pCO_2 of cave air	as BU4	as BU4
cave temperature	9.5°C	10.5°C

Table 6.2.: Input values of the Correlation Approach for the application to BU1 and AH1

For the stalagmite from Atta Cave - AH1 - climate data from the DWD (German weather service www.dwd.de) station in Attendorn close to the cave are used. The actual relation between $\delta^{18}O_{prec}$ and temperature at Atta Cave could not be established during the monitoring period (March 1997 - December 1997). Therefore, Wackerbarth *et al.* [2010] concluded that the correlation derived for Bunker Cave is the best choice. Drip interval (d_{std}=300s) and mean cave temperature for calibration can be retrieved from the literature [Niggemann, 2000] (T=9.5°C - 1°C colder than Bunker Cave). From this work it can also be derived that the drip site of AH1 reveals neither a seasonal cycle in $\delta^{18}O_{drip}$ nor in the Ca^{2+} content indicating a well mixed water body and, therefore, a long residence time (one or more years). For the calculation of kinetic fractionation a problem is the determination of the pCO_2 of cave air and soil air required. No measurements were carried out during the cave monitoring. Wackerbarth *et al.* [2010] assumed that the pCO_2 values from Bunker Cave can also be regarded as being representative

for Atta Cave.
For the temperature reconstruction using BU1, the same parameters as for BU4 can be used except the average drip interval over the monitoring period from the associated drip site (d_{std}=410s) which is shorter than for BU4.

With these adjustments, the $\delta^{18}O_{calcite}$ (T) curves can be calculated for each stalagmite. As performed for BU4 the established models can be tested by comparing the modelled $\delta^{18}O_{calcite}$ value for ΔT=0°C and the measured value.
AH1 shows an isotopic composition of -5.88‰ at the uppermost calcite sample [Niggemann, 2000]. The simulated value is -5.69‰ which is a very good estimation of the true value. The temperature reconstruction curve is biased by 0.2‰ to match this value at ΔT=0°C.
For BU1 the youngest $\delta^{18}O_{calcite}$ value is 0.2 ka old and its isotopic composition is -5.97‰. The model yields this value for the present day conditions. Due to the lack of knowledge of the present day $\delta^{18}O_{calcite}$ value of BU1 the $\delta^{18}O_{calcite}$ -temperature relationship used to reconstruct temperatures is not shifted.
The results of the different temperature reconstructions are presented in figure 6.6.

6.2.3.1. Temperature reconstructions

The individual temperature reconstructions are plotted in figure 6.7 together with the stalagmite $\delta^{18}O_{calcite}$ records. The temperature variations reconstructed from AH1 and BU1 agree with the reconstruction from BU4 for the respective periods. The younger part of BU1 reveals a higher variability than the older part. A pattern, that is also present in the BU4 temperature reconstruction.
In principle the three different stalagmites should show the same temperature history, since the caves are close to each other (<30km). However, not every aspect of the isotope system is covered by the presented model (for example: the true variance of the drip interval in the past). Therefore, the $\delta^{18}O_{calcite}$ records differ slightly from each other. BU1 and BU4 are very similar. AH1 in contrast shows a slightly different basic level of the $\delta^{18}O_{calcite}$ values and some different features in the pattern. Regarding this, the model run results in remarkably similar surface temperatures.
The climate of the region of the past seems to have experienced rather cold and dry[3] conditions from 500 to 1000 years before present as well as at 3.5 ka and around 6 ka. Rather warm phases seem to have prevailed from 1 ka to 3ka and from 3.5 ka to 5.5 ka. These tendencies are a reliable feature of the temperature reconstruction. Absolute temperatures can only be derived, if the correlation between winter temperature and winter precipitation is known. Very high temperature variations e.g. in the phase between 1ka and 2 ka suggest a pronounced variation in the slope between winter temperature and winter precipitation that could indicate a strong NAO-like circulation pattern.

[3] Due to the correlation between winter temperature and winter precipitation lower temperatures coincide with drier conditions and vice versa.

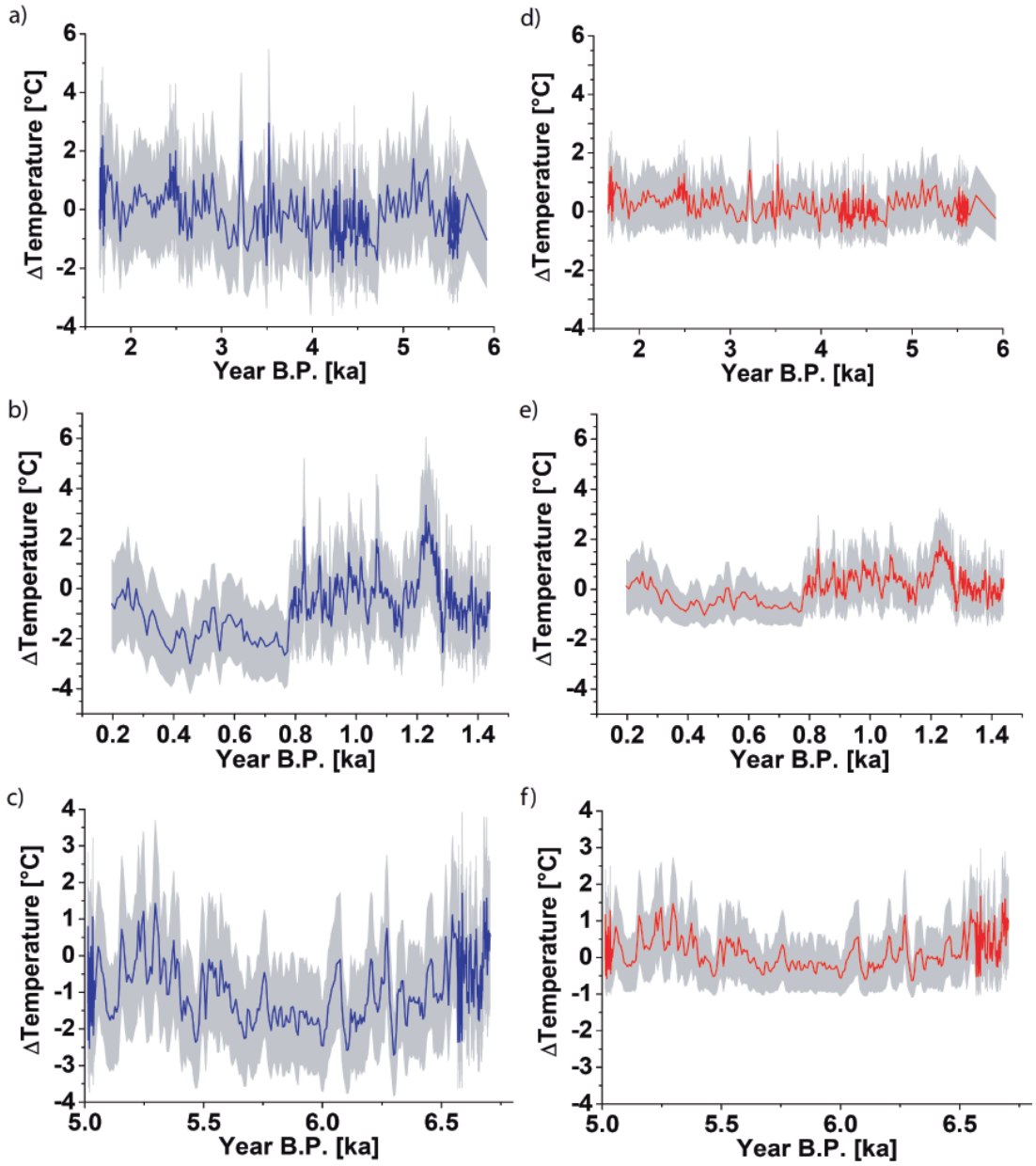

Figure 6.6.: Temperature reconstruction from AH1 (a and d), the younger part of BU1 (b and e) and the older part of BU1 (c and f) for the assumed correlation between winter temperature and winter precipitation of 10%/°C (blue curves) and 30%/°C (red curves). The error is estimated by a Monte-Carlo-Simulation with 2000 runs (see text).

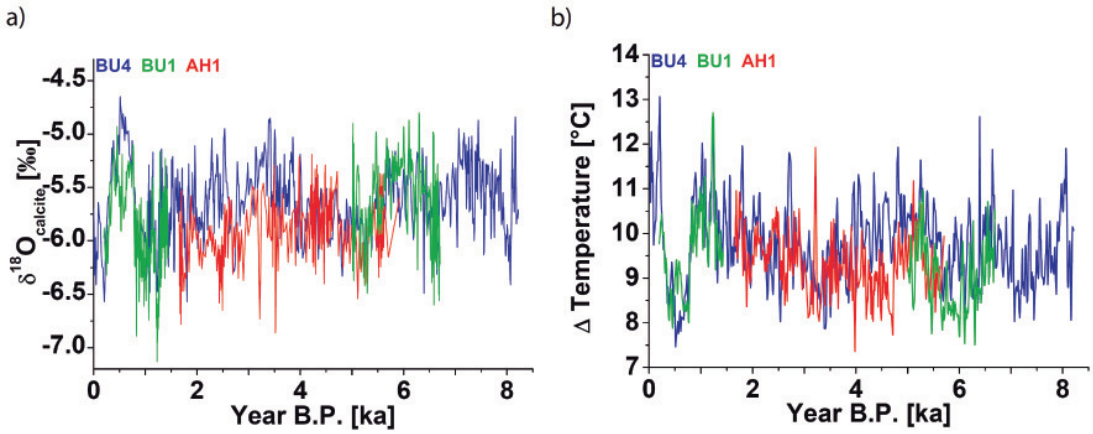

Figure 6.7.: a) $\delta^{18}O_{calcite}$ and b) reconstructed temperature from of BU1, AH1 and BU4 for the assumed correlation between winter temperature and winter precipitation of 10%/°C. The stalagmite records are smoothed by a 20 years moving average.

6.3. Comparison: Correlation- vs Dual-Proxy Approach

Both presented approaches to reconstruct temperatures from $\delta^{18}O_{calcite}$ signals of stalagmites have advantages and disadvantages.
The Correlation Approach does not need many additional input parameters for the forward model, except the assumption of a general correlation between winter temperature and winter precipitation. However, it is not realistic, that this correlation was constant in the past resulting in an uncertainty that cannot be neglected.
The Dual-Proxy Approach yields an independent pair of temperature and precipitation for each $\delta^{18}O_{calcite}$ value with the help of a second stalagmite proxy - the Mg/Ca ratio. The disadvantage of this model is that in contrast to the $\delta^{18}O$ signal which is mainly influenced by surface parameters the Mg/Ca ratio is controlled by multiple parameters in the highly complex karst system. Fortunately the parameters can be calibrated with the drip water Mg/Ca ratio and other observed drip water values. However, it is also possible that substantial modification in the soil and karst layers changed the system in the past that would make an adjustment of the parameters in the Mg/Ca model necessary.
Beside the different procedures to determine the mean annual temperature, the models are based on different assumptions.
The Correlation Approach is based on the $\delta^{18}O$ forward model in the configuration that varies only winter precipitation instead of the annual precipitation to suit the meteoric conditions at the cave location. This reduction was necessary, since the correlation between temperature and precipitation are only defined in winter months (NDJFM), and allowed, because the main infiltration occurs anyway in this season.
In contrast, the Dual-Proxy approach relies on the forward model in the setup which varies temperature and precipitation identical and to the same extent for all the months. The reduction to variations only in the winter month is not necessary in this model setup. Though the approaches differ in many features, the simulation should lead finally to similar temperature reconstructions. Figure 6.8 shows the comparison of the two resulting temperature time series for the BU4 record.

The temperature variations resulting from the Dual-Proxy approach are obviously larger than from the Correlation Approach. However, the similarity of the time dependent pattern is remarkable.
Figure 6.8 a) and b) show the comparison between the inverse models for the undetrended Mg/Ca record of BU4. The precipitation record is significantly lower in the Dual-Proxy Approach (blue) than in the Correlation Approach (red). The comparison of the temperature simulation based on the detrended Mg/Ca record are shown in figure 6.8 c) and d). The temperature variation changes slightly due to the detrending, but still reveals the same pattern as the temperature reconstruction based on the Correlation-Approach. The general precipitation level is shifted to a higher level and shows more variation than the Correlation-Approach based precipitation reconstructions.
Temperature. The differences in the amplitude of the simulated temperatures can be explained by the different gradients $\Delta T(\delta^{18}O)$ in the model approaches. For the Correlation Approach the $\Delta T(\delta^{18}O)$ gradient results from the correlation between winter precipitation and winter temperature (see figure 6.4). The range of 1.5‰ of $\delta^{18}O$ values

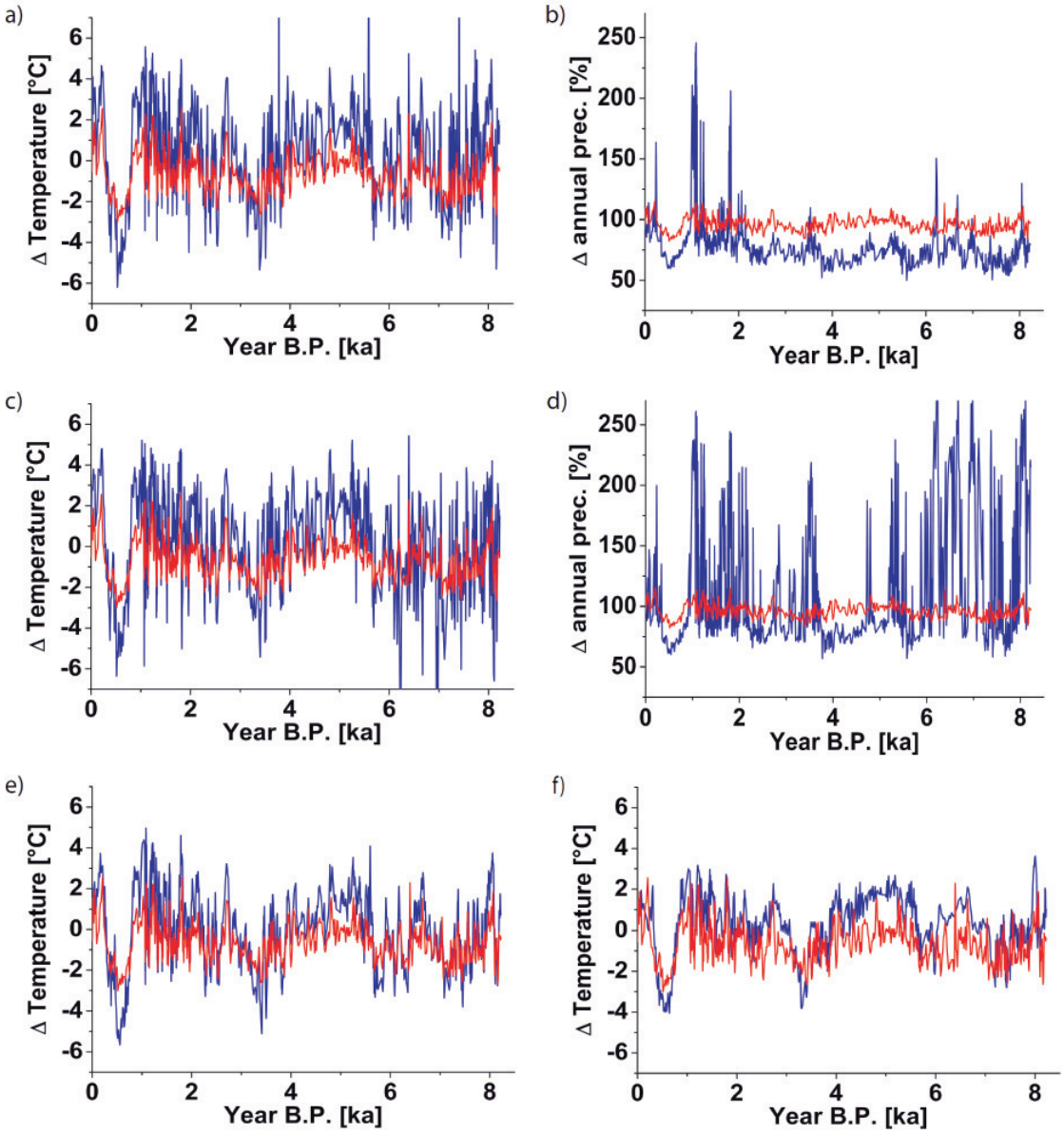

Figure 6.8.: Simulated temperature (a) and precipitation (b) reconstructions using the $\delta^{18}O_{calcite}$ data from BU4 in the two different model inversion approaches (Correlation Approach: red, Dual-Proxy Approach: blue). c) and d) show the same for the detrended Mg/Ca record. e) and f) illustrate the results of c) if the input data for the Dual-Proxy Approach are smoothed by a 10-point (e) and 20-point (f) moving average.

result in 4°C temperature variations (figure 6.9 red squares) for the curve representing a correlation of 10%/°C between winter temperature and winter precipitation. For the Dual-Proxy Approach, the range of resulting temperature variations of 1.5‰ is about 11°C (figure 6.9 blue squares), which is much steeper than in the Correlation Approach. The temperature gradient of the $\delta^{18}O$ signal in the Correlation Approach might be a more realistic representation of the true relationship. Mangini *et al.* [2005] found the

same relationship by establishing a temperature calibration between $\delta^{18}O_{calcite}$ values of an Alpine stalagmite and corresponding temperatures.
Hence, a particular $\delta^{18}O$ variation leads to much higher temperature changes in the Dual-Proxy-Approach.
Precipitation. The simulated precipitation varies also stronger in the Dual-Proxy Approach. It should be kept in mind that the Dual-Proxy Approach yields true annual precipitation values, while the Correlation Approach keeps the precipitation fix between April and October. This explains the obvious difference between the precipitation simulations and suggests that the Mg/Ca might be a better estimate for the precipitation due to the independence of the precipitation determination. The results including the detrended Mg/Ca record yield the more realistic values (identical to section 6.1.2), since the low precipitation values including the undetrended Mg/Ca record are an effect of the general trend towards higher Mg/Ca values with older ages due to the depletion of loess.. At least the model results should be compared and discussed for a climate record of a certain time.

In principle, the Dual-Proxy Approach is a very sensitive system, since a multitude of parameters influence the Mg/Ca ratio in addition to climate parameters. Therefore, it can be useful to carry out a smoothing of the measured stalagmite data, before they are used as input for the temperature reconstruction. This reduced the natural variation of the input data, especially in case of the Mg/Ca ratio which might not be grasped by the model. In figure 6.8 e) and f) the temperature deviations from both approaches are presented in which the input data for the Dual-Proxy Approach are smoothed by a 10-point running mean (10 Mg/Ca or $\delta^{18}O_{calcite}$ values in the averaging window containing in average 85 years) and 20-point running mean. In this configuration the temperature deviation agree with the reconstruction of the Correlation Approach for positive deviations from the present day temperature.
Both models agree in the general, negative relationship between surface temperature and the $\delta^{18}O_{calcite}$ from stalagmites. In addition, the model results show the same warmer and colder periods, though the absolute temperature reconstruction is afflicted with uncertainties.

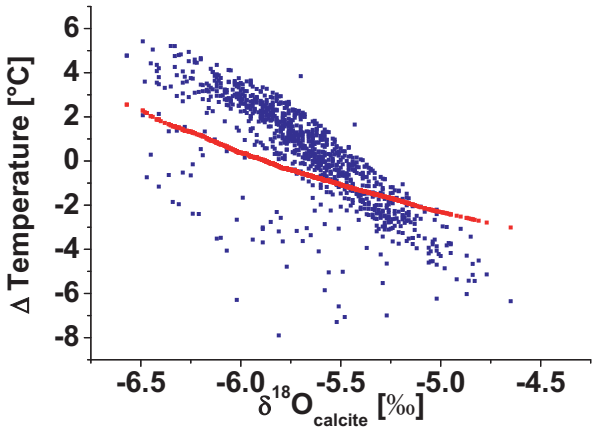

Figure 6.9.: The simulated temperature depending on corresponding $\delta^{18}O_{calcite}$ input value of the Correlation Approach (red) and Dual-Proxy Approach (blue).

7. Forcing the ODSM with ECHAM5-wiso

In the previous sections the ODSM was applied as a forward model to analyse the influence of different parameters on $\delta^{18}O_{drip}$ and $\delta^{18}O_{calcite}$ as well as an inverse model to derive temperatures from existing $\delta^{18}O_{calcite}$ record of stalagmites. The model inversion had to assume that the correlation between winter temperature and winter precipitation was constant in the past. The inverse model obeys the terms of the forward model see section 4.3.2.5, in which climate conditions of each month depends on the others. It is not possible in this model setup to identify a different seasonality (for example a particular wet spring) from the $\delta^{18}O$ record of the stalagmite except more or less winter influence. However, this is probably one of the driving factors of the $\delta^{18}O_{calcite}$ system. To include this in the analyses a cooperation was established between the Alfred-Wegener-Institut (AWI) and the DAPHNE Forschergruppe. At the AWI a state-of-the-art atmospheric general circulation model was enhanced by explicit isotope diagnostics (ECHAM5-wiso, Werner *et al.* [2011]). The output parameters of this model (temperature, precipitation, evapotranspiration and $\delta^{18}O_{prec}$) can be used as input parameters for ODSM which calculates the resulting $\delta^{18}O_{drip}$ and $\delta^{18}O_{calcite}$ according to the input parameters. This approach allows to abandon the inverse modelling and analyse the $\delta^{18}O$ record of stalagmites with a rather comparative technique. With the output parameters from ECHAM5-wiso as input parameters for the ODSM, the $\delta^{18}O_{calcite}$ value of a stalagmite for any time and place all over the world can be simulated. By comparing the simulated and the measured $\delta^{18}O_{calcite}$ value from this time, the climate setup (ECHAM5-wiso output) can be analysed and variations between different time slices understood.
However, it is not advisable to apply this approach to a cave without knowledge of the present-day cave system. The present day situation is needed to evaluate, if the model approach is a valid representation of the climate regime and cave system. Therefore the approach is first applied for present day and with the insights of this experiment expanded to the past.

7.1. Present day experiment

7.1.1. Included caves

The approach to replace observed measurement data by simulated climate values is tested at seven European caves which provide a comprehensive cave monitoring ($\delta^{18}O_{drip}$ and $\delta^{18}O_{calcite}$ of modern calcite samples, cave temperature) and climate observations (temperature, precipitation, $\delta^{18}O_{prec}$). The present-day test aims to identify the caves in which the approach works well and can be applied for past times. A compilation of geographic position, mean annual temperature, mean annual amount of meteoric precipitation, weighted mean $\delta^{18}O_{prec}$, mean $\delta^{18}O_{drip}$ and $\delta^{18}O_{calcite}$ of modern calcite

samples is shown in table 7.2 and table 7.1. For more details see the respective references (table 7.1) and appendix A.
For comparison the ECHAM5-wiso output for the respective caves is also given in table 7.2.

Cave	**Lat.**	**Long.**	**Altitude**	$\delta^{18}\mathbf{O_{drip}}$	$\delta^{18}\mathbf{O_{calcite}}$
Soylegrotta (Norway) Lauritzen and Lundberg (1999)	66.55°	13.93°	100-200m	-10±0.23‰ 1991-1992	-7.33‰
Korallgrottan (Sweden) Sundqvist et al. 2007	64.89°	14.16°	540-600m	-12.02±0.41‰ 2005-2006	-9.41‰
Tartair Cave (Scotland) Fuller et al. (2008)	58.14°	-4.93°	300-500m	-7.09±0.26‰ 2003-2005	-5.2±0.35‰
Bunker Cave (Germany) Riechelmann et al. (in press)	51.37°	7.66°	100m	-7.92±0.28‰ 2003-2009	5.92±0.19‰
Katerloch (Austria) Boch et al. (2010)	47.25°	15.55°	900m	-8.7±0.1‰ 2005-2007	-6.3‰
Giazzera Cave (Italy) see appendix A	45.85°	11.09°	900-1300m	-9.5±0.24‰ 2002-2003 2006-2008	-6.7‰
Clamouse Cave (France) Frisia et al. (2002)	43.70	3.61	75m	-6.2 1999-2001	-4.9‰

Table 7.1.: Cave locations and compilation of isotope data from monitoring programs. Further information about the caves can be found in appendix A and the respective references.

7.1.2. ECHAM5-wiso

ECHAM5 is the fifth generation of an atmospheric general circulation model. It was developed at the Max-Planck-Institute in Hamburg (Germany). It was thoroughly tested under present-day conditions (e.g., Roeckner *et al.* [2003] and Roeckner *et al.* [2006]) and used for the last Intergovernmental Panel on Climate Change assessment [Randall *et al.*,

2007]. By the work of Joussaume *et al.* [1984], Jouzel *et al.* [1987] and Hoffmann *et al.* [1998] the ECHAM5 model has been enhanced by a water isotope module in the model's hydrological cycle allowing an explicit simulation of water isotopes in the entire hydrological cycle, from ocean evaporation through cloud condensation and precipitation (rain- and snowfall) to surface water runoff.
On a global scale, the ECHAM5-wiso simulation results are in good agreement with available observations of the isotopic composition of precipitation, both on an annual as well as on a seasonal time scale. For more details on the isotopic enabled ECHAM5-wiso model see Werner *et al.* [2011].

ECHAM5-wiso was implemented to performed an experiment for present day conditions (1956-1999 in a monthly resolution) with a two years spin-up time. The surface forcing and boundary conditions represent observed monthly sea-surface temperatures and sea-ice cover (as in the Atmospheric Model Intercomparison Project (AMIP)-style forcing, [Gates *et al.*, 1999]). The isotopic composition of the ocean is set to the observed modern value (global gridded dataset compiled in LeGrande and Schmidt [2006]). The atmosphere is left free to evolve.
It is important to note, that the modelled climate parameters for a month cannot be directly compared to observed values from this particular month as a consequence of the evolution of the atmosphere. The monthly pattern will change slightly depending on the starting month of the model calculation. However, the long term mean values and variations of the climate output are a robust parameter of the model and should be preferred in comparison with observational data.
The presented ECHAM5-wiso experiment was carried out in a relatively high resolution (T106L31), which describes a resolution of approximately 1.1° by 1.1° and 31 layers in the vertical. Additional information can be found in Langebroek *et al.* [in press].

7.1.3. Forcing realisation

The ODSM is used in the forward model setup. In section 4.2 the ODSM was forced with meteorological data from a weather service station. In this section the weather and isotope data are replaced by the ECHAM5-wiso output data. The output is supplied in a monthly resolution leading to a monthly resolution of the simulated $\delta^{18}O_{drip}$ and $\delta^{18}O_{calcite}$ values. The residence time of the water in the soil and karst layer can be defined in this setup. It consists of two components: i) the mixing time, defining how much monthly water parcels are mixed in soil and karst and ii) the transition time which describes how long it takes for a water parcel to travel from surface to the cave. The mixing time results in a smoothing of the $\delta^{18}O_{prec}$ signal while the transition time leads to a temporal shift of the signal. In the context of this application the transition time is not important, since only mean values are compared between measured and observed $\delta^{18}O_{calcite}$ values instead of the pattern of a time series. The mixing time is important because it determines the variance of the $\delta^{18}O_{drip}$ signal. This parameter can be calibrated to the observed variance in the $\delta^{18}O_{drip}$ data, though the problem remains that the modelled $\delta^{18}O_{drip}$ is in general much smoother than the observed data, because the ODSM cannot grasp the short term variance of the drip water. The mixing time is

therefore set to a default value of 48 months, but it should be kept in mind how the variance of the simulated drip water $\delta^{18}O$ value changes, if the mixing time is varied.
For the ODSM forcing two sets of experiments were performed. In one forcing setup (Setup 1 "ECHAM") the mean monthly temperature, the monthly amount of precipitation and $\delta^{18}O_{prec}$ as computed by ECHAM5-wiso are used as input. In the second setup (Setup 2 "Thornthwaite") the evapotranspiration is replaced by a calculated value using the equation of Thornthwaite and Mather [1957]. The amount of infiltrating water depends then on temperature, latitude and a temperature-dependent heat index. In this context this equation is preferred to Haude's equation Haude [1954], because the humidity and temperature at 2 p.m. and the vegetation type required for Haude's equation are not supplied by ECHAM5-wiso. These parameters must be known, if the model should be applied to caves worldwide. Therefore, the Thornthwaite equation is used in this application.
The ODSM assumes equilibrium fractionation, since the true kinetic fractionation requires parameters, which are not given for all the caves. In the discussion of the results this subject is commented on.

General comment The ECHAM5-wiso output is supplied and calculated in a resolution of 1° x 1° per grid box and corresponds in general roughly to the measured data sets. Before conclusions can be drawn, which setup matches best the $\delta^{18}O$ measurements, the fact has to be considered, that substantial differences between modelled and observed data may occur (see table 7.2). Especially the amount of precipitation and related $\delta^{18}O_{prec}$ depend strongly on the topographic position of the cave in the grid box. These small scale spatial variations can be accounted for by adjusting the ECHAM5-wiso output values for a particular cave by adding the offset between the long term climatic observations at the cave location and the long term mean of the ECHAM5-wiso output values table 7.2. This adjustment is done for the mean annual temperature, the annual amount of precipitation and the precipitation weighted mean $\delta^{18}O_{prec}$ for each cave according to the respective difference between measured and simulated values. No adjustment is applied for the simulated seasonal cycle of these variables.
The experiments help to evaluate, which setup seems to represent true climate conditions at a cave's location and how the model approach must be applied for past times experiments under the assumption that the discrepancy is a constant offset occurring due to the geographical position of the cave in the grid box.

7.1.4. Local adjustments of the ECHAM5-wiso results

As discussed in the section before the input adjustment of the ODSM can help to understand which setup is the best representation of the cave conditions. To understand the resulting shift of the simulated mean $\delta^{18}O_{drip}$ and $\delta^{18}O_{calcite}$ values, the sensitivity of $\delta^{18}O_{drip}$ and $\delta^{18}O_{calcite}$ to $\delta^{18}O_{prec}$, temperature and precipitation are discussed in the following section. As an example the sensitivities are displayed for Bunker Cave in figure 7.1.

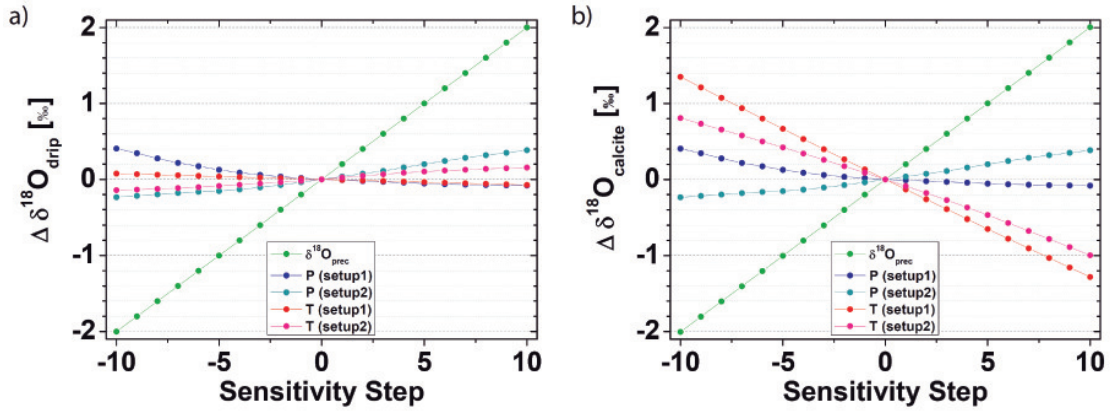

Figure 7.1.: Sensitivity of $\delta^{18}O_{drip}$ and $\delta^{18}O_{calcite}$ to temperature, precipitation and $\delta^{18}O_{prec}$. Each parameter is varied in a certain range: temperature from -5°C to +5°C, precipitation from -50mm/month to +50mm/month and $\delta^{18}O_{prec}$ from -2‰ to +2‰. The respective parameter shift is added to the whole time series and the ODSM recalculates the mean $\delta^{18}O_{drip}$ (a) or $\delta^{18}O_{calcite}$ (b) with this modified data set. Note, that this figure shows the sensitivity with respect to the standard experiment (centre dot).

$\delta^{18}O_{prec}$ sensitivity A shift of the $\delta^{18}O_{prec}$ can be regarded as an offset. Each month's $\delta^{18}O_{prec}$ is varied to the same extent. The size of the isotope fractionation during evapotranspiration does not depend on the initial $\delta^{18}O$ value. The resulting mean annual drip water $\delta^{18}O$ is therefore shifted to the same extent as the $\delta^{18}O_{prec}$.

Temperature sensitivity The temperature sensitivity is very different in Setup 2 compared to Setup 1. The reason is that in Setup 2 the evapotranspiration depends on temperature, while in Setup 1 the evapotranspiration is a fix output value of the ECHAM5-wiso model. In this setup the $\delta^{18}O_{drip}$ value depends only on temperature due to the enrichment during evapotranspiration.
In setup 2, however, the temperature determines the amount of evapotranspiration and through this the ratio of infiltration to precipitation, which is the dominant factor in the enrichment during evaporation (see figure 4.2).
The sensitivity of $\delta^{18}O_{drip}$ is positive at each location, although the absolute gradient differs slightly. This originates from the non-linear function describing the evapotranspiration. Compared to the $\delta^{18}O_{prec}$ or precipitation sensitivity the temperature sensitivity of $\delta^{18}O_{drip}$ is rather small (see figure 7.1).
The fractionation from drip water to speleothem calcite (equation 4.7) has a temperature gradient of about -0.23‰/°C. Hence, the temperature sensitivity of $\delta^{18}O_{calcite}$ is affected by this gradient (see also figure 7.1b).

Precipitation sensitivity The influence of a changing amount of precipitation is complex. Two mechanisms must be distinguished:

- **Change of the seasonal infiltration pattern.** If the monthly mean precipitation amount decreases by an absolute amount, the smaller infiltration in summer

experiences a stronger relative change than the amount of winter infiltration. This shifts the weight to the winter season. In this case $\delta^{18}O_{drip}$ will be more depleted.

- **Effect on isotopic enrichment during evapotranspiration.** A decrease in precipitation may increase the $\delta^{18}O_{drip}$ due to the enrichment during evapotranspiration caused by diminishing infiltration/precipitation ratio.

These two effects have opposite consequences and counteract each other. Therefore the particular situation at the cave must be considered to estimate which effect prevails.

	Model results Annual mean	1σ standard deviation	**Observational Data**	**Applied Adjustment**
Soylegrotta				
P [mm]	1120	180		
T [°C]	0.2	0.7	2.7 (1966-1989)	+2.5
$\delta^{18}O_{prec}$ [‰]	-10.7	0.6	-9.8	+0.9
ET [mm]	440	40		
T cave [°C]				+2.5
Koralgrottan				
P [mm]	1000	110	860 (1961-1990)	-140
T [°C]	-0.5	0.8	1 (1961-1990)	+1.5
$\delta^{18}O_{prec}$ [‰]	-12.4	0.7	-13.7 (1975-1988)	-1.3
ET [mm]	340	20		
T cave [°C]			2	+2.5
Tartair				
P [mm]	870	130	1900 (1971-2000)	+1030
T [°C]	7.7	0.4	7.1 (1971-2000)	-0.6
$\delta^{18}O_{prec}$ [‰]	-8.1	0.5	-7.1 (2003-2005)	+1
ET [mm]	540	50		
T cave [°C]			7.1	-0.6
Bunker				
P [mm]	1140	140	900 (1978-2007)	-240
T [°C]	8.4	0.7	10.5	+2.1
$\delta^{18}O_{prec}$ [‰]	-7.7	0.6	-7.7 (2003-2009))	
ET [mm]	600	30		
T cave [°C]			10.5	+2.1
Katerloch				
P [mm]	750	150	870 (1973-2004)	+120
T [°C]	8.5	0.7	8 (2006-2008)	-0.5
$\delta^{18}O_{prec}$ [‰]	-9	1	-8.8 (1973-2004)	+0.2
ET [mm]	540	50		
T cave [°C]			6	-2.5
Giazzera				
P [mm]	910	160	970 (1992-2004)	+60
T [°C]	10.9	0.7	13.3 (1992-2004)	+2.4
$\delta^{18}O_{prec}$ [‰]	-7.1	0.7	-8.7 (1997-2007)	+0.6
ET [mm]	610	50		
T cave [°C]			8.5	-2.4
Clamouse				
P [mm]	760	120	600 (2003-2007)	-160
T [°C]	11	0.6	14.5 (1997-2007)	+3.5
$\delta^{18}O_{prec}$ [‰]	-6.4	0.5	-5.8	+0.6
ET [mm]	560	50		
T cave [°C]			14.5	3.5

Table 7.2.: Compilation of ECHAM5-wiso results and observational climate data for each cave. Behind the observational data the period of observation is given. The last column shows the difference between modelled and observed data, which is used in our adjusted model simulation (see section 7.1.4)

7.2. Results

In the following section the simulated $\delta^{18}O_{drip}$ and $\delta^{18}O_{calcite}$ is described for the seven caves. To understand the spatial European pattern of $\delta^{18}O_{drip}$, the European pattern of the $\delta^{18}O_{prec}$ signal is discussed first.
The results are then discussed for both, the original and the adjusted ECHAM5-wiso output values.

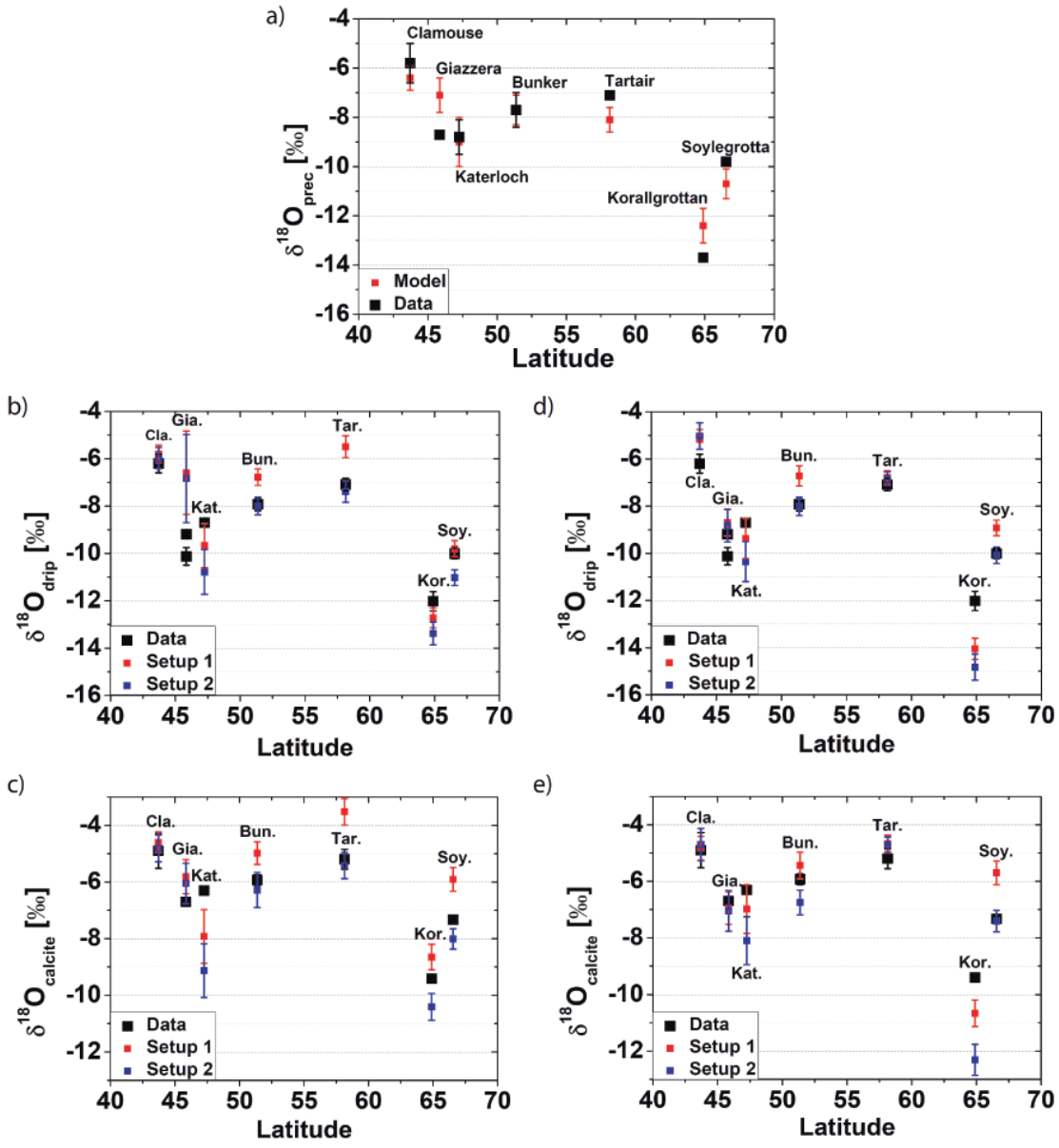

Figure 7.2.: Comparison of observational data (black) and model results (red: Setup 1, blue: Setup 2) for each cave for a) $\delta^{18}O_{prec}$, b) $\delta^{18}O_{drip}$ c) $\delta^{18}O_{calcite}$ d) $\delta^{18}O_{drip}$ using adjusted input parameters and e) $\delta^{18}O_{calcite}$ using adjusted input parameters.

7.2.1. Results of unadjusted input values

7.2.1.1. δ^{18}O of precipitation

The results of simulated $\delta^{18}O_{prec}$ are displayed in figure 7.2a). The pattern can be understood, when the three main influences on $\delta^{18}O_{prec}$ are considered. Two processes influence the isotopic composition of an air mass by: i) a change of the temperature in the air mass influencing the isotopic fractionation during condensation and ii) the rain-out effect which describes the fact that a successive removing of the formed water droplets in the air mass leads to isotopic depletion of the remaining air mass since the heavier species of the oxygen isotopes is enriched in the droplets. These two processes reflect in the isotope effects described by [Mook, 2006], i) the temperature effect, referring directly to a depleted $\delta^{18}O_{prec}$ signal with colder surface temperatures, ii) the altitude effect describing the isotopic depletion, when an air mass is lifted to higher altitudes due to cooling of the air mass accompanied with a rain-out effect, iii) the latitude-effect by which an air mass depletes with increasing latitude due to lower temperatures and iv) the continental effect describing the depletion of an air mass through successive rain-out on the path from the coast across landmasses.
To summarise, in principle the $\delta^{18}O_{prec}$ value at a cave location should be depleted with decreasing surface temperatures (increasing latitudes), increasing distance from the coast and increasing altitudes and vice versa.
In the next section the actual δ^{18}O pattern measured at the caves is discussed and afterwards compared to simulated values.

Observed $\delta^{18}O_{prec}$. The observed data in figure 7.2a) from **Soylegrotta** and **Korallgrottan** (high latitude, cold surface temperature) show depleted $\delta^{18}O_{prec}$. Korallgrottan is more depleted compared to Soylegrotta, since Korallgrottan is located more inland than Soylegrotta, leading to additional depletion through the rain-out effect at Korallgrottan.
Tartair Cave is comparably close to the ocean (the source of precipitation) as Soylegrotta, but the mean annual temperature is about 6°C warmer than in Soylegrotta. Therefore the measured $\delta^{18}O_{prec}$ value should be heavier - as displayed in figure 7.2a).
The observed $\delta^{18}O_{prec}$ value for **Bunker Cave** is identical to Tartair Cave, despite the annual temperature which is about 3.5°C warmer at Bunker Cave. However, Bunker Cave is not directly at the coast like Tartair Cave. Thus, precipitation depletes on the path from ocean to Bunker Cave counteracting the temperature effect.
Though **Katerloch Cave** lies farther south than Bunker Cave, the location is at a rather high altitude (≈1000m). An air mass depletes during its way upwards to the cave. Hence, the $\delta^{18}O_{prec}$ signal should be depleted. In addition the mean annual temperature is colder than at Bunker cave and the location is farther from the ocean - two effects that increase the depletion of the $\delta^{18}O_{prec}$.
Giazzera Cave is located at the same altitude as Katerloch Cave. Surface temperature is about 5°C warmer at Giazzera Cave. Therefore the $\delta^{18}O_{prec}$ should be higher than in Katerloch Cave. However both value are nearly the same.
The $\delta^{18}O_{prec}$ at **Clamouse** shows the highest observed value. The temperature is high at the cave and it is very close to the Mediterranean. In addition to high temperature, low altitude and latitude this could enrich the $\delta^{18}O_{prec}$ signal. A Mediterranean influence

yields higher $\delta^{18}O_{prec}$ values, since the Mediterranean Sea is isotopically heavier than the Atlantic ocean due to high evaporation rates from the relatively small water basin compared to the Atlantic ocean. Additionally little mixing and exchange of Mediterranean water masses with the oceans occur [Lachniet, 2009].

Simulated $\delta^{18}O_{prec}$. The comparison between simulated and observed values must be done with some caution since the temporal interval of the observation is in some cases rather short. Only for Bunker Cave, Katerloch Cave and Clamouse Cave the variation could be given for periods longer than 10 years. For Bunker Cave and Katerloch Cave the standard deviation of the annual weighted $\delta^{18}O_{prec}$ is 0.7‰, suggesting that the variation might be in this range also for the other caves.
In general the expected mean $\delta^{18}O_{prec}$ pattern is also displayed in the simulated $\delta^{18}O_{prec}$ values with some small differences.
For **Soylegrotta** the simulated $\delta^{18}O_{prec}$ is too low which might originate from simulated annual mean temperatures (table 7.2), which are 2.5°C lower than the observed data leading to higher depletion.
For **Korallgrottan** the simulated $\delta^{18}O_{prec}$ value is too high compared to observed data. The reason could be an underestimation of the continental effect depleting the $\delta^{18}O$ signal of the air mass on the transport to the cave.
The modelled $\delta^{18}O_{prec}$ value at **Tartair Cave** is again too low, while for **Bunker Cave** and **Katerloch Cave** the modelled values agree well with the data.
The $\delta^{18}O_{prec}$ at **Giazzera Cave** is heavier than the monitoring data, which could possibly be caused by a pronounced influence of the Mediterranean in the model. For **Clamouse Cave** the influence seems to be present, though the simulated temperatures are 3.5°C too low resulting in slightly lower $\delta^{18}O_{prec}$ values at the cave's location.
However, if the assumption is correct, that the variation of the observed values lies at about 0.7‰, all the modelled and observed values agree in the range of their errors.

7.2.1.2. $\delta^{18}O$ of drip water and calcite

Two main factors decide on depletion or enrichment of the $\delta^{18}O_{drip}$ with respect to $\delta^{18}O_{prec}$, which are closely linked to evapotranspiration and infiltration.

- Evapotranspiration enriches a water parcel isotopically and can shift the annual mean $\delta^{18}O_{drip}$ towards heavier $\delta^{18}O$ values compared to precipitation
- The seasonality of infiltration biases the $\delta^{18}O$ signal towards the months with highest contribution to the annual drip water. For the relevant caves this is a shift towards lower $\delta^{18}O$ values.

Which factor prevails depends on the evaporation rate in each month.

Simulated $\delta^{18}O_{drip}$ and $\delta^{18}O_{calcite}$ - Setup 1 ECHAM5-wiso In most caves (except Katerloch and Korallgrottan) the mean annual $\delta^{18}O_{drip}$ (figure 7.2 b) (red dots)) is heavier than the corresponding $\delta^{18}O_{prec}$. The enrichment during evaporation dominates

the bias towards the colder, isotopically lighter months in these caves. In Korallgrottan and Katerloch Cave it is the other way round.
This pattern passes on to the respective $\delta^{18}O_{calcite}$ values (figure 7.2 c) (red dots)). The range of $\delta^{18}O_{calcite}$ compared to $\delta^{18}O_{drip}$ for the different caves is smaller than in $\delta^{18}O_{drip}$, because the isotopic fractionation from drip water to calcite is anticorrelated to temperature resulting in smaller enrichment in warmer caves and larger enrichment in colder caves.

Simulated $\delta^{18}O_{drip}$ and $\delta^{18}O_{calcite}$ - Setup 2 Thornthwaite Although the pattern of $\delta^{18}O_{drip}$ is similar to Setup 1, the absolute $\delta^{18}O_{drip}$ values in Setup 2 are lower than in Setup 1 for every cave and also lower than the observed $\delta^{18}O_{drip}$ value (except Giazzera Cave). The difference originates from the ET_{pot} values in the different setups.
As an example the values for evapotranspiration per month from Setup 1 and Setup 2 and the resulting infiltration at Bunker cave are illustrated in figure 7.3 a). For the other caves the absolute, monthly values are different, but the general behaviour is the same except for Giazzera and Clamouse, where the annual patterns of evapotranspiration in Setup 1 and Setup 2 are similar to each other.

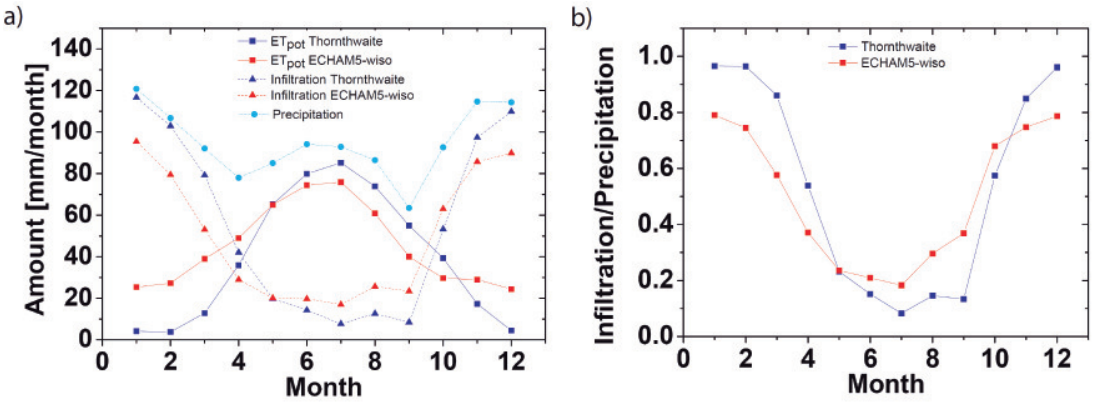

Figure 7.3.: a) Seasonal cycle of precipitation, infiltration and evapotranspiration (ET_{pot}) at Bunker Cave as computed by ECHAM5-wiso or after Thornthwaite. b) Ratio of infiltration to precipitation using ECHAM5-wiso or Thornthwaite evapotranspiration.

The infiltration calculated from Thornthwaite (Setup 2) is higher from November to April and lower from May to October than in Setup 1. The weight on the winter season and the resulting shift to lower $\delta^{18}O$ value is therefore more pronounced in Setup 2. The resulting drip water $\delta^{18}O$ is subsequently lighter than in Setup 1.
In figure 7.3 b) the ratio of infiltration to precipitation determining the degree of isotopic enrichment during evaporation is given. The lower the ratio, the more enriched is the remaining water parcel. It is obvious that in the month with highest infiltration rates representing the highest contribution to the annual mean drip water (winter, early spring, late autumn) the ratio is higher in Setup 2 than in Setup 1. This is an additional explanation why the $\delta^{18}O_{drip}$ from Setup 1 is more enriched than the drip water $\delta^{18}O$ from Setup 2.

The $\delta^{18}O_{calcite}$ signal in Setup 2 reveals the same pattern as $\delta^{18}O_{drip}$ identically to Setup 1.

7.2.2. Results of adjusted input values

Table 7.2 compiles the comparison between modelled and observed temperature, precipitation and $\delta^{18}O_{prec}$ values. In the last column the parameters are shown, which are used for the ECHAM5-wiso output adjustment. The results are presented in figure 7.2 d) and e).
If the simulated $\delta^{18}O_{drip}$ value does not match the observed drip water $\delta^{18}O$ values, two reasons can cause the discrepancy.

- The seasonal pattern of infiltration might be wrong. Too heavy simulated $\delta^{18}O_{drip}$ values correspond to an overestimated weight of the warmer season while too low $\delta^{18}O_{drip}$ values indicate a stronger influence of the colder season.
- The enrichment of the water parcel during evapotranspiration might be overestimated. The part of the Rayleigh fractionation (equation 4.3) that describes the evaporation uses as enrichment factor by Majoube [1971], which is defined as the enrichment during evapotranspiration from an open water parcel. The evaporation from the upper soil layer might be smaller due to mixing with soil water or the characteristics of the soil. This could be a major problem in warmer regions, since evaporation rates are higher than in colder regions.

The seasonality of infiltration and the seasonal pattern of evapotranspiration are the most likely factors for wrong $\delta^{18}O_{drip}$ values after the adjustment. In the following paragraphs the results of the adjusted models will be discussed in this context.

Simulated $\delta^{18}O_{drip}$ After the adjustment of the input parameters Setup 2 seem to simulate the measured $\delta^{18}O_{drip}$ values slightly better than Setup 1.
Four cave drip water $\delta^{18}O$ values (Soylegrotta, Tartair Cave, Bunker Cave, Giazzera Cave) are calculated correctly using Setup 2. However, in case of Tartair Cave and Giazzera Cave Setup 1 also yields good results. In addition Setup 1 prevails at Katerloch Cave. For Korallgrottan and Clamouse Cave the measured value can neither be simulated by Setup 1 nor 2.
If one setup is clearly the better choice at a certain cave, this means that the seasonal pattern of infiltration is better represented in this setup, which is the case for the caves where only one setup is able to simulate the drip water $\delta^{18}O$ value. If both setups yield approximately the same $\delta^{18}O_{drip}$, this indicates that the seasonal pattern of evapotranspiration is rather similar. For the warm caves this is indeed the case (Giazzera and Clamouse). For Tartair Cave the setups agree in their simulated $\delta^{18}O_{drip}$ value. This is not caused by similar evapotranspiration pattern, but due to the extremely high amount of precipitation per year. Some mm per month of evapotranspiration more or less do not have too much consequence for the amount of infiltration.
These three cases indicate that the model setups are equivalent either in a warm climate

where the evapotranspiration pattern of the setups is similar or for caves where the amount of precipitation is very high.
To assess the reason why for Clamouse Cave and Korallgrottan the simulated $\delta^{18}O_{drip}$ is still wrong is complicated. The seasonal infiltration pattern could be the reason or the cave system can bear some features not included. These caves should be handled with care and it must be kept in mind that there is an offset between measured and simulated values, if a past time experiment is applied to one of the caves.

Simulated $\delta^{18}O_{calcite}$ The simulated $\delta^{18}O_{calcite}$ is presented in figure 7.2e). From the literature of the respective caves (see appendix A) it can be assumed that for the colder caves (Soylegrotta, Korallgrottan, Tartair Cave and Katerloch Cave) the calcite precipitation took place near equilibrium. For Bunker Cave as well as for Giazzera and Clamouse Cave significant offsets between the predicted equilibrium $\delta^{18}O_{calcite}$ value are observed. For Bunker Cave the gap between equilibrium and kinetic $\delta^{18}O_{calcite}$ value can be closed using the model for kinetic fractionation as presented in section 4. For the other caves the required input parameters are not known. However, it should be kept in mind that the modelled equilibrium value is lower than the true kinetic value.
For the caves, in which calcite precipitation happens very close to equilibrium conditions, the respective setup which was the best representation of the measured $\delta^{18}O_{drip}$ is also the best for the calcite $\delta^{18}O$ value (Soylegrotta, Tartair Cave, Katerloch Cave).
For Bunker Cave the measured $\delta^{18}O_{calcite}$ value is enriched compared to the modelled equilibrium value from Setup 2. This does not mean that Setup 1 should be preferred, since kinetic fractionation is known to occur there.
For Giazzera a kinetic offset is also visible. The $\delta^{18}O_{drip}$ measured in the cave is lower than the simulated value and must be lower also in the $\delta^{18}O_{calcite}$ as the simulated value. However, it is higher than the modelled $\delta^{18}O_{calcite}$. This shift can be attributed to kinetic fractionation.
The calcite $\delta^{18}O$ value from Clamouse Cave is apparently in a very good agreement with the simulated values. However, if the drip water $\delta^{18}O$ values are known, it is obvious that this is only a kinetic effect. This caves illustrates very impressively, that the present day study is a very helpful tool to evaluate the results of the model approach.

7.2.3. Conclusion and comment

The present day application of the model approach is an important test, if this comparative technique can help to analyse the $\delta^{18}O$ value as a climate proxy.
It is obvious that the main problem is the determination of evapotranspiration, since an adjustment is not possible. The present day study identifies caves in which the modelled conditions are a good representative of the true situation.
The best way how the presented approach can be used for climate research is first to apply the present day experiment to a cave to understand the differences between modelled climate and actual climate. Hereupon a simulated, artificial $\delta^{18}O_{calcite}$ record could be established, if the model output from ECHAM5-wiso were supplied as a time series of the simulated climate of the past. The comparison of the stalagmite and the simulated $\delta^{18}O_{calcite}$ record allows to draw conclusions about the climate of the past. An agree-

ment of both time series suggests that the ECHAM5-wiso output values of this time are close to the true climate parameters. A disagreement can indicate that significant changes in the fractionation between drip water and calcite influenced the stalagmite $\delta^{18}O_{calcite}$ value or the ECHAM5-wiso output values do not represent the true climate of this period. To identify, if the fractionation changes are the reason for the discrepancy between model and stalagmite $\delta^{18}O_{calcite}$ value, the study should rely on more than one stalagmite. The present day experiment showed that Soylegrotta, Tartair Cave, Bunker Cave, Katerloch Cave and Giazzera Cave are adequate caves for the application of such a study.
However, computation time of such a time series is expensive and long. Instead time slices can replace a transient time series. Unfortunately the growth periods of the stalagmites from the investigated caves are different and to find a time slice in which all stalagmites grew is almost not possible. McDermott *et al.* [2011] gave a comprehensive overview of European stalagmites, their growth periods and $\delta^{18}O_{calcite}$ values. From this set stalagmites can be selected which grew during the modelled time slice. However, these stalagmites are rarely accompanied with a monitoring of the parent cave. Without a cave monitoring it is hard to derive how the model approach must be applied to the cave.

7.3. 6k experiment

As discussed in the previous section, the approach to force the ODSM with ECHAM5-wiso output data should be applied to caves which provide a present day monitoring of cave environment and climate conditions for a better evaluation of the results. However, caves with a comprehensive monitoring are rare and in addition stalagmites from these caves do not offer calcite values from any given time slice in which the climatological and isotopic mean values are simulated by ECHAM5-wiso.
This problem can be approached by involving a set of stalagmites instead of one single speleothem. This helps to identify true climate signals from cave internal variations. In addition it is advisable not to focus on absolute $\delta^{18}O_{calcite}$ values but on relative values. Therefore, in this experiment stalagmites are used which grew at 6k as well as in modern times. The study yields the $\delta^{18}O_{calcite}$ difference between present day and 6k. If an offset resulting from kinetic fractionation exists for present day conditions between simulated and measured $\delta^{18}O$ values, it can be assumed that also in past times kinetic fractionation enriched the $\delta^{18}O_{calcite}$ value. The simulated $\delta^{18}O$ values would be too low in both cases even, if the climate parameters were modelled correctly. The comparison of relative values is therefore a tool to bypass this problem. However, it must be kept in mind that the kinetic fractionation might not be a constant offset.
In addition, an offset between absolute simulated and measured $\delta^{18}O_{calcite}$ values can originate from the discrepancy between the grid model values and the local conditions at the cave (as discussed before). Under the assumption that the offset between model and true climate parameter remains constant in time, the comparison of relative values is the best tool to compare model and data.

7.3.1. Studied stalagmites and measured $\Delta\delta^{18}O_{calcite}$

The study from McDermott (McDermott *et al.* [2011]) gives an excellent overview of European stalagmites, their growth periods and corresponding $\delta^{18}O_{calcite}$ values. From this compilation twelve caves where selected which supply $\delta^{18}O_{calcite}$ values from present day as well as from 6ka BP. The stalagmites are given at the end of this section in table 7.4. The difference of $\delta^{18}O_{calcite}$ (6k-PD) are illustrated in figure 7.4 (also table 7.4).
The snapshot at 6k of the COMNISPA record from the Spannagel Cave was calculated from Vollweiler [2010] in which an update of the first stalagmite record [Vollweiler *et al.*, 2006] was given.
The spatial, European pattern does not show a homogeneous behaviour. Some stalagmites (from Korallgrottan, Hölloch, Savi and Garma) reveal a strong depletion in their $\delta^{18}O_{calcite}$ value between 6k and 0k while others show a strong enrichment (Poleva, Crag, Carburangeli) and others are nearly on the same isotope level as present day.
For a time slice which differs clearly in the climate parameters from today (for example from the last Glacial) the isotope values were expected to show a consistent gradient to lower or higher values for the entire set of stalagmites (Cheng *et al.* [2009], Dykoski *et al.* [2005], Zhao *et al.* [2010]). However, the climate changes during the Holocene are not comparable with large scale variation as the last Glacial.
The arising question is, which climatological, hydrological or isotopic European pattern

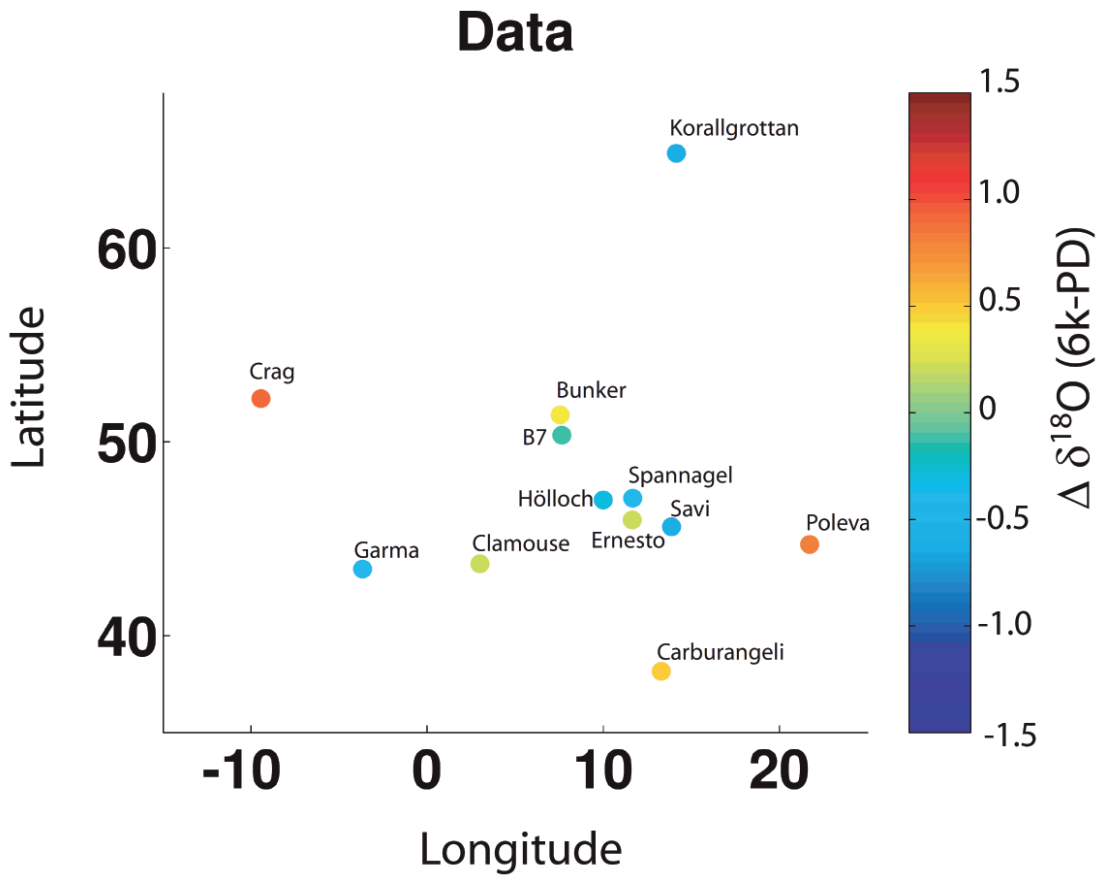

Figure 7.4.: $\Delta\delta^{18}O_{calcite}$ in ‰ between 6k and present day.

could explain the observed $\delta^{18}O_{calcite}$ values.
In this context the cooperation with ECHAM5-wiso can be enlightening and offer insights to climate analyses from stalagmites, which could otherwise not be detected.
In the following section the climate and isotope parameters which are simulated by ECHAM5-wiso are presented and the resulting $\delta^{18}O_{calcite}$ is shown in order to compare the modelled and observed $\delta^{18}O_{calcite}$ values.

7.3.2. ECHAM5-wiso setup

The present day experiment performed with the ECHAM5-wiso was forced with observed sea surface temperatures and the sea ice cover. For a model run from past times it is necessary to force the ECHAM5-wiso with a model for these parameters. Three different models are used for the coupled simulation: CCSM [Collins *et al.*, 2006], COSMOS (http://cosmos.enes.org/) and ECHO-G [Legutke and Voss, 1999]. From these models the mean values over 50 years were used as forcing for the 6k time slice.
In addition, the present day (PD) experiment differs from the 6k experiment in the insolation due to different orbital parameters and the concentration of green house gases in the atmosphere. The setup of the forcing is exactly as applied in the PMIP experiments (http://pmip2.lsce.ipsl.fr/ - see 'Experimental Design' and 'Boundary Conditions' for

the different forcings).

- **Present day experiment (mean 1956-1999)**
  - **CO_2** : 348ppm
  - **CH_4** : 1650ppb
  - **N_2O** : 306ppb
  - **Orbital configuration**: depending on the year (1956-1999)
- **Mid Holocene experiment (6k)**
  - **CO_2** : 280ppm
  - **CH_4** : 650ppb
  - **N_2O** : 270ppb
  - **Orbital configuration**: based on year 6k

With these experimental setup Petra Langebroek from the AWI in Bremerhaven run the ECHAM5-wiso for 12 years. The first two years were used as spin-up, in the other ten years the atmosphere is free to evolve. Therefore the monthly values vary from year to year. The output is given as mean monthly values.

7.3.3. 6k results

7.3.3.1. ECHAM5-wiso simulation

In figures 7.5, 7.6 and 7.7 the differences between the PD experiment and the 6k experiment (6k-PD) are given for temperature (figure 7.5), for precipitation (figure 7.6) and for $\delta^{18}O_{prec}$ (figure 7.7) for each cave location of this study.

Simulated temperature anomaly The simulated **mean annual temperature** in the CCSM mode shows slightly warmer temperatures for western Europe at 6ka, which diminishes with increasing longitude. The eastern cave locations have nearly no temperature gradient for T_{mean}.
The ECHO-G mode agrees with this slightly warmer pattern at 6ka but with a slight north-south gradient towards warmer temperature in the south.
In contrast to both the mean annual temperature reveal a strong cooling between present day and 6k.
This behaviour is also present in the simulated **winter temperatures**. CCSM shows a west-east trend from warmer to identical temperatures with a particular warming in Germany and the northern Alps. ECHO-G produces slightly warmer temperatures while the cooling of the COSMOS mode is even more pronounced in the winter month.
Also in the **summer temperatures** the west-east trend in the CCSM mode from warmer to colder temperatures is visible. ECHO-G shows a very strong warming during summer in central Europe. The COSMOS mode yields warmer temperatures in eastern and southern Europe.
To conclude: The COSMOS mode clearly yields the coldest temperature (although with

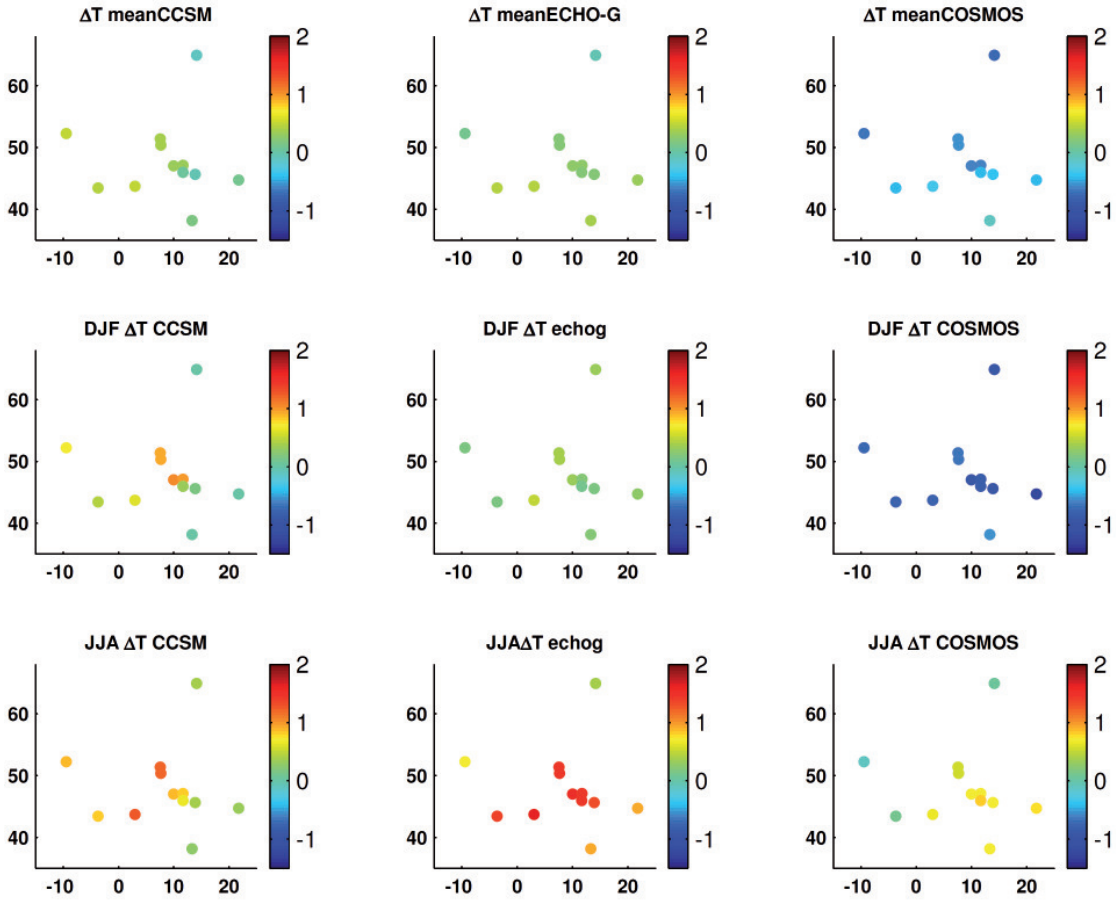

Figure 7.5.: Temperature anomalies (6k-PD) in °C in Europe (x-axis: longitude, y-axis: latitude) simulated by ECHAM5-wiso coupled with three different forcing models (CCSM, COSMOS, ECHO-G). First row: annual mean temperature, second row: winter temperature, third row: summer temperature.

warmer temperatures during summer), while CCSM ans ECHO-G reveal roughly the same behaviour of slightly warmer temperatures. CCSM reveals in addition a northwest-southeast trend towards colder temperatures.

Simulated precipitation anomaly In contrast to the simulated temperature anomalies, the pattern of the simulated precipitation anomalies is very inhomogeneous. The **annual mean precipitation anomaly** is positive for all over Europe in the CCSM mode, while the pattern derived by ECHO-G is not consistent and shows little difference from present day as in the COSMOS mode.
Only some aspects should be discussed:
The **CCSM mode** reveals an remarkable increase of precipitation rate in northern Europe during the winter month at 6ka while the amount of precipitation is lower than present day in southern Europe. This pattern should be kept in mind. In the summer

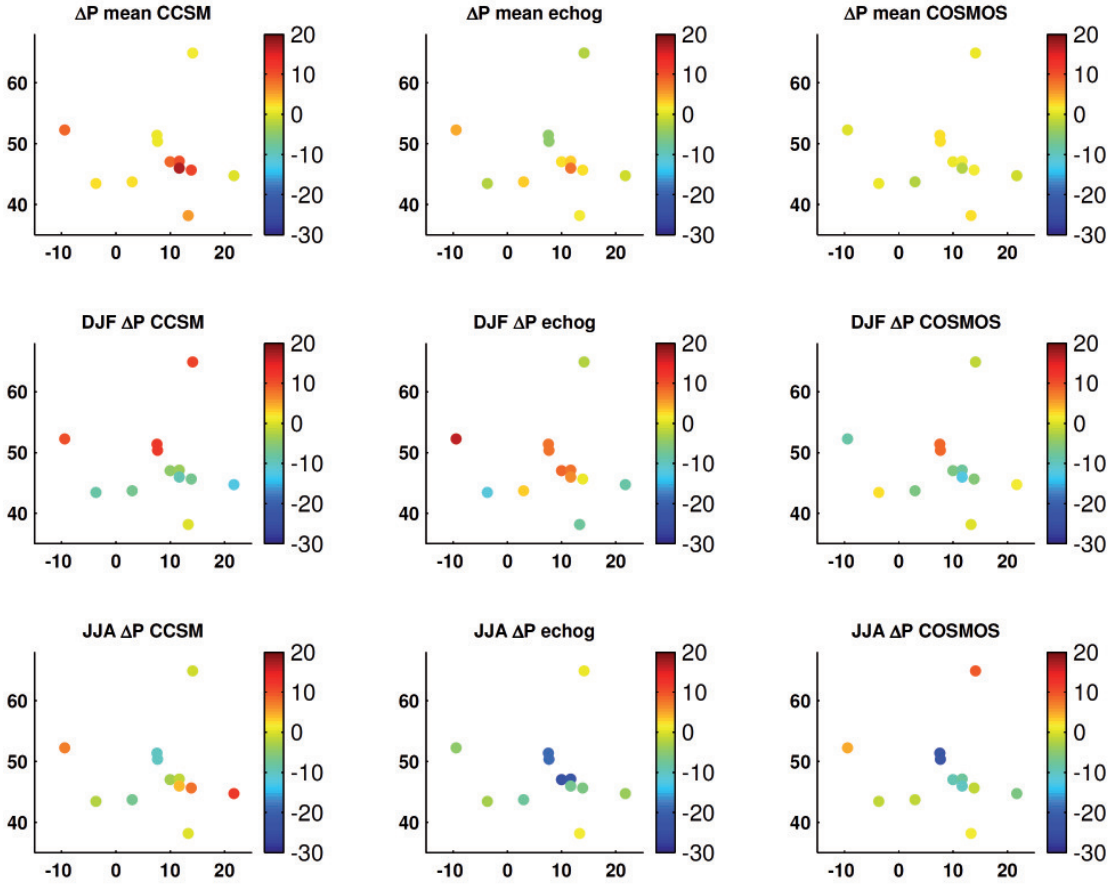

Figure 7.6.: Precipitation anomalies (6k-PD) in mm/month in Europe (x-axis: longitude, y-axis: latitude) simulated by ECHAM5-wiso coupled with three different forcing models (CCSM, COSMOS, ECHO-G). First row: annual precipitation, second row: winter precipitation, third row: summer precipitation.

month it is vice versa except the location of Crag Cave, which experiences throughout all month a rise in precipitation. Except in the winter season, the Alps seem to be exposed to wetter pronounced conditions.
A trend of the precipitation anomalies is not visible in the **ECHO-G mode**. However it agrees with the wetter conditions in the Alps predicted by the CCSM mode. The precipitation anomalies yielded by **COSMOS** mode cannot be summarised as drier or warmer conditions. The precipitation pattern seems to vary all over Europe.

Simulated $\delta^{18}\mathbf{O_{prec}}$ anomalies The European pattern of $\delta^{18}O_{prec}$ is more homogeneous than the precipitation anomalies. This is not surprising since the $\delta^{18}O_{prec}$ is also influenced by the surface temperature at the cave location.
In general the **mean $\delta^{18}\mathbf{O_{prec}}$** is lightest in the COSMOS mode, slightly heavier at 6ka in the ECHO-G mode and reveals a trend from slightly heavier to slightly lighter values corresponding to the temperature trend in the CCSM mode.

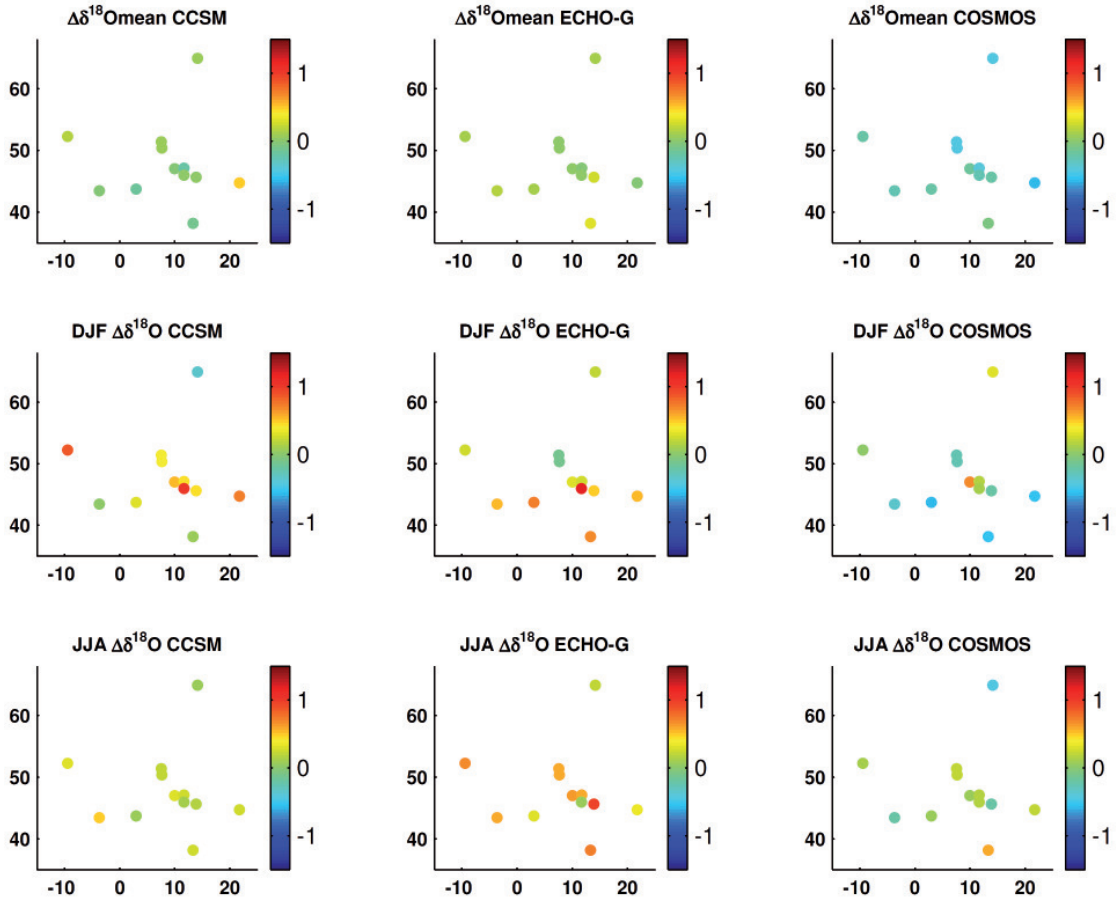

Figure 7.7.: $\delta^{18}O_{prec}$ anomalies (6k-PD) in ‰ in Europe (x-axis: longitude, y-axis: latitude) simulated by ECHAM5-wiso coupled with three different forcing models (CCSM, COSMOS, ECHO-G). First row: annual mean $\delta^{18}O_{prec}$, second row: winter $\delta^{18}O_{prec}$, third row: summer $\delta^{18}O_{prec}$.

However, the $\delta^{18}O_{prec}$ values are also influenced by different parameters and can be affected by the circulation and the source of the precipitation.
The winter situation yielded by ECHO-G is a good example. The temperature anomaly pattern shows a homogeneous behaviour for all the cave locations. In contrast to that, the $\delta^{18}O_{prec}$ anomaly has a clear north-south trend with heavier $\delta^{18}O$ values in the Mediterranean. This could result from a stronger influence at 6k of the Mediterranean Sea as a source of precipitation.

7.3.3.2. Simulated $\delta^{18}O_{calcite}$ anomalies

The next step is to calculate the resulting $\delta^{18}O_{calcite}$ anomalies with the ODSM from the respective ECHAM5-wiso output values. The results are composed in figure 7.8. There are two graphics for each model forcing - Setup 1 and Setup 2 (as described in section 7.1.3) The specific numbers are given in table 7.3.
At first glance the simulated $\delta^{18}O_{calcite}$ pattern looks in general more regular and structured as the stalagmite data. This is probably due to the lower resolution of the input climate values which is not comparable to the data which represent a smaller scale climate. The CCSM mode agrees roughly in most $\delta^{18}O_{calcite}$ anomalies for the Mediterranean stalagmites and up to B7 Cave. For higher latitudes (Tartair, Korallgrottan) the modelled values differ from real $\delta^{18}O_{calcite}$ values. The ECHO-G mode reveals also some agreements with the data, however, less than the CCSM mode. In Setup 1 ECHO-G seem to match the stalagmite data better than in Setup 2. The $\delta^{18}O_{calcite}$ anomalies simulated by the COSMOS mode reveal a lower isotopic pattern in 6k than in the present for nearly all the caves. This originates from the low simulated $\delta^{18}O_{prec}$ in this mode. The resulting $\delta^{18}O_{calcite}$ value pattern does not resemble the data.

	Data	**CCSM Setup 1**	**ECHO-G Setup 1**	**COSMOS Setup 1**	**CCSM Setup 2**	**ECHO-G Setup 2**	**COSMOS Setup 2**
Korall.	-0.7	0.1	0.2	-0.0	0.2	0.2	0.3
Crag	0.9	-0.1	0.0	0.2	-0.0	-0.2	0.2
Bunker	0.4	-0.3	-0.6	-0.6	0.0	-0.4	-0.2
B7	-0.1	-0.3	-0.6	-0.6	0.0	-0.4	-0.2
Spannagel	-0.4	-0.5	-0.8	-0.4	-0.4	-0.5	-0.0
Hölloch	-0.3	-0.2	-0.9	-0.2	-0.1	-0.5	0.1
Savi	-0.6	0.5	0.4	-0.2	0.5	0.4	-0.3
Ernesto	0.2	0.4	0.1	-0.0	0.2	0.1	-0.2
Poleva	0.8	1.3	0.1	-1.0	1.2	0.3	-1.0
Clamouse	0.2	-0.0	-0.2	-0.5	0.1	-1.1	-0.5
Garma	-0.4	-0.6	-0.4	-0.5	-0.2	-0.4	-0.5
Carbur.	0.5	0.2	1.0	0.4	0.3	0.6	-1.5

Table 7.3.: $\delta^{18}O_{calcite}$(6k-PD) values of the stalagmites and the corresponding modelled values of the different forcings.

To prove this statement the correlation between modelled and stalagmite $\delta^{18}O_{calcite}$(6k-PD) is displayed in figure 7.9. The black lines represent the 1:1 lines. In the figures the Root Mean Square Deviation, **RMSD**, is given calculated as

$$\mathrm{RMSD} = \sqrt{\frac{\sum_{i=1}^{n}(\delta^{18}\mathrm{O(6k\text{-}PD)_{Model}} - \delta^{18}\mathrm{O(6k\text{-}PD)_{Data}})_i^2}{n}} \tag{7.1}$$

where n is the number of samples (here: n=12). The RMSD is a measure for the deviation of the modelled from the measured $\delta^{18}O_{calcite}$(6k-PD) values.
The CCSM implementation shows in both setups the best (lowest) RMSD values.

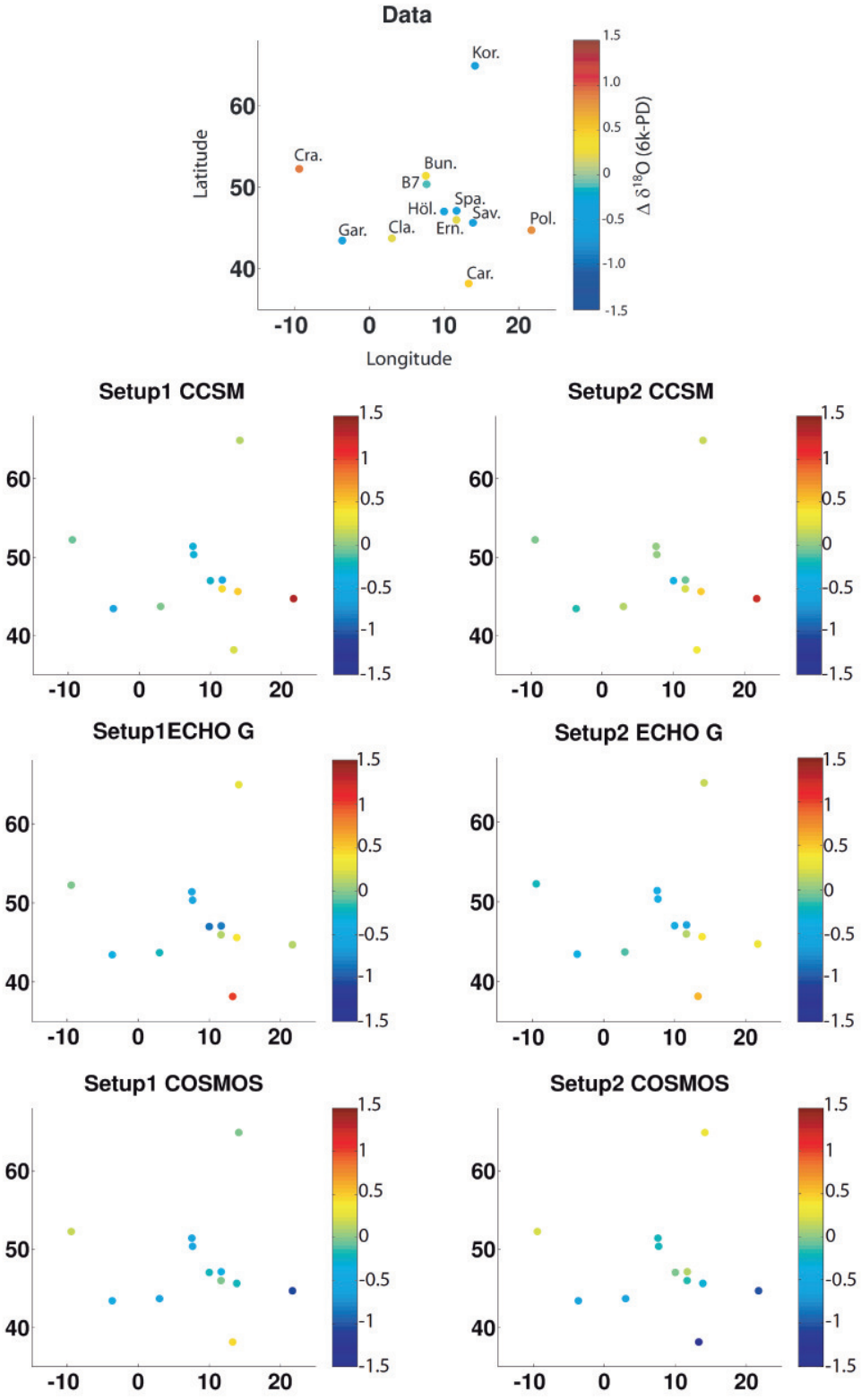

Figure 7.8.: $\delta^{18}O_{calcite}$ difference 6k-PD in Europe simulated by ECHAM5-wiso coupled with three different models (CCSM, COSMOS, ECHO-G)

The ECHO-G mode approaches the measured $\delta^{18}O_{calcite}$(6k-PD) values better in Setup 1 than in Setup 2, however, both RMSD values are lower than in the CCSM mode. The COSMOS mode reveals in both modes a significantly higher RDSM value than the other modes.
In addition, the linear regressions between modelled and measured $\delta^{18}O_{calcite}$(6k-PD) values are calculated (dashed, blue line in figure 7.9) and the slope, **m**, is noted on the figures for comparison to the 1:1 line (black lines in figure 7.9 where m=1).
The linear regressions show a slope smaller than 1 in all the model modes. However, the CCSM mode results in the slope with the highest value. The linear regression of the modelled values of the ECHO-G mode has also a positive slope in Setup 1, but approaches m=0 in Setup 2. The slopes in the COSMOS modes are even worse and have negative values. Figure 7.9 indicates that the CCSM mode seems to be the best choice to simulate the stalagmite $\delta^{18}O_{calcite}$(6k-PD) values.

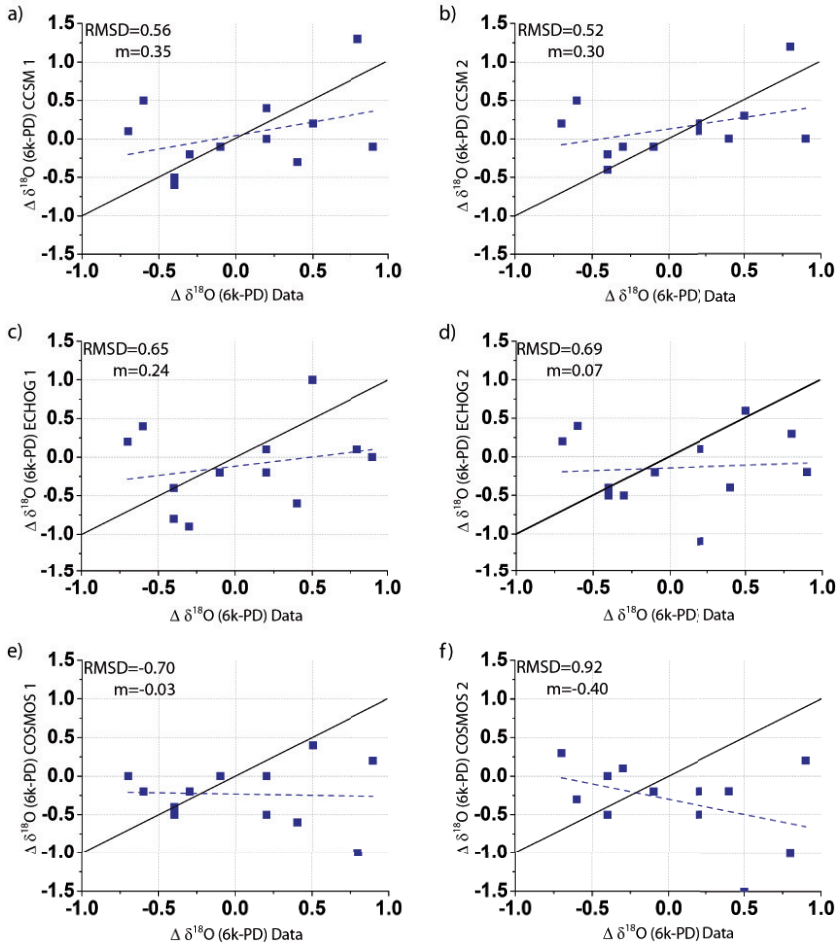

Figure 7.9.: Modelled versus stalagmite $\delta^{18}O_{calcite}$(6k-PD) values for the different model setups. The value of the Root Mean Square Deviation, **RMSD**, gives an evaluation of how well the modelled $\delta^{18}O_{calcite}$(6k-PD) values agree with the data. In addition, the slopes, **m**, of linear regressions between modelled and stalagmite $\delta^{18}O_{calcite}$(6k-PD) values (blue, dashed lines) are displayed in order to compare to the 1:1 lines (black line).

Discussion of discrepancies Since some $\delta^{18}O_{calcite}$ anomalies could not be simulated correctly, a discussion of some general problems and uncertainties helps to understand the origin of discrepancies between simulated and observed values.
On one hand the influence of kinetic fractionation between drip water and speleothem calcite can be a factor responsible for shifts in the $\delta^{18}O_{calcite}$ value of the speleothems which is not included in the model so far due to lack of knowledge of the required parameters to simulate kinetic fractionation. To some extent this problem is compensated by the use of anomalies instead of absolute values.
On the other hand due to the lack of sufficiently small scaled model output parameters the climate conditions of the gridbox simulated by ECHAM5-wiso could not be an adequate representation of the true condition at the cave.
In the following, possible reasons are discussed for the $\delta^{18}O_{calcite}$ anomalies, which no model setup could simulate correctly.
Korallgrottan For the stalagmite from Korallgrottan kinetic effects can be neglected due to very low cave temperatures. The mismatch between simulated values and data must arise from the ECHAM5-wiso output parameters. The $\delta^{18}O_{prec}$ value has the main influence (see figure 7.1). The only ECHAM5-wiso output, which shows low annual mean $\delta^{18}O_{prec}$ values is the COSMOS mode (see figure 7.7). However, the winter season, which has the largest influence on cave drip water is rather enriched than depleted at 6k. One possible explanation for very light isotope values could be an increased influence of the Norwegian Sea. As a source of precipitation this would lead to lighter $\delta^{18}O_{prec}$ values due to the low $\delta^{18}O_{prec}$ value compared to the Northern Atlantic where European precipitation usually originates [Lachniet, 2009]. This influence might be underestimated in ECHAM5-wiso. Another explanation can be the annual pattern of precipitation. The COSMOS setup predicts an increase of summer precipitation at 6k while the other seasons diminish. This leads to a bias towards heavier summer precipitation in the drip water and calcite.
Crag Cave The stalagmite from Crag Cave shows a strong enrichment in 6k. The COSMOS mode is the best simulation of the $\delta^{18}O_{calcite}$ anomaly. Kinetic fractionation could in principle play a major role in this cave since cave temperature is relatively warm. However, the COSMOS mode (which yields the best agreement with the measured value) shows rather cold temperatures which could diminish the amplitude of fractionation compared to today instead of enriching it [Mühlinghaus *et al.*, 2009]. Therefore, kinetic fractionation is no reason for the mismatch between simulation and observed values. A more likely reason is that the simulated $\delta^{18}O_{prec}$ is already too low.
Bunker Cave At Bunker Cave kinetic influence was proven in section 4.2. Slightly warmer cave temperatures (as predicted by CCSM mode) would lead to an increased influence of kinetic fractionation. In addition, Bunker Cave is very close to B7 Cave ($< 10km$). The climatic conditions are bound to be similar at the caves. However, the stalagmite of B7 does not show the same significant enrichment at 6ka. This indicates, that kinetic fractionation is a realistic reason why the model yields too low $\delta^{18}O_{calcite}$ anomalies.
Savi Cave The simulated $\delta^{18}O_{calcite}$ anomalies for Savi cave show too heavy values compared to the stalagmite value. For a warm cave as Savi kinetic fractionation could play a major role. The only model mode which approaches the measured anomaly is the COSMOS mode (setup 2) and is still too high by 0.3‰. Again two reasons could

explain the offset: i) a reduction of the amplitude of the kinetic fractionation at 6k and ii) an overestimated influence of the Mediterranean. It is possible that the precipitation approaching the cave did not primarily originate from the Adriatic Sea but from the Atlantic or western Mediterranean crossing northern Italy and depleting successively. This would lead to lower $\delta^{18}O_{calcite}$ values.
Poleva Cave The stalagmite from Poleva Cave shows a very strong enrichment at 6k compared to today. In other modes than CCSM this enrichment cannot be observed at all. The CCSM mode, however, overestimates the value. This might origin from the very enriched $\delta^{18}O_{prec}$ value in the CCSM mode in Autumn. With regard to the situation at Savi Cave where the model also yields too enriched $\delta^{18}O_{calcite}$ anomalies, it is possible that at Poleva Cave the model slightly overestimates the influence of the Mediterranean Sea.

7.3.4. Conclusions from the 6k experiment

First, there is to say that an evaluation of the model forcings is hard from one time slice and 12 stalagmites. An appropriate way is to use more time slices (calculated by ECHAM5-wiso) in combination with as much stalagmite data (from different caves as well as other stalagmites from the same cave) as possible to assess, if discrepancies between model and stalagmite data are a temporary or temporally varying problem (stalagmite kinetics) or a systematical offset (resulting from for example the geographical position of the cave). Any conclusion from this study must be further tested.
From this study the CCSM coupled ECHAM5-wiso seems to be the best climate model setup to simulate stalagmite data from Europe. Why the CCSM might be a more realistic climate model for the European climate situation could be for the explanation in the next section.

Meteorological interpretation of the ECHAM5-wiso output in CCSM mode The CCSM mode reveals some features which are not present in the other ECHAM5-wiso results. In this context only the winter results of the CCSM must be attended. The temperature anomaly at 6k shows an overall warming (from 0.02°C for Korallgrottan and Poleva up to 1°C at Hölloch Cave) which is pronounced in Central Europe. The precipitation anomalies reveal a strong precipitation increase for Northern Europe (including B7 and northwards) and a decrease in southern Europe with a minimum at Poleva Cave. The $\delta^{18}O_{prec}$ anomalies have positive values for the entire set of cave locations except the location at Korallgrottan (depleted by 0.4‰). Strong enrichment is revealed by the location at Tartair Cave, Ernesto Cave and Poleva Cave.
The pattern of these three parameters display striking similarities with the synoptic phenomenon of a strong positive phase of the North Atlantic Oscillation. In this mode a characteristic pattern of temperature, precipitation and $\delta^{18}O_{prec}$ can be observed in Europe, which would lead to a certain spatial $\delta^{18}O_{calcite}$ distribution.
The basics of the NAO system are described in the section 2.7. Trigo *et al.* [2002] determined correlation coefficients between the NAO index and precipitation and temperature for the European winter climate by analysing the NCEP reanalysis data set of 1958-1997. The results are in agreement with the general European pattern published by Hurrell

[1995] and the work of Baldini *et al.* [2008]. The latter is a very useful paper, since in addition to climate data sets, they analysed isotopic dataset and detected correlations between temperature, precipitation and $\delta^{18}O_{prec}$ value to the NAO index from all over Europe.
In the following the impact of a positive NAO on temperature, precipitation, $\delta^{18}O_{prec}$ and the resulting $\delta^{18}O_{calcite}$ in Europe is outlined as it can be summarised from the given references above. Figure 7.10 illustrates this topic.
If the NAO is in a positive mode, strong westerlies from the Atlantic transport a large amount of precipitation to Mid- and Northern Europe during the winter month. The winter temperature is also higher than in a negative NAO phase. This mode is also accompanied by a significant, positive correlation of the NAO index to $\delta^{18}O_{prec}$ (see Baldini *et al.* [2008]). These conditions account for the German caves, the caves in the northern Alps and presumably also Garma Cave which cannot be assigned to the typical Mediterranean area.
For the location at Crag Cave the correlations to temperature and $\delta^{18}O_{prec}$ are positive due to the source of precipitation, but a correlation to the amount of winter precipitation cannot be detected in the data set from Baldini *et al.* [2008]. Maybe due to the cave position which is exposed to the Atlantic Sea, the storm tracks do not play a significant role.
High latitude locations (here location for Korallgrottan) reveal a negative correlation to $\delta^{18}O_{prec}$ and the amount of winter precipitation [Baldini *et al.*, 2008]. This could result from an influence of the Norwegian Sea, however, the positive correlation to winter temperature suggest, that the air masses come from southern direction. An explanation for the anticorrelation to $\delta^{18}O_{prec}$ and amount of winter precipitation can be offered by a NAO+ phase in which the precipitation arriving at the cave is highly depleted due to the latitude effect. If precipitation originates from the Northern Sea, the air mass is lighter at the source (after evaporation) due to the lower isotopic composition of the Norwegian Sea, however, the depletion due to progressive rain-out yields lower $\delta^{18}O_{prec}$ values at the location of Korallgrottan than the source effect (Mook [2006], Lachniet [2009]).
In southern Europe[1] winter precipitation originates primarily from the Mediterranean in a positive NAO mode and is reduced, compared to the negative NAO mode, in which precipitation has its origin in the Atlantic. Temperature is also positively correlated to the NAO index due to the diminished Atlantic influence (which carries colder air compared to the Mediterranean as source of precipitation). The same is valid for the $\delta^{18}O_{prec}$ value. Precipitation from the Mediterranean Sea is isotopically heavier than from the Atlantic. This can also be derived from the study by Baldini *et al.* [2008].
In addition, a strong positive NAO phase is accompanied by a weak Siberian anticyclone restraining cold air from the North to influence the climatic condition in south-east Europe (important for location of Poleva Cave). The positive correlation to temperature and anticorrelation to precipitation was shown by (Winterhalder [2011], Tomozeiu *et al.* [2002], Tomozeiu *et al.* [2005]).

The expected $\delta^{18}O_{calcite}$ pattern can be observed in figure 7.10. For the locations in Northern Spain (Garma Cave), Germany (Bunker, B7) and Austria (Hölloch, Spannagel)

[1] meaning south of the Alps that behave as a kind of meteorological divide

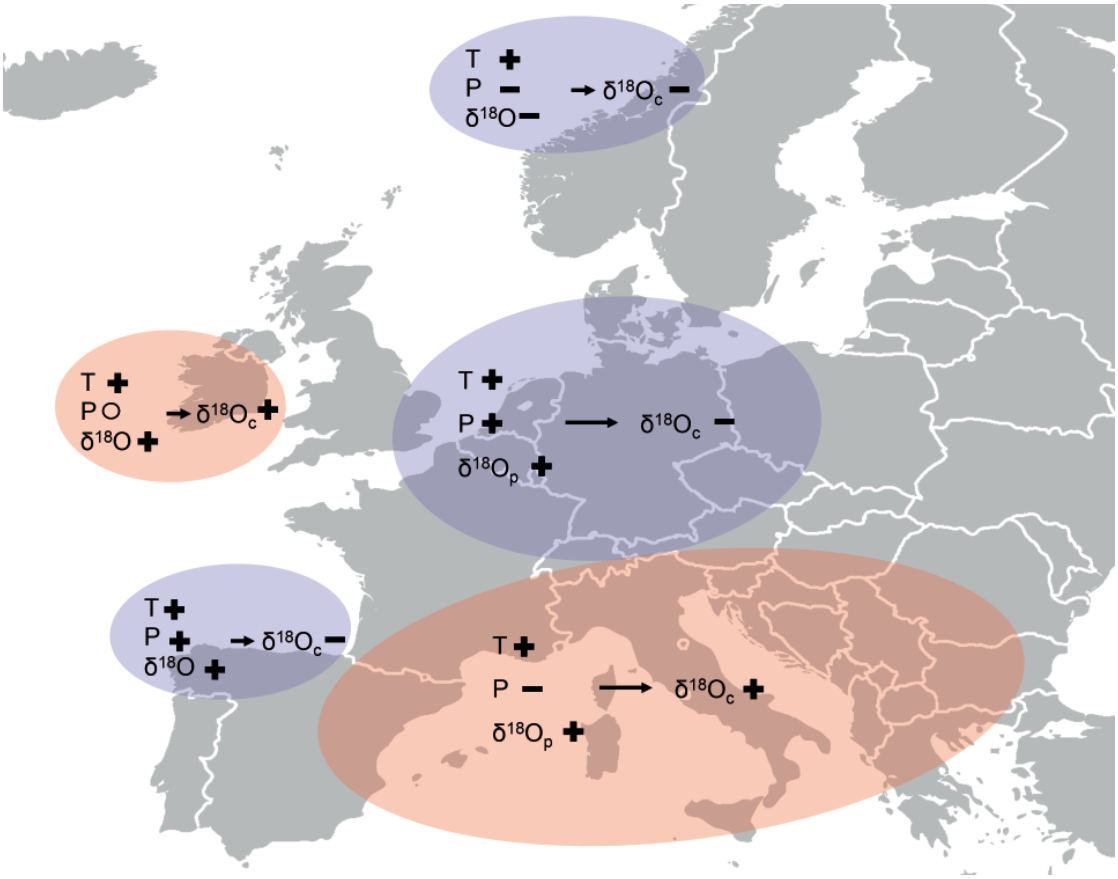

Figure 7.10.: Scheme illustrating the impact of the positive NAO mode on the European pattern of temperature, precipitation, $\delta^{18}O_{prec}$ and the resulting, hypothetical $\delta^{18}O_{calcite}$ as discussed in the text. '+' represents an increase, '-' represents a decrease and the circle represents invariance of the respective parameters.

the increased weight of isotopically lighter winter precipitation due to the positive correlation between NAO index and winter precipitation leads to lower $\delta^{18}O_{calcite}$ values. The influence of the biased weight of winter season dominates in this case the influence of increasing $\delta^{18}O_{prec}$ values of winter precipitation (see section 6.2). For the location at Korallgrottan, the negative correlation of NAO index to $\delta^{18}O_{prec}$ yields lower $\delta^{18}O_{calcite}$ values in a positive NAO mode.
Although Crag Cave belongs in principle to the northern caves, the missing correlation of the amount of precipitation to the NAO index leads to an invariant weight of winter precipitation. The positive shift of the $\delta^{18}O_{prec}$ dominates the system leading to enriched $\delta^{18}O_{drip}$ and consequently to a heavier $\delta^{18}O_{calcite}$ value.
In southern Europe (Clamouse, Ernesto, Savi, Poleva, Carburangeli) the isotopic composition of precipitation increase in a NAO+ situation. In contrast to the situation in northern Europe winter precipitation diminishes under NAO+ conditions. The weight of the winter season is thus also reduced shifting the mean annual $\delta^{18}O_{drip}$ towards the summer $\delta^{18}O_{prec}$. Finally, this leads to heavier $\delta^{18}O_{calcite}$ values.

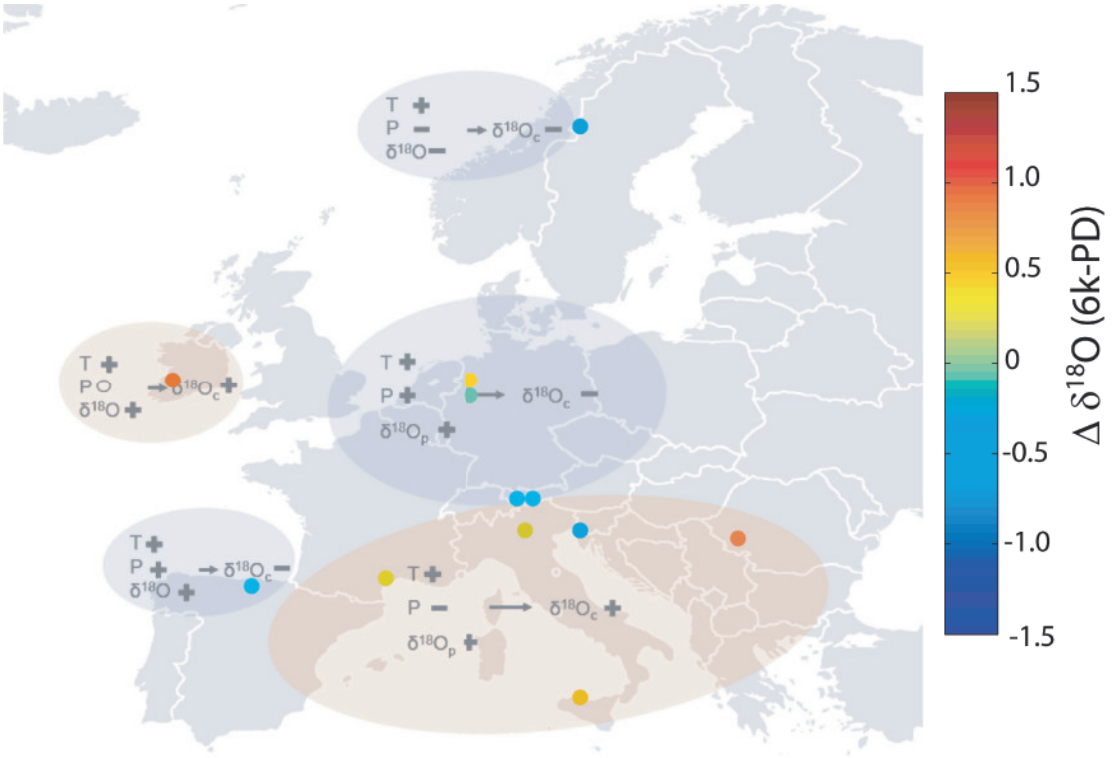

Figure 7.11.: Expected parameter variation during a positive NAO mode and the assumed resulting $\delta^{18}O_{calcite}$ values. Coloured dots represent the measured $\delta^{18}O_{calcite}$ anomalies from the discussed speleothems (see figure 7.4.

This pattern is indeed found in the stalagmite data (figure 7.11). The stalagmites Korallgrottan, B7, Spannagel, Hölloch and Garma Cave show depleted $\delta^{18}O_{calcite}$ values as expected, while the samples from Crag Cave, Clamouse, Ernesto, Poleva and Carburangeli Cave are enriched. The extent of the respective enrichment or depletion depends on the related cave system and the response to surface variations. This is not considered in this study.
Only two caves (Bunker and Savi Cave) disagree with the expected $\delta^{18}O_{calcite}$ values. Bunker Cave is enriched instead of depleted. Due to the previous studies with the Bunker Cave stalagmite (section 6.3 and figure 6.8) this problem can be understood. The model approaches (Dual-Proxy Approach and Correlation Approach) which were used to reconstruct temperatures from the $\delta^{18}O_{calcite}$ record of BU4 disagree at 6k with each other. While the Correlation Approach (inclusion of the NAO based correlation between winter temperature and winter precipitation) states a negative temperature anomaly at 6k, the Dual-Proxy Approach ($\delta^{18}O_{calcite}$ model combined with the Mg/Ca model) yields a positive temperature anomaly. The Correlation approach thus yields drier conditions, while the Dual-Proxy Approach disagrees with this. This might suggest, that the enrichment of $\delta^{18}O_{calcite}$ was not caused by a true climate signal, but by kinetic fractionation which was underestimated in the ODSM.

The stalagmite from Savi Cave was not studied here. Therefore, any explanation would be pure speculation.
The conclusion of a strong positive NAO mode at 6ka B.P. can be compared with the profound study of Wanner *et al.* [2008]. By comparison of a climate model with the indications from proxy data, they also show evidence that in this time the NAO was in a pronounced, positive mode. The same statement is supported by Jansen *et al.* [2007] suggesting an overall temperatures increase for Europe compared to pre-industrial times. Both studies encourage that at 6 ka B.P. the presented model approach yields the true climate situation.

In the $\delta^{18}O_{calcite}$ values which were simulated by the CCSM coupled with ODSM the predicted, NAO+ related pattern is visible showing a clear depletion of $\delta^{18}O_{calcite}$ value for Garma, Hölloch, Spannagel, Bunker, B7 Cave and an enrichment in the Mediterranean region. Problems occur only with the $\delta^{18}O_{calcite}$ values from Korallgrottan and Tartair Cave. Although the ECHAM5-wiso output yields the strong NAO+ phase pattern, the other seasons weaken the pattern of the winter season. This might mean that the influence is to some extent underestimated in the model or on the other hand, that the other seasons show a pattern which does not represent the true climate. As mentioned before these statements must be tested for different time slices before profound conclusions can be drawn about the best forcing mode of the ODSM. However, it becomes clear that the approach to simulate $\delta^{18}O_{calcite}$ values by using a General Climate Model as input for the ODSM is a helpful tool to understand $\delta^{18}O_{calcite}$ changes of the past and in addition conclusions can be drawn about circulation pattern in the past.

Cave	**Stal.**	**Lat.**	**Lon.**	**Alt.**	$\delta^{18}\mathbf{O_{cal}}$ PD	$\delta^{18}\mathbf{O_{cal}}$ 6k
Korallgrottan (Sweden) Sundqvist et al. 2007	K1	64.89°	14.16°	570m	-8.55‰	-9.2‰
Crag Cave (Ireland) McDermott et al. (2001)	CC3	52.23	-9.44°	60m	-3.8‰	-2.9‰
Bunker Cave (Germany) Riechelmann (2010)	BU4	51.38°	7.55°	100m	-5.8‰	-5.4‰
B7 Cave (Germany) Niggemann et al. (2003)	B7-5	51.34°	7.65°	185m	-5.7‰	-5.8‰
Spannagel Cave (Austria) Vollweiler (2010)	COMNISPA	47.09°	11.67°	2500m	-7.9‰	-8.3‰
Hölloch Cave (Germany) Wurth et al. (2004)	StalHoel1	47°	10°	1440m	-7.97‰	-8.27‰
Ernesto Cave (Italy) McDermott et al. (2009)	ER76	45.96°	11.65°	1165m	-7.8‰	-7.6‰
Savi Cave (Italy) Frisia et al. (2005)	SV1	45.61°	13.88°	441m	-6.1‰	-6.74‰
Poleva Cave (Romania) Constantin et al. (2007)	PP9	44.77°	21.73°	390m	-8.62‰	-7.8‰
Clamouse Cave (France) McDermott et al. (1999)	CL26	43.7°	3°	75m	-4.95‰	-4.76‰
Garma Cave (Spain) Baldini et al. (2008)	Gar01	43.43°	-3.66°	75m	-3.99‰	-4.39‰
Carburangeli (Italy) Frisia et al. (2006)	CR1	38.15°	13.3°	22m	-6‰	-5.5‰

Table 7.4.: Cave locations and compilation of isotope data of the studied 12 speleothems extracted from McDermott *et al.* [2011].

8. Conclusions and Outlook

8.1. Conclusions

This work aimed for a deeper understanding of the processes modifying the values of two different climate proxies from stalagmites - the $\delta^{18}O_{calcite}$ value and the Mg/Ca ratio. From literature both parameters are known to be sensitive to climate variations. However, quantitative analyses remain a challenging task, since climate signals are masked by different other parameters which are not directly linked to climate. In addition, the true climate parameters affect the proxies in different ways and to a different extent and interfere with each other making the interpretation of the proxies ambiguous. This work has established models, which are supposed to enhance the understanding of climate signals recorded in speleothem calcite. The following paragraphs summarise the results of the presented models.

Forward Modelling Here, the models were primarily applied for Bunker Cave in western Germany. The advantage of this cave is the extensive, ongoing monitoring program established in 2007, which is necessary to calibrate the models and confirm the model results.
The model design of the $\delta^{18}O$ model and the Mg/Ca model differ in one essential point from each other - the initial signal of the respective parameter. In the Mg/Ca system, the initial signal originates from the host rock above the cave, while the initial $\delta^{18}O_{calcite}$ value bears an atmospheric signal. In context of model calibration this is an advantage for the $\delta^{18}O$ model, since the initial value can be measured. On the other hand the atmospheric origin of the $\delta^{18}O$ signal leads to a sensitivity of this initial value to climate parameters resulting in additional uncertainties, which the Mg/Ca advantageously lacks.
Conclusions from the Mg/Ca model The Mg/Ca ratio shows a more pronounced sensitivity to precipitation compared to temperature. The relation to precipitation is clearly negative. This is a logical result, since the amount of precipitation or infiltration drives Prior Calcite Precipitation, PCP, and thus the Mg/Ca ratio of the stalagmite.
By comparison of the possible variability of the modelled Mg/Ca values to the stalagmite record of BU4, it becomes obvious that PCP as the only process occurring in the karst matrix cannot explain the natural variability. Two additional processes bear the potential to enhance the range of the Mg/Ca variability. These are the dissolution of dolomite and the re-dissolution of calcite in the karst matrix, which does not belong to the host rock, but was deposited during PCP occurred at an earlier stage. Both types of rock show significantly different Mg/Ca ratios and can finally explain the observed Mg/Ca range of a stalagmite.
Conclusions from the $\delta^{18}O$ model The $\delta^{18}O_{calcite}$ value reveals also a strong sensitivity to temperature and precipitation. However, the correlations are less distinct than

for the Mg/Ca model.
In contrast to the Mg/Ca model the initial $\delta^{18}O$ value reveals a pronounced seasonal cycle. While for the Mg/Ca model the total amount of precipitation is the relevant feature, for the $\delta^{18}O_{drip}$ value the seasonality of precipitation plays a major role. Therefore the results of a changed seasonality (more or less winter precipitation[1]) need to be investigated. The impact on the $\delta^{18}O_{calcite}$ sensitivity to temperature and precipitation variations is a clearly negative correlation between $\delta^{18}O_{calcite}$ and precipitation as well as temperature.

The comparison of the $\delta^{18}O_{calcite}$ and Mg/Ca record of stalagmite BU4 shows major similarities indicating that both are influenced by climate variability in the same way. This encourages the suggestion that the $\delta^{18}O_{calcite}$ model, which allows the seasonal contribution to change, is the more realistic representation of the natural system. If the $\delta^{18}O_{calcite}$ model is applied in this configuration, both proxy models show the same sensitivity to precipitation. However, it must be kept in mind that in this configuration the $\delta^{18}O$ model draws only conclusions about the amount of winter (NDJFM) precipitation, while the amount of precipitation of the other months is constant. For the $\delta^{18}O$ model this is an advantage, since it was proven that the changing contribution of precipitation of the winter season is one of the major parameters controlling the $\delta^{18}O$ value of stalagmites. However, for the Mg/Ca the more important factor is the total annual amount of precipitation. The application of the setup with varying influence of the winter season to the Mg/Ca model is therefore not advisable.
For both models the kinetic isotope fractionation between drip water and calcite can affect the proxies to a major extent and therefore had to be included in the model setup. A function had to be defined describing the relationship between drip interval and meteoric precipitation for this purpose. The influence of this function on the model results is fortunately a minor factor compared to climate signals. However, it must be noted that uncertainties remain whether the true behaviour of kinetic fractionation can be captured by the model.

Inverse Modelling Two approaches of inverse modelling were presented in this work to reconstruct temperature and precipitation from $\delta^{18}O_{calcite}$ values. The **Dual-Proxy Approach** involves both analysed proxies - Mg/Ca and $\delta^{18}O$ - and yields by comparison of both proxy models temperature-precipitation solution sets that fit to the respective proxy values of a certain stalagmite sample.
The **Correlation Approach** uses a correlation between winter temperature and winter precipitation to derive temperature values from the $\delta^{18}O_{calcite}$ record. The correlation is based on the general relationship between temperature and precipitation during the winter season in Northern Europe caused by the regime of the North Atlantic Oscillation.
The model approaches are based on different forward models. While the Correlation Approach is based on a varying influence of the winter season, the Dual-Proxy approach assumes identical and uniform variation of temperature (and precipitation) for all the

[1] For the investigated cave as in general caves in Europe stronger long term variations are visible in the winter than the other seasons. See 2.7 for details

months.
Both bear characteristic advantages and disadvantages. A disadvantage of the Correlation Approach is the defined correlation between winter temperature and winter precipitation, which could have changed in the past. In addition, modern correlation coefficients between these parameters are small (R^2=0.21) so that the relation is better described as a trend than a clear correlation.
The advantage of the Correlation Approach is, that most of the parameters which influence the $\delta^{18}O$ value can be connected to climate. In contrast, the Dual-Proxy Approach depends on several parameters which are not linked to climate (initial Ca^{2+} content, initial Mg/Ca ratio, natural behaviour of flow paths and PCP characteristics). This evokes uncertainties and is a disadvantage of the Dual-Proxy Approach. On the other hand, the advantage of the Dual-Proxy Approach is that temperature and precipitation are derived independently from each other.

Temperature reconstruction. Although both approaches have significant differences in the model realisation, the temperature histories reconstructed from the proxy records of BU4 reveal remarkably similar patterns (figure 6.8). Reconstructed temperatures using the Correlation Approach generally show smaller variations than the Dual-Proxy Approach. The reason might be that Mg/Ca is influenced by geological parameters, which are misleadingly ascribed to temperature changes. If the proxy values are smoothed reducing small scale variations, both temperature reconstructions agree well with each other.
Precipitation reconstruction. The Dual-Proxy Approach shows significant higher variations of the total annual amount of precipitation than the Correlation Approach. The reason is that the Correlation Approach yields winter precipitation (NDJFM), while the other monthly precipitation values are constant. The Dual-Proxy Approach determines directly the total annual precipitation. This causes higher values in general.
The reconstructed precipitation time series agree less between the approaches than the temperature reconstructions. The differences occur from the model design. While precipitation is bound to show the same variation as temperature using the Correlation Approach, in the Dual-Proxy Approach precipitation can evolve in a different pattern than temperature.
Closer inspection of the precipitation pattern reveals that the variations resulting from the Dual-Proxy Approach increase strongly, when the precipitation resulting from the Correlation Approach shows higher values. In contrast, the variation of the precipitation reconstructions agrees, when precipitation values are low (e.g. between 0.5 ka and 1ka or 4-5.5 ka in figure 6.8). This suggests that in phases where the Correlation Approach predicts a warmer and wetter climate (NAO+ situation) the general variability of water supply is very different to colder and drier phases (NAO-). A positive NAO phase evokes massive storm tracks across the northern Europe. However, where exactly the water masses precipitate as rain depends on the geographical conditions and on the exact trajectory of the respective storm track.
A suggestion is that the Correlation Approach detects the general mode regarding the NAO during winter times, but the Dual-Proxy Approach gives a more realistic value of the extent of precipitation at the cave location. For a negative NAO mode it is vice versa. The storm tracks are reduced, when winter conditions become drier. Dry air from

the north carries in general less precipitation, leading to a more uniformly distributed precipitation pattern. This explains why in colder and drier conditions both modelled precipitation reconstructions tend to agree with each other.
It is also possible that the Dual-Proxy Approach yields the more realistic values due to the independent determination of precipitation. The idea might occur to calibrate the model for the Correlation Approach with the 'true' precipitation values resulting from the Dual-Proxy Approach. However, the Dual-Proxy Approach cannot reflect changing seasonal contributions (wetter or drier winter) which is an essential point for the Correlation Approach. These very different model assumptions should not be mixed, before a correlation between the amount of winter precipitation and the precipitation of the rest of the year could be defined (which could not be derived by analysing observational data).
Reconstructed climate variations. The suggested temperature variation from the reconstruction using BU4 range about ±2°C (peak to peak) between present day and 8ka before present (figure 6.8). Both reconstructions show a pronounced colder period around 0.5 ka, that can be associated with the Little Ice Age, which is known as a colder period in Europe. Colder temperatures are accompanied with reduced precipitation in both models. At about 1.5 ka a warmer and wetter phase started ending at around 1 ka which could be connected with the Medieval Climate Anomaly. Also the warmer period from 3.5 to 5.5 ka was published before ([Joerin *et al.*, 2006], [Schönwiese, 2008]). The presumed Holocene optimum at around 6.5 ka [Schönwiese, 2008] agrees with a significant warm phase in the Holocene climate study of Joerin *et al.* [2006]. The temperature reconstruction of BU4 indicated in this time also increasing temperature, though not significant higher than the other warm phases.
These results suggest that the established, inverse models are able to identify large scale climate phases. The Correlation Approach tends to detect the general synoptical mode (NAO+, NAO-), while the Dual-Proxy Approach is a helpful tool to derive the specific phases when at the cave strong precipitation events occurred or when the actual amount of precipitation was less pronounced although climate was in a general wetter mode. If the results are discussed deliberately, the models represent a valuable tool for climate.
In addition, the model results indicate that the assumption of a NAO regime on winter season climate of the investigated cave can be confirmed.

ECHAM5-wiso forced Modelling The approach to force a stalagmite $\delta^{18}O_{calcite}$ model (here: ODSM) with climate and isotope data from a General Circulation Model (here: ECHAM5-wiso) has not been performed before.
Present day experiment. The present day experiment was necessary to establish a general forcing procedure and evaluate the results.
The differences of the simulated, climate parameters (mean annual temperature, total annual precipitation, weighted mean $\delta^{18}O_{prec}$) and measured values are presumably caused by general offsets between the averaged climate parameters of the grid box and the respective parameter values at the cave location. This instance justifies the presented adjustment of the input parameters for testing, if the forcing approach can be applied.
However, some discrepancies occur between modelled and measured $\delta^{18}O_{drip}$ and $\delta^{18}O_{calcite}$ values. First, although the simulated, mean annual climate parameters reflect after the

adjustment the actual parameters, the seasonal pattern can reveal differences shifting the weight of monthly $\delta^{18}O_{prec}$ values. This leads to offsets between modelled and measured $\delta^{18}O_{drip}$ and $\delta^{18}O_{calcite}$ values. Secondly, kinetic fractionation requires cave specific parameters, which could not be supplied for all the included stalagmites. Therefore, kinetic fractionation could not be applied which is a significant uncertainty in the warmer and drier caves.
Important insights can be derived from the sensitivity tests. They show that the $\delta^{18}O_{drip}$ and $\delta^{18}O_{calcite}$ signals react highly sensitive to the $\delta^{18}O_{prec}$ and a little less to temperature. The former is an important conclusion, because it shows that it is a relevant factor from where on the ocean the precipitation originates and which trajectories the air mass followed.
These insights were needed to design an experiment in which the ODSM is forced with ECHAM5-wiso output data for a calculated time slice (here at 6ka B.P.).
The 6k experiment. For the experiment, ECHAM5-wiso was driven by three different models, which prescribe sea surface temperature and sea ice cover (CCSM, COSMOS, ECHO-G), which were supplied by observational data in the present day experiment.
It is advisable for this experiment to compare the differences between modelled and measured, relative $\delta^{18}O_{calcite}$ values ($\delta^{18}O_{calcite}$(6k-PD)) to reduce two effects: i) the discrepancy between modelled and measured values originating from kinetic fractionation and ii) the offset between measured and simulated $\delta^{18}O_{calcite}$ resulting from the offset between simulated and actual climate data evoked by the geographical position of the cave in the grid box.
The experiment was performed for twelve, European caves. The respective, measured $\delta^{18}O_{calcite}$ values reveal a pattern suggesting a strong NAO+ mode at 6ka. This pattern could be confirmed by ECHAM5-wiso (with CCSM forcing).
The experiment showed that forcing the ODSM with ECHAM5-wiso output data is a very useful tool to analyse the $\delta^{18}O_{calcite}$ signal from speleothems and indicated that it is advantageous to apply the model to several stalagmites. While one stalagmite alone can yield a misleading interpretation, a set of stalagmites as presented in the 6k experiment helps to better identify true climate signals.
The 6k experiment emphasized the influence of the NAO regime for European climate and confirmed therefore that the model inversion (Correlation Approach and Dual-Proxy Approach) are qualified approaches to analyse climate changes using $\delta^{18}O_{calcite}$ and Mg/Ca values from stalagmites.

Future work suggestions For future work the following guidelines should be regarded when the presented models are applied:
Suggestion I. It should be refrained from universal statements describing the influence of a certain parameter on the $\delta^{18}O$ or Mg/Ca incorporation in stalagmites. Each cave represents a unique response to environmental changes.
Suggestion II. It is advantageous to apply both presented approaches of inverse modelling to a stalagmite in the context of climate reconstruction, since each approach supplies helpful information on climate conditions.
Suggestion III. To diminish small scale variation (kinetic influence, effects in soil and karst affecting the drip water characteristics) in the proxy records it is helpful to use

several stalagmites from one region to detect common climate signals.
Suggestion IV. The European winter climate is driven by a large synoptic pattern (NAO). To analyse the temporal evolution of this pattern involving a set of stalagmites from all over Europe is advisable. This helps to reduce the probability of falsely interpreting stalagmite signals.

8.2. Outlook

Modelling in the context of climate research is about finding a compromise between including enough parameters to reflect the processes influencing the respective proxy in a realistic way without creating to many degrees of freedom, making applications and reversing of the models complicated.
The presented models already seem to represent the processes influencing the respective stalagmite proxies in a realistic way. However, four main points could improve the climate reconstruction:

- **Tie points.** In the inverse models certain relations were established for present day conditions (NAO strength, relation between drip water and infiltration amount), which might have significantly changed in the past. If tie points existed on which the temperature or precipitation in the past is known, the relations could be recalibrated by forcing the model to yield the requested temperature and adjusting the established relations. Such tie points can be supplied by noble gas temperatures derived from water in fluid inclusions for certain depth along the stalagmite's growth axis. Although the noble gas thermometry may become a robust and reliable technique for palaeo temperature reconstructions (Aeschbach-Hertig *et al.* [1999], Kluge *et al.* [2008]), the required sample size is still too big (0.5g-1g [Kluge, 2008]) to yield a high resolution record like δ^{18}O or Mg/Ca. However, the independently derived temperature reconstructions could be valuable to improve the climate reconstruction of the presented models.

- **Precipitation source.** The isotopic composition of meteoric precipitation depends beside other parameter on the origin of air masses. The isotopic composition of the northern Atlantic where precipitation is usually formed is enriched compared to the high northern Atlantic or Norwegian Sea (see figure 2.2). So far this effect is not included in the developed models, however, it can lead to diminished variance of the reconstructed temperature. If the temperature during winter is low, the $\delta^{18}O_{prec}$ value is also rather low due to the temperature effect. For Bunker Cave this coincides with the meteorologic situation in which precipitation is transported by air masses from the north, which exhibit lower initial δ^{18}O values. The measured δ^{18}O value at the cave location is in the model ascribed only to lower temperature, but actually part of the lower δ^{18}O value may be due to the origin of precipitation. For the opposite situation the δ^{18}O value is rather high, which is interpreted as higher temperatures. However, part of the increased δ^{18}O value is due to the more southern (Atlantic) vapour source.
  If the origin of precipitation could be included in the model, quantitative tem-

perature reconstructions could be improved. This could be derived by analysing the deuterium excess (intercept of the relation between $\delta^{18}O$ and $\delta^{2}H$) from fluid inclusions. The deuterium excess of the Meteoric Water Line Gat [1996] of precipitation is beside other parameters (water recycling, evaporation of water droplets) related to the moisture source due to the humidity during evaporation [Merlivat and Jouzel, 1979]. For ice cores this technique has been applied to identify palaeo moisture origins [Masson-Delmotte *et al.*, 2005]. Matthews *et al.* [2000] presented a study on the deuterium excess on speleothems. However, due to large required sample amounts for the $\delta^{18}O$ determination compared to $\delta^{2}H$ (5ml and 2μg, respectively - method: [Clark and Fritz, 1997]), the $\delta^{18}O$ value was calculated in comparison with the surrounding speleothem calcite. However, the study reveals the potential of this technique.

- **Drip rate determination.** One critical point of the models is the kinetic fractionation or in particular the relationship between precipitation and drip interval. This correlation is poorly investigated. However, $\delta^{13}C$ of speleothem calcite is dominantly sensitive to the drip interval [Deininger, 2010]. If this proxy could be included in the current models, a better estimation for the true drip interval could be given leading to more precise determination of the kinetic fractionation factor in past times.

- **Transient ECHAM5-wiso run.** Restricted by computation time it was so far only possible to apply the new approach of forcing the ODSM with the ECHAM5-wiso output data for one time slice. The study revealed that this experiment can be highly useful for interpreting $\delta^{18}O_{calcite}$ values. More time slices or even a transient run should be aimed for.

With these ideas the model performance could lead to an advanced interpretation of stalagmite records. As the next step the model should be applied to other stalagmites from different European regions. This might be the best option to achieve robust results in palaeo climate research using speleothems. A model can never include all small scale variations which might influence a specific proxy. Therefore, the detection of common features in a selection of stalagmites allows to separate cave internal variations from large scale climate patterns and can finally lead to identification of true climate signals.

A. Caves included in the ECHAM5-wiso experiment

Soylegrotta (Norway)
Lauritzen and Lundberg [1999] presented a temperature calibration of the δ^{18}O signal of a stalagmite from Soylegrotta (modern calcite δ^{18}O is -7.33‰). Hendy tests (according to Hendy [1971] the simultaneous isotopic enrichment along growth layers) indicate that the stalagmite grew in equilibrium with its parent drip water. Lauritzen and Lundberg (1999) monitored one annual cycle of the δ^{18}O of precipitation and cave drip water. The δ^{18}O revealed a very stable pattern throughout this year. The cave temperature agrees with the mean annual temperature from the weather service station in Neverdal (1966-1989). Unfortunately the amount of precipitation is not recorded. The mean $\delta^{18}O_{prec}$ over the monitoring period is -9.90‰. This value should be handled with care, since the weighted mean $\delta^{18}O_{prec}$ might be different.

Korallgrottan (Sweden)
In Korallgrottan Sundqvist *et al.* [2007] established a monitoring program from 2000-2006. One year of drip water from eight drip sites was sampled and analysed. In this period the δ^{18}O signal varies by 2‰ maximum. In comparison with meteoric precipitation this signal is smoother and heavier. The mean $\delta^{18}O_{drip}$ is about -12.2‰ whereas the precipitation weighted mean δ^{18}O is -13.7‰ (Burgman *et al.* [1980], Calles and Westman [1989]). In Sundqvist *et al.* [2007] an actively growing stalagmite is discussed whose uppermost calcite sample reveals a $\delta^{18}O_{calcite}$ value of -9.41‰. Hendy-tests [Hendy, 1971] confirm that the stalagmite seems to have grown in a quasi-equilibrium state. Long term meteorologic data were taken from the weather service station in Jormlien and Ankarvattnet (1961-1990). The mean cave temperature is 1°C higher than the surface temperature.

Tartair Cave (Scotland)
Two annual cycles of drip water sampling are presented in Fuller *et al.* [2008]. They analysed water from 13 drip sites which show a damped δ^{18}O signal with respect to precipitation. The mean $\delta^{18}O_{drip}$ (-7.09‰) agrees with the δ^{18}O of precipitation measured close to the cave in Inchnadamph. The δ^{18}O values of contemporary calcite (-5.2‰) refer to two stalagmite tips which were actively growing when collected in the cave. For surface temperature and annual amount of precipitation Fuller et al. (2008) refer to long term averages from 1971-2000 in Proctor *et al.* [2000].

Bunker Cave (Germany) In the context of the DFG grant 668 (DAPHNE) a monitoring program has been carried out since 2003 which includes $\delta^{18}O_{prec}$ and $\delta^{18}O_{drip}$ from eight drip sites [Riechelmann *et al.* [a], in press]. They show a diminished annual

$\delta^{18}O_{drip}$ signal (mean: -7.92) with respect to precipitation and the mean value is slightly lower. Below four of the drip sites watch glasses were installed to analyse modern calcite precipitates. Their mean value is -5.92‰. It should be noted, that in comparison with the parent drip water all the precipitates show signs of kinetic fractionation.
The climatic data is taken from the German Weather Service (Deutscher Wetterdienst - DWD, www.dwd.de) from the station Hagen-Fley of the years 1978-2007.

Katerloch Cave (Austria)
Boch *et al.* [2010] provide a comprehensive monitoring of Katerloch Cave between 2005 and 2007 including six drip sites which were analysed for $\delta^{18}O$. A smoothed $\delta^{18}O$ signal is displayed which is in agreement with the weighted mean $\delta^{18}O_{prec}$ (GNIP station: Graz 1973-2004). Modern calcite ranges between -5‰ and -7‰. Boch et al. (2009) hint that calcite precipitation takes place in equilibrium.
Temperature are supplied by the monitoring program (2005-2007) and isotope and precipitation data by the GNIP station from Graz (1973-2004). The cave temperature is 2-4°C lower than surface temperature depending on the cave chamber.

Cogola Grande di Giazzera (Italy) Giazzera Cave was monitored from 2001-2003 Miorandi *et al.* [2007] in the context of the AQUAPAST project and from 2006-2009 in the context of the DAPHNE research group. In this period three different drip sites were analysed each over one year. Two of the drip sites reveal a mean $\delta^{18}O$ value of -9.2‰ though the drip site which belongs to a modern stalagmite has a mean $\delta^{18}O$ value of -10.1‰. The $\delta^{18}O$ value at the top of the stalagmite GZ-1 is -6.7‰ and affected by kinetic effect.
Close to the cave meteorologic data are available between 1992 and 2004 as well as isotope data (2002-2004). The annual mean $\delta^{18}O_{prec}$ (-8.8‰) is clearly heavier than the mean $\delta^{18}O_{drip}$ (-9.5‰) indicating the loss of summer precipitation due to evaporation.
The temperature data show that the cave temperature is 5°C colder than surface temperature (annual mean 13.3°C). All the data were supplied by courtesy of Andrea Borsato.

Grotte de Clamouse (France)
Drip water sampling in Clamouse Cave was carried out between 1999 and 2001 [Plagnes *et al.*, 2002]. In Frisia *et al.* [2002] an overview of the important cave features is given. The $\delta^{18}O_{drip}$ shows a stable value between -5.8‰ and -6.6‰. The calcite fractionation is close to equilibrium [Plagnes *et al.*, 2002].
Modern precipitates range between -4.26 and -5.54‰.
Meteorologic and isotope data can be derived from the GNIP station in Avignon from 1997 to 2007, though temperature values are available only from 2003 to 2007. According to the isotope data a shift to lighter values from rainwater to drip water can be observed.

B. Weather service station Hagen Fley: Data

Date	Humidity (2p.m.) [%]	Mean Temp. [°C]	Prec. [mm/month]	$\delta^{18}O_{prec}$ [‰]
1988-01-15	70.13	6.46	93.20	-9.44
1988-02-15	69.86	4.17	108.80	-11.02
1988-03-15	71.71	4.66	168.40	-8.99
1988-04-15	48.50	8.92	13.40	-10.15
1988-05-15	49.48	14.95	37.60	-4.32
1988-06-15	65.03	15.44	56.50	-6.56
1988-07-15	57.68	17.14	109.60	-7.84
1988-08-15	53.61	17.35	51.70	-6.81
1988-09-15	65.80	13.98	92.80	-7.62
1988-10-15	72.48	10.77	50.30	-7.08
1988-11-15	68.93	5.78	70.90	-8.39
1988-12-15	81.06	6.11	135.50	-8.52
1989-01-15	67.39	5.03	37.50	-7.12
1989-02-15	64.32	5.11	69.20	-7.72
1989-03-15	56.52	8.31	89.90	-7.43
1989-04-15	62.83	7.48	84.70	-9.17
1989-05-15	38.10	14.60	16.20	-6.03
1989-06-15	45.83	15.81	77.60	-6.16
1989-07-15	49.84	18.46	53.20	-5.94
1989-08-15	48.16	17.72	46.90	-9.63
1989-09-15	60.70	15.19	62.90	-7.62
1989-10-15	57.03	12.07	78.40	-6.41
1989-11-15	56.60	4.86	36.90	-5.81
1989-12-15	69.87	5.03	114.00	-11.41
1990-01-15	75.10	5.39	71.10	-9.34
1990-02-15	55.46	7.93	140.10	-10.05
1990-03-15	58.81	8.33	38.30	-6.31
1990-04-15	51.53	8.25	53.60	-6.44
1990-05-15	42.42	14.34	20.10	-5.36
1990-06-15	56.37	15.72	116.30	-5.14
1990-07-15	47.16	17.33	28.50	-6.01
1990-08-15	46.52	19.29	81.10	-6.29
1990-09-15	66.73	12.47	95.10	-5.85
1990-10-15	55.03	12.03	37.50	-17.37
1990-11-15	78.27	5.90	96.20	-8.09
1990-12-15	76.94	3.19	114.00	-12.13

Date	Humidity (2p.m.) [%]	Mean Temp. [°C]	Prec. [mm/month]	$\delta^{18}O_{prec}$ [‰]
1991-01-15	67.90	3.18	69.50	-7.99
1991-02-15	57.36	-0.65	25.00	-12.80
1991-03-15	54.29	8.40	39.10	-8.78
1991-04-15	41.97	8.07	31.90	-7.20
1991-05-15	49.65	10.74	45.10	-8.24
1991-06-15	56.77	13.85	82.90	-6.77
1991-07-15	50.61	19.59	55.30	-6.88
1991-08-15	50.29	17.83	78.20	-6.32
1991-09-15	56.97	15.00	51.00	-9.12
1991-10-15	63.35	9.51	42.90	-6.30
1991-11-15	71.53	5.83	122.60	-9.52
1991-12-15	73.13	3.18	110.80	-6.93
1992-01-15	76.74	2.69	38.80	-6.25
1992-02-15	68.83	4.95	46.20	-6.12
1992-03-15	59.55	6.87	106.20	-8.80
1992-04-15	55.77	8.85	65.70	-6.73
1992-05-15	42.42	15.57	17.80	-6.14
1992-06-15	59.23	16.97	88.00	-7.73
1992-07-15	51.26	19.00	73.80	-5.96
1992-08-15	55.39	18.97	99.20	-7.80
1992-09-15	57.30	14.29	53.70	-4.82
1992-10-15	68.87	7.64	103.70	-10.56
1992-11-15	71.80	7.61	127.10	-9.89
1992-12-15	76.81	3.58	77.10	-8.64
1993-01-15	68.55	4.73	148.60	-8.73
1993-02-15	72.29	1.11	35.40	-6.66
1993-03-15	48.65	5.40	12.30	-3.18
1993-04-15	53.53	11.50	68.10	-7.10
1993-05-15	52.55	14.79	127.90	-6.46
1993-06-15	50.40	16.54	28.80	-5.88
1993-07-15	54.32	16.81	149.50	-7.06
1993-08-15	53.81	15.58	35.20	-6.21
1993-09-15	66.93	12.86	124.50	-7.36
1993-10-15	71.00	8.70	101.30	-10.16
1993-11-15	70.40	1.93	52.20	-10.91
1993-12-15	81.32	5.04	210.30	-10.03
1994-01-15	75.68	5.07	125.40	-7.83
1994-02-15	62.11	1.98	25.10	-8.66
1994-03-15	59.55	7.89	134.60	-5.83
1994-04-15	54.23	9.02	62.60	-9.86
1994-05-15	60.52	13.12	71.90	-7.27
1994-06-15	55.00	16.49	95.40	-5.99
1994-07-15	43.87	21.72	45.80	-3.98
1994-08-15	50.06	17.95	40.90	-5.94
1994-09-15	66.00	13.69	75.20	-10.34
1994-10-15	59.16	9.03	88.20	-7.72
1994-11-15	77.17	9.51	104.40	-8.32
1994-12-15	75.13	5.68	109.50	-8.19

Date	Humidity (2p.m.) [%]	Mean Temp. [°C]	Prec. [mm/month]	$\delta^{18}O_{prec}$ [‰]
1995-01-15	71.26	2.93	174.10	-7.83
1995-02-15	69.18	6.41	110.00	-8.66
1995-03-15	55.77	4.65	88.90	-5.83
1995-04-15	58.17	9.59	46.50	-9.86
1995-05-15	46.71	13.14	56.40	-8.31
1995-06-15	57.63	15.17	45.10	-7.85
1995-07-15	44.84	20.72	68.70	-5.39
1995-08-15	38.87	19.43	47.40	-6.50
1995-09-15	65.83	13.68	115.40	-6.87
1995-10-15	63.48	13.51	24.80	-4.33
1995-11-15	66.90	6.42	42.90	-7.52
1995-12-15	80.13	-0.28	56.10	-11.85
1996-01-15	68.03	-0.28	7.20	-18.22
1996-02-15	74.21	-0.04	88.00	-10.96
1996-03-15	54.48	3.05	12.00	-7.57
1996-04-15	40.23	9.11	6.20	-4.72
1996-05-15	59.55	11.52	99.60	-7.29
1996-06-15	51.93	16.10	49.00	-4.79
1996-07-15	54.03	16.66	69.20	-8.96
1996-08-15	55.55	17.24	173.50	-8.96
1996-09-15	64.30	11.88	49.10	-5.80
1996-10-15	67.23	10.17	109.00	-7.03
1996-11-15	80.93	5.68	92.40	-10.96
1996-12-15	74.58	-0.23	54.30	-10.70
1997-01-15	71.77	-1.23	7.70	-7.90
1997-02-15	67.39	6.56	132.50	-7.70
1997-03-15	57.03	7.80	51.10	-4.76
1997-04-15	47.00	7.68	63.00	-5.38
1997-05-15	53.35	12.94	80.40	-6.76
1997-06-15	47.37	16.38	82.80	-6.84
1997-07-15	57.68	17.63	77.10	-7.06
1997-08-15	48.00	20.27	36.10	-6.74
1997-09-15	52.67	13.85	31.30	-5.57
1997-10-15	60.26	8.91	95.60	-6.24
1997-11-15	70.13	6.40	29.10	-8.98
1997-12-15	77.06	4.78	80.90	-9.08
1998-01-15	69.71	4.54	81.60	-9.17
1998-02-15	60.64	6.63	14.80	-5.55
1998-03-15	61.90	7.20	132.60	-5.79
1998-04-15	67.57	9.72	88.90	-10.26
1998-05-15	56.19	14.87	58.00	-6.23
1998-06-15	62.73	16.65	115.90	-5.93
1998-07-15	64.42	16.37	77.50	-4.62
1998-08-15	57.10	16.82	60.50	-7.34
1998-09-15	68.90	14.41	168.10	-10.52
1998-10-15	76.16	9.62	214.90	-13.00
1998-11-15	75.03	3.68	64.70	-9.41
1998-12-15	79.06	4.20	49.00	-8.60

Date	Humidity (2p.m.) [%]	Mean Temp. [°C]	Prec. [mm/month]	$\delta^{18}O_{prec}$ [‰]
1999-01-15	76.71	5.39	91.30	-8.18
1999-02-15	75.71	2.73	111.20	-5.55
1999-03-15	59.68	7.38	72.70	-5.79
1999-04-15	56.43	9.97	75.40	-8.74
1999-05-15	48.65	14.53	56.70	-4.51
1999-06-15	50.63	16.03	62.30	-4.60
1999-07-15	47.74	19.85	38.40	-6.33
1999-08-15	53.71	17.58	83.00	-5.86
1999-09-15	52.93	17.66	66.60	-7.96
1999-10-15	61.45	10.39	68.60	-5.44
1999-11-15	74.17	5.55	77.90	-8.97
1999-12-15	76.26	4.56	157.30	-10.44
2000-01-15	74.74	4.01	67.50	-6.59
2000-02-15	64.03	5.59	121.20	-8.57
2000-03-15	69.13	6.63	109.60	-5.97
2000-04-15	50.43	10.97	30.90	-8.27
2000-05-15	56.32	15.59	58.60	-5.97
2000-06-15	49.53	17.55	48.60	-3.97
2000-07-15	67.55	15.69	159.90	-7.28
2000-08-15	54.13	17.91	66.10	-6.05
2000-09-15	66.00	15.74	83.20	-5.93
2000-10-15	65.55	11.62	77.80	-7.52
2000-11-15	67.50	8.53	53.20	-9.77
2000-12-15	68.97	5.62	51.00	-12.54
2001-01-15	73.97	3.07	70.80	-9.55
2001-02-15	65.86	4.85	86.20	-9.84
2001-03-15	73.97	5.79	100.20	-9.91
2001-04-15	57.77	8.48	98.40	-8.13
2001-05-15	49.10	15.33	111.80	-6.62
2001-06-15	51.43	15.79	82.40	-7.32
2001-07-15	46.03	19.50	74.10	-6.29
2001-08-15	45.65	19.52	59.60	-4.77
2001-09-15	67.80	13.02	131.20	-6.39
2001-10-15	57.10	14.45	56.50	-6.30
2001-11-15	70.73	6.09	98.50	-8.01
2001-12-15	78.39	2.39	74.10	-9.55

Table B.1.: Data from 1988-2001 from DWD station Hagen Fley - www.dwd.de

Bibliography

[Aeschbach-Hertig *et al.* 1999] Aeschbach-Hertig, W. ; Peeters, F. ; Beyerle, U. ; Kipfer, R.: Interpretation of dissolved atmospheric noble gases in natural waters. *Water Resources Res.* 35. p. 2779–2792. 1999

[Baker and Bradley 2010] Baker, A. ; Bradley, C.: Modern stalagmite d18O: Instrumental calibration and forward modelling. *Gloplacha* 71. p. 201–206. 2010

[Baldini *et al.* 2006] Baldini, J.U.L. ; McDermott, F. ; Fairchild, I.J.: Spatial variability in cave drip water hydrochemistry: Implications for stalagmite paleoclimate records. *Chem. Geol.* 235. p. 390–404. 2006

[Baldini *et al.* 2008] Baldini, L.M. ; McDermott, F. ; Foley, A.M. ; Baldini, J.U.L.: Spatial variability in the European winter precipitation d18O-NAO relationship: Implications for reconstructing NAO mode climate variability in the Holocene. *Geoph. Res. Lett.* 35. p. L04709. 2008

[Bar-Matthews *et al.* 1999] Bar-Matthews, M. ; Ayalon, A. ; Kaufman, A. ; Wasserburg, G.J.: The eastern Mediterranean palaeoclimate as a reflection of regional events: Soreq Cave, Israel. *Earth Planet Sci. Lett.* 166. p. 85–95. 1999

[Boch *et al.* 2010] Boch, R. ; Spötl, C. ; Frisia, S.: Origin and palaeoenvironmental significance of lamination in stalagmites from Katerloch Cave, Austria. *Sedimentology* 2010

[Bradley *et al.* 2010] Bradley, C. ; Baker, A. ; Jex, C.N. ; Leng, M.J.: Hydrological uncertainties in the modelling of cave drip-water d18O and the implications for stalagmite palaeoclimate reconstructions. *Quat. Sci. Rev.* 29. p. 2201–2214. 2010

[Burgman *et al.* 1980] Burgman, J.O. ; Eriksson, E. ; Kostov, L. ; Sundblad, G.: Oxygen-18 variation in monthly precipitation over Sweden. *Uppsala University, Department of Physical Geography, Division of Hydrology* 24. 1980

[Burns *et al.* 2001] Burns, S.J. ; Fleitmann, D. ; Matter, A. ; Neff, U. ; Mangini, A.: Speleothem evidence from Oman for continental pluvial events during interglacial periods. *Geology* 29. p. 623–626. 2001

[Calles and Westman 1989] Calles, B. ; Westman, F.: Oxygen-18 and Deuterium in precipitation in Sweden. *Department of Physical Geography, Division of Hydrology, Report Series A* 47. p. 20. 1989

[Cheng *et al.* 2009] Cheng, H. ; Edwards, L.R. ; Broecker, W.S. ; Denton, G.H. ; Kong, X. ; Wang, Y. ; Zhang, R. ; Wang, X.: Ice Age Terminations. *Science* 326. p. 248–252. 2009

[Clark and Fritz 1997] Clark, I. ; Fritz, P.: *Environmental Isotopes in Hydrology.* LewisPublishers,NewYork.. 1997

[Cobb *et al.* 2007] Cobb, K.M. ; Adkins, J.F. ; Partin, J.W. ; Clark, B.: Regional-scale climate influences on temporal variations of rainwater and cave dripwater oxygen isotopes in northern Borneo. *Earth Planet Sci. Lett.* 263. p. 207–220. 2007

[Collins *et al.* 2006] Collins, W. D. ; Bitz, C. M. ; Blackmon, M. L. ; Bonan, G. B. ; Bretherton, C. S. ; Carton, J. A. ; Chang, P. ; Doney, S. C. ; Hack, J. J. ; Henderson, T. B. ; Kiehl, J. T. ; Large, W. G. ; McKenna, D. S. ; Santer, B. D. ; Smith, R. D.: The Community Climate System Model Version 3 (CCSM3). *J. Climate* 19. p. 2122–2143. 2006

[Cruz *et al.* 2007] Cruz, F. ; Burns, S. ; Jercinovic, M. ; Karmann, I. ; Sharp, W. ; Vuille, M.: Evidence of rainfall variations in Southern Brazil from trace element ratios (Mg/Ca and Sr/Ca) in a Late Pleistocene stalagmite. *Geochim Cosmochim Acta* 71. p. 2250–2263. 2007

[Cruz *et al.* 2005] Cruz, F.W. ; Burns, S.J. ; Karmann, I. ; Sharp, W.D. ; Vuille, M. ; Cardoso, A.O. ; Ferrari, J.A. ; Silva Dias, P.L. ; Viania, O: Insolation-driven changes in atmospheric circulation over the past 116,000 years in subtropical Brazil. *Nature* 434. p. 63–66. 2005

[Dansgaard 1964] Dansgaard, W: Stable isotopes in precipitation. *Tellus* 16. p. 438–468. 1964

[Deininger 2010] Deininger, M.: *Klimaarchiv Stalagmit - Modellierung der Bildungsprozesse und Rekonstruktion von Paläoklimaparametern*, Ruprecht-Karls-University, Heidelberg, master thesis, 2010

[Denniston *et al.* 1999] Denniston, R.F. ; Gonzalez, L.A. ; Asmerom, Y. ; Baker, R.G. ; Reagan, M.K. ; Bettis, E.A.: Reagan, M.K., Bettis III, E.A., 1999a. Evidence for increased cool season moisture during the middle-Holocene. *Geology* 27. p. 815–818. 1999

[Dreybrodt 2008] Dreybrodt, W.: Evolution of the isotopic composition of carbon and oxygen in a calcite precipitating H2O - CO2 - CaCO3 solution and the related isotopic composition of calcite in stalagmites. *Geochim. Cosmochim. Acta* 72 (19). p. 4712–4724. 2008

[Dykoski *et al.* 2005] Dykoski, C. ; Edwards, R.L. ; Cheng, H. ; Yuan, D. ; Cai, Y. ; Zhang, M. ; Lin, Y. ; Qing, J. ; An, Z. ; Revenaugh, J.: A high-resolution, absolute-dated Holocene and deglacial Asian monsoon record from Dongge Cave, China. *Earth Planet Sci. Lett.* 233. p. 71–86. 2005

[Fairchild *et al.* 2000] Fairchild, I.J. ; Borsato, A. ; Tooth, A.F. ; Frisia, S. ; Hawkesworth, C.J. ; Huang, Y. ; McDermott, F. ; Spiro, B.: Controls on trace element (Sr–Mg) compositions of carbonate cave waters: implications for speleothem climatic records. *Chem. Geol.* 166. p. 255–269. 2000

[Fairchild *et al.* 2006] Fairchild, I.J. ; Smith, C.L. ; Baker, A. ; Fuller, L. ; Spoetl, C. ; Mattey, D. ; McDermott, F.: Modification and preservation of environmental signals in speleothems. *Earth Sci. Rev.* 75. p. 105–153. 2006

[Fairchild and Treble 2009] Fairchild, I.J. ; Treble, P.C.: Trace elements in speleothems as recorders of environmental change. *Quat. Sci. Rev.* doi:10.1016/j.quascirev.2008.11.007.. 2009

[Fensterer 2011] Fensterer, C.: *Holocene Caribbean Climate Variability reconstructed from Speleothems from Western Cuba*, Ruprecht-Karls-University, Heidelberg, phd thesis, 2011

[Fohlmeister *et al.* 2011] Fohlmeister, J. ; Scholz, D. ; Kromer, B. ; Mangini, A.: Modelling Carbon Isotopes of Carbonates in Cave Drip Water. *Geochim. Cosmochim. Acta* 75 18. p. 5219–5228. 2011

[Fricke and O'Neil 1999] Fricke, H.C. ; O'Neil, J.R.: The correlation between 18O/16O of meteoric water and surface temperature: its use in investigating terrestrial climate change over geologic time. *Earth Planet. Sci. Lett.* 170. p. 181–196. 1999

[Friedmann and O'Neil 1977] Friedmann, I. ; O'Neil, J.R.: *Compilation of stable isotope fractionation factors of geochemical interest (ed M. Fleischer).* In: Data of Geochemistry 6th edition, p. 1–12, U. S. Geol. Survey Prof. Paper 440 KK. 1977

[Frisia *et al.* 2002] Frisia, S. ; Borsato, A. ; Fairchild, I.J. ; McDermott, F. ; Selmo, E.M: Aragonite-Calcite Relationships in Speleothems (Grotte de Clamouse, France) Environment, Fabrics and Carbonate Geochemistry. *J. Sed. Res.* 72 5. p. 687–699. 2002

[Fuller *et al.* 2008] Fuller, L. ; Baker, A. ; Fairchild, I.J. ; Spötl, C. ; Marca-Bell, A. ; Rowe, P. ; Dennis, P.F.: Isotope hydrology of dripwaters in a Scottish cave and implications for stalagmite plaeoclimate research. *Hydrol. Earth Syst. Sci.* 12. p. 1065–1074. 2008

[Gat 1996] Gat, J.R.: Oxygen ans hydrogen isotopes in the hydrologic cycle. *Annu. Rev. Earth Planet. Sci.* 24. p. 225–262. 1996

[Gates *et al.* 1999] Gates, W.L. ; Boyle, J.S. ; Covey, C.C. ; Dease, C.G. ; Doutriaux, C.M. ; Drach, R.S. ; Fiorino, M. ; Gleckler, P.J. ; Hnilo, J.J. ; Marlais, S.M. ; Phillips, T.J. ; Potter, G.L.D. ; Sperber, K.R. ; Taylor, K.E. ; Williams, D.N.: An overview of the results of the Atmospheric Model Intercomparison Project (AMIP I). *Bull. Amer. Meteor. Soc.* 80. p. 29–55. 1999

[Genty *et al.* 2003] Genty, D. ; Blamart, D. ; Ouahdi, R. ; Gilmour, M. ; Baker, A. ; Jouzel, J. ; Van-Exter, S.: Precise dating of Dansgaard–Oeschger climatic oscillations in western Europe from stalagmite data. *Nature* 421. p. 833–837. 2003

[Haude 1954] Haude, W: Zur praktischen Bestimmung der aktuellen und potentiellen Evaporation und Evapotranspiration. *Mitt. Deutsch. Wetterdienst Nr. 8* Band 8. p. 1–15. 1954

[Haude 1955] Haude, W.: Zur Bestimmung der Verdunstung auf möglichst einfache Weise. *Mitt. Deutsch. Wetterdienst Nr. 11* Band 2. p. 1–24. 1955

[Häckel 1999] Häckel, Hans: *Meteorologie, 4. überarbeitete Auflage.* Ulmer. 1999

[Henderson and Slowey 2000] Henderson, G.M. ; Slowey, N.C.: Evidence from U–Th dating against Northern Hemisphere forcing of the penultimate deglaciation. *Nature* 404. p. 61–66. 2000

[Hendy 1971] Hendy, C.: The Isotopic Geochemistry of Speleothems – I. The Calculation of the Effects of Different Modes of Formation on the Isotopic Composition of Speleothems and Their Applicability as Palaeoclimatic Indicators. *Geochim. Cosmochim. Acta* 35. p. 801–824. 1971

[Hendy and Wilson 1968] Hendy, C.H. ; Wilson, A.T.: Palaeoclimatic data from speleothems. *Nature* 219. p. 48–51. 1968

[Hoffmann *et al.* 1998] Hoffmann, G. ; Werner, M. ; Heimann, M.: Water isotope module of the ECHAM atmospheric general circulation model - A study on timescales from days to several years. *J. Geophys. Res.* 103. p. 16871–16896. 1998

[Hu *et al.* 2008] Hu, C. ; Henderson, G.H. ; J., Huang ; Chen, Z. ; Johnson, K.R: Report of a three-year monitoring programme at Heshang Cave, Central China. *Intern. J. Speleo.* 37. p. 143–151. 2008

[Huang and Fairchild 2001] Huang, Y. ; Fairchild, I.J.: Partitioning of Sr2+ and Mg2+ into calcite under karstanalogue experimental conditions. *Geochim. Cosmochim. Acta* 65. p. 47–62. 2001

[Hurrell 1995] Hurrell, J. W.: Decadal Trends in the North Atlantic Oscillation: Regional Temperatures and Preciptiation. *Science* 269. p. 676–679. 1995

[Hurrell and van Loon 1997] Hurrell, J.W. ; Loon, H. van: Decadal variations in climate associated with the North Atlantic Oscillation. *Clim. Change* 36. p. 301–326. 1997

[IAEA/WMO 2006] IAEA/WMO: *Global Network of Isotopes in Precipitation. The GNIP Database.* Accessible at: http://isohis.iaea.org. 2006

[Jansen *et al.* 2007] Jansen, E. ; Overpeck, J. ; Briffa, K.R. ; Duplessy, J.-C. ; Joos, F. ; Masson-Delmotte, V. ; Olago, D. ; Otto-Bliesner, B. ; Peltier, W.R. ; Rahmstorf, S. ; Ramesh, R. ; Raynaud, D. ; Rind, D. ; Solomina, O. ; Villalba, R. ; Zhang, D.: *Climate Change 2007: The Physical Science Basis. Contribution of Working Group I to the Fourth Assessment Report of the Intergovernmental Panel on Climate Change.* In: Palaeoclimate., p. 434–498, Cambridge University Press, Cambridge, United Kingdom and New York, NY, USA.. 2007

[Jex *et al.* 2010] Jex, C. ; Baker, A. ; Fairchild, I.J. ; Eastwood, W.J. ; Leng, M. ; Sloane, H.J. ; Thomas, L. ; Bekaroglu, E.: Calibration of speleothem d18O with instrumental climate records from Turkey. *Gloplacha* 71. p. 207–217. 2010

[Joerin *et al.* 2006] Joerin, U.E. ; Stocker, T.F. ; Schlüchter, C.: Multicentury glacier fluctuations in the Swiss Alps during the Holocene. *The Holocene* 16. p. 697–704. 2006

[Johnson *et al.* 2006] Johnson, K.R. ; Hu, C. ; Belshaw, N.S. ; Henderson, G.M.: Seasonal trace-elements and stable-isotope variations in a Chinese speleothem: The potential for high resolution paleomonsoon reconstruction. *Earth Planet. Sci. Lett.* 244. p. 3461–3475. 2006

[Jones *et al.* 1997] Jones, P.D. ; Jonsson, T. ; Wheeler, D.: Extension to the North Atlantic Oscillation using early instrumental pressure observations from Gibraltar and south-west Iceland. *Int. J. Climatol.* 17. p. 1433–1450. 1997

[Joussaume *et al.* 1984] Joussaume, S. ; Sadourny, R. ; Jouzel, J.: A general circulation model of water isotope cycles in the atmosphere. *Nature* 311. p. 24–29. 1984

[Jouzel *et al.* 1987] Jouzel, J. ; Russell, G.L. ; Suozzo, R.J. ; Koster, D. ; White, J.W.C. ; Broecker, W.S.: Simulations of the HDO and H18O atmospheric cycles using the NASA GISS general circulation model: The seasonal cycle for present- day conditions. *J. Geophys. Res.* 92. p. 14739–14760. 1987

[Karmann *et al.* 2007] Karmann, I. ; Cruz, F.W. ; Viana Jr., O. ; Burns, S.J.: Climate influence on trace element geochemistry of waters from Santana–Pe´ rolas cave system, Brazil. *Chem. Geol.* 244. p. 232–247. 2007

[Kim and O'Neil 1997] Kim, S.-T. ; O'Neil, J. R.: Equilibrium and nonequilibrium oxygen isotope effects in synthetic carbonates. *Geochim. Cosmochim. Acta* 61 16. p. 3461–3475. 1997

[Kluge 2008] Kluge, T.: *Fluid inclusions in speleothems as a new archive for the noble gas palaeothermometer*, Ruprecht-Karls-University, Heidelberg, phd thesis, 2008

[Kluge *et al.* 2008] Kluge, T. ; Marx, T. ; Scholz, D. ; Niggemann, S. ; Mangini, A. ; Aeschbach-Hertig, W.: A new tool for palaeoclimate reconstruction: Noble gas temperatures from fluid inclusions in speleothems. *Earth Planet. Sci. Lett.* 28. p. 412–432. 2008

[Kluge *et al.* 2010] Kluge, T. ; Riechelmann, D.F.C ; Wieser, M. ; Spötl, C. ; Sültenfuss, J. ; Schröder-Ritzrau, A. ; Niggemann, S. ; Aeschbach-Hertig, W.: Dating cave drip water by tritium. *J. Hydrol.* 394. p. 396–406. 2010

[Lachniet 2009] Lachniet, M.S: Climatic and environmental controls on speleothem oxygen-isotope values. *Quart. Sci. Rev.* 28. p. 412–430. 2009

[Langebroek *et al.*] Langebroek, P.M. ; Werner, M. ; Lohmann, G.: *Climate information imprinted in oxygen-isotopic composition of precipitation in Europe.* – Earth Planet. Sci. Lett. in press

[Lauritzen and Lundberg 1999] Lauritzen, S.-E. ; Lundberg, J.: Calibration of the speleothem delta function: an absolute temperature record fort he Holocene in northern Norway. *Holocene* 9. p. 659–669. 1999

[Lebrón and Suárez 1998] Lebrón, I. ; Suárez, D.L.: Kinetics and mechanisms of preciptitation of calcite as affected by pCO2 and organic ligands at 25 °C. *Geochim. Cosmochim. Acta* 62. p. 405–416. 1998

[Lee and Fung 2007] Lee, J.E. ; Fung, I.: "Amount effect" of water isotopes and quantitative analysis of post-condensation processes. *Hydrol. Process.* 22. p. 1–8. 2007

[LeGrande and Schmidt 2006] LeGrande, A.N. ; Schmidt, G.A.: Global gridded data set of the oxygen isotopic composition in seawater. *Geophys. Res. Lett.* 33. p. L12604. 2006

[Legutke and Voss 1999] Legutke, S. ; Voss, R.: The Hamburg atmosphere-ocean coupled circulation model ECHO-G / DKRZ, Hamburg, Germany. 1999. – Forschungsbericht

[Linge *et al.* 2001] Linge, H. ; Lauritzen, S.E. ; Lundberg, J. ; Berstad, I.M.: Stable isotope stratigraphy of Holocene speleothems: examples from a cave system in Rana, northern Norway. *Palaeogeography* 167. p. 209–224. 2001

[Luterbacher *et al.* 2002] Luterbacher, J. ; E., Xoplaki ; D., Dietrich ; Jones, P.D. ; Davies, T.D. ; Portis, D. ; Gonzalez-Rouco, J.F. ; Storch, H. von ; D., Gyalistras ; Casty, C. ; Wanner, H.: Extending North Atlantic oscillation reconstructions back to 1500. *Atmos. Sci. Lett.* 2. p. 114–124. 2002

[Majoube 1971] Majoube, M.: Fractionnement en oxygen-18 et en deuterium entre l'eau et sa vapeur. *Journal de Chimie Physique.* 68. p. 1423–1436. 1971

[Mangini *et al.* 2005] Mangini, A. ; Spötl, C. ; Verdes, P.: Reconstruction of temperature in the Central Alps during the past 2000 yr from a d18O stalagmite record. *Earth Planet. Sci. Lett.* 68. p. 1423–1436. 2005

[Mangini *et al.* 2007] Mangini, P. ; Spoetl, C. ; Scholz, D. ; Vollweiler, N. ; Kromer, B.: Persistent influence of the North Atlantic hydrography on central European winter temperature during the last 9000 years. *Geophys. Res. Lett.* 34. p. L02704. 2007

[Masson-Delmotte *et al.* 2005] Masson-Delmotte, V. ; Jouzel, J. ; Landais, A. ; Stievenard, M. ; Johnsen, S.J. ; White, J.W.C. ; Werner, M. ; Sveinbjornsdottir, A. ; Fuhrer, K.: GRIP Deuterium Excess Reveals Rapid and Orbital-Scale Changes in Greenland Moisture Origin. *Science* 309. p. 118–121. 2005

[Matthews *et al.* 2000] Matthews, A. ; Ayalon, A. ; Bar-Matthews, M.: D/H ratios of fluid inclusions of Soreq cave (Israel) speleothems as a guide to the Eastern Mediterranean Meteoric Line relationships in the last 120 ky. *Chem. Geol.* 166. p. 183–191. 2000

[McDermott 2004] McDermott, F.: Palaeo-climate reconstruction from stable isotope variations in speleothems: a review. *Quat. Sci. Rev.* 23. p. 901–918. 2004

[McDermott *et al.* 2011] McDermott, F. ; Atkinson, T.C. ; Fairchild, I.J. ; L.M., Baldini ; Mattey, D.P.: A first evaluation of the spatial gradients in d18O recorded by European Holocene speleothems. *Gloplacha* in press. 2011

[McDonald and Drysdale 2004] McDonald, J. ; Drysdale, R.: The 2002–2003 El Nino recorded in Australian cave drip waters: Implications for reconstructing rainfall histories using stalagmites. *Geophys. Res. Lett.* 31. p. L22202. 2004

[McDonald *et al.* 2007] McDonald, J. ; Drysdale, R. ; Hill, D. ; Chisari, R. ; Wong, R.: The hydrochemical response of cave drip waters to sub-annual and inter-annual climate variability, Wombeyan Caves, SE Australia. *Chem. Geol.* 244. p. 605–623. 2007

[McMillan *et al.* 2005] McMillan, E.A. ; Fairchild, I.J. ; Frisia, S. ; Borsato, A. ; McDermott, F.: Annual trace element cycles in calcite–aragonite speleothems: evidence of drought in the western Mediterranean 1200–1100 yr BP. *J. Quat. Sci.* 20. p. 423–433. 2005

[Merlivat and Jouzel 1979] Merlivat, L. ; Jouzel, J.: Global Climatic Interpretation of the Deuterium-Oxygen 18 Relationship for Precipitation. *J. Geoph. Res.* 84. p. 3029–5033. 1979

[Mühlinghaus 2008] Mühlinghaus, C.: *The principles of growth and isotopic fractionation of stalagmites - A numerical model to reconstruct temperature and precipitation records from stalagmites grown under disequilibrium conditions*, University of Heidelberg, phd thesis, 2008

[Mühlinghaus *et al.* 2009] Mühlinghaus, C. ; Scholz, D. ; Mangini, A.: Modelling fractionation of stable isotopes in stalagmites. *Data of Geochemistry 6th edition (ed. by Fleischer, M.)* 73. p. 7275–7289. 2009

[Miorandi *et al.* 2007] Miorandi, R. ; Borsato, A. ; Frisia, S. ; Zandonati, M.: Monitoraggio di aria e acqua di percolazione in alcune grotte del Trentino. Studi Trentini di Scienze Naturali. *Acta Geol.* 82. p. 151–164. 2007

[Mook and de Vriess 2000] Mook, W.G. ; Vriess, J.J. de: *Environmental Isotopes in the Hydrological Cycle. Principles and Applications.* In: Volume 1: Introduction - Theory, Methods, Review, IAEA. 2000

[Mook 2006] Mook, Willem G.: *Introduction to Isotope Hydrologie.* Taylor&Francis/Balkema. 2006

[Morse and Bender 1990] Morse, J.W. ; Bender, M.L.: Partition coefficients in calcite: examination of factors influencing the validity of experimental results and their application to natural systems. *Chem. Geol.* 82. p. 265–277. 1990

[Neff *et al.* 2001] Neff, U. ; Burns, S.J. ; Mangini, A. ; Mudelsee, M. ; Fleitmann, D. ; Matter, A.: Strong coherence between solar variability and the monsoon in Oman between 9 and 6 kyr ago. *Nature* 411. p. 290–293. 2001

[Nielsen and Toft 1984] Nielsen, A. ; Toft, J.: Electrolyte crystal growth kinetics. *J. Crystal Growth* 67. p. 278–288. 1984

[Niggemann 2000] Niggemann, S.: Klimabezogene Untersuchungen an spat- bis postglazialen Stalagmiten aus Massenkalkhöhlen aus dem Sauerland. *Beiträge zur Speläologie I: Bochumer geol. U. geotechn. Arb., 55, pp. 5–129. Bochum.* Detlef K Richter and Georg Wurth. 2000

[Niggemann *et al.* 2003] Niggemann, S. ; Mangini, A. ; Mudelsee, M. ; Richter, D.K. ; Wurth, G.: Sub-Milankovitch climatic cycles in Holocene stalagmites from Sauerland, Germany. *Earth Planet Sci. Lett.* 216. p. 539–547. 2003

[O'Neil *et al.* 1969] O'Neil, J.R. ; Clayton, R.N. ; Mayeda, T.K.: Oxygen Isotope Fractionation in Divalent Metal Carbonates. *J. Chem. Phys.* 51. p. 5547–5558. 1969

[Partin *et al.* 2007] Partin, J.W. ; Cobb, K.M. ; Adkins ; J.F. ; Clark, B. ; Fernandez, D.P.: Millennial-scale trends in west Pacific warm pool hydrology since the Last Glacial Maximum. *Nature* 449. p. 452–455. 2007

[Penman 1948] Penman, H.L.: Natural evaporation from open water, bare soil and grass. *Proc. Roy. Soc. London A* 193. p. 120–145. 1948

[Plagnes *et al.* 2002] Plagnes, V. ; Causse, C. ; Genty, D. ; Paterne, M. ; Blamart, D.: A discontinuous climatic record from 187 to 74 ka from a speleothem of the Clamouse Cave (south of France). *Earth Planet. Sci. Lett.* 201. p. 87–103. 2002

[Proctor *et al.* 2000] Proctor, C.J. ; Baker, A. ; Barnes, W.L. ; Gilmour, M.A.: . A thousand year speleothem proxy record of North Atlantic climate from Scotland. *Cli. Dynam.* 16. p. 815–820. 2000

[Randall *et al.* 2007] Randall, D.A. ; Wood, R.A. ; Bony, S. ; Colman, R. ; Fichefet, T. ; Fyfe, J. ; Kattsov, V. ; Pitman, A. ; Shukla, J. ; Srinivasan, J. ; Stouffer, R. ; Sumi, A. ; Taylor, K.: *Climate Change 2007: The Scientific Basis.* In: Contribution of Working Group 1 to the Fourth Assessment Report of the Intergovernmental Panel on Climate Change., p. p. 881, Cambridge University Press, Cambridge, United Kingdom and New York, NY, USA. 2007

[Richards and Dorale 2003] Richards, D. ; Dorale, J.: Uranium chronology and environmental applications of speleothems. *Rev. Mineral.* 52. p. 407–460. 2003

[Riechelmann 2010] Riechelmann, D. F. C.: *Aktuospeläologische Untersuchungen in der Bunkerhöhle des Iserlohner Massenkalks (NRW/Deutschland): Signifikanz für kontinentale Klimaarchive.*, Ruhr-University Bochum, phd thesis, 2010

[Riechelmann *et al.* a] Riechelmann, D.F.C ; Schröder-Ritzrau, A ; Scholz, D. ; Fohlmeister, J. ; Spötl, C. ; Richter, D.K. ; Mangini, A.: *Monitoring Bunker*

Cave (NW Germany): A prerequisite to interpret speleothem isotopic and geochemical time series from this site. – J. Hydrol. in press

[Riechelmann *et al.* b] Riechelmann, S. ; Buhl, D. ; Schröder-Ritzrau, A. ; Spötl, C. ; Riechelmann, D.F.C. ; Richter, D.K. ; Immenhauser, A.: *Hydrogeochemistry and fractionation pathways of Mg isotopes in a continental weathering system: Lessons from field experiments.* – in review

[Roberts *et al.* 1998] Roberts, M.S. ; Smart, P.L. ; Baker, A.: Annual trace element variations in a Holocene speleothem. *Earth Planet Sci. Lett.* 154. p. 237–246. 1998

[Rodwell *et al.* 1999] Rodwell, M.J. ; Rowell, D.P. ; Folland, C.K.: Oceanic forcing of the wintertime North Atlantic Oscillation and European climate. *Nature* 398. p. 320–323. 1999

[Roeckner *et al.* 2006] Roeckner, E. ; Brokopf, R. ; Esch, M. ; Giorgetta, M. ; Hagemann, S. ; Korn-blueh, L. ; Manzini, E. ; Schlese, U. ; Schulzweida, U.: Sensitivity of simulated climate to horizontal and vertical resolution in the ECHAM5 atmosphere model. *J. Climate* 19. p. 3771–2791. 2006

[Roeckner *et al.* 2003] Roeckner, E. ; Bäuml, G. ; Bonaventura, L. ; Brokopf, R. ; Esch, M. ; Giorgetta, M. ; Hagemann, S. ; Kirchner, I. ; Kornblueh, L. ; Manzini, E. ; Rhodin, A. ; Schlese, U. ; Schulzweida, U. ; Tompkins, A.: The Atmospheric General Circulation Model ECHAM5. Part I: Model Description. / Max Planck Institute for Meteorology, MPI-Report 349. 2003. – Forschungsbericht

[Romanov *et al.* 2008] Romanov, D. ; Kaufmann, G. ; Dreybrodt, W.: d13C profiles along growth layers of stalagmites: Comparing theoretical and experimental results. *Geochim. Cosmochim. Acta* 72. p. 438–448. 2008

[Rozanski *et al.* 1993] Rozanski, K. ; Araguás-Araguás, L. ; Gonfiantini, R.: *Climate Change in Continental Isotopic Records.* In: Isotopic patterns in modern global precipitation, p. 1–37, American Geophysical Union, Washington. 1993

[Scheffer and Schachtschabel 1984] Scheffer, F. ; Schachtschabel, P.: *Lehrbuch der Bodenkunde.* Ferdinand Enke Verlag Stuttgard1984. 1984

[Schiff 1975] Schiff, H.: Berechnung der potentiellen Verdunstung und deren Vergleich mit aktuellen Verdunstungswerten von Lysimetern. *Arch. Met. Geoph. Biokl., Ser. B* 23. p. 331–342. 1975

[Schmidt *et al.* 2007] Schmidt, G.A. ; LeGrande, A.N. ; Hoffmann, G.: Water isotope expressions of intrinsic and forced variability in a coupled ocean-atmosphere model. *J. Geophys. Res* 112. p. D10103. 2007

[Schönwiese 2008] Schönwiese, C.D.: *Klimatologie.* UTB, Stuttgart. 2008

[Scholz *et al.* 2009] Scholz, D. ; Mühlinghaus, C. ; Mangini, A.: Modelling the evolution of d13C and d18O in the solution layer on stalagmite surfaces. *Geochim. Cosmochim Acta* 73. p. 2592–2602. 2009

[Spötl *et al.* 2005] Spötl, C. ; Fairchild, I.J. ; Tooth, A.F.: Cave air control on dripwater geochemistry, Obir Caves (Austria): Implications for speleothem deposition in dynamically ventilated caves. *Geochim Cosmochim Acta* 69 10. p. 2451–2468. 2005

[Spötl and Mangini 2002] Spötl, C. ; Mangini, A.: Stalagmite from the Austrian Alps reveals Dansgaard–Oeschger events during isotope stage 3: implications for the absolute chronology of Greenland ice cores. *Earth Planet Sci. Lett.* 203. p. 507–518. 2002

[Spötl *et al.* 2007] Spötl, C. ; Offenbecher, K.-H. ; Boch, R. ; Meyer, M. ; Mangini, A. ; Kramers, J. ; Pavuza, R.: Tropstein-Forschung in österreichischen Höhlen - ein Überblick. *Jahrbuch der Geologischen Bundesanstalt* 147. p. 117–167. 2007

[Sundqvist *et al.* 2007] Sundqvist, H.S. ; Seibert, J. ; Holmgren, K.: Understanding conditions behind speleothem formation in Korallgrottan, northwestern Sweden. *J. Hydrol* 347. p. 13–22. 2007

[Tang and Feng 2001] Tang, K. ; Feng, X.: The effect of soil hydrology on the oxygen and hydrogen isotopic composition of plant' source water. *Earth Planet. Sci. Lett.* 185. p. 355–367. 2001

[Thornthwaite and Mather 1957] Thornthwaite, C.W. ; Mather, J.R.: Instructions and tables for computing potential Evapotranspiration and the water balance. *Publications in Climatology* 10. p. 3. 1957

[Tomozeiu *et al.* 2002] Tomozeiu, R. ; A., Busuioc ; S., Stefan: Changes in seasonal mean maximum air temperature in Romania and their connection with large-scale circulation. *Intern. J. Clim.* 22. p. 1181–1196. 2002

[Tomozeiu *et al.* 2005] Tomozeiu, R. ; S., Stefan ; A., Busuioc: Winter precipitation variability and large-scale circulation patterns in Romania. *Theo. Appl. Clim.* 81. p. 193–201. 2005

[Tooth and Fairchild 2003] Tooth, A.F. ; Fairchild, I.J.: Soil and karst aquifer hydrological controls on the geochemical evolution of speleothem-forming drip waters, Crag Cave, southwest Ireland. *J. Hydrol* 273. p. 51–68. 2003

[Treble *et al.* 2003] Treble, P. ; Shelley, J.M.G. ; Chappell, J.: Comparison of high resolution sub-annual records of trace elements in a modern (1911-1992) speleothem with instrumental climate data from southwest Australia. *Earth Planet Sci. Lett.* 216. p. 141–153. 2003

[Trigo *et al.* 2002] Trigo, M.R. ; Osborn, T.J. ; Corte-Real, J.M.: The North Atlantic Oscillation influence on Europe: climate impacts and associated physical mechanisms. *Clim. Res.* 20. p. 9–17. 2002

[Trouet *et al.* 2009] Trouet, V. ; Esper, J. ; Graham, N.E. ; Baker, A. ; J.D. ; Scourse, D.C.: Persistent Positive North Atlantic Oscillation Mode Dominated the Medieval Climate Anomaly. *Science* 324. p. 78–80. 2009

[Vollweiler 2010] Vollweiler, N.: *COMNISPA – ein präzise datiertes Klima-Archiv aus holozänen alpinen Stalagmiten*, Ruprecht-Karls-Universität, Heidelberg, phd thesis, 2010

[Vollweiler *et al.* 2006] Vollweiler, N. ; Scholz, D. ; Mühlinghaus, C. ; Mangini, A. ; Spötl, C.: A precisely dated climate record for the last 9 kyr from three high alpine stalagmites, Spannagel Cave, Austria. *Geophys. Res. Lett.* 33. p. L20703. 2006

[Vose *et al.* 1998] Vose, R.S. ; Peterson, T.C. ; Hulme, M.: *The Global Historical Climatology Network Precipitation Database: Version 2.0. In Proceedings of the Ninth Symposium on Global Change Studies.* American Meteorological Society, Boston, Massachusetts. 1998

[Wackerbarth *et al.* 2010] Wackerbarth, A. ; Scholz, D. ; Fohlmeister, J. ; Mangini, A.: Modelling the d18O value of cave drip water and speleothem calcite. *Earth Planet. Sci. Lett.* 299. p. 387–397. 2010

[Wang *et al.* 2001] Wang, Y.J. ; Cheng, H. ; Edwards, R.L. ; An, Z.S. ; Wu, J.Y. ; Shen, C.-C. ; Dorale, J.A: A High-Resolution Absolute-Dated Late Pleistocene Monsoon Record from Hulu Cave, China. *Science* 294. p. 2345–2348. 2001

[Wanner 2001] Wanner, H.: North Atlantic Oscillation – Concepts and Studies. *Surv. Geophys.* 22. p. 321–382. 2001

[Wanner *et al.* 2008] Wanner, H. ; Beer, J. ; Bütikofer, J. ; Crowley, T.J. ; Cubasch, U. ; Flückiger, J. ; Goosse, H. ; Grosjean, M. ; Joos, F. ; Kaplan, J.O. ; Küttel, M. ; Müller, S.A. ; Prentice, C. ; Solomina, O. ; Stocker, T.F. ; Tarasov, P. ; Wagner, M. ; Widmannm, M.: Mid- to Late Holocene climate change: an overview. *Quat. Sci. Rev.* 27. p. 1791–1828. 2008

[Werner *et al.* 2011] Werner, M. ; Langebroek, P.M. ; Carlsen, T. ; Herold, M. ; Lohmann, G.: Stable water isotopes in the ECHAM5 general circulation model: Towards high resolution isotope modelling on a global scale. *J. Geoph. Res.* 2011

[Winograd *et al.* 1992] Winograd, I.J. ; Coplen, T.B. ; Landwehr, J.M. ; Riggs, A.C. ; Ludwig, K.R. ; Szabo, B.J. ; Kolesar, P.T. ; Revesz, K.M.: Continuous 500,000-year climate record from vein calcite in Devils Hole, Nevada. *Science* 258. p. 255–260. 1992

[Winterhalder 2011] Winterhalder, S.: *Ein präzise datierter Multiproxyrecord des Spätholozäns aus einem südeuropäischen Stalagmiten (Closani-Höhle, Rumänien)*, Ruprecht-Karls-Universität Heidelberg, master thesis, 2011

[Zhao *et al.* 2010] Zhao, K. ; Wang, Y. ; Edwards, L. ; Cheng, H. ; Liu, D.: High-resolution stalagmite d18O records of Asian monsoon changes in central and southern China spanning the MIS 3/2 transition. *Earth Planet Sci. Lett.* 298. p. 191–198. 2010

[Zhou *et al.* 2005] Zhou, Y. ; Wang, S. ; Xie, X. ; Luo, W. ; Li, T.: Significance and dynamics of drip water responding to rainfall in four caves of Guizhou, China. *Chin. Sci. Bull.* 50. p. 154–161. 2005

Danksagung

Vor allen anderen möchte ich meinem Doktorvater Herrn Prof. Dr. Augusto Mangini danken, der mich durch seine Hingabe an die Paläoklimaforschung von Anfang an sowie immer wieder für dieses Thema begeistern konnte. Ich bin dankbar für die Möglichkeit selbständig und eigenverantwortlich zu arbeiten und seine Bereitschaft jederzeit das Erarbeitete zu diskutieren. Ich habe in hohem Maße von seinem wissenschaftlichen Intellekt und seiner Betreuung profitiert, die mir half mich methodisch, fachbezogen und persönlich weiterzuentwickeln.

An zweiter Stelle gilt mein Dank Herrn Prof. Dr. Werner Aeschbach-Hertig, der sich bereiterklärt hat diese Arbeit als Zweitgutachter zu lesen und zu beurteilen.

Desweiteren danke ich Petra Langebroek, Martin Werner und Gerrit Lohmann vom Alfred-Wegener-Institut in Bremerhaven, die mir ermöglichten die in dieser Arbeit verwendeten Daten des ECHAM5-wiso zu verwenden. Ohne ihre Bereitschaft zu vertrauensvollem, wissenschaftlichen Austausch, wäre ein Großteil meiner Arbeit nicht möglich gewesen.
Ich danke vor allem Petra für das zeitraubende Zusammenstellen der Daten und ihre ausführlichen Erklärungen ohne die das ECHAM5-wiso für mich immer noch eine Blackbox wäre. Groetjes nach Bergen!

Keine wissenschaftliche Arbeit entsteht durch einen einzelnen. Ich danke Andrea, Denis und Jens, die mich während der drei Jahre durch fachliche Diskussionen, Ideen und Anregungen begleitet haben und sich auch bereit erklärt hatten, diese Arbeit Korrektur zu lesen. In diesem Zusammenhang danke ich auch Felix, Nicole und Phil für ihre Kommentare und Vorschläge.

Ich danke jedem einzelnen meiner Arbeitsgruppe, die doch so viel mehr als das ist. Wenn man nach vier Jahren die Mensa immer noch nicht satt hat, dann liegt das zweifellos an der Gesellschaft.

Mein größter Dank gilt denen, deren Nähe mir ein Zuhause gibt, wo immer ich auch stehen bleibe. Ohne euch - Felix, Nicole, Pascal, Petra, Phil und Wiebke - wäre ich nicht so mutig und beharrlich weitergegangen. Allen voran aber stehen die, die mir früher wie heute die Orientierung sind und mit mir manchmal unverständlichem Optimismus an mich glauben: meine Familie - meine Eltern, meine Schwester und Rainer.

Erklärungen gemäß §8 (3) b) und c) der Promotionsordnung::

- Ich erkläre hiermit, dass ich die vorgelegte Dissertation selbst verfasst und mich keiner anderen als der von mir ausdrücklich bezeichneten Quellen und Hilfen bedient habe.
- Ich erkläre hiermit, dass ich an keiner anderen Stelle ein Prüfungsverfahren beantragt bzw. die Dissertation in dieser oder anderer Form bereits anderweitig als Prüfungsarbeit verwendet oder einer anderen Fakultät als Dissertation vorgelegt habe.

Heidelberg, den ....
Unterschrift